SYNTHETIC STUDIES BASED ON COVALENT PROTEIN MODIFIERS

Thesis presented for the degree of Doctor of Philosophy

Kathryn Marie Evans

March 2006

School of Chemistry

University of St Andrews

DECLARATIONS

I, Kathryn Marie Evans, hereby certify that this thesis, which is approximately 65 000 words in length, has been written by me, that it is the record of work carried out by me and that it has not been submitted in any previous application for a higher degree.

Date: 13/3/06 Signature of candidate:

I was admitted as a research student in October 2002 and as a candidate for the degree of Doctor of Philosophy in March 2006; the higher study for which this is a record was carried out at the University of St Andrews between 2002 and 2006.

Date: 13/3/06 Signature of candidate:

I hereby certify that the candidate has fulfilled the conditions of the Resolution and Regulations appropriate for the degree of Doctor of Philosophy in the University of St Andrews and that the candidate is qualified to submit this thesis in application for that degree.

Date: 13/3/06 Signature of supervisor:

(Dr. N. J. Westwood)

COPYRIGHT DECLARATION

In submitting this thesis to the University of St Andrews I understand that I am giving permission for it to be made available for use in accordance with the regulations of the University Library for the time being in force, subject to any copyright vested in the work not being affected thereby. I also understand that the title and abstract will be published, and that a copy of the work may be made and supplied to any bona fide library or research worker.

Date: 13/3/06 Signature of candidate:

ABSTRACT

PART I

Small molecule covalent protein modifiers are of importance in therapeutics, biological research, and chemical proteomics. In the majority of cases, the chemical mechanism of covalent protein modification is obvious. However, this is not always true.

Chapter 1 introduces the small molecule 2,3-bis(bromomethyl)quinoxaline 1,4-dioxide (**1**), an inhibitor of the Apicomplexan parasite *Toxoplasma gondii* invasion into host cells. This small molecule was initially viewed as a general alkylating agent but was subsequently shown to exhibit selectivity in a range of secondary biological assays linked to the invasion process.

Chapter 2 discusses the mechanism of the reaction of **1** (and structurally related quinoxaline derivatives) with primary and secondary amines. The first experimental evidence in support of a reaction pathway that involves two equivalents of the amine is provided. This work has been reported in the Journal of Organic Chemistry, **2005**, *70*, 5055-5061. The identified mechanism is proposed to provide a plausible hypothesis for the biological selectivity observed.

Chapter 3 investigates the effects of incorporating a substituent into 2,3-bis(bromomethyl)quinoxaline derivatives on the mechanism of reaction with amines. Key steps in the mechanism, namely the initial S_N2 displacement reaction and a tautomerisation step were affected by a substituent incorporated at the C-6/7 position of **1**. The findings discussed are supported by NMR analysis, X-ray crystallographic data and computational studies.

Chapter 4 describes the first phase of studies in designing an affinity reagent based on **1** to probe its biological mode of action. The successful synthesis of a biotinylated derivative of **1** is disclosed. Preliminary biological results using the biotin-containing chemical probe are presented. Interestingly, for several proteins non-sulfur protein-based nucleophiles are implicated in the reaction with **1**.

PART II

Chapter 1: Part II of this thesis reports synthetic applications of a butenyl protecting group and demonstrates its applicability to phenol and aniline functional groups. The relevance of the butenyl protecting group is demonstrated further in the synthesis of a phenol-containing derivative of (*S*)-(–)-blebbistatin, a known myosin inhibitor. The concepts behind the protecting group have been integrated into a novel traceless linker that has subsequently been shown to be applicable to solid phase synthesis.

ACKNOWLEDGEMENTS

First and foremost I would like to thank Dr. Nick Westwood for the opportunity to work in his lab in St Andrews and for all his encouragement, guidance and support throughout my PhD. I also thank him for helping me develop my scientific thinking and for removing the incessant split infinitives I initially wrote into this thesis!

Thank you so much to all the guys in the group, past and present, for their daily support and advice but mostly their friendship, and for making the lab not too bad a place to be Monday to Friday. In particular to the postdocs who helped me out over the three years with their advice: Russell, Stephen, and Jon, and to the guys who were there throughout, Cristina, Fede, Helmet, Nick, Neil, Nico, Richard, Rach, and Su.

Thanks to all the staff at St Andrews whom I've worked alongside; Doug (for the molecular modelling and his helpful discussions), Melanja and Tomas (for their NMR expertise), Caroline, Catherine, and Alex (mass spectrometry), Sylvia (elemental analysis), Bobby (workshop), and Colin (glassblowing). Thank you to Gary and Jeralyn at the University of Vermont for their collaboration and answering all of my biology related questions (there were lots!).

A big thank you goes to all the friends I've made in St Andrews along the way; there are just too many to name, but especially to Rosie, Sophia, Sumi, Phill, Arjun, Mairead, Kate, and Dave. An additional thanks to both Sumi and Lindsay for their fantastic hospitality whilst writing my thesis and Fergus for sharing his room! They will all help me remember St Andrews with a smile and much more besides.

I wish to say a big thank you to Gareth for his friendship, strength and for being with me every step of the way. I also wish to thank his family for their kindness, support and of course the great dinners; Ali, Fergus, Pat and Dave – thanks.

Last of all, the biggest thanks go to my family; my sister, Jo for being a great friend (and the cakes!) and my nephew Jack (little monkey!) for being such good fun, my parents Angela and Keith for their endless love and support for the last 26 years (and still going!) and my grandparents, Midge, Gudd, Jack and Joyce for building the family I am proud to be a part of. I love you all very much, thank you.

In loving memory of Nan

STANDARD ABBREVIATIONS AND ACRONYMS

α	observed optical rotation in degrees
[α]	specific rotation
Å	angstrom
AcOH	acetic acid
Boc	*tert*-butoxycarbonyl
br	broad (spectral)
n-Bu	normal (primary) butyl
c	concentration, optical rotations g/100 mL
c.	*circa*, latin, around
°C	degrees Celsius
calcd	calculated
$CDCl_3$	deuterated chloroform
CD_3OD	deuterated methanol
cf.	confer imper, latin, compared to
CI	chemical ionisation
cm^{-1}	wavenumber(s)
COSY	proton-proton correlation spectroscopy
*m*CPBA	*meta*-chloroperoxybenzoic acid
δ	chemical shift in parts per million downfield from tetramethylsilane
d	day(s); doublet (spectral)
DCM	dichloromethane
DEAD	diethyl azodicarboxylate
DMF	*N*,*N*-dimethylformamide
DMSO	dimethylsulfoxide
DMSO-d_6	deuterated dimethylsulfoxide
DOS	Diversity-Oriented Synthesis
ECL	enhanced chemiluminescence
ee	enantiomeric excess
EI	electron impact
equiv.	equivalents
Et	ethyl
et al.	*et alia*, latin, and others

Et_2O	diethyl ether
ES^+	electrospray ionisation, operating in positive mode
ES^-	electrospray ionisation, operating in negative mode
g	gram(s)
h	hour(s)
HMBC	Heteronuclear Multiple Bond Correlation
HPLC	high-performance liquid chromatography
HRMS	high-resolution mass spectrometry
HRP	horseradish peroxidase
HSQC	Heteronuclear Single Quantum Coherence
Hz	hertz
IR	infrared
J	coupling constant (in NMR spectroscopy)
kDa	kilodaltons (mass)
L	litre(s)
LAC	lowest active concentration (defined as I(M), medium level of inhibition)
LCMS	liquid chromatography mass spectrometry
LiHMDS	lithium bis(trimethylsilyl)-amide, lithium hexamethyldisilazane
lit.	literature
µ	micro
m	multiplet (spectral); metre(s); milli
M	molar (moles per litre); mega
M^+	parent molecular ion
MALDI	matrix-assisted laser desorption ionisation
Me	methyl
MeOH	methanol
MHz	megahertz
ML	microlitre(s)
ML	millilitre (s)
min	minute(s); minimum
µM	micromolar (micromoles per litre)
mM	millimolar (millimoles per litre)
mol	mole(s)
mmol	millimole(s)

mp	melting point
MS	mass spectrometry
m/z	mass-to-charge ratio
NEt_3	triethylamine
nm	nanometre(s)
NMMII	non-muscle myosin II
NMR	nuclear magnetic resonance
Nu	nucleophile
Pd/C	palladium on carbon
PEG	polyethylene glycol
Ph	phenyl
ppm	part(s) per million
i-Pr	isopropyl
Py	pyridine
q	quartet (spectral)
RT	room temperature
s	singlet (spectral); second(s)
SDS-PAGE	sodium dodecyl sulfate polyacrylamide gel electrophoresis
S_N1	unimolecular nucleophilic substitution
S_N2	bimolecular nucleophilic substitution
SM	starting material
t	triplet (spectral)
T. gondii	*Toxoplasma gondii*
TBAF	tetra-*n*-butylammonium fluoride
TFA	trifluoroacetic acid
THF	tetrahydrofuran
TIPS	triisopropylsilyl
TLC	thin-layer chromatography
TMS	trimethylsilyl; trimethylsilane
t_R	retention time (in chromatography)
TS	transition state
UV	ultraviolet
ν	wavenumber, cm^{-1}
v/v	volume per unit volume (volume-to-volume ratio)

w/w	weight per unit weight (weight-to-weight ratio)
YFP	yellow fluorescent protein

CONTENTS

PART I

PART II

PART I

CHAPTER 1

SYNTHETIC STUDIES BASED ON COVALENT PROTEIN MODIFIERS

1.0 SMALL MOLECULES AS TOOLS TO STUDY COMPLEX BIOLOGICAL PROCESSES

After the sequencing of the human genome[1] there lies ahead the exciting but daunting task of assigning structure and function to the proteins that are encoded within it. One important approach towards defining how a protein functions within a cell or organism involves the use of small molecules. Small molecules are typically organic, non-peptide compounds with a molecular weight of < 1500 Da, derived from synthetic routes or natural products.[2] Small molecules that modulate the activity of specific proteins are powerful tools for studying protein function.[3] They therefore have great potential to aid scientists in their efforts to understand key biological processes. When these processes are central to health and disease, the small molecule can help to identify potential targets for new therapies.

There are an increasing number of examples in the literature of the use of non-covalently binding small molecules to perturb systematically a biological system.[4-7] Two recent examples are those of monastrol (**1**)[8] and blebbistatin (**2**)[9] (Figure 1.1). Mayer and co-workers observed that monastrol (**1**) arrested mammalian cells in mitosis (the process of nuclear cell division in eukaryotic cells) and induced a mono-astral array at the spindles surrounded by a ring of chromosomes (Figure 1.1, A).[8] The cellular target for monastrol (**1**) was established as the mitotic motor protein, Eg5, a bipolar kinesin required to establish and maintain spindle bipolarity. All previously known small molecules that specifically affect the mitotic machinery targeted tubulin (e.g. Taxol® (**3**) and vinca alkaloids such as vinblastine (**4**)). Therefore, monastrol (**1**) provides an alternative perspective from which mitosis can be viewed and will be a useful tool for studying mitotic mechanisms. **1** has indeed being used in further research studies and already boasts 301 citations of the original paper (as of the 10th March 2006) reflecting the appetite for new chemical tools.

Blebbistatin (**2**) is a recently discovered small molecule tool for studying myosin function.[9] So named because of its ability to inhibit cell *blebb*ing, blebbistatin **(2)** has been shown to be a selective inhibitor of non-muscle myosin II (NMMII), a motor protein essential for cells to divide and move. NMMII is implicated in the process of cytokinesis (Figure 1.1, B). During cell division blebbistatin (**2**) was observed to inhibit reversibly contraction of the cleavage furrow and block the final cleavage motion after the cells had duplicated and separated their chromosomes. No disruption of contractile ring assembly was observed.[9]

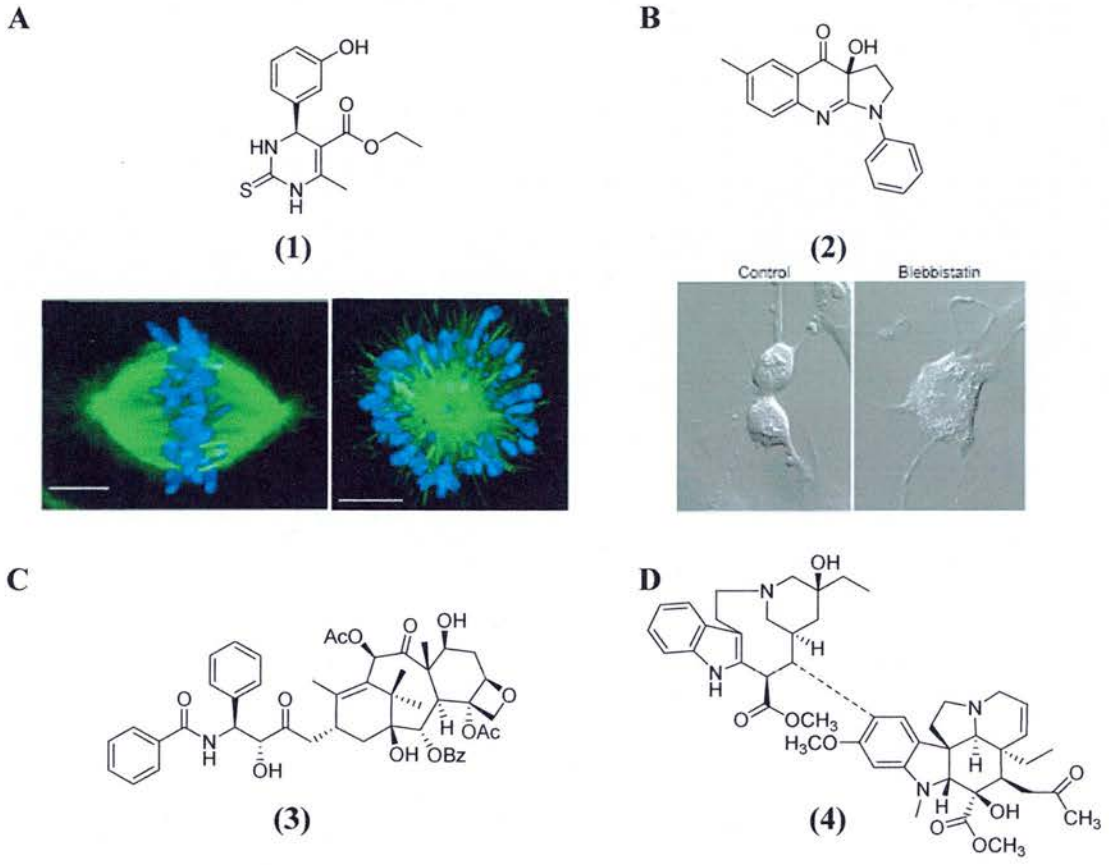

Figure 1.1. A. Monastrol (**1**) treatment of mitotic cells halt spindle assembly at an early stage of cell division. The normal bipolar spindle is replaced with a monoastral microtubule array (green) surrounded by a ring of chromosomes (blue). Image reproduced from T. Mayer *et al. Science* **1999**, *286*, 971-974.[8] **B.** Addition of (±)-blebbistatin (**2**) (right) to cytokinetic *Xenopus* tissue culture cells inhibits contraction of the cleavage furrow and prevents normal division of the cell into two daughter cells ((left), control, without (±)-blebbistatin (**2**)). Image reproduced from A. Straight *et al. Science* **2003**, *299*, 1743-1747.[9] **C.** The structure of Taxol ® (**3**). **D.** The structure of vinblastine (**4**).

1.1 THE DISCOVERY OF MONASTROL (1) AND BLEBBISTATIN (2) USING CHEMICAL GENETICS

The use of small molecules to probe biological systems is now often described as 'chemical genetics' or 'chemical genomics' because of its conceptual similarity to classical genetics (Table 1.1).[10] Monastrol (**1**) and blebbistatin (**2**) are both fruits of chemical genetic approaches. The identification of blebbistatin (**2**) is the product of a successful reverse chemical genetic (RCG) study. RCG involves screening libraries of small molecules against a purified protein of interest. Small molecules that alter the function of the chosen protein can then be used to elucidate its role within a biological system, by analysing the small molecule's effects in cells. Blebbistatin (**2**) was discovered by using a non-muscle myosin II (NMMII) assay to screen a library of over 16 000 small molecules.[9] In contrast, monastrol (**1**) was discovered through a forward chemical genetic (FCG) approach. FCG involves screening libraries of small molecules for their ability to induce a *phenotype* of interest in cells and then searching the proteome to identify the protein target(s) of the active 'hits'.[11] Once a hit compound has been identified the question then becomes: How did the small molecule elicit the response?

Table 1.1. Parallels between classical and chemical genetic approaches.

Forward Genetics (from phenotype to gene/protein)		**Reverse Genetics (from gene/protein to phenotype)**	
Classical Genetic Approach	*Chemical Genetic Approach*	*Classical Genetic Approach*	*Chemical Genetic Approach*
Random mutagenesis (e.g. irradiating cells)	Screen by adding library of small molecules to cells	Mutate single gene to target a protein of interest in cells (e.g. gene knockout)	Screen by adding library of small molecules to a purified protein of interest
Screen and select mutants with a phenotype of interest	Select small molecules that produce the phenotype of interest	Generate cells or animals with mutant gene	Add the molecules that bind to the protein of interest to cells or animals
Identify mutated gene	Identify the protein(s) target whose function is modified by the small molecule	Look for key phenotypes/ consequence(s)	Look for key phenotypes/ consequence(s)

Table adapted from B. R. Stockwell *Nature Reviews Genetics* **2000**, *1*, 116-125.[12]

Whilst classical genetics is and will continue to be incredibly powerful, chemical genetics has several advantages. This approach can be used to investigate protein function in systems not amenable to traditional genetic manipulation, e.g. disruption of an essential gene typically results in a lethal phenotype. Small molecules usually bind non-covalently to proteins and their effects can therefore, usually be reversed by simply "washing out" the compound. A small molecule can take affect within seconds of addition and this kinetic advantage allows the study of dynamic processes.[13] Small molecules can be added or removed at any time with excellent temporal resolution and are tuneable (allow a gradient of phenotypes). Furthermore, small molecules are easily applicable to cross-species studies and their use provides a closer link to drug discovery than classical genetic studies.[2]

In summary, the stated goal of chemical genetics is to provide, for each protein encoded by the genome, a small molecule tool to decipher the cellular function of the protein.[14,15] The RCG approach enables the identification of new lead small molecules or core structures with which to develop and study biological processes associated with known proteins. FCG has the potential to implicate new proteins in a given biological system. Both approaches are potentially relevant to drug discovery. However, one of the most significant challenges in the FCG approach is the identification of the cellular target of bioactive small molecules and therefore, the development of new target identification methods is an essential area of research.[16-18]

1.2 DIFFERENT (CHEMISTRY BASED) TARGET ID STRATEGIES

Several methods for cellular target identification of a small molecule are available and fall into one of two disciplines, either biology or chemistry-based. Examples of biological techniques include the generation of mutants, transcriptional profiling, protein microarrays, and phage display.[6,19] However, in the context of this thesis the emphasis is upon those methods which require the input of synthetic organic chemistry and these are discussed in turn in the sections that follow.

1.2.1 Affinity Chromatography

Small molecule-based affinity chromatography involves immobilisation of the bioactive small molecule of interest by "tethering" it to a matrix or solid support (pull-down approach) (Figure 1.2, A). The resulting affinity matrix is then used to capture the binding partners of the bioactive small molecule by incubation with crude or prefractionated cell lysates.[20] Binding of the proteins relies on the specific *reversible* interaction between a protein (or group of proteins) and the ligand while non-specifically or unbound proteins wash through the column (Figure 1.2, B). Elution of the captured protein(s) is achieved by reversing the interaction with the ligand either by competition with free ligand or by changing the pH, ionic strength or the polarity of the elution buffer (Figure 1.2, C to D). Mass spectroscopic analysis of the eluted proteins, following analysis by 1- or 2D gel electrophoresis, facilitates target identification.

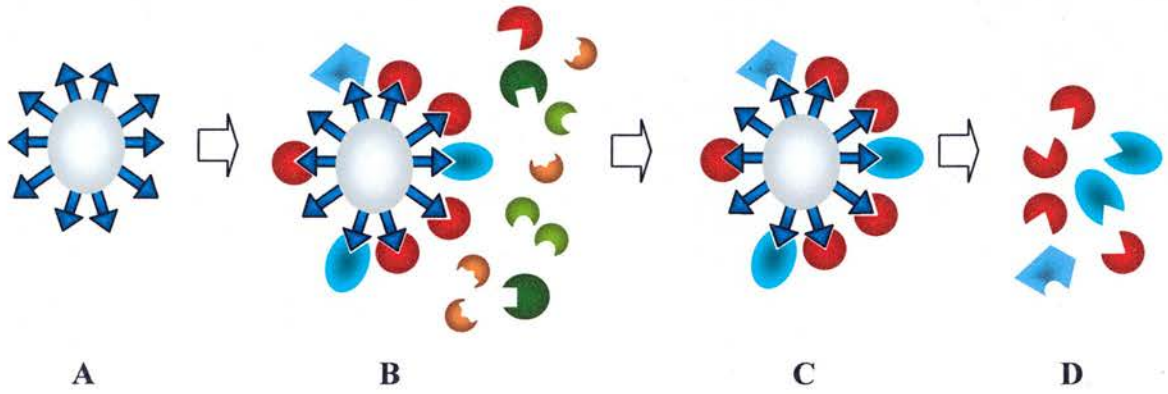

Figure 1.2. Schematic representation of the key stages involved in affinity chromatography. **A.** Immobilisation of the small molecule (depicted as a blue triangle) via a linker/spacer unit (blue rectangle) to the affinity resin beads (grey sphere). **B.** Cellular extract is applied under conditions that favour specific binding of the target protein(s) to the complementary small molecule (blue triangle). Non-specific binding often occurs (blue rhomboid), particularly from high abundance components of the extract. **C.** The bound protein(s) is recovered by elution. **D.** Captured proteins are identified by N-terminal microsequencing or MS fingerprinting.

Affinity chromatography has been used to successfully identify protein binding partners for numerous small molecules including Rapamycin (**5**),[21] FK506 (**6**),[22] Trapoxin (**7**),[23] and Purvalanol (**8**),[24] demonstrating its effectiveness as a target identification method. However, this approach still has its disadvantages and is often plagued by high levels of non-specific binding of proteins to the affinity matrix or the inability to identify an attachment site for a linker that retains biological activity.[25] In addition, it is often

difficult to determine whether immobilisation of the small molecule to an affinity matrix interferes with its binding ability.

1.2.2 Tagging

A small molecule 'hit' can be synthetically modified to form an affinity reagent or chemical probe. A chemical probe is comprised of the bioactive small molecule (typically bearing a reactive functional group) that is linked through a spacing unit to a label or tag (Figure 1.3).[26] The purpose of the chemical tag is for identification of proteins modified by the probe and for subsequent use as part of the purification technique.

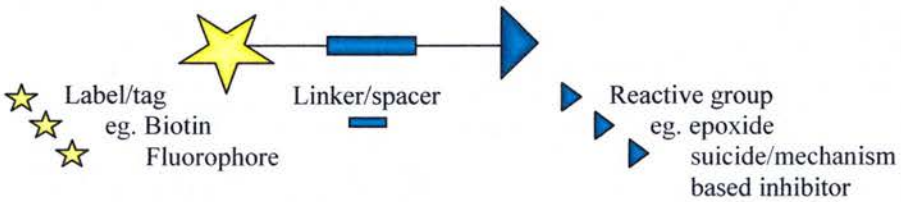

Figure 1.3. The structure of a chemical probe, comprising of three basic groups i) a label or tag which serves as a reporter molecule for visualisation and/or purification of probe-modified proteins, ii) a linker unit that acts as a spacer to prevent steric hinderence from the tag, and iii) the bioactive small molecule, typically containing a reactive functional group.

The most commonly used chemical tags include biotin (Figure 1.4, A), fluorophores (e.g. Figure 1.4, B), and radiolabels (e.g. Figure 1.4, C). Radiolabels that are incorporated into a bioactive small molecule and used in biological studies are ^{14}C, ^{32}P, ^{35}S, ^{3}H, and $^{125/131}I$, with ^{125}I being the radioactive atom of choice for reasons including availability, cost and sensitivity.[27] Commonly employed fluorescent tags include Alexa Fluors (Molecular Probes), fluorescein analogues and BODIPY derivatives (Molecular Probes) (for further discussion see Chapter 4, Section 3.3). Fluorescent tags and radiolabelling techniques have notable benefits over biotin, one of these being that they can be directly visualised by scanning an SDS-gel hence reducing experimental time. Successful target identification studies using fluors and radiolabels[28,29] are reported in the literature.

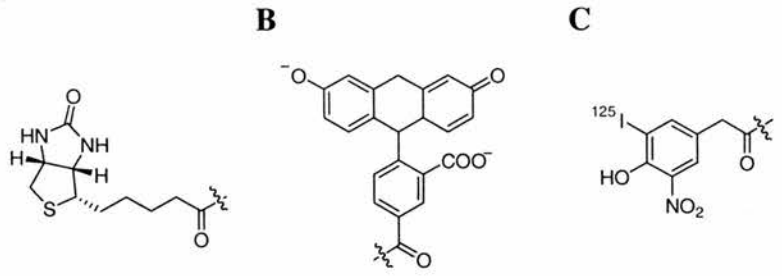

Figure 1.4. Examples of typical reporter tags that can be used to label small molecules for target identification purposes, including biotin (**A**), fluorescein (**B**), and insertion of radioactive iodine, 1-(4-hydroxy-3-iodo-5-nitrophenyl)propan-2-one derivative shown (**C**).[26]

Incorporation of a biotin group for detection and purification of labelled proteins takes advantage of the high affinity biotin-streptavidin system (association constant, 10^{15} M^{-1}).[30] Biotin facilitates detection by simple western blot approaches using a reporter attached to avidin (e.g. fluorescently labelled or using a chemiluminescent readout generated by an avidin conjugated peroxidase) in place of the standard secondary antibody.[26] Despite the advantages of alternative tagging methods, the use of biotinylated reagents remains the most common. This is partly because purification can be achieved through gel-based methods or through the use of immobilised streptavidin beads. Quantitative analysis indicates that the detection limit of the biotinylated protein is less than 10^{-14} mol, which is of the same order of magnitude as radioisotopic methods.[31] For this reason the use of biotin plays a key role in work described in this thesis and will be highlighted in more detail at various stages.

A good example of the use of a biotinylated chemical probe is reported for myoseverin (**9**, Figure 1.5). Myoseverin (**9**) was discovered following a FCG phenotypic screen by Schultz and co-workers, who observed that **9** caused morphological changes in myotubes (involved in skeletal muscle cell differentiation, Figure 1.5).[32] Synthesis of a myoseverin (**9**) derivative containing a linker arm facilitated attachment of a biotin group to give the affinity probe **10**. **10** was incubated with muscle cells and biotinylated proteins were isolated from the lysate using streptavidin coated magnetic beads. Tubulin was identified as a binding partner for **10** following immunoblotting with a tubulin specific antibody. This emphasised an important role for microtubules (usually associated with the process of cell division) in non-dividing cells.

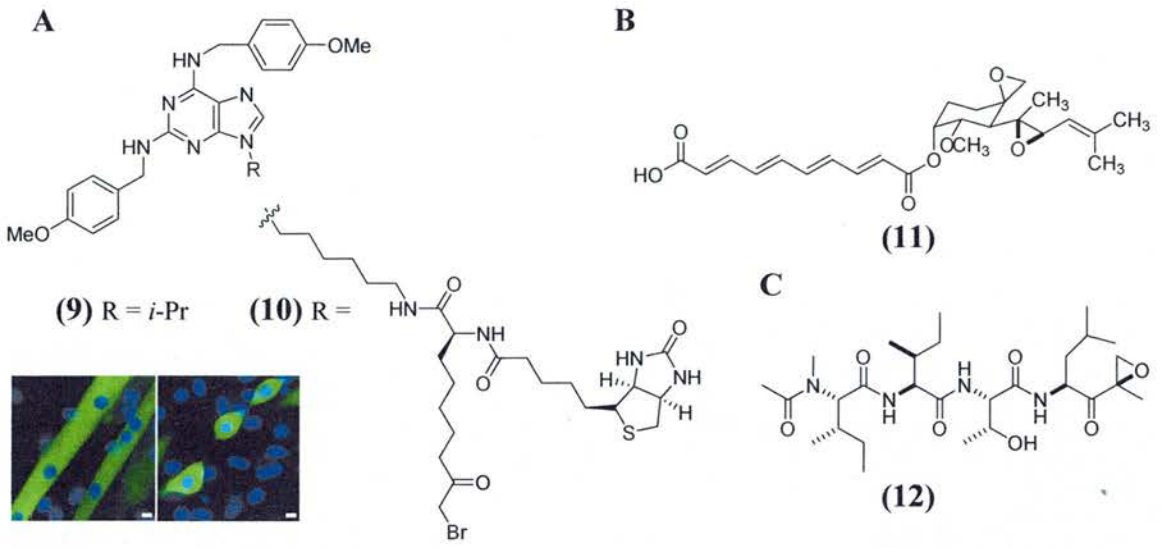

Figure 1.5. A. Biotinylated myoseverin affinity probe (**10**). Insert: Myoseverin treated muscle cells resulted in a change in cell morphology visible by phase contrast microscopy. Long, cylindrical myotubes of untreated cells (left) were replaced by chains of smaller rounded cells (right). Image reproduced from P. G. Schultz *et al. Nature Biotechnol.* **2000**, *18*, 304-308. **B.** The structure of fumagillin (**11**). **C.** The structure of epoxomicin (**12**).

The use of biotin was the key component in the identification of the protein targets for the small molecules fumagillin (**11**)[33] and epoxomicin (**12**)[34]. Both studies were carried out by Crews and co-workers and are similar but not identical in their approach to that of Schultz. Crews took advantage of the ability of **11** and **12** to bind irreversibly to their target proteins. Fumigillin (**11**) was known to be a highly effective potent inhibitor of angiogenesis (new blood vessel formation). In order to investigate the molecular mode of action underlying its activity, Crews *et al.* synthesised a fumagillin (**11**) analogue possessing a tethered biotin group. Using this chemical probe, fumagillin (**11**) was identified as a covalent modifier of methionine aminopeptidase (MetAP-2). A similar approach employing biotin labelled epoxomicin (**12**) concluded that **12** specifically covalently labelled a subunit of the 20S proteasome and subsequent functional assays indicated that **12** was a potent proteasome inhibitor.

1.2.3 Photoaffinity Labelling

Photoaffinity labelling involves the integration of semi-controlled covalent modification of the protein target with labelling technologies. This approach requires the modification of the bioactive small molecule to contain a photoreactive group (e.g. aryl azide or diazirine) and a tag (e.g. biotin, radiolabel see Section 1.2.2). Initial incubation of the photoaffinity reagent with a crude protein extract is carried out to establish binding of

any protein(s) that recognise the ligand. Subsequent irradiation of the mixture at a defined wavelength causes photoactivation of the small molecule and results in covalent modification of the binding protein(s) linking them to the small molecule. This approach requires that after a covalently labelled protein is identified, competitors are co-incubated with the photoaffinity reagent and the experiment repeated to determine selectivity. Selectively labelled proteins can then be identified and analysed by mass spectrometric techniques. In this way, photoaffinity labelling not only identifies small molecule binding partners but provides structural information about the binding site through locating the site of covalent modification. This approach has therefore proved to be a popular and successful technique,[35,36] in particular when used in conjugation with a biotin tag (Figure 1.6).[31]

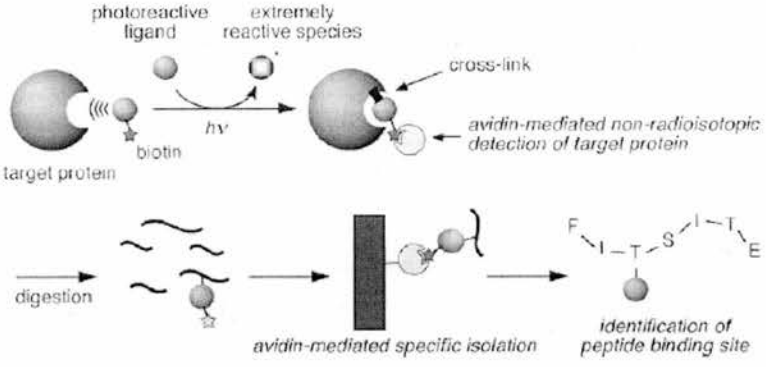

Figure 1.6. Outline of photoaffinity mediated biotinylation of proteins. A small molecule containing a photoreactive group and a biotin tag is incubated with a cell lysate. Irradiation induces covalent bond formation between the small molecule and its established target protein(s). The biotin tag facilitates purification of modified proteins for identification. Image reproduced from T. Tomohiro *et al. Chem. Rec.* **2005**, *5*, 385-395.

Konoki *et al.* have employed the biotinylated affinity reagent (**13**) in a quest to identify okadaic acid-binding protein(s) in a marine sponge *Halichondria okadai* (Figure 1.7).[37] Photoaffinity labelling followed by SDS-PAGE analysis indicated labelling of protein phosphatase 2A (PP2A), a known binding protein for okadaic acid. In addition, using crude extracts of the sponge three further proteins were labelled by **13** and are proposed to be involved in self-resistance mechanisms of the sponge against okadaic acid. Unfortunately, however in this instance no mass spectrometric analysis of these proteins is reported. The diazirine based biotinylated photocrosslinking reagent has been extended to identify carbohydrate binding sites on proteins by conjugation to sugars.[38]

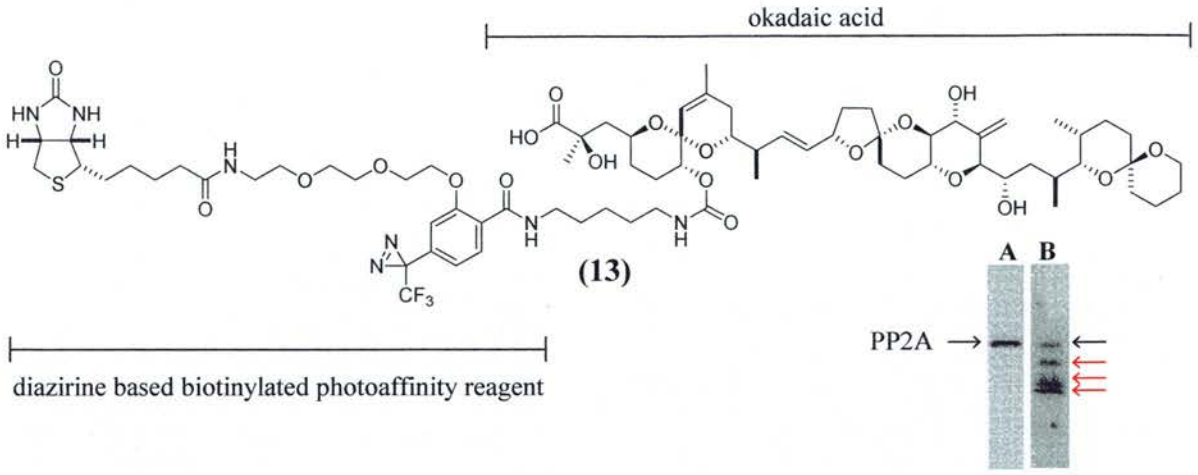

Figure 1.7. The biotinylated photoaffinity reagent used by Konoki *et al.* to identify binding proteins of okadaic acid in a marine sponge *Halichondria okadai*. Insert: A. Labelling of PP2A, a known binding protein of okadaic acid, by **13** was detected (black arrow). B. Three further proteins were labelled from *H. okadai* cell lysate (red arrows). Image reproduced from K. Konoki *et al. Tetrahedron* **2000**, *56*, 9003-9014.

1.2.4 Bioorthoganol Two-step Labelling

Two-step labelling strategies involve the incorporation of a functional group into a biomolecule (e.g. protein) that can later be conjugated to a reporter tag through a chemoselective ligation reaction (Figure 1.8).[39] Such chemical reactions are required to be orthogonal to the diverse functionality present in biological systems thereby permitting analysis of proteins modified by chemical probes in living cells. For this, the azide has secured a prominent role as a unique chemical handle for bioconjugation.[40]

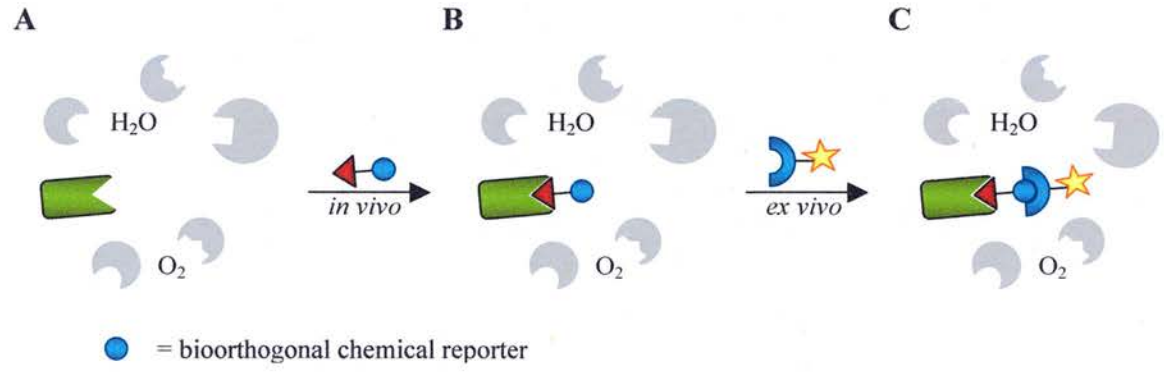

Figure 1.8. Schematic illustrating the bioorthogonal chemical reporter strategy. **A.** The small molecule (red triangle) is modified to incorporate a chemical reporter group (blue circle). **B.** The small molecule binds to its protein target (green rectangle) in cells. **C.** In the second step the reporter molecule covalently tags the small molecule-protein complex with an exogenously delivered probe. Adapted from J. A. Prescher and C. R. Bertozzi *Nat. Chem. Biol.* **2005**, *1*, 13-21.[41]

Bertozzi and co-workers have made extensive use of the azide functional group as a chemical reporter of glycosylation, employing the Staudinger ligation reaction with its phosphine coupling partner to tag azidosugars introduced into cellular glycoconjugates (Figure 1.9).[42,43] The Bertozzi group have also made the first steps toward *in vivo* activity based profiling of glycosides using an azide equipped mechanism-based glycoside inhibitor.[40]

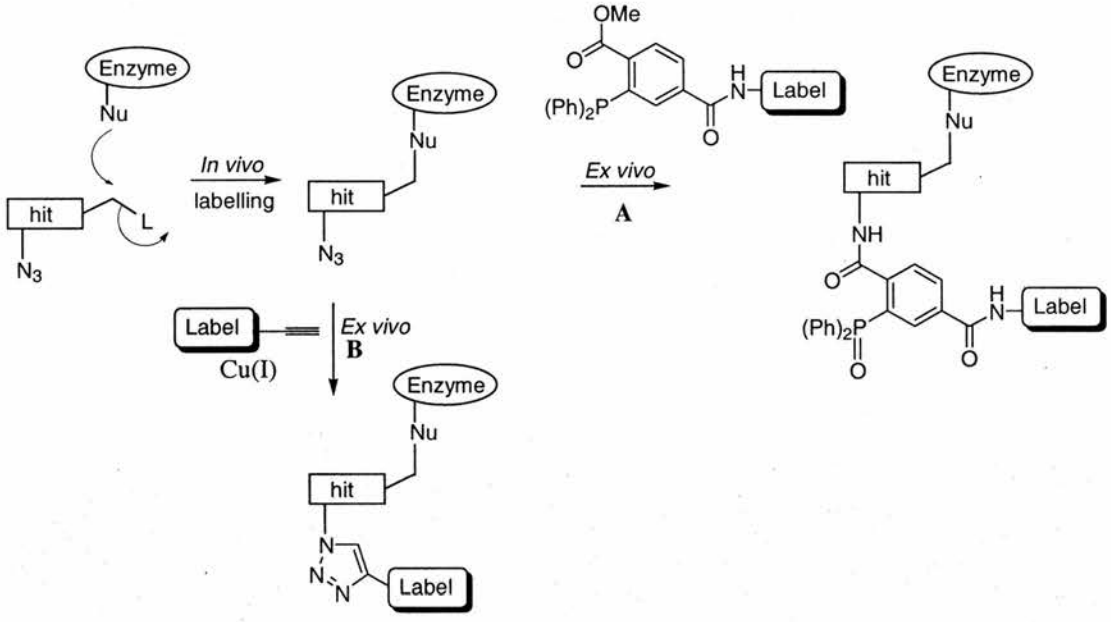

Figure 1.9. Principle behind two-step labelling using either: **A** Bertozzi-Staudinger ligation or **B** Huisgen-type cyclisation, so-called "click" chemistry.[45] The Bertozzi-Staudinger ligation is the reaction between an azide and a phosphine to form a phospha-aza-ylide which can be trapped by an acyl group to yield a stable amide bond. Sharpless' "click" chemistry utilises an azide and a terminal alkyne and proceeds in the presence of a copper catalyst to give a triazole product.

An alternative mode of bioorthogonal reactivity for the azide is in a [3 + 2] cycloaddition reaction with alkynes, first described by Huisgen.[44] This approach has been exploited by Sharpless and co-workers by their development of a copper(I)-catalysed version allowing the reaction to proceed at physiological temperatures.[45] Additionally, this method controls the regioselectivity of the reaction exclusively yielding the 1,4-disubstituted 1,2,3-triazole product.

1.2.5 Yeast 3-Hybrid

Another method developed for the detection of small molecule-protein interactions is the yeast three-hybrid system. This method exploits the tools that were previously

developed for investigating protein-protein interactions and only few studies have made use of this system for identifying protein binding partners of small molecules (for examples see references 46, 47 and 48. In short, this method requires modification of the small molecule to form a 'hybrid' compound to a second small molecule, such as methotrexate (**14**) (Figure 1.10). The 'hybrid' molecule is then used as a sophisticated chemical probe to label binding-partners in a cell lysate.

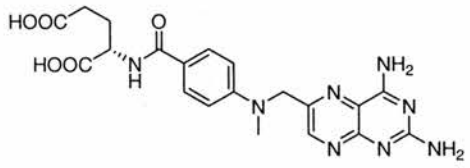

(14)

Figure 1.10. The structure of methotrexate (**14**).

As discussed above, the physical interaction (i.e. non-covalent versus covalent) between a small molecule and its protein target can be exploited several different ways to aid the process of target identification. Covalent modifiers are less amenable to some of the approaches discussed, for example affinity chromatography. From a target identification perspective covalent modifiers are more applicable to affinity labelling strategies, which exploit the irreversible binding to aid purification techniques.

2.0 COVALENT MODIFIERS

There are numerous examples of small molecules that covalently modify their respective protein targets, including natural products[49] and commercial drugs.[50,51] Specific small molecules that covalently modify their target protein(s) are of considerable medical importance. A recent review article lists 19 enzyme targets for which prescribed drugs elicit their chemotherapeutic effect through irreversible covalent protein modification.[51] These include the β–lactam antibiotics (e.g. amoxicillin (**15**)), aspirin (**16**), fosfomycin (**17**), and α-difluoromethylornithine (**18**).

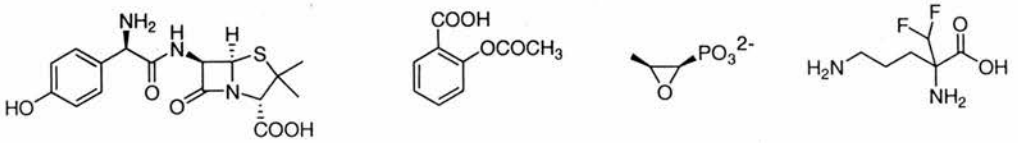

(15) Penicillin Binding Proteins (PBPs)

(16) COX-1

(17) UDP-*N*-acetylglucosamine 1-carboxyvinyltransferase.

(18) ornithine decarboxylase

Figure 1.11. Selected commercial drugs which elicit their chemotherapeutic effect by covalent modification of their respective target proteins. Amoxicillin (**15**), aspirin (**16**), fosfomycin (**17**), and DL- α-difluoromethylornithine (**18**).

Amoxicillin (**15**) is an example of a *β*–lactam antibiotic which targets the penicillin binding proteins (PBPs), i.e. bacterial transpeptidases and carboxypepidases. This class of small molecules typically function via a nucleophilic ring-opening of the *β*–lactam by attack on C-4 by an activated serine hydroxyl. The ring-opening of the *β*–lactam releases ~25 kcalmol^{-1} of strain energy[52] in forming a stabilised covalent acyl-enzyme complex to effectively inhibit these enzymes. Aspirin (**16**) has been shown to acetylate Ser-530 of its target cyclooxygenase-1 (COX-1) (and later, COX-2) enzyme and that this acetylation hinders the access of arachidonic acid to the active site.[53] The therapeutic efficacy of aspirin (**16**) in myocardial infarction has been clearly attributed to its inhibiton of platelet COX-1 activity.[53] Fosfomycin (**17**) is an antibacterial drug that alkylates an active site cysteine residue in its target enzyme, UDP-*N*-acetylglucosamine 1-carboxyvinyltransferase.[54] α-Difluoromethylornithine (**18**) is an antiprotozoal agent and acts as a substrate for its target enzyme, ornithine decarboxylase. PLP-dependent decarboxylation generates a reactive intermediate that can be attacked by either a lysine or a cysteine protein residue. **18** has been shown by X-ray crystallography to modify covalently Cys-360 in the ornithine decarboxylase enzyme of *Trypanosoma brucei*.[51]

Other examples include carbamazepine (**19**), diclofenac (**20**), and tamoxifen (**21**) (Figure 1.12). In these three cases, covalent binding to cellular proteins by reactive metabolites/intermediates is suggested to be responsible for the associated side-effects of these drugs.[50]

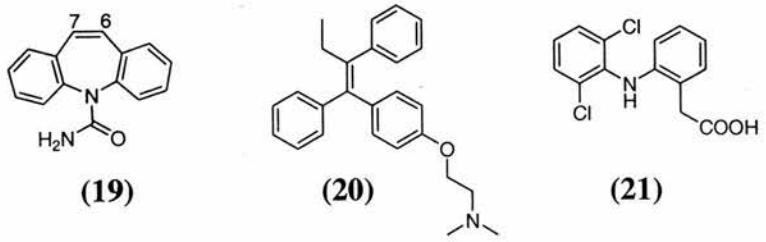

(19) **(20)** **(21)**

Figure 1.12. Selected commercial drugs which elicit undesirable side-effects through covalent modification of cellular proteins and/or DNA. Carbamazepine (**19**), tamoxifen (**20**), and diclofenac (**21**).

In vitro and *in vivo* biochemical studies using chromatographic (HPLC and LC-MS) and immunological (e.g. ELISA) techniques have provided credence to this hypothesis.[50] Carbamazepine (**19**) can undergo metabolic oxidation of the C-6–C-7 bond by P-450 enzymes to give the corresponding epoxide derivative. This metabolite may be responsible for the anticonvulsant activity of **19**.[55] Tamoxifen (**20**) can also be oxidatively metabolised forming catechol products that can covalently bind proteins and DNA. Diclofenac (**21**) is metabolised to acyl glucuronides for which two mechanisms have been suggested for covalent binding; transacylation and/or Schiff's base formation (glycation).[50]

Biologically active natural products are also evident that are endowed with electrophilic functional groups that covalently modify nucleophilic residues in specific protein targets. Many of these mechanisms involve simple reactive motifs including the electrophilic carbon centres of epoxides (e.g. E64 (**22**), Figure 1.13 and fumigillin (**11**) Figure 1.5), α,β-unsaturated systems (e.g. Leptomycin B (**23**), Figure 1.14) and β-lactone ring systems (e.g. lipstatins). Selected examples are discussed in the following section.

E64 (**22**) is a covalent inhibitor of several cysteine proteases. The reaction mechanism of E64 (**22**) with papain was elucidated by ^{13}C NMR spectroscopy by Yabe *et al.*[56] In principle, reaction of **22** could lead to products derived from nucleophilic attack on the epoxide on either C-2 or C-3. An analogue of **22** was prepared, regiospecifically labelled at C-2. Incubation of ^{13}C-labelled **22** with activated papain in phosphate buffer at pH 6.8 produced a new resonance at 76.5 ppm in the ^{13}C NMR spectrum corresponding to a secondary alcohol at C-2. The alternate product, which would be formed from attack at C-2 and would therefore possess a secondary alcohol at C-3, would be expected to produce a signal near 50 ppm and was not observed. Inactivation of cysteine proteases has been shown to occur via a regioselective S_N2 mechanism at C-3 to give a thioether product and this mode of attack has been extensively characterised by X-ray crystallography.[49]

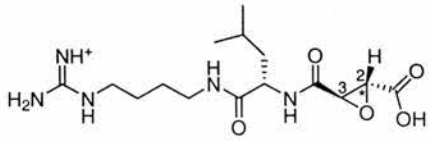

(22)

Figure 1.13. The structure of E64 (**22**). A known cysteine protease inhibitor containing a reactive *trans*-epoxysuccinic acid unit. Yabe *et al.* prepared a ^{13}C-labelled analogue of **22** at C-2 (*) to investigate the mechanism of covalent modification by the cysteine protease papain.[56]

The cellular target of Leptomycin B (**23**) was identified as CRM1, a non-enzymatic nuclear export signalling protein.[57] The mechanism of covalent modification of CRM1 is credited to the sulfhydryl group of Cys-529 reacting via a 1,4 conjugate addition to the α,β-unsaturated δ-lactone of **23**. Kudo and co-workers have elegantly shown by ^{1}H NMR (and correlated spectroscopic methods) that *N*-acetyl-L-cysteine methyl ester formed an adduct with **23** consistent with this mode of attack.[57] In addition, to validate whether **23** could specifically covalently modify CRM1 *in vivo*, i.e. in the presence of other cysteine-containing proteins, a biotinylated analogue (**24**) was synthesised (Figure 1.14). A 102 kDa protein was identified as a covalent binding partner for **24** and binding of this protein was successfully competed by **23**. The protein was identified as CRM1, demonstrating that **23** can selectively bind CRM1 in the cell.

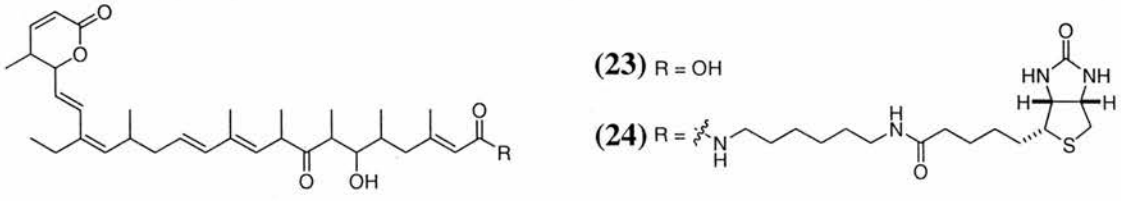

(23) R = OH

(24) R =

Figure 1.14. The structure of leptomycin B (**23**) and the biotinylated derivative (**24**) synthesised by Kudo *et al.*[57] **24** was used in cells to demonstrate selective covalent modification of the target protein CRM1.

Trapoxin (**7**) is an irreversible inhibitor of histone deacteylase activity.[58] Trapoxin (**7**) possesses two structural features that have led to a proposed mechanism of action involving covalent modification. First, trapoxin (**7**) contains an electrophilic epoxyketone that is essential for biological activity and second, the aliphatic side-chain is approximately isosteric with *N*-acetyl lysine thus trapoxin (**7**) is likely to act as a substrate mimic (Figure 1.15).[23]

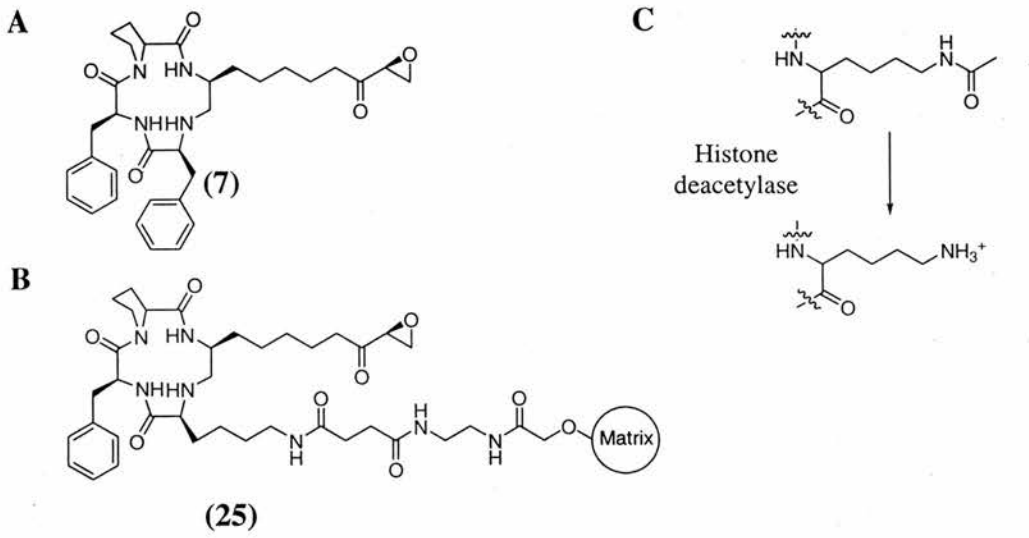

Figure 1.15. A. The structure of trapoxin (**7**). The epoxyketone side chain of **7** is approximately isosteric to lysine and likely alkylates an active site nucleophile. **B.** Immobilisation of **7** to form the affinity matrix, K-trap (**25**). Covalent linkage to the resin was achieved by replacement of one of the phenylalanine residues with a lysine. **C.** Deacetylation of lysine by histone deacetylase.

To purify and isolate histone deacetylase, Schreiber and co-workers synthesised an immobilised analogue of trapoxin (**7**), known as K-Trap (**25**). Affinity chromatography experiments using **25** led to the discovery of histone deacetylase-1 (HDAC-1) as a binding partner. HDAC-1 was found to be 60% identical to the yeast protein, RPD3, necessary for transcriptional repression. Importantly, this result provided a link between the role of histone deacetylases to the repression of gene transcription.[23] This work provides another illustration of the importance of synthetic organic chemistry in helping to solve biological problems.

Lysine has also been shown to be an important protein-based nucleophile for covalent modification. The ε–amino group of Lys-802 of phosphatidylinositol 3-kinase (PI 3-kinase) attacks C-20 of the natural product wortmannin (**26**).[49] An addition-elimination mechanism results in the formation of a vinylogous carbamate. This mode of attack covalently modifies and irreversibly inhibits the target protein.

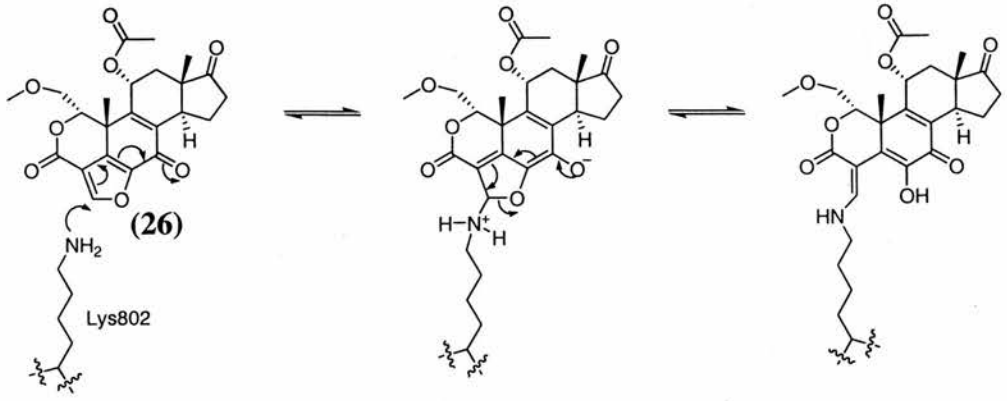

Figure 1.16. Nucleophilic attack by a lysine residue on the doubly activated furan ring of wortmannin **(26)** at C-20 results in covalent modification of PI 3-kinase. Image reproduced from C. Drahl *et al. Angew. Chem. Int. Ed.* **2005**, *44*, 5788-5809.

In summary, small molecules use a remarkably diverse set of mechanisms to covalently modify enzymes. The small molecules involved possess a range of structural features. Typically the mode of covalent attack involves a nucleophilic residue on the target protein and a sufficiently electrophilic centre on the small molecule.

2.1 APPLICATION OF COVALENT MODIFIERS IN CHEMICAL PROTEOMICS

Covalent modifiers of protein function are useful tools for studying biological processes, despite the fact that they cannot be washed out in cell-based assays. More recently, less specific small molecules that covalently modify sub-proteomes have been used in the emerging field of chemical proteomics.[59,60] This is known as activity-based protein profiling (ABPP). This method uses small molecule affinity based probes (ABP) to investigate protein families by functional based profiling. An ABP takes on a similar anatomy to that of a traditional affinity probe discussed in Section 1.2.2 (Figure 1.3). This consists of a reactive warhead group, a linker unit (in this case it could contain selective binding elements that can aid overall specificity e.g. a peptide unit), and a tag. This approach relies on the ability of a small molecule containing an electrophilic functional group to form an irreversible, covalent bond with a protein nucleophile.

Focus of work in this area was based around the preparation and use of ABPs for enzyme classes with known covalent inhibitors. To date, ABPs have been developed for over a dozen classes of enzymes including serine and cysteine proteases and hydrolases, oxidoreductases, kinases, tyrosine phosphatases and penicillin binding proteins.[60,61]

Applying an ABP to study the various stages of the life-cycle of the parasite *Plasmodium falciparum*, Greenbaum *et. al.* identified a specific cysteine protease, falcipain 1, relating to the invasion process.[62]

Until the development of two-step labelling strategies ABPP strategies had been conducted *in vitro* but adoption of these techniques is now driving *in vivo* studies. Cravatt and co-workers evaluated the application of click chemistry in ABPP.[63] Utilising an azide containing phenyl sulfonate ester group they were able to demonstrate *in vivo* profiling of glutathione *S*-transferases, aldehyde dehydrogenase and enoyl CoA hydratases. The use of the Staudinger ligation has also been reported for profiling enzyme activities in living cells.[64]

However, covalent inhibitors do not exist for the majority of proteins. Therefore, recent research efforts have been channelled into the discovery of active site-directed profiling reagents for proteins lacking cognate affinity labels.[65] The current need for the development of new chemical probes and probe classes that can be used to target diverse sets of protein families is widely regarded as a key issue within the field of chemical proteomics.[26]

In summary, the chemical genetic approach has the power to deliver small molecules that can be used as chemical tools to dissect a given biological pathway and answer fundamental questions. Small molecules that have the ability to covalently modify their protein target can provide important mechanistic answers through their use as chemical probes. The development of chemical probes that covalently modify their respective protein target(s) is also of great importance in the field of chemical proteomics. Bioorthogonal ABPP strategies are versatile techniques for functional analysis of the proteome.

3.0 THE SMALL MOLECULE APPROACH TO STUDYING HOST CELL INVASION

A forward chemical genetic approach has been applied in parasitology to identify inhibitors of host cell invasion by the parasite *T. gondii*.[11] This work was initiated by Dr.

Nick Westwood in the laboratory of Professor Gary E. Ward (University of Vermont) and at ICCB, Harvard Medical School in the laboratory of Professor T. J. Mitchison FRS.

3.1 *Toxoplasma gondii*

Toxoplasma gondii is an obligate, intracellular, protozoan parasite, belonging to the same phylum, Apicomplexa, as the malaria causing parasite *Plasmodium falciparum*. *T. gondii* is the causative agent of toxoplasmosis, a disease that now affects more than a quarter of the world's population. In most humans the disease is asymptomatic, however in immuno-compromised patients or the unborn foetus, the disease is serious and often fatal. Invasion into the host cell is key to the parasite's survival (Figure 1.17). The pathology of toxoplasmosis is a direct result of repeated cycles of host cell invasion, parasite replication, and host cell lysis.[11]

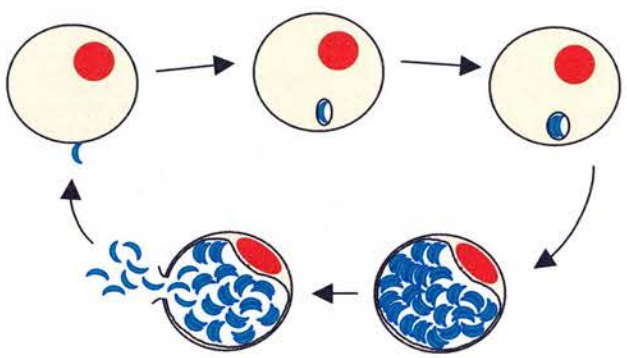

Figure 1.17. Cartoon overview of the lifecycle of *T. gondii*. The lifecycle consists of (i) host cell invasion, a rapid process taking only approximately 15 to 20 seconds, (ii) parasite replication and (iii) host cell lysis. *T. gondii* parasites require the confines of a host cell in order to replicate and survive.

As denoted by the name, members of the phylum Apicomplexa contain an elaborate 'apical complex', consisting of the secretory organelles (micronemes, rhoptries and dense granules), a group of unique cytoskeletal structures: the polar rings, which serve as a microtubule-organising centre and, in some species, a conoid.[66,67] In *T. gondii*, the conoid is a truncated cone, approximately 280 nm in length and 380 nm in diameter.[68] Electron microscopy (EM) studies have shown that the conoid consists of 10-12 ribbon-like fibres tightly wound into a counterclockwise spiral like a compressed spring.[68,69] In *T. gondii*, these conoid fibres are composed of tubulin organised into a novel polymeric form.[68,70]

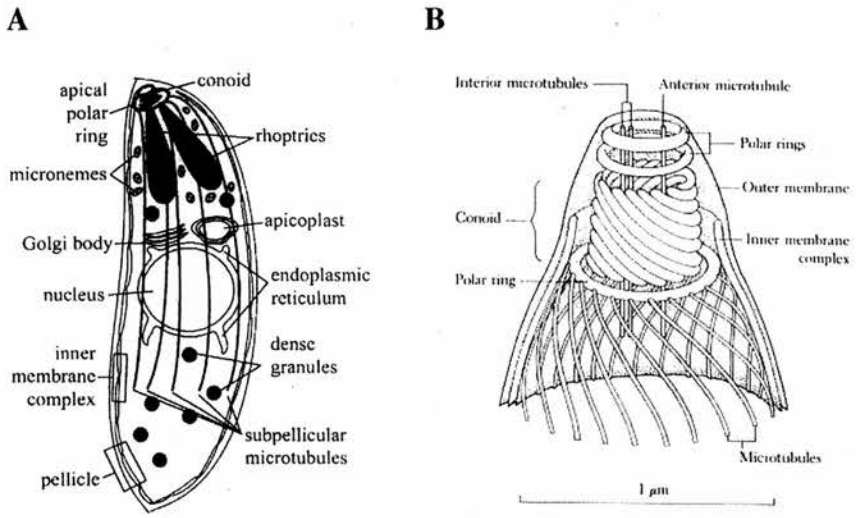

Figure 1.18. A. The morphology of an apicomplexan parasite. Image reproduced from N. S. Morrissette and L. D. Sibley *Microbiology and Molecular Biology Reviews* **2002**, *66*, 21-38. **B.** The 'apical complex' of *T. gondii.* Image reproduced from Cell Biology of *Toxoplasma gondii*, E. R. Pfefferkorn, in *Modern Parasite Biology*, David J. Wyler editor, W.H. Freeman and Company 1990. The conoid, present in some members of the phylum, defines the apical end of the parasite.[70] This small cone-shaped spiral of fibres, is thought to play a role in the invasion process and can be protruded from or retracted into the apical polar ring.[69]

3.2 KEY STEPS IN THE INVASION PROCESS

Invasion by the *T. gondii* tachyzoite is a complex process involving several apparently discrete events (Figure 1.19). The process is initiated following recognition of the host cell and the parasite becomes attached to the host cell surface. Conoid extension occurs, closely followed by sequential secretion from three distinct secretory organelles.[71] The final stages involve penetration of the host cell membrane and active internalisation, driven by complex machinery, known as the glideosome (contains a myosin motor).[72] The process culminates in encapsulation of the parasite inside the host cell within a parasitophorous vacuole (PV).

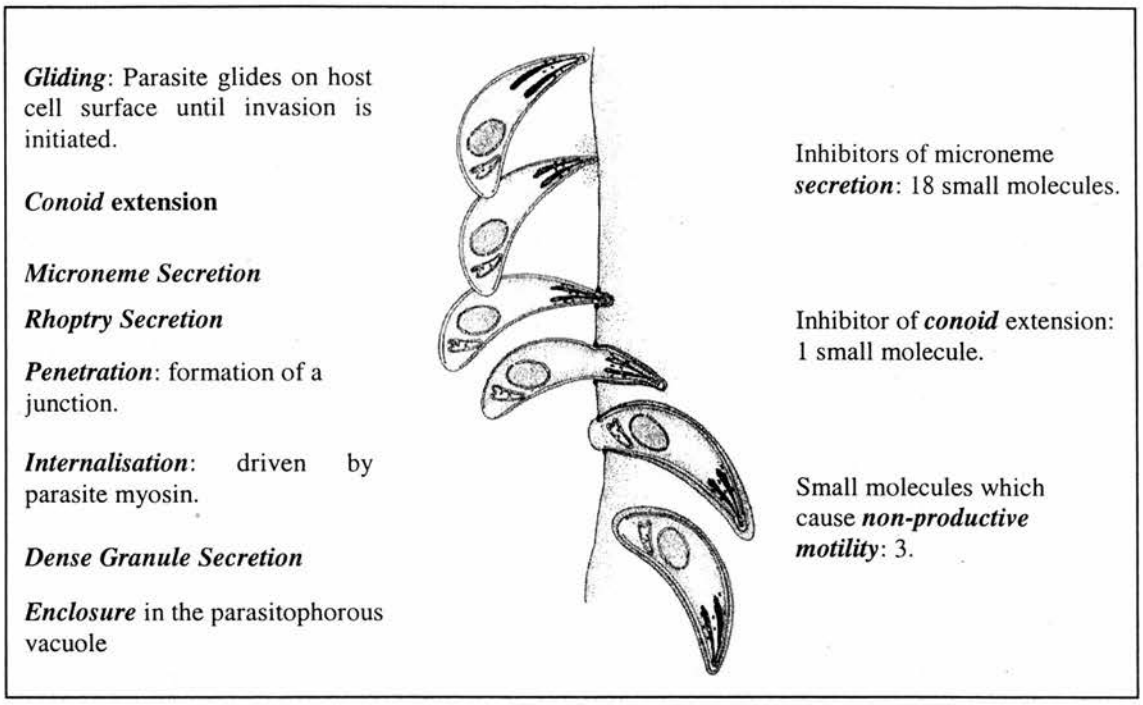

Figure 1.19. Overview of the invasion process. The parasite glides along the surface of the host cell. Conoid extension occurs followed by an increase in secretion of proteins from the micronemes and rhoptries. The parasite is driven into the developing parasitophorous vacuole (PV) by a myosin motor.[73] Proteins (and possibly lipids) secreted from the dense granules modify the functional properties of the PV. Small molecules were identified from the high throughput screen which inhibited different stages of invasion (see right-hand side of figure and reference 72). Image reproduced from Cell Biology of *Toxoplasma gondii*, E. R. Pfefferkorn, in *Modern Parasite Biology*, David J. Wyler editor, W.H. Freeman and Company 1990.

Host cell invasion is extremely well orchestrated by the parasite yet the mechanisms involved remain relatively poorly understood at the molecular level. This provided the driving force for the development of a phenotype based assay to identify small molecules that block the invasion process.[11] The goal was to use these small molecules to dissect in greater detail the pathways involved in invasion.

3.3 THE IDENTIFICATION OF SMALL MOLECULE INHIBITORS OF *Toxoplasma gondii* INVASION

A high-throughput screen was carried out by Carey *et al.*, which identified small molecules that inhibited the *Toxoplasma gondii* invasion process (Figure 1.20).[11] In brief, a commercially available library of 12 160 small molecules (from Chembridge) was screened. DMSO stock solutions of each small molecule were added to confluent monolayers of BSC-1 cells plated in 384-well format. Parasites expressing yellow fluorescent protein (YFP) were added and the plates incubated for 15 minutes at 23 °C

(parasites unable to invade at this temperature), then 60-90 minutes at 37 °C (optimum temperature for invasion to occur). After washing, any remaining extracellular parasites were labelled with a fluorescently labelled antibody to SAG1, a known surface antigen on the parasites. The parasites that had successfully invaded cells were then "counted" from images captured using fluorescence microscopy and using a sophisticated automated algorithm. Parasites that remained external to the host cells fluoresce at wavelengths that were pseudo-coloured both green and red (expressing both YFP and labelled by the fluorescent antibody respectively) following microscopy. Internalised parasites fluoresce at the wavelength that was pseudo-coloured green only (only expressing YFP) (Figure 1.20). Merging the two sets of images captured, at the two corresponding wavelengths, resulted in those parasites internal to host cells appearing green whereas external parasites appeared yellow (combination of green and red). A small molecule was classified as an inhibitor of invasion if it was observed to reduce the number of internal parasites to < 20% compared to a control (DMSO only treated).

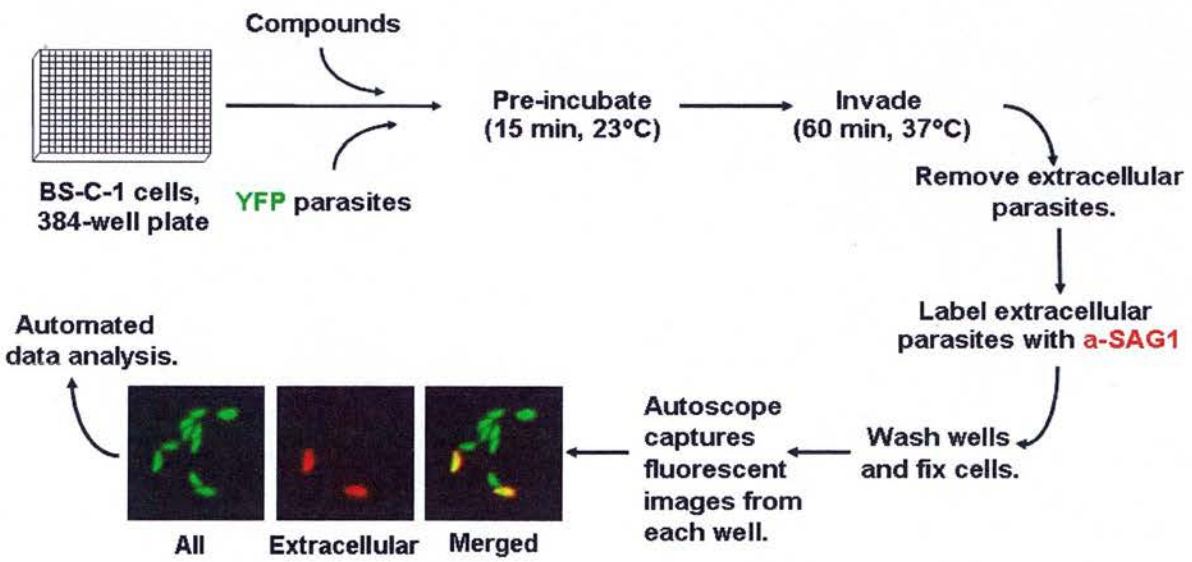

Figure 1.20. A forward chemical genetics approach to identify inhibitors of *Toxoplasma gondii* invasion.[11] 12 160 small molecules were screened in 384-well format and compared to DMSO (control). Intracellular and extracellular parasites were distinguished by fluorescence microscopy; extracellular parasites were pseudo-coloured red and green and therefore appeared yellow in merged images whereas intracellular parasites were green only. Small molecules that reduced the invasion levels to < 20% compared to control wells were considered inhibitors. Image reproduced from K. L. Carey *et al. Proc. Natl. Acad. Sci. USA* **2004**, *101*, 7434-7438.

Of the 12 160 small molecules tested, 24 were found to reproducibly inhibit *T. gondii* invasion into host cells and were noncytotoxic (on the timescale of the assay). Additionally, 6 small molecules were deemed enhancers of invasion (> 200% compared to

a control). To determine whether the observed effect of each of these 'hits' was reversible the small molecule was "washed out" after the initial 15 minute incubation period.[11] This resulted in the classification of five small molecules as irreversible inhibitors. For these five, target cell identification was assessed by independently pretreating host cells and parasites with or without the small molecule and, after washing, all four combinations assayed for invasion. Three small molecules were found to act specifically on the parasite.

Further secondary assays were carried out on all 30 hits, designed to probe key steps in the invasion process (Figure 1.19). Further details regarding the secondary experiments are reported in the primary paper by Carey *et al.*[11] One of the three parasite specific, irreversible inhibitors gave rise to a particularly interesting selectivity profile. 2,3-Bis(bromomethyl)-quinoxaline 1,4-dioxide **(27)** was only observed to inhibit Ca^{2+} ionophore-induced conoid extension. All of the other 29 small molecules inhibited/enhanced another component(s) and therefore **27** was unique.

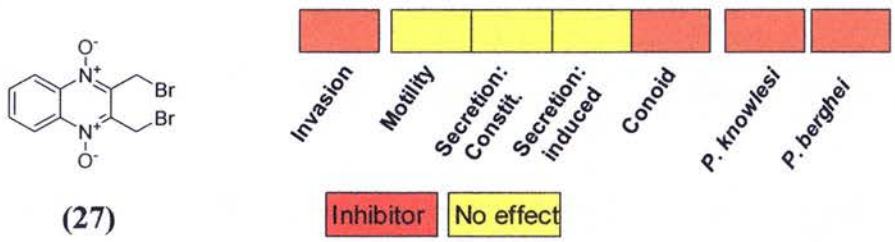

Figure 1.21. 2,3-Bis(bromomethyl)-quinoxaline 1,4-dioxide (**27**) exhibited a selective biological activity profile across a range of secondary assays designed to probe the components of the invasion machinery.

3.4 CONOID EXTENSION

In extracellular motile *T. gondii* parasites the conoid repeatedly extends and retracts beyond the polar rings and the apical end of the subpellicular microtubules (Figure 1.22). Hu *et al.* demonstrated that the pitch of the conoid fibres increases upon extension.[68] The exact function of the conoid and its cycles of extension/retraction remain unclear, though it is widely thought that the conoid plays some role in invasion. [69,74,75]

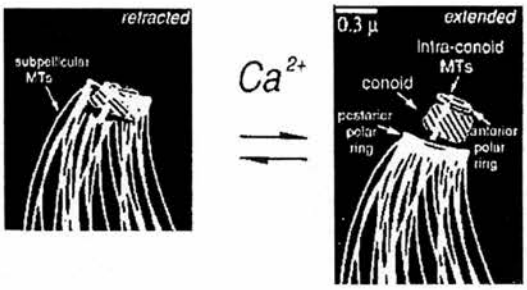

Figure 1.22. Cartoon illustrating conoid retraction and extension in response to changes in parasite intracellular Ca^{2+} levels. Image reproduced from K. Hu *J. Cell. Biol.* **2002**, *156*, 1039-1050.

Conoid extension can be experimentally induced by treating extracellular parasites with calcium ionophores, such as ionomycin (**28**) or A23187 (**29**) (Figure 1.23).[11,68,74,75] Other compounds known to induce conoid extension are thapsigargin (**30**) and caffeine (**31**), which are also thought to act by increasing intracellular calcium levels.[75]

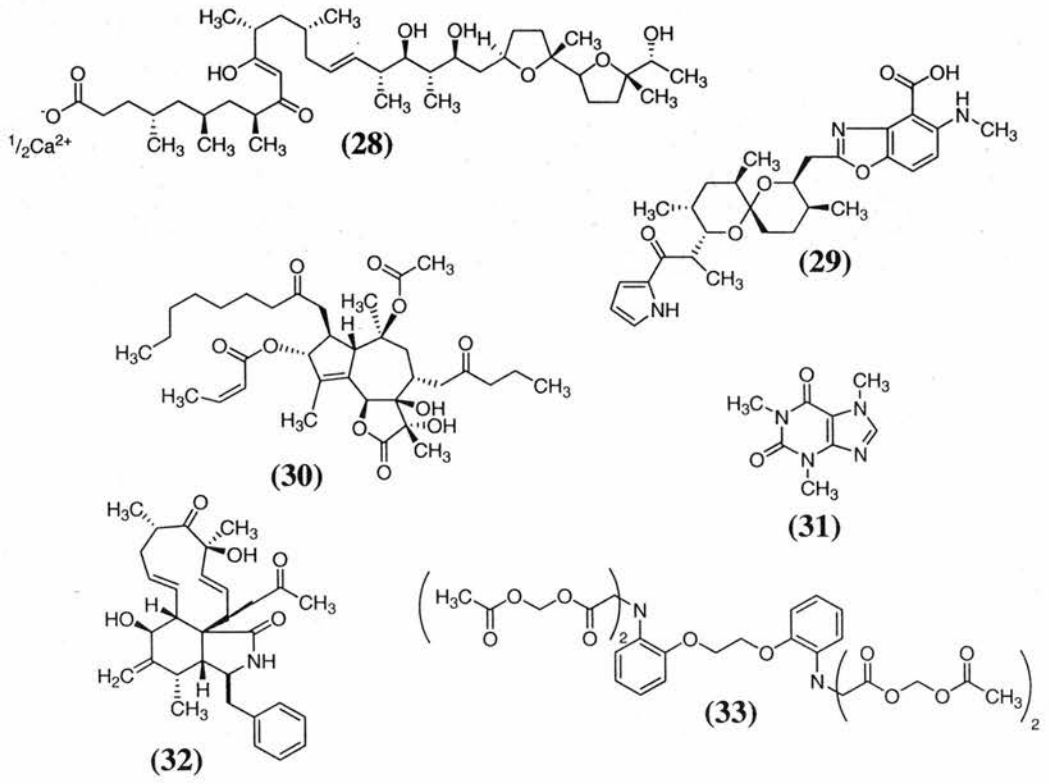

Figure 1.23. Small molecules known to have an affect on conoid extension. Ionomycin calcium salt (**28**), A23187 (**29**), thapsigargin (**30**), and caffeine (**31**) are all known inducers of conoid extension. Cytochalasin D (**32**) is known to inhibit Ca^{2+} induced conoid extension and the Ca^{2+} chelator BAPTA/AM (**33**) inhibits conoid extension.

Cytochalasin D (**32**) (Figure 1.23) inhibits conoid extension in response to calcium ionophore treatment, suggesting that either actin polymerization or actin-myosin-based motility is involved in conoid extension in response to a calcium signal.[75]

The effect of **27** on conoid extension was determined by the addition of buffer containing the calcium ionophore **28** or DMSO to parasites pretreated with **27**, and then visualising extended conoids by phase microscopy. **27** efficiently blocked ionomycin-induced conoid extension (Figure 1.24) in a similar manner to that reported for **32**.

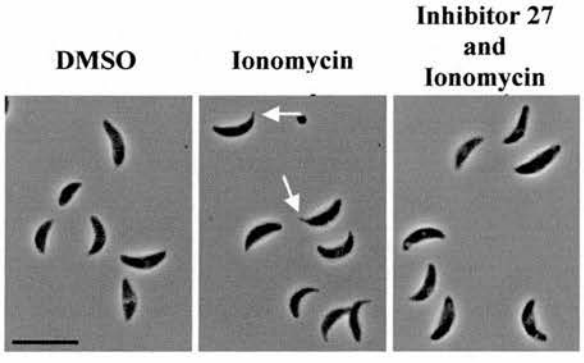

Figure 1.24. Conoid extension assay. Phase micrographs of tachyzoites treated for 15 mins. with medium containing: DMSO (control); 1 μM ionomycin or 50 μM of **27** followed by 1 μM ionomycin. The conoids of >50% of the ionomycin-treated tachyzoites were extended (e.g. arrows). Extension was completely blocked by pre-treatment with **27**. (Bar = 10 μm.) Image reproduced from K. L. Carey *et al. Proc. Natl. Acad. Sci. USA* **2004**, *101*, 7434-7438.

Interestingly, **27** was shown to have no effect on either constitutive or induced microneme secretion,[11] both processes that are dependent on calcium levels. **27** also had no detectable effect on parasite intracellular calcium levels as visualised by the calcium-sensitive fluorescent indicator Fluo4-AM (reference [11] and G. E. Ward, unpublished data). It is therefore the belief that **27** acts by a mechanism different from that of BAPTA/AM (**33**), a known Ca^{2+} binding agent.

Dose-response assays established that the lowest active concentration of **27** required to inhibit effectively, invasion of the parasites was 12.5 μM. Through an extensive collaborative effort, **27** has also been shown to act as an inhibitor of invasion of the related Apicomplexan parasites *Plasmodium knowlesi* (50% invasion of red blood cells at 50 μM) and *Plasmodium berghei*. An analogue of **27** in which the two bromine atoms were substituted for hydroxyl groups (**34**) no longer blocked invasion or conoid extension

in *T. gondii* parasites.[11] This observation suggests that **27** acts on its molecular target(s) by alkylation, consistent with its irreversible nature.

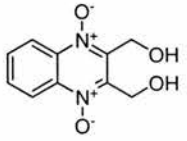

(34)

Figure 1.25. An analogue of **27** in which the bromine atoms have been replaced by hydroxyl groups. **34** did not inhibit invasion of *T. gondii* parasites into host cells and had no effect on conoid extension.

In summary, the complex process of host cell invasion by this parasite remains relatively poorly understood despite its essential role in the parasite's lifecycle. **27** could therefore prove to be a useful tool in raising the level of understanding of this process. It is proposed that **27** acts through irreversible covalent modification of its biological target.[11] Importantly in the context of this thesis, biological studies using **27** were consistent with a degree of selectivity associated with its mode of action. **27** did not inhibit motility of the parasites or microneme secretion but did inhibit the ionomycin-induced extension of an apical cytoskeletal structure in the parasite known as the conoid. It was therefore of interest whether there may be a chemical explanation for this activity profile. Collectively, these reasons highlighted **27** as an interesting small molecule for study. Furthermore, since **27** is proposed as a covalent protein modifier it may find additional applications as a chemical proteomic tool.

4.0 PROJECT AIMS

A deep understanding of the mechanism of action of small molecules is of great importance when dealing with biological systems. In the majority of cases, the way in which a small molecule can interact with a protein in order to form a covalent bond, is clear from assessment of the structural features possessed by that compound. However, examples are available in the published literature where, based on structure, the compound was proposed to operate via a given mechanism that was subsequently refuted. These include the mode of action of the *N*-sulfonylaryl β-lactam inhibitors of human leukocyte elastase (HLE).[76,77] Firestone *et al.* proposed a mechanism in which the β-lactam initially reacts with the enzyme to form a hydrolytically labile acyl-enzyme complex which is followed by a β–elimination of the *N*-substituent[76] but subsequent studies by the groups of

Knight[78] and Schofield[79] demonstrated that the initial proposed elimination reaction does not occur and the complex formed is the stable acyl-enzyme ester.

Whilst the apparent ability of **27** to be selective is at first sight surprising this is also the case for other small molecules identified by FCGs. **35** is a recent example of one of the hits (Figure 1.26) reported by Yarrow and co-workers, using a small-molecule high-throughput screen designed to identify modulators of cell monolayer wound healing.[80] The small molecule **35** possesses an *N*-hydroxy succinamide ester moiety well-established to be displaced easily by a nucleophile. It seems unlikely that this small-molecule can selectively modify a single protein target.

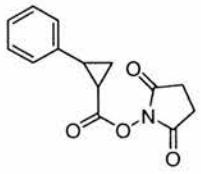

(35)

Figure 1.26. Small molecule **35**, a mascot for one of the structural classes, isolated from a HT screen by Yarrow and co-workers. Stereochemistry not specified.

To chemically address how **27** could have a selective activity profile, one of the goals at the outset of this research project involved mechanistic and reactivity studies of **27** with nucleophiles of relevance to protein chemistry. A more long long-term goal of identifying a protein target(s) for **27** was also set. Traditional target identification strategies, as outlined in Section 1.2, necessitate the design and synthesis of suitable reagents. Therefore the generation of a set of reagents for application as chemical probes was a target. Inherent in this goal is the preparation of a derivative of **27** that can be modified to contain a linker unit (for affinity studies *in vitro*) or reactive functional group (e.g. an azide) and retain its biological activity. In collaboration with Prof. Gary E. Ward at the University of Vermont, it was planned to test derivatives and any chemical probes that retained the desired biological activity could then be applied towards identifying binding partners for **27**.

In short, the goals identified for this research project were:

Part I.

I. Chemical reactivity analysis of **27** with nucleophiles of relevance to protein chemistry (Chapter 2).
II. Synthesis of derivatives of **27** for biological and chemical analysis (Chapter 3).
III. Synthesis of derivatives of **27** relevant to target identification strategies (Chapter 4).

Part II.

IV. Development of the chemistry that forms the basis of Part I Chapter 4 (Chapter 1).

CHAPTER 2

THE REACTIVITY OF 2,3-BIS(BROMOMETHYL)QUINOXALINE 1,4-DIOXIDE (27) WITH NUCLEOPHILES

1.0 A SELECTIVE ALKYLATING AGENT?

Chapter 2 focuses in more detail on one of the small molecule inhibitors identified from the *Toxoplasma gondii* invasion screen (see Chapter 1).[11] The majority of the research presented in this chapter was carried out in collaboration with Dr Russell Pearson and has recently been published in the Journal of Organic Chemistry.[81]

It is believed that the small molecule, **27**, around which this study is based, is capable of covalent modification of a protein (or subset of proteins) and that this is responsible for the observed inhibition of invasion by the parasites into host cells (see Chapter 1, Sections 3.3 and 3.4). In support of this assumption, **27** was shown to be an irreversible inhibitor of invasion, and an analogue of **27** in which the bromine atoms were substituted for hydroxyl groups no longer blocked invasion or conoid extension.[11] In addition, secondary assays also revealed a unique activity profile for **27** (see Chapter 1). Of the 24 small molecule inhibitors identified from the screen, **27** was the only compound to act specifically on the parasite and inhibit conoid extension. This profile suggests that **27** may be a promising, useful tool for exploring the possible role played by conoid extension in the invasion process of *T. gondii*. **27** was initially viewed as a general alkylating agent. This assumption was based upon the presence of the two electrophilic carbon atoms that are susceptible to attack by nucleophiles (either protein or nucleic acid based), with bromide as a good leaving group. However, this assumption does not fit easily with the selective activity profile associated with **27**.

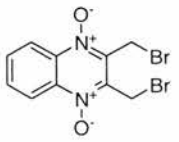

(27)

Figure 2.1. The small molecule 2,3-bis(bromomethyl)quinoxaline 1,4-dioxide (**27**). **27** possesses two reactive electrophilic bromomethylene groups and characteristic *N*-oxide functionality.

It was decided that the detailed chemical mechanism by which **27** might react with a protein was of particular interest, as this information may aid studies within the group to determine the biological mode of action of **27** through affinity-based protein target identification (ID) studies. The mode of action of **27** (and related compounds that have antibacterial activity, see Chapter 3) remains unassigned but almost certainly involves alkylation of nucleophilic residues present in one or more proteins. This provokes the intriguing question "How can **27** be a selective alkylating agent?" This chapter presents one plausible hypothesis.

1.1 Potential Cellular Targets of 27

As discussed previously, **27** has the capacity to act as an electrophile and can therefore alkylate cellular/biological macromolecules, potentially inhibiting their function and disrupting cellular pathways. The cellular targets of electrophiles include certain S, O and N atoms present in proteins, DNA, RNA, lipids and carbohydrates.

1.2 Therapeutic Agents that Form Covalent Bonds with DNA Targets

DNA is an important cellular nucleophile. The double helical structure possesses a significant number of nucleophilic N and O atoms that can form adducts with an electrophile. A number of small molecules are known to covalently modify DNA. Of these, one of the most familiar is the molecule Mitomycin C (**36**) (Figure 2.2). Mitomycin C (**36**) is an antitumour antibiotic that is metabolically activated by reduction of the quinone ring to the hydroquinone system. This reduction results in the unmasking of an electrophilic site at C-1, which then cross links to DNA.[55]

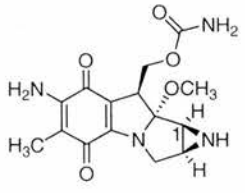

(36)

Figure 2.2. Mitomycin C (**36**), a known covalent modifier of DNA.

For this reason, a number of quinone derivatives have been evaluated as bioreductive alkylating agents. Both mono- and bisalkylating agents have been developed. Sartorelii *et al.* have shown that compounds based on **37** with better leaving groups (Scheme 2.1, X and Y) were the most efficacious as antineoplastic agents.[82] The same researchers later demonstrated that derivatives of **37** with a 5- or 6-chloro substituent (electron-withdrawing) on the benzene ring of the naphthoquinones, appeared to possess equal antitumour activity to the corresponding 5- or 6-methyl substituted (electron-donating) analogues, but no attempt at rationalisation was presented.[83]

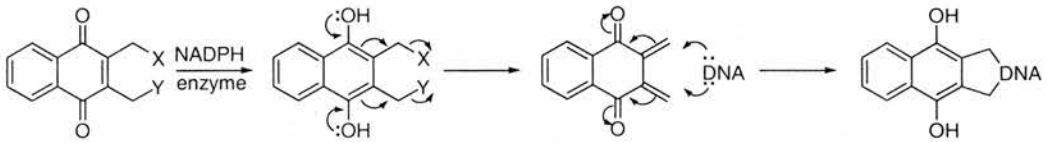

(37)

Scheme 2.1. Quinone derivatives developed by Sartorelii *et al.* as bioreductive alkylating agents.[82] The arrows are designed to signify the overall outcome of the reaction rather than a detailed reaction mechanism.

Cisplatin (*cis*-diamine-dichloro-platinum, *cis*-$[PtCl_2(NH_3)_2]$) (**38**) is another excellent example of a small molecule capable of covalently modifying DNA, forming two covalent bonds by displacement of both chloride ligands. Cisplatin has been identified to form intrastrand cross-links, of which the most common are Pt complexes between N-7 of two adjacent guanines.[55]

However, DNA seems like an unlikely target for **27** since the relatively short timescale of the original assay (approximately 2 hours) is probably too short to account for the affect of DNA disruption to induce the observed phenotypic change. A more probable target for **27** is a cellular protein. This assumption raises a multitude of possibilities in considering what class/type of protein **27** is capable of covalently modifying.

1.3 NUCLEOPHILIC AMINO ACIDS

The most significant amino acid residues when considering covalent adduct formation are those that have ionisable side chain functional groups (Table 2.2). These are aspartic and glutamic acid, lysine, arginine, cysteine, histidine, serine and tyrosine. In their unprotonated state each is a potent nucleophile and can engage in a covalent bond forming

reaction. These possible amino acids can therefore be involved in an alkylation reaction (Table 2.1).

Table 2.1. Selected examples of ionisable functional groups on amino acid side chains which participate in nucleophilic (covalent) catalysis and can therefore be involved in an alkylation reaction with RCH_2X.

Amino Acid	*Nucleophilic Side Chain*	*Alkylated form by reaction with RCH_2X*	*Examples in nucleophilic enzymatic reactions*
Serine	$-CH_2-OH$	$-CH_2-O-CH_2-R$	Serine proteases, esterases, lipases
Tyrosine (phenolic anion)	$-Ar-OH$	$-Ar-O-CH_2-R$	DNA topoisomerase
Aspartic acid (n = 1) Glutamic acid (n = 2)	$-(CH_2)_n-CO_2H$	$-(CH_2)_n-CO_2-CH_2-R$	Epoxide hydrolase, haloalkane dehalogenase
Cysteine	$-CH_2-SH$	$-CH_2-S-CH_2-R$	Cysteine proteases, acyl transferases
Lysine	$-(CH_2)_4-NH_2$	$-(CH_2)_4-NH-CH_2-R$	Acetoacetate decarboxylase, class I aldolases

Ar = aromatic and X = halogen. Table adapted from 'Introduction to Enzyme and Coenzyme Chemistry' T. D. H. Bugg.[84]

Nonpolar, hydrophobic amino acids play a role in determining the three-dimensional structure as they are typically buried inside the protein. In contrast, charged and polar groups are found on the surface where they can interact with the solvent unless paired in hydrogen-bonding.[84]

Table 2.2. pK values of ionisable functional groups in proteins pK* values are dependent on temperature, ionic strength, and the microenvironment of the ionisable group.

Group	*Acid*		*Base* + H^+	*Typical* pK*
α-COOH	—COOH	⇌	$—COO^-$ + H^+	3.1
Aspartic acid	—COOH	⇌	$—COO^-$ + H^+	4.4
Glutamic acid	—COOH	⇌	$—COO^-$ + H^+	4.4
Histidine	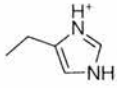	⇌	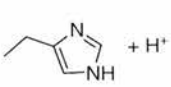	6.5
α-NH_3^+	$—NH_3^+$	⇌	$—NH_2$ + H^+	8.0
Cysteine	—SH	⇌	$—S^-$ + H^+	8.5
Tyrosine	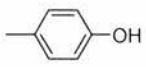	⇌	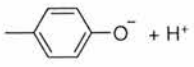	10.0
Lysine	$—NH_3^+$	⇌	$—NH_2$ + H^+	10.0
Arginine	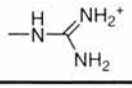	⇌	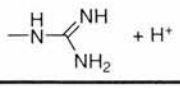	12.0

Table adapted from Stryer, L. Biochemistry.[85]

1.4 BIS-ALKYLHALIDES AND THEIR ASSOCIATED REACTIVITY WITH AMINO ACIDS

The reaction of an alkyl halide, such as **27**, is rarely confined to a specific functional group. For example, compounds of this type are known to react with a sulfhydryl group of cysteine, both imidazoyl side chain nitrogens of histidine, the thioether of methionine, and the ε-amino group of lysine residues and N-terminal α–amines.[27] Bis-alkylhalides contain reactive halogen groups capable of cross-linking through sulfhydryl-, primary amine-, or histidine-containing functionalites by nucleophilic substitution (Figure 2.3). At physiological pH alkyl halides are mainly specific for sulfhydryl groups, however at more alkaline pH they readily react with nitrogen nucleophiles.[27]

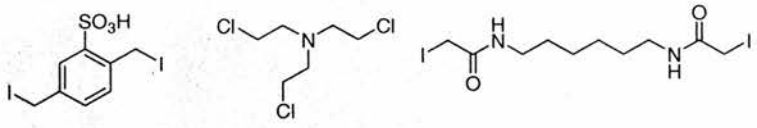

(39) **(40)** **(41)**

Figure 2.3. Some typical bis-alkylhalides belonging to the three main classes, **A** – **C**. **A.** α, α′-Diiodo-*p*-xylene sulfonic acid (**39**). Benzyl halides typically contain iodine or bromine. **B.** Tri(2-chloroethyl)amine (**40**). An alkylhalide in which the halogen atom is *β* to a nitrogen or sulfur atom. **C.** *N*,*N*′-Hexamethylene-bis(iodoacetamide) (**41**). A haloacetyl derivative.

1.5 SULFUR NUCLEOPHILES OF RELEVANCE TO COVALENT PROTEIN MODIFICATION

The sulfhydryl group of cysteine is arguably ranked of highest nucleophilicity, relative to the major groups in protein molecules (based on the theory of nucleophilicity).[27,86] However, cysteine is one of the most rarely used amino acids in the proteins of most organisms studied so far.[87,88] Thiols can exist in proteins in reducing conditions but are more often present in the oxidised form as a disulfide bridge, where they play a crucial role in stabilising protein structures. For example, proteins contained within oxidising cell compartments (e.g. endoplasmic reticulum and periplasm) and extracellular proteins often rely on the formation of covalent disulfide bonds to support their correct folding and maintain structural stability.[87] Whereas, thiol groups present in proteins contained in the cytosol (reducing environment) are reduced and often found in the substrate binding pockets or in the active site of enzymes.[87] Covalent adduct formation can occur by alkylation of a sulfhydryl group to form a stable thioether bond. Cysteine proteases contain a catalytically active cysteine sulfhydryl group, Cys-25, in the active site

(Scheme 2.2). An imidazole group, present in close proximity, polarises and deprotonates the sulfhydryl group facilitating nucleophilic attack of the electrophilic carbon belonging to the amide carbonyl.

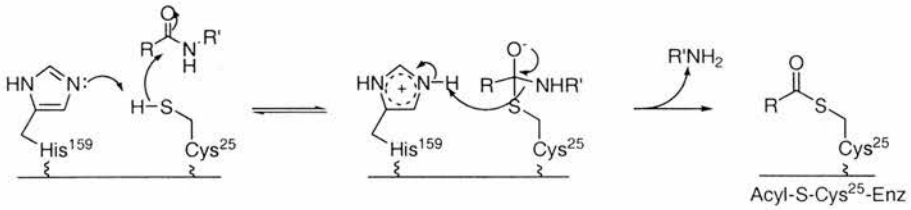

Scheme 2.2. Cysteine protease. The cysteine sulfur in the active site acts as a nucleophile.

Alkylation of the cysteine sulfur by a variety of reagents including chloromethyl ketones e.g. Tos-Lys-CH_2Cl (TLCK),[89] peptidyl-diazomethanes[90] e.g. Cbz-Phe-CHN_2,[91] and epoxysuccinyl peptides e.g. E64 (**22**),[49,89] renders the enzyme catalytically inactive. There is some debate over the degree of polarisation of the sulfhydryl group in a cysteine protease and hence whether the sulfur exists as the thiol or the ionised thiolate form.

A strictly conserved active site cysteine thiol across the family of aldehyde dehydrogenase enzymes is also known to act as a catalytic nucleophile.[92] The reaction mechanism involves attack on an aldehyde carbon present in the substrate to form a thiohemiacetal intermediate. Noyori and co-workers have also shown that sepharose-bound thiols (such as cysteine and glutathione), regarded to be plausible mimics of protein thiols, react by nucleophilic 1,4-conjugate addition to the α,β-unsaturated system of cyclopentenone prostaglandins under physiological conditions.[93]

1.5.1 The Reaction of 27 With Sulfur-based Nucleophiles

Reaction of **27** with its cellular target may involve covalent modification by a sulfur-based nucleophile. For this reason, the reaction of **27** with 4 equivalents of benzylmercaptan in $CDCl_3$ was studied using 300 MHz ^{1}H NMR spectroscopy. After 17 hours at room temperature, no new signals were observed in the ^{1}H NMR spectrum and **27** remained unmodified. In contrast, reaction of **27** with sodium 2-methyl-2-propanethiolate (NaS^{t}Bu, **42**) was observed to occur immediately. Unfortunately attempts to identify the product(s) by ^{1}H NMR analysis proved challenging and isolation was unsuccessful due to rapid decomposition.

It is also difficult to envisage how attacking a general sulfur nucleophile could provide any degree of selectivity to **27**. In addition, the relatively low abundance of sulfhydryl groups (average cysteine composition quoted as being 1.7-2.8%) in comparison to primary amino groups (average lysine composition quoted as being 5.7-7.0%)[88,94,95] implies that a protein containing a sulfur bound nucleophile may not be the target of **27**.

1.6 OXYGEN NUCLEOPHILES OF RELEVANCE TO COVALENT PROTEIN MODIFICATION

Another common mechanism for covalent adduct formation is through attack of an activated oxygen atom at an electrophilic site in a small molecule, for example, a serine hydroxyl activated in the catalytic triad of a serine protease (Scheme 2.3). For an oxygen atom to have sufficient nucleophilicity to carry out such a reaction it must be activated within its surrounding microenvironment as, in general, oxygen is a less potent nucleophile compared to its sulfur counterpart.

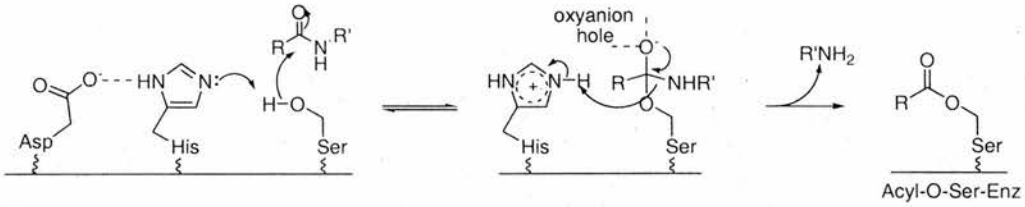

Scheme 2.3. Serine protease. The serine in the active site acts as a nucleophile.

The *β*–lactam class of serine protease inhibitors includes monocyclic *β*–lactams (**43**) (azetidinones) and bicyclic structures such as penicillin (**44** R = CH_2Ph, penicillin G), the cephalosporins (**45**) and penems (**46**) (Figure 2.4). The mechanism of inhibition of serine proteases by *β*–lactam containing small molecules occurs by an initial nucleophilic attack of the hydroxyl group of the active site serine on the C-2 carbonyl of the *β*–lactam.[96] Wilmouth *et al.* describe the crystal structure of porcine pancreatic elastase (PPE) (E.C.3.4.21.36) and the monocyclic *β*–lactam **47**.[79] The ring-opened *β*–lactam is covalently bound within the active site of the enzyme through the serine oxygen forming a stable acyl-enzyme complex in which, importantly, the carbonyl oxygen is not located in the oxyanion hole of the active site.

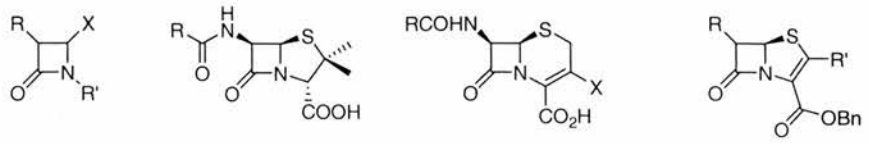

(43) (44) (45) (46)
(47)

Figure 2.4. General structure of the monocyclic β–lactams; azetidinones, **(43)** (**47**, R = Et, X = CO_2H, R´ = Ts), penicillins (**44** R = CH_2Ph, penicillin G), cephalosporins (**45**) and penems (**46**).

1.6.1 The Reaction of 27 With PPE

To investigate the possibility that **27** could bind to a protein containing a nucleophilic oxygen, incubation with porcine pancreas elastase (PPE) was carried out. PPE was chosen based on previous literature[79,97-99] and because of its relatively open active site to presumably enable facile incorporation of **27**. Model studies were carried out with a β–lactam containing compound to confirm the activity of the enzyme. However, upon incubation of **27** with PPE, no covalent reaction products were detected by LC-MS.

1.7 NITROGEN NUCLEOPHILES OF RELEVANCE TO COVALENT PROTEIN MODIFICATION

Despite the distinct possibility that the cellular target(s) for **27** could be a sulfur-based nucleophile we chose to investigate initially the probability of it being a protein-based amine nucleophile. The most abundant target for protein labelling is primary amines, which are present predominately at the N-terminus of proteins or in lysine residues. Lysines are widely distributed in proteins and usually exposed on the surface of a protein, making them easy to derivatise.

According to the theoretical pK_a values, at pH < 8.5 nucleophilic substitution reactions using amines or sulfur-based nucleophiles should be inefficient. In reality however, the actual pK_a can differ significantly from the theoretical value, for instance, the ε-amino group on lysine (p$K_a \simeq 10$) exists uncharged in sufficient quantity to react and be modified close to neutrality (pH 7.2) (Figure 2.5). The discrepancy results from micro-environmental effects experienced by residues within the three-dimensional structure of the protein.[27] For example, the enzyme acetoacetate decarboxylase contains an active site

lysine with a pK_a value found to be 5.9, much less than the expected value of ~9.[84] It is important to note then that changes in pK_a which have been observed to occur in proteins due to micro-environmental effects invokes an overlap of the pK_a range for thiols and amine-containing residues so that in practice pH alone cannot be used to target solely e.g an –SH or NH_2 functional group in a protein alkylation reaction.

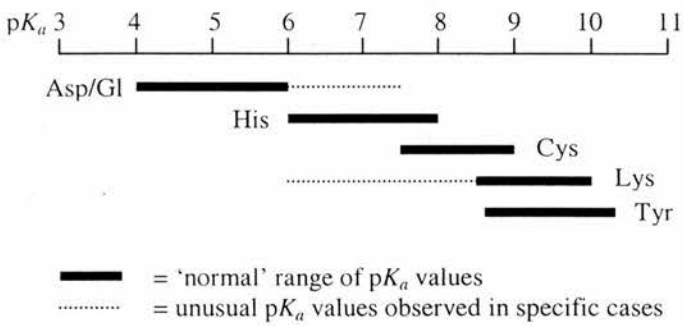

Figure 2.5. Range of pK_a values observed for amino acid side chains in enzyme active sites. Image reproduced from 'Introduction to Enzyme and Coenzyme Chemistry' T. D. H. Bugg.[84]

In addition, intramolecular compartmentalisation within a cell enables different chemical (pH) environments to be maintained between compartments. This, in turn, enables a different complement of enzymes, operating at different optimum pH levels, to function harmoniously inside a single cell.

To summarise, **27** is believed to be capable of covalent modification of a target protein(s). Although, interestingly **27** was observed to exhibit a selective inhibitory profile in the secondary biological assays, only displaying an effect on coniod extension. Reasoning that identification of the molecular target of **27** would provide insight into the invasion process of the *Toxoplasma gondii* parasite and/or information about the function of the conoid, a programme to study the detailed chemical mechanism by which **27** reacts with amines was initiated.

1.7.1 The Reaction of 27 With Amines

From all the possible cellular nucleophiles discussed in Section 1.1 the reaction of **27** with primary amines was chemically intriguing. The reaction of **27** with amines has been the subject of previous literature reports.[100 -103] Landquist and Silk reported that upon treatment with aliphatic primary amines, **27** gave "red mixtures which did not yield

the desired derivatives" rather than the simple displacement products (**48**, Scheme 2.4) or the corresponding cyclic tertiary amines (**52**, Scheme 2.4).[100]

In 1969, Anderson and Fleming proposed a mechanism for the conversion of **27** to **51** on reaction with methylamine via path A, Scheme 2.4.[101]

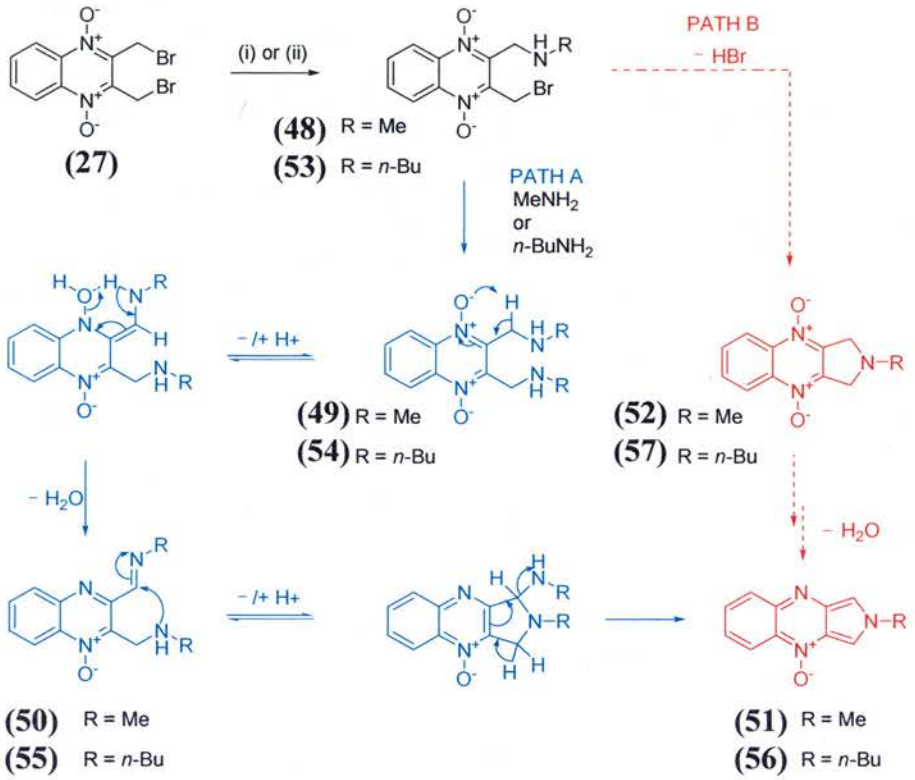

Scheme 2.4. Two possible reaction pathways for conversion of **27** to **51/56**. Path A (blue) involves a double nucleophilic substitution reaction involving two equivalents of the amine. Path B (red) involves a cyclisation pathway utilising only one equivalent of the amine. *Reagents and conditions:* (i) methylamine, -80 °C;[101] (ii) *n*-butylamine, 25 °C.

This pathway (Scheme 2.4, path A, blue) was proposed to proceed by a double nucleophilic displacement of two bromide ions by two equivalents of the primary amine, methylamine (R = methyl) to form the disubstituted intermediate **49**. The tautomer of **49** was then proposed to eliminate water to form the imine **50**. Nucleophilic attack of the second amine-nitrogen at the electrophilic carbon of the imine can then occur with loss of one equivalent of amine to give the extended aromatic product **51**.

No evidence in support of this mechanism was provided by the authors or is known to be presented elsewhere in the literature. The authors did not provide any accompanying rationalisation for their chosen pathway. Several alternative plausible mechanisms were

considered by us for the transformation of **27** through to **51**. Of these, the foremost involved a seemingly favourable intramolecular cyclisation reaction to yield the intermediate **52**.[104] This chemically intuitive route could take place, via rearrangement and overall dehydration, to afford the observed product **51** (Scheme 2.4, path B, red). Further investigations into the chemical mechanism of the reaction of **27** with a primary (and secondary) amine are presented herein, designed to probe the pathway suggested by Anderson and Fleming.

1.7.2 Biological Consequences of this Reaction Mechanism for the Mode of Action of 27 and the Possibility of a Selective Alkylating Reagent?

Despite sulfur being a more apparent target nucleophile to react with **27**, the mechanism proposed by Anderson and Fleming presented an intriguing biological hypothesis outlined in Figure 2.6.[105]

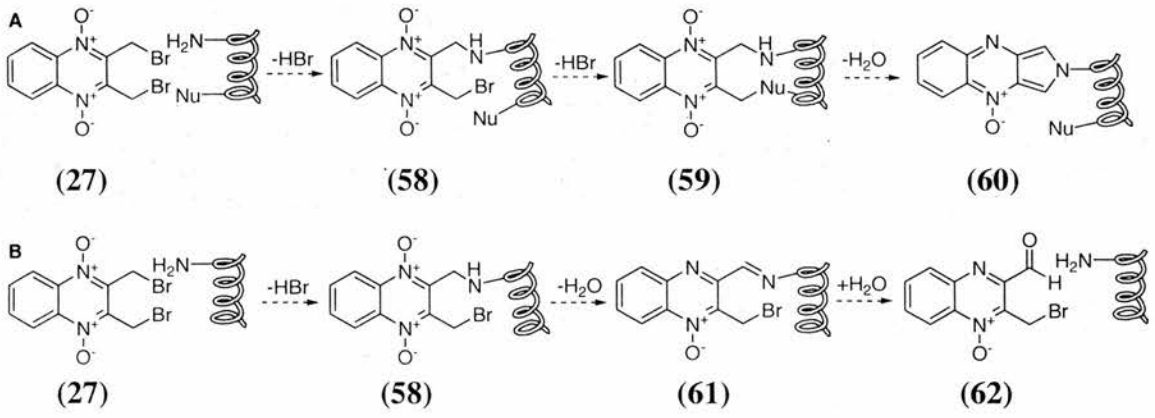

Figure 2.6. A schematic representation of one method for covalent protein modification of a protein by **27**. **A** Covalent modification is subject to the requirement that a second nucleophile is in close proximity and positioned at the correct orientation to attack the initially formed protein-inhibitor complex **58**. **B** Involvement of only a single nucleophile is predicted to result in no overall covalent modification of the protein. If a second nucleophile is unavailable, an initial covalent modification is expected (**58**) to be followed by loss of the *N*-oxide functionality (**61**) and subsequent hydrolysis leading to turnover of **27** and reformation of native enzyme.

By this model, a double nucleophilic event is required for irreversible covalent modification of a target protein(s), giving rise to the inhibitor bound as the extended *o*-quinonoidal system (**60**) (cf. **51**). Both nucleophiles are required to be in close proximity to one another with the second positioned in the correct orientation to facilitate attack on the initially formed protein-inhibitor complex (**58**) (cf. **48**). If a second nucleophile is unavailable then it is envisaged that upon formation of the imine intermediate (in a

situation analogous to that for **50**) that hydrolysis would be favoured in an aqueous environment. Involvement of only a single nucleophile would be predicted then to result in no overall covalent modification of a protein. Instead hydrolysis would result in dissociation of the inhibitor as a turnover product of **27**, bearing an aldehyde functionality and reformation of the native enzyme.

The fact that **27** could react with a nitrogen-based nucleophile via an analogous mechanism to that proposed[101] is an intriguing possibility, even more so since this hypothesis provides one explanation for the apparent selectivity observed for **27**. In addition, it was anticipated that we could gain additional insights into the mechanism by studying the related quinoxaline (**64**, Scheme 2.5) and quinoxaline mono-*N*-oxide (**69**, Scheme 2.7) in parallel.

2.0 STUDY OF THE REACTION OF QUINOXALINES, QUINOXALINE MONO-*N*-OXIDES AND QUINOXALINE DI-*N*-OXIDES WITH AMINES

2.1 SYNTHESIS OF QUINOXALINE DERIVATIVES

Literature studies reveal several protocols for the synthesis of 2,3-bis(bromomethyl)quinoxaline 1,4-dioxide (**27**) or related analogues. Previous work in the Westwood lab followed the synthesis of Landquist and Silk in which the parent quinoxaline **64** was prepared by bromination of the commercially available 2,3-methylquinoxaline **63** (Scheme 2.5).[100] Although **64** was obtained by bromination in anhydrous DCM the method was not reliable. In general low yields were obtained that were the result of incomplete bromination. Landquist and Silk also reported *N*-oxidation of 2,3-bis(bromomethyl)quinoxaline **64**, using peracetic acid (1.2 to 2 M) and heating to 50 °C, to afford both mono-*N*(1) (**69**) and di-*N*(1,4) (**27**) oxidised products.[100]

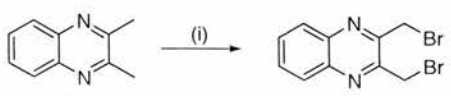

(63) **(64)**

Scheme 2.5. Bromination of 2,3-methylquinoxaline (**63**) to give **64** was found to be an unreliable method.[100] *Reagents and conditions:* (i) Br_2, DCM, reflux, 10 mins.

An alternative approach to **27** was employed by Haddadin *et al.* (Scheme 2.6), which utilises the Beirut reaction.[106] This involves condensation of benzofurazan oxide

(benzo[1,2,5]oxadiazole-1-oxide) (**65**) with butanone using pyrrolidine in acetonitrile. Bromination in ethyl acetate was then used to give **27** in an 85% yield.

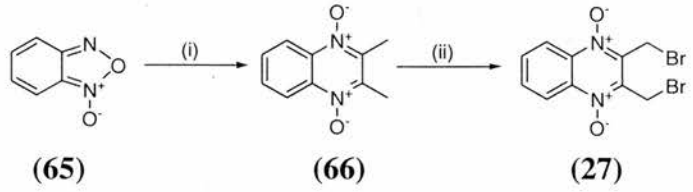

(**65**) (**66**) (**27**)

Scheme 2.6. Preparation of **27** used by Haddadin *et al.*[106] *Reagents and conditions:* (i) butanone, pyrrolidine, MeCN, warming, 65%; (ii) Br_2, ethyl acetate, heat, 85%.

The strategy used here for the synthesis of **27** was based on two literature reactions and proved to be more robust (Scheme 2.7). This route involved a condensation reaction between commercially available 1,4-dibromo butane-2,3-dione (**68**) and *o*-phenylenediamine (**67**)[100,107,108] to afford 2,3-bis(bromomethyl)quinoxaline **64**. The ^{1}H NMR of **64** showed the presence of an AA´XX´ system, as expected.

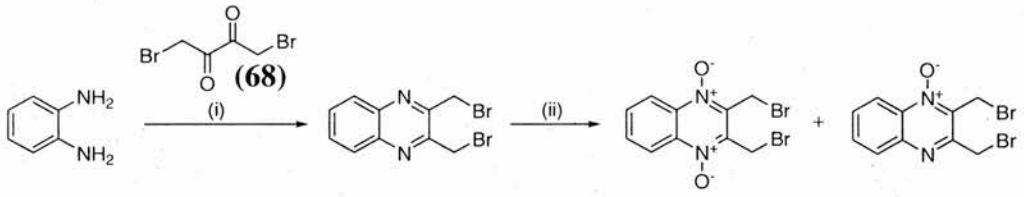

(**67**) (**64**) (**27**) (**69**)

Scheme 2.7. Adopted synthesis of 2,3-bis(bromomethyl)quinoxaline 1,4-dioxide (**27**), via condensation and *m*CPBA oxidation. *Reagents and conditions:* (i) THF, 0 °C to RT, 17 h, 88%; (ii) *m*CPBA, DCM, RT, 42 h, 65% (**27**), 18% (**69**).

Oxidation of the parent quinoxaline **64**, was carried out typically using five equivalents of purified *m*CPBA in THF to give predominantly the 1,4 dioxide product (**27**) as a bright yellow crystalline solid.[106] The mass spectrometric analysis of **27** showed the presence of three peaks consistent with the characteristic isotope pattern for the presence of two bromine atoms at *m/z* 373 $[M^{81} + Na]^+$, 371 $[M^{81,79} + Na]^+$, and 369 $[M^{79} + Na]^+$ for the mass plus sodium. Additionally, the ^{1}H NMR of **27** showed a pronounced downfield shift of the signals corresponding to *H*-5 and *H*-8 (the AA´ part of the AA´XX´ system). Deady *et al.* have previously observed that N-5 oxidation of 11*H*-indeno[1,2-*b*]quinoxalin-11-ones of general structure **70** caused a downfield shift of *c.* 0.5 ppm for two one proton doublets corresponding to H-4 and H-6 (Scheme 2.8).[108] In addition, *N*-oxidation of quinoline, has been reported to result in a downfield shift of 0.7 ppm for the signals

corresponding to the *peri* proton, H-8.[109] Reduction in the number of equivalents of *m*CPBA used to oxidise **69** (or reaction times) tailors the reaction to favour the singly oxidised product **69**. (see Section 2.8). The ^{1}H NMR for the mono-oxidised product **69** showed a downfield shift of 0.5 ppm for H-8 (8.57 ppm) compared to H-5 (8.07 ppm).[110]

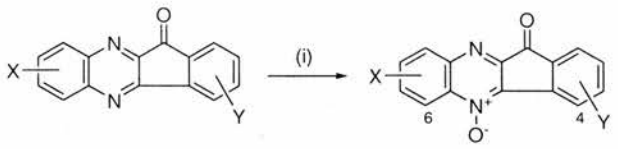

(70) **(71)**

Scheme 2.8. *N*-oxidation technique used by Deady *et al.* to assign the isomer structure of the 11*H*-Indeno[1,2-b]quinoxalin-11-ones (**70**). *Reagents and conditions:* (i) 30% H_2O_2, AcOH, heat.

2.2 Reaction of 2,3-Bis(Bromomethyl)quinoxaline (64) with *n*-Butylamine

500 MHz ^{1}H NMR spectroscopy was used to track the reaction of 2,3-bis(bromomethyl)quinoxaline **64** with *n*-butylamine. *n*-Butylamine was chosen as a lysine mimic. The reaction of **64** at an initial concentration of 20 mM with three equivalents of *n*-butylamine was performed in $CDCl_3$ at 25 °C. ^{1}H NMR spectra were acquired at regular time points over a 17 hour period and the signals corresponding to the starting material **64**, major reaction intermediate **72** and products **73** and **74** were tracked.

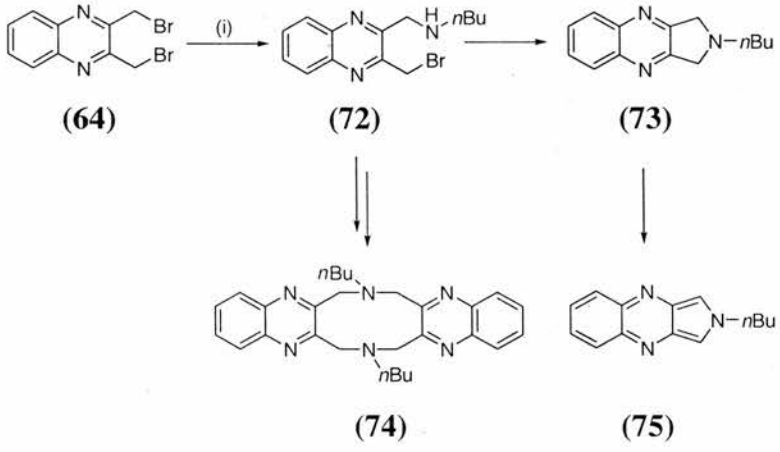

(64) **(72)** **(73)**

(74) **(75)**

Scheme 2.9. Products formed on reaction of **64** with *n*-butylamine. *Reagents and conditions:* (i) *n*-butylamine (3 equiv.), $CDCl_3$, 25 °C.

The ^{1}H NMR spectra collected at specific time points throughout the course of the reaction were compared. Signals were assigned that corresponded to compounds on the reaction pathway, guided by integration. Peaks were chosen that represented each intermediate on the pathway (for an example see Appendix). These peaks were analysed individually over several time points and their integration calculated as a percentage ratio compared to the $CHCl_3$ signal (i.e. integral of the signal corresponding to the intermediate under study + the integral of $CHCl_3$ = 100) and were normalised to correct for the number of integrated protons. The variation in the integral percentage was then plotted as a function of time.

The ^{1}H NMR experiment showed that two major products, **73** and **74**, were formed on reaction of **64** with *n*-butylamine (Scheme 2.9 and Figure 2.7). The ^{1}H NMR spectra of **73** and **74** were similar (benzylic methylene singlet at 4.14 ppm for **73** and 4.37 ppm for **74**). Mass spectrometric analysis of purified compounds (including high resolution) was consistent with the assigned structures for **73** and **74**.

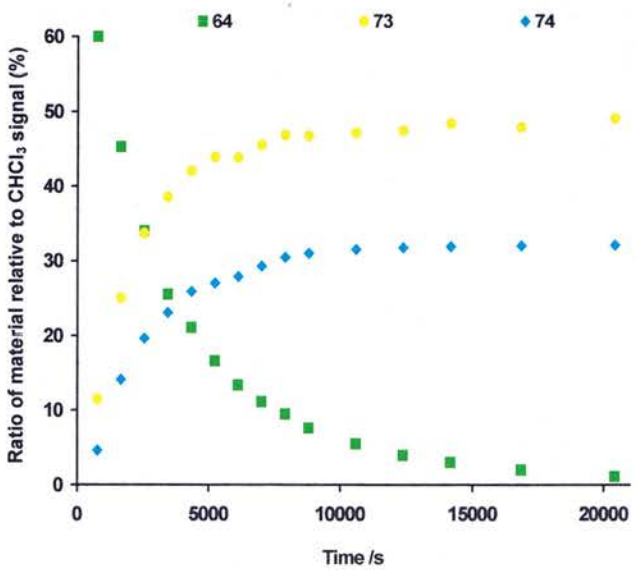

Figure 2.7. Relative abundance of compounds **64**, **73** and **74**. *Reagents and conditions:* *n*-butylamine (3 equiv.), $CDCl_3$, 25 °C.

From Figure 2.7, the observed ratio of **73**:**74** after 17 hours was 3:2. During the course of the reaction, minor signals corresponding to **75** were also observed due to decomposition of **73**. Compound **75** was isolated on a preparative scale as a red oil

showing a singlet at 7.61 ppm in the ^{1}H NMR spectrum characteristic of the new aromatic protons in the five-membered ring.

Compound **73** was formed by the cyclisation of **72** although this step must be relatively slow for an intramolecular reaction, as reflected by the observed formation of **74**. A corresponding ten-membered ring compound (**76**) has been previously reported in the literature as a minor component (8-10%) resulting from the reaction of **64** with *tert*-butylamine (Figure 2.8).[111] However, with the exception of a melting point no further structural characterisation was reported. In addition the authors stated that the structure was tentatively assigned and may require revision. In light of our isolation of **74** their assignment of **76** seems likely to be correct.

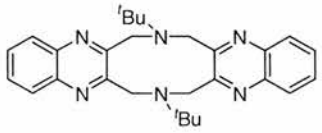

(76)

Figure 2.8. Minor component tentatively assigned as the 10-membered ring. **76** was isolated from the reaction of **64** with *t*-butylamine by Kreher *et al.*[111]

The formation of **74** can occur by a favoured intermolecular reaction of **72** with **64** followed by incorporation of a second molecule of *n*-butylamine and macrocyclisation. Alternatively, **74** can be produced by reaction of two molecules of **72**. The latter of these two options is deemed unlikely, at least during the early stages of the reaction, due to the relatively low concentration of **72** present compared with **64**.

The formation of **74** initially seemed surprising given that an intramolecular cyclisation reaction would usually be expected to be relatively fast. However, a previous article in the literature by King and Tsang reported a similar observation.[112] Two reaction pathways were observed in a study of the relative rate of bimolecular nucleophilic substitution of dibenzylethylsulfonium fluoroborate (**79**) compared to the corresponding reaction with the cyclic sulfonium fluoroborate (**83**) (Figure 2.9). Upon reaction with thiocyanate anion **79** was found to react 8000 times faster than **83** and gave only the products, **80** and **81**, from an S_N2 reaction at the benzylic centre. No dibenzyl sulfide (**77**) or ethyl thiocyanate (**78**) were formed. By contrast, **83** gave a mixture of products from reaction at both the benzylic carbon, **84** (20%), and CH_2 of the ethyl group, **82** (80%). The differential product formation is rationalised by the ability of the benzyl groups in **79** to freely adopt a stabilised TS by conjugation with the aromatic ring as shown in A, Figure

2.9. In the case of **83** in order to react to give **84** it is proposed to go via a constrained TS that is close to a 'coplanar' arrangement as shown in B, Figure 2.9. This renders the rate of attack at the benzylic carbon less favourable compared with the alternative, CH_2 of the ethyl group, and in comparison to the benzylic carbon centre of **79**. This TS implied in this study is analogous to that for the intramolecular cyclisation reaction of **64**.

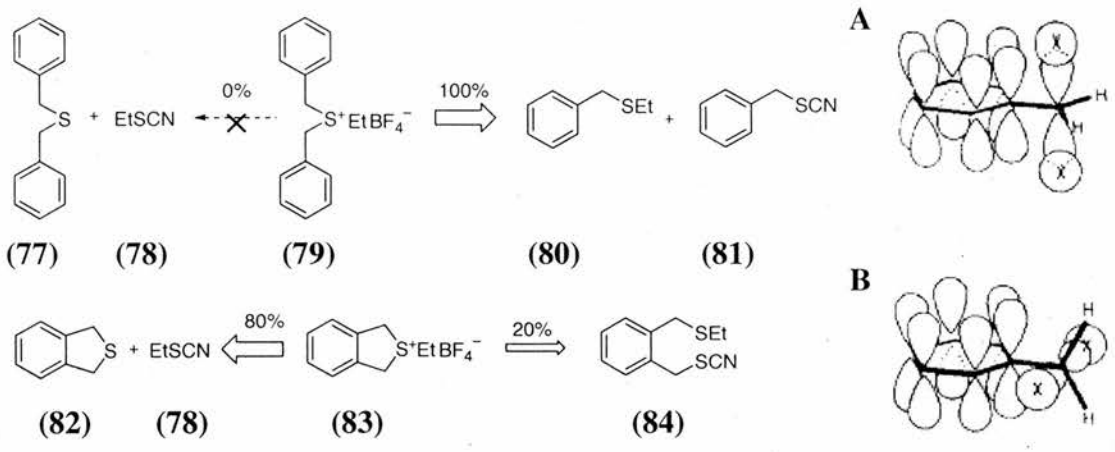

Figure 2.9. The differential reactivity of **79** in comparison to **83** observed by King and Tsang.[112] **79** can freely adopt the 'orthogonal' arrangement (Insert A) allowing it to undergo an S_N2 displacement 8000 times faster than **83**. **83** contains a constrained ring system forcing a more 'coplanar' TS arrangement (Insert B) that disfavours the S_N2 reaction at the benzylic carbon and favours displacement of the Et group. Images reproduced from J. F. King and G. T. Y. Tsang *J. Chem. Soc. Chem. Commun.* **1979**, 1131-1132.

As anticipated, repeating the reaction at an initial concentration of 4 mM of **64** (a five-fold dilution) increased the ratio of **73**:**74** to 7:2 further in favour of the intramolecular reaction. Interestingly, a route to **74** involving the reaction of the disubstituted compound, **85** with **64** was ruled out due to the absence of signals in the ^{1}H NMR corresponding to **85**. At the five-fold dilution, signals corresponding to the formation of **72** were transiently observed, although isolation of **72** was not possible, as predicted.

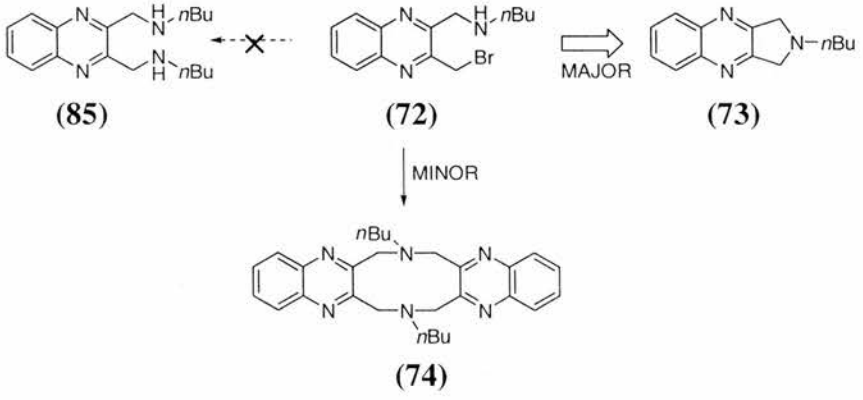

Scheme 2.10. A summary of the reaction pathways available to intermediate **72**.

In summary, an analogue of **27** lacking the *N*-oxide functional groups (**64**) forms the cyclised product **73** as the major product upon reaction with *n*-butylamine (Scheme 2.10).

2.3 Reaction of 2,3-Bis(bromomethyl)quinoxaline (64) with Diethylamine

The situation is further simplified upon reaction of **64** with a secondary amine, diethylamine, under analogous conditions. This results almost exclusively in the formation of **87** (>90% as judged by ^{1}H NMR analysis of the reaction mixture, 74% isolated yield, Scheme 2.11). It is worthwhile noting that in an attempt to obtain crystals of **87** for analysis; the reaction was repeated on a preparative scale at an increased concentration (105 mM cf. 20 mM). **87** was collected following crystallisation and subsequent ^{1}H NMR analysis of the reaction filtrate indicated signals corresponding to the disubstituted compound **88** as a minor component. This result indicates that product formation is dependant upon the reaction concentration and that the cyclisation reaction is in competition with a second nucleophilic substitution, as expected. Further comparison of the reaction at 20, 50 and 100 mM showed that increasing the concentration of this reaction allowed for the formation of **88** however, even at 100 mM, **87** was still the minor product.

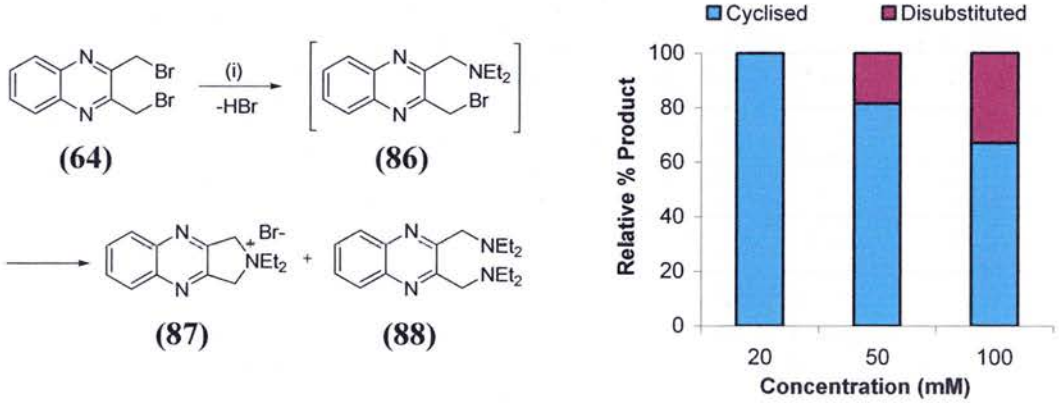

Scheme 2.11. Reaction of **64** with a secondary amine. At 20 mM, **87** was observed as the only product. *Reagents and conditions:* (i) diethylamine (4 equiv), $CDCl_3$, 25 °C, 74% yield (**87**).

Compound **87** was assigned as the tertiary amine salt based on symmetrical ^{1}H NMR signals and a shift in the benzylic methylene observed as a singlet at 5.55 ppm, cf. singlet at 4.35 ppm for the benzylic methylene in compound **93** (see Section 2.5, Scheme 2.16) in $CDCl_3$. Due to the limited solubility of **87**, in chloroform, heavy water (D_2O) was also used as the solvent to acquire ^{1}H and ^{13}C NMR. It is interesting to note that in D_2O, signals corresponding to the benzylic methylenes quickly diminished until they were no

longer observed due to rapid deuterium-proton exchange. For D_2O solutions there is no accepted reference for carbon chemical shifts[113] and so 1,4-dioxane was added and its signal defined as 59.85 ppm. Furthermore, the signal at 64.6 ppm (in D_2O) attributed to the benzylic methylene carbons of **87** is observed as an apparent quintet in the ^{13}C NMR spectrum, as expected, resulting from coupling to deuterium (Figure 2.10). The assignment of the carbon signal was further confirmed by a HSQC experiment in $CDCl_3$ (where H–D exchange was not possible, Figure 2.11).

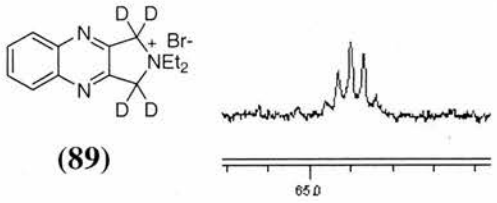

(89)

Figure 2.10. **87** undergoes rapid deuterium exchange in D_2O to give **89**. The resonance corresponding to the benzylic methylene carbon is observed as a quintet in the ^{13}C NMR as a result of $^{1}J_{C,D}$ coupling.

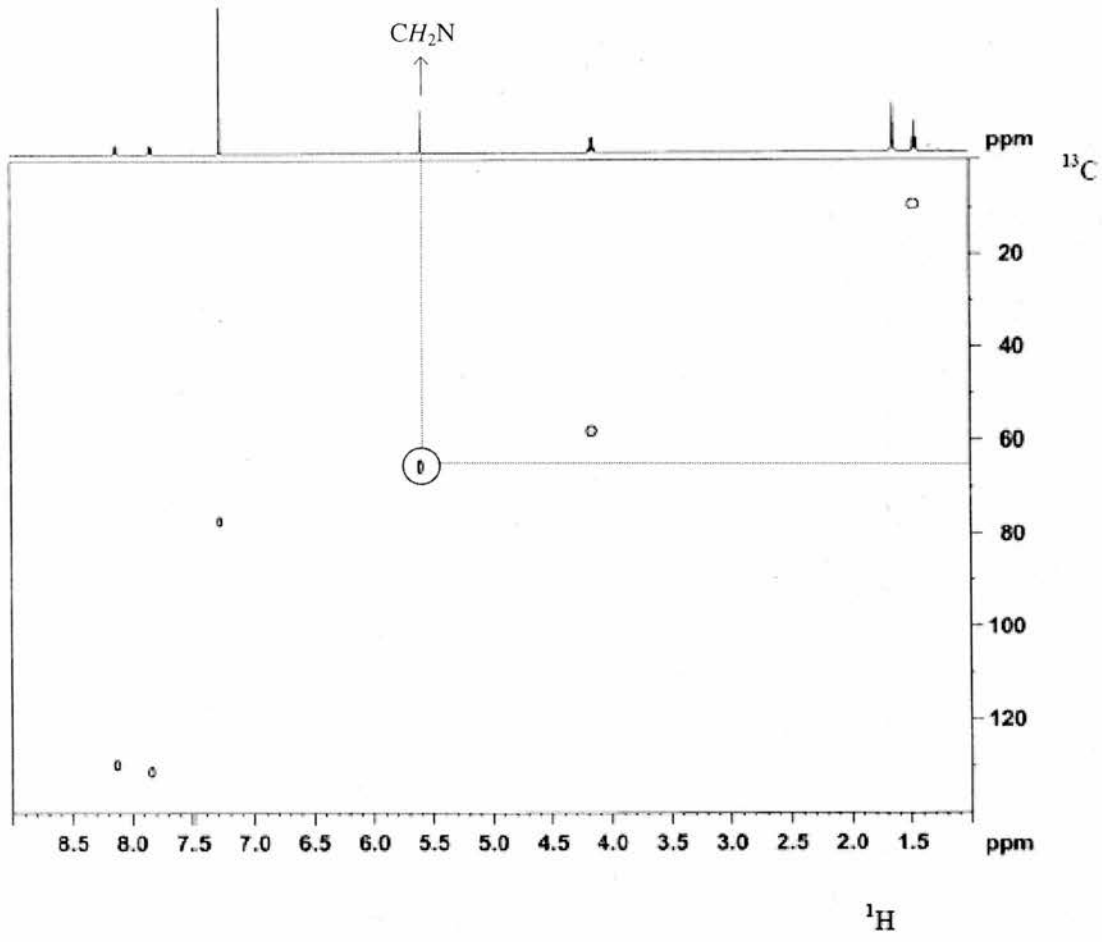

Figure 2.11. 500 MHz ^{1}H and ^{1}H–^{13}C HSQC in $CDCl_3$ for **87**. The HSQC spectrum correlates an identified proton signal (i.e. the benzylic protons, 2 × CH_2N) to the carbon to which it is directly bonded (i.e. 2 × CH_2N, 64.9 ppm) confirming the assignment of the quintet observed at 64.6 ppm to the benzylic methylene carbons in D_2O.

In contrast to the reaction of **64** with *n*-butylamine at 20 mM, a ^{1}H NMR spectrum of this reaction taken after 1 hour shows no signals corresponding to the presence of **64** (cf. time interval at 4346 seconds (1.2 hours) in Figure 2.7). The expected increase in rate of the first nucleophilic displacement (for a secondary versus primary amine) coupled with a proposed reduction in the rate of the reaction of the mono-substituted intermediate **86** with any remaining **64** (cf. reaction of **72** with **64**) on steric grounds probably explains the high efficiency of the conversion of **64** to the quaternary amine **87**.

To summarise, the reaction of **64** with *n*-butylamine is contrary to that predicted by Anderson and Fleming, over 35 years ago, for reaction of the di-*N*-oxide counterpart (**27**) with methylamine. The observation that the reaction intermediates **72** and **86** prefer to undergo a cyclisation pathway raises questions regarding the formation of **56** from **27**. For example, if the proposed mechanism is correct, what factors contribute to the differential reactivities of intermediate **53** and intermediate **72**? It was therefore decided to study the reaction of 2,3-bis(bromomethyl)quinoxaline 1,4-dioxide (**27**) with *n*-butylamine with the same approach to investigate in further detail the proposed mechanism.

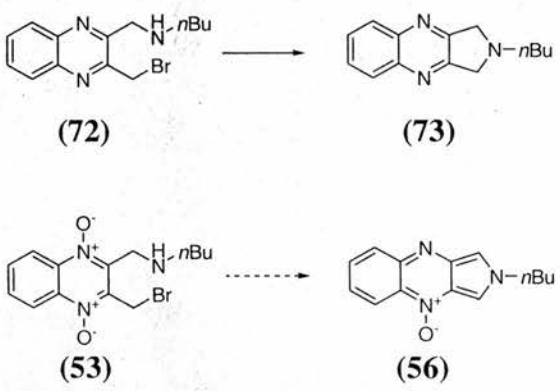

Scheme 2.12. Intermediate **72** has been observed to cyclise to give a major product **73**. If the mechanism proposed by Anderson and Fleming is correct, what role do the *N*-oxides in **53** have towards determining the product outcome?

2.4 Reaction of 2,3-Bis(Bromomethyl)quinoxaline 1,4-dioxide (27) with *n*-butylamine

The reaction of **27** with a nitrogen-based nucleophile became further intriguing following the results with **64**. Figure 2.12 shows a simplified representation of the analysis of the reaction of **27** with *n*-butylamine.

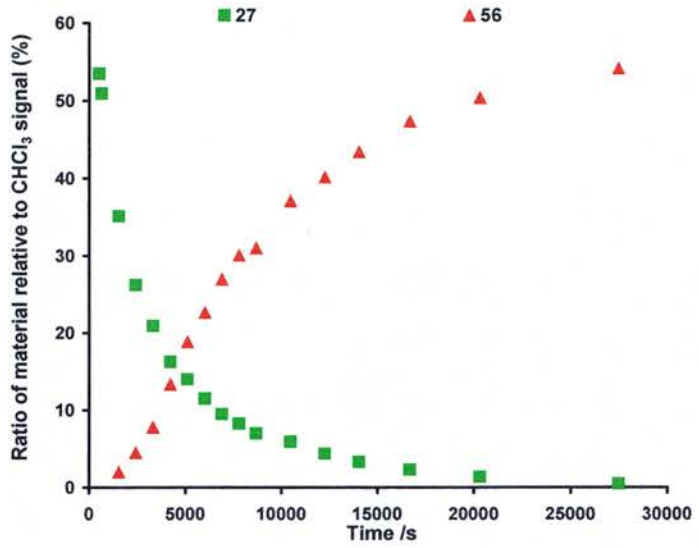

Figure 2.12. Relative abundance of **27** and **56** following reaction of **27** with *n*-butylamine. The sigmoidal shape of the curve for the formation of **56** indicates the presence of an intermediate(s) in the transformation of **27** to **56**. *Reagents and conditions:* (i) **27** (20 mM), *n*-butylamine (3 equiv.), $CDCl_3$, 25 °C.

The disappearance of ^{1}H NMR signals corresponding to **27** with concomitant formation of those associated with **56** was observed. **56** possessed characteristic ^{1}H NMR signals; two doublets at 7.67 and 7.61 ppm assigned to the new, non-equivalent, aromatic signals in the pyrrole ring and a triplet at 4.39 ppm corresponding to the NCH_2 group. When carried out on a preparative scale **56** was isolated following rapid column chromatography in a 90% yield as a dark red oil and was found to decompose rapidly in the absence of solvent in light and air.

Signals corresponding to several intermediates were also observed, but a detailed analysis became possible only when the experiment was repeated at a five-fold dilution (Figure 2.13). Unexpectedly, the reaction of **27** with *n*-butylamine showed that when the *N*-oxide functional groups are present a double nucleophilic substitution reaction utilising two equivalents of amine is preferred over the direct cyclisation pathway.

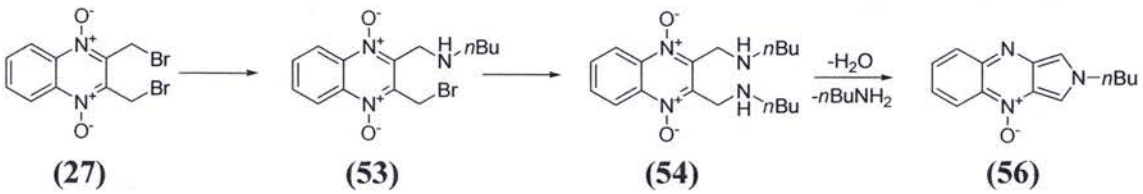

(27) **(53)** **(54)** **(56)**

Scheme 2.13. Reaction path A for the conversion of **27** to the extended aromatic product **56**.

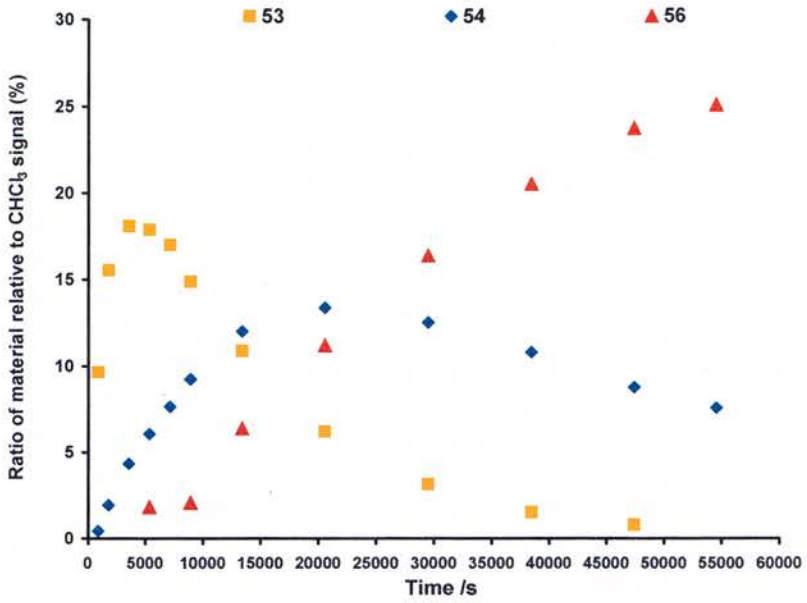

Figure 2.13. Tracking key intermediates **53** and **54** together with the major product **56** from reaction of **27** with *n*-butylamine. *Reagents and conditions:* (i) **27** (4 mM), *n*-butylamine (3 equiv.), $CDCl_3$, 25 °C.

The observed formation of signals corresponding to **53** followed by the delayed formation of **54** is consistent with the majority of **56** being formed by path A (Scheme 2.4 and 2.13). The fact that the ^{1}H NMR signals corresponding to formation of **54** increase whilst those corresponding to the presence of **53** are decreasing is also supportive of the proposed reaction mechanism. Integration and summation of key ^{1}H NMR signals associated with compounds **27**, **53**, **54** and **56** at intervals throughout the time course, indicate that these four compounds make up > 90% of the reaction mixture at all times.

The ^{1}H NMR spectra of **53** and **54** differ considerably in the aromatic region, where **53** has four signals and **54** has two signals, each one a characteristic part of an AA´XX´ system, consistent with their respective symmetry. In addition **53** has a signal at 4.99 ppm (singlet) for the CH_2Br, which is absent in **54** (singlet at 4.28 ppm, benzylic methylenes).

Attempts to isolate **53** by quenching the reaction with silica resulted in the isolation of the aldehyde **62**, the product of hydrolysis of the corresponding imine **90**. A question arose as to whether **62** was the active compound in the original biological screen. **62** was analysed in the assay and was found to have a lowest active concentration (LAC, see Chapter 3, Section 3.2) of 25 μM. Further analysis showed that reaction of **62** with substoichiometric equivalents of *n*-butylamine resulted in formation of the imine intermediate **90** (Scheme 2.14) that did not proceed through to **56**, as expected. This result

confirms further the requirement for 2 equivalents of an amine nucleophile to form the covalent adduct **56**. The reduced biological activity of **62** supports the role of **27** as the active small molecule for inhibition of invasion of *T. gondii*.

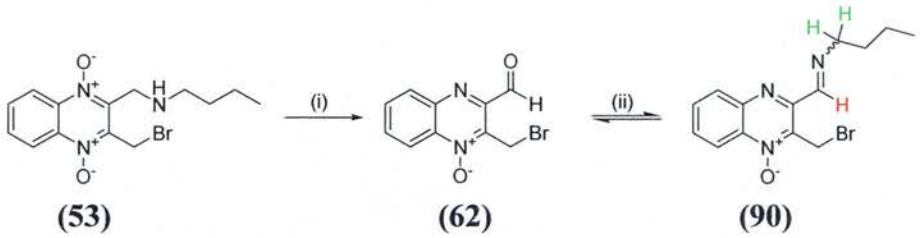

(53) **(62)** **(90)**

Scheme 2.14. Attempts to isolate **53** resulted in the purification of **62**. Subsequent reaction of **62** with substoichiometric equivalents of *n*-butylamine gave rise to the imine intermediate (**90**). *Reagents and conditions:* (i) *n*-butylamine (3 equiv.), $CHCl_3$, RT, 30 mins. (ii) *n*-butylamine (0.25 equiv.), $CDCl_3$, RT.

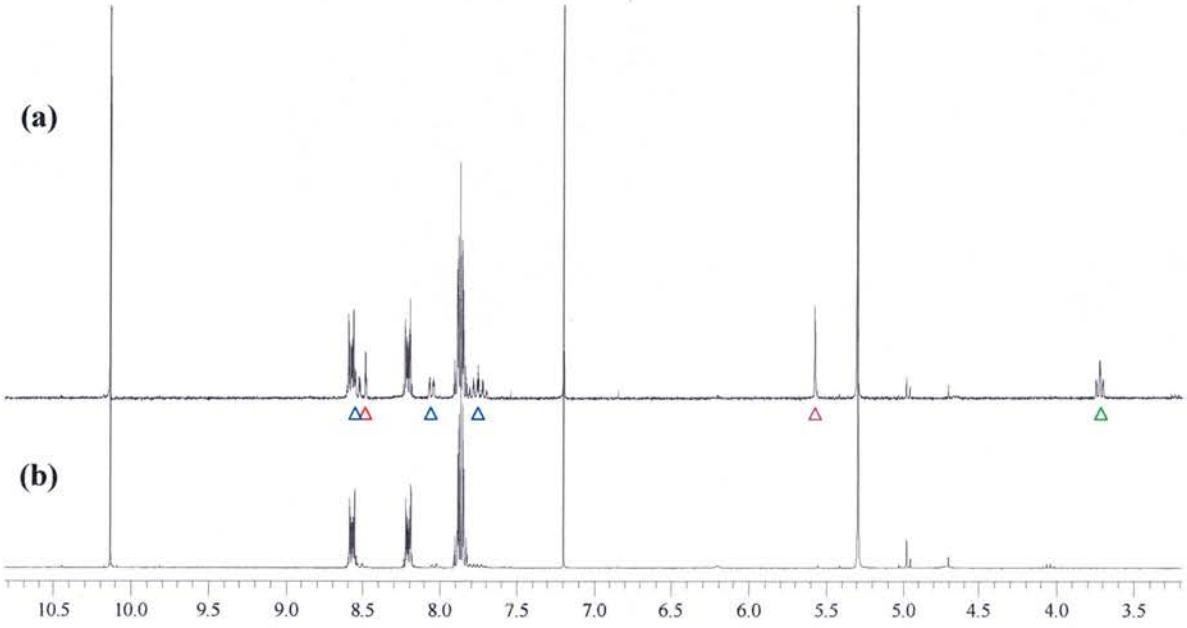

Figure 2.14. **(a)** ^{1}H NMR spectrum following reaction of **62** with substoichiometric equivalents of *n*-butylamine. Peaks corresponding to the imine intermediate **90** were observed: the unsymmetrical aromatic system (4H, blue triangle), imine proton (1H, red triangle), CH_2Br (purple triangle), and the NCH_2 (2H, green triangle). No peaks in the ^{1}H NMR corresponding to **56** were observed. **(b)** ^{1}H NMR of **62**.

Further analysis of the ^{1}H NMR for the reaction of **27** with *n*-butylamine identified **90** as a minor component of the reaction mixture. Whilst **90** could be converted to product **56**, it is believed that this was only a minor route.

These studies therefore provide the first direct experimental evidence in support of the mechanism for reaction of 27 that involves two equivalents of the amine nucleophile, as originally proposed by Anderson and Fleming (Scheme 2.4, path A). These experiments also rule out several alternative reaction mechanisms that could be drawn for the transformation of **27** to **56**. In particular, a mechanism that proceeds via the cyclised intermediate **57**, since no evidence (including for example, NMR resonances or isolated material) could be found for this intermediate.

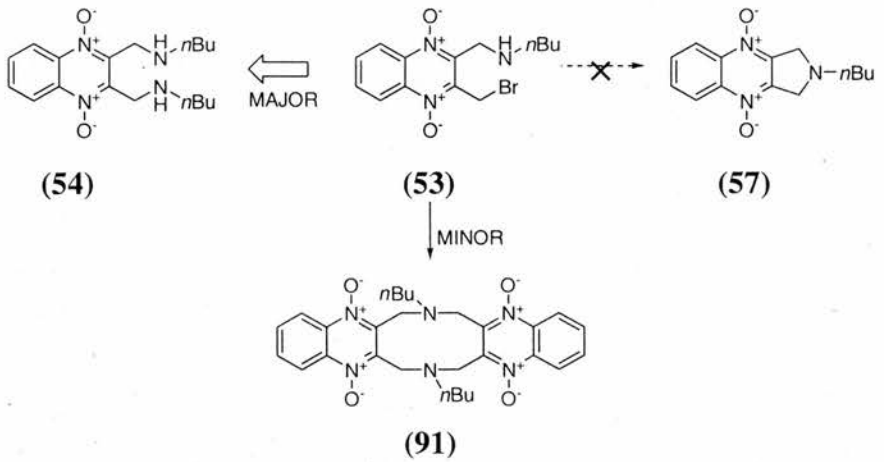

Scheme 2.15. A summary of the reaction pathways available to intermediate **53**.

2.5 Reaction of 2,3-Bis(Bromomethyl)quinoxaline 1,4-dioxide (27) with Diethylamine

Under analogous reaction conditions as previously used for **64**, compound **27** was reacted with diethylamine. In contrast to **64**, which gave almost exclusively the cyclised product, **27** prefers to undergo a double nucleophilic displacement using two equivalents of the amine, resulting in greater than 90% formation of the disubstituted product **93** (as judged by ^{1}H NMR analysis of the reaction mixture) (Scheme 2.16).

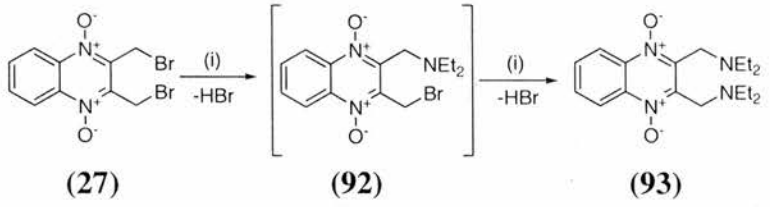

Scheme 2.16. Reaction of **27** with a secondary amine. *Reagents and conditions:* (i) diethylamine (4 equiv.), $CDCl_3$, 25 °C.

2.6 SUMMARY OF THE OBSERVED DIFFERENCES BETWEEN THE TWO SYSTEMS

Two different mechanistic pathways have been shown to be in operation for the reaction of **27** and **64** with primary or secondary amines. The differential reactivity occurs despite the fact that the only structural difference between the two substrates is the presence of *N*-oxide functionalities.

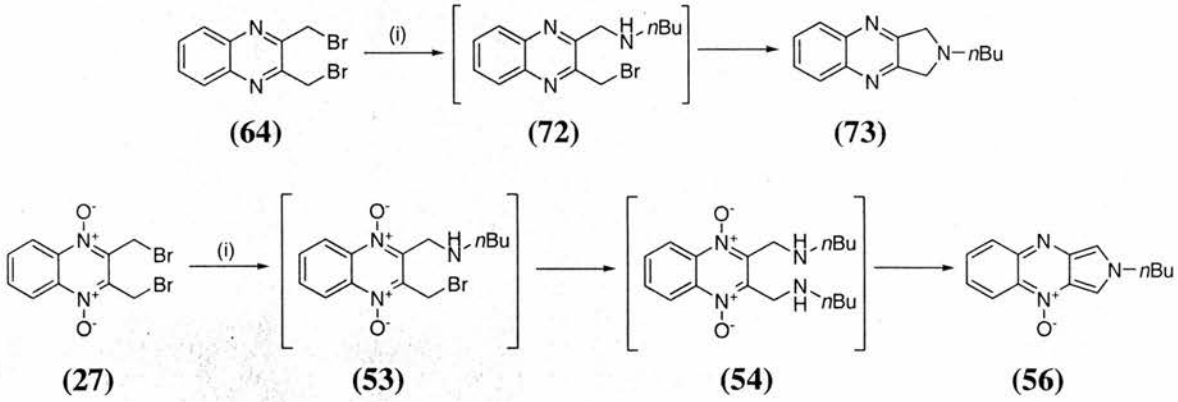

Scheme 2.17. A summary of the outcome of the reaction products of **64** and **27** with *n*-butylamine. *Reagents and conditions:* (i) *n*-butylamine (3 equiv.), $CDCl_3$, 25 °C.

Since in both scenarios the initial substitution remains the same, the question becomes, "how does the presence of the *N*-oxide cause the mono-substituted intermediates **53** and **72** to follow different pathways?" In order to explain the observed differences, several different avenues were explored and these will be discussed in turn.

2.7 RATIONALISATION OF THE OBSERVED REACTION

Several explanations were considered in order to explain the difference in reactivity between the quinoxaline, **64**, and its di-*N*-oxide equivalent, **27**. Two of these centred on the possibility that the secondary nitrogen atom in intermediate **53** cannot act as a nucleophile.

2.7.1 The Protonation State of the Amine

The first of these possibilities was the protonation state of the secondary amine in **53**. This possibility arises because 1 equivalent of HBr is produced in the substitution reaction. The option was ruled out based on the observed chemical shifts of the benzylic

methylene groups adjacent to the N atom in **53** (4.26 ppm for **53**; cf. 5.59 ppm for **87**, Figure 2.15).

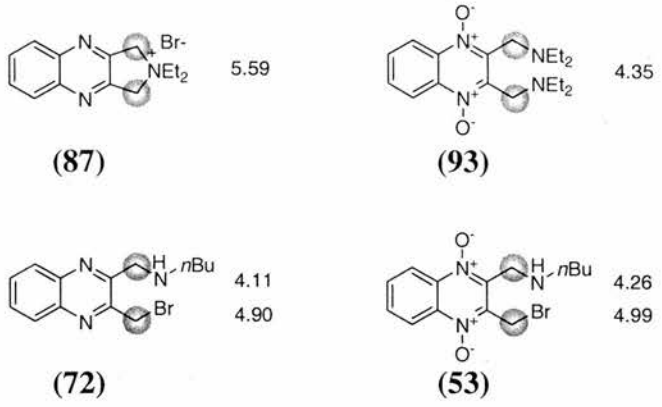

Figure 2.15. Relative ^{1}H NMR shifts of the benzylic methylene protons/ppm

2.7.2 Rate of Formation of the Imine

The second of the possibilities that would render the secondary nitrogen in **53** non-nucleophilic is that it is rapidly converted to the corresponding imine **90** and therefore cannot undergo a cyclisation reaction. In order to evaluate this theory, the unsymmetrical mono-brominated derivative (**94**) was synthesised. Due to the presence of only one bromine atom a second nucleophilic displacement reaction cannot occur and therefore the mechanism of reaction with *n*-butylamine according to Path A (Scheme 2.4) would not be expected to proceed further than the imine intermediate **96**. If conversion of **53** to the imine (**55**) were a fast process, then it would be expected that in the case of **94** reacting with *n*-butylamine, a rapid build of the imine **96** would be observed with the possibility that no signals corresponding to **95** would be present (Scheme 2.18).

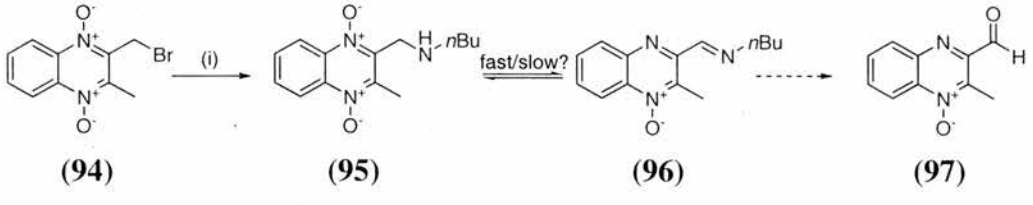

Scheme 2.18. If reaction of **94** to the imine **96** were a fast process the secondary nitrogen would be rendered non-nucleophilic and therefore unable to act as a nucleophile.

The synthesis of **94** began with the preparation of 1-bromobutane-2,3-dione (**99**). Of the few literature syntheses of **99**, Engel and Schieberle report in *J. Agric. Food Chem.* the bromination of butane-2,3-dione (**98**) using bromine.[114] Repetition of this procedure

yielded several brominated products therefore a more selective method for bromination was sought. Commercially available butane-2,3-dione (**98**) was treated with copper (II) bromide in chloroform. Catalytic 18-crown-6 was added to the reaction mixture to aid solubilisation of the copper (II) bromide (as a substitute for ethyl acetate) in a modification of a literature procedure.[115,116] The reaction was monitored by ^{1}H NMR and after 2.5 days heating at reflux and purification of the crude reaction, 1-bromobutane-2,3-dione (**99**) was obtained in an adequate yield. The synthesis then proceeded in an analogous manner to that for **27**, via cyclocondensation with *o*-phenylenediamine (**67**), and subsequent *N*-oxidation using *m*CPBA (Scheme 2.19).

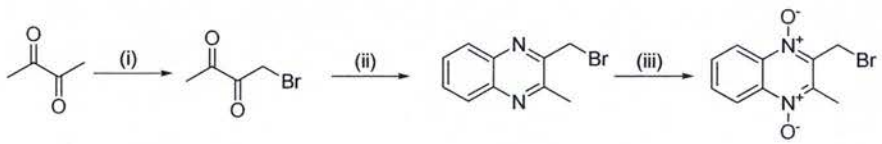

(98) **(99)** **(100)** **(94)**

Scheme 2.19. Synthesis of 2-(bromomethyl)-3-methylquinoxaline 1,4-dioxide (**94**). *Reagents and conditions:* (i) 18-crown-6 (cat), $CHCl_3$, reflux, 2.5 d, 37%; (ii) *o*-phenylenediamine (**67**) (1.05 equiv.), THF, 0 °C to RT, 17 h, 37%; (iii) *m*CPBA (5 equiv.), DCM, RT, 20 h, 50%.

To identify the rate of imine formation, the reaction of **94** with *n*-butylamine was studied in an analogous manner to that of **27** and **64.** The signals corresponding to **94**, the intermediates **95** and imine **96** (Scheme 2.18) were followed and their relative abundance is presented in Figure 2.16.

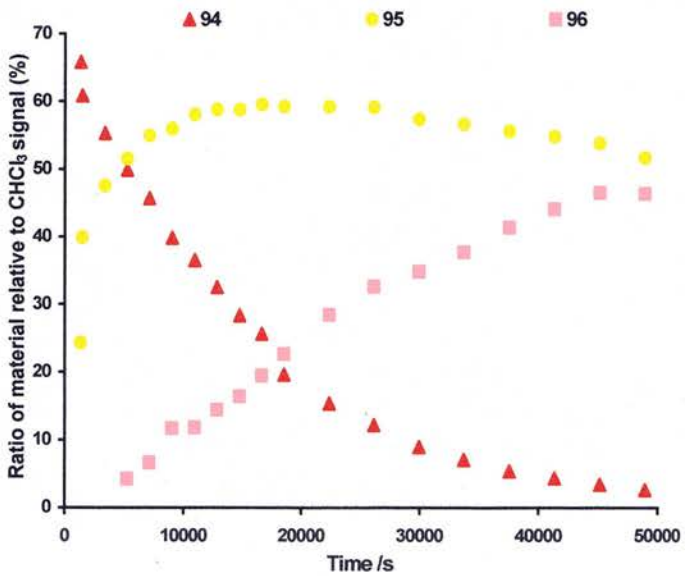

Figure 2.16. Relative abundance of **94**, **95** and **96** following reaction of **94** with *n*-butylamine. *Reagents and conditions:* (i) *n*-butylamine (3 equiv.), $CDCl_3$, 25 °C.

From the data presented in Figure 2.16 it was evident that there is only a small build up of imine **96** after 5244 s, despite **95** being the major material in the reaction mixture. The fact that **95** is observed in significant amounts indicates that the conversion to the imine **96** is relatively slow. Hydrolysis of **96** to aldehyde **97** is not observed over 17 hours. Whilst **94** to **95** is observed as a relatively fast transformation, the subsequent conversion of **95** to imine **96** is relatively slow (> 40 000 s, the decrease in **95** is approximately equal to the formation of **96**) under the reaction conditions and time scale used in these studies. In conclusion, there is no evidence to suggest that **95** (cf. **53**) is quickly converted to the corresponding imine in appreciable amounts. Thus the role of the *N*-oxide in controlling the reactivity of **27**, in the presence of primary and secondary amines, can not be explained by rapid imine formation.

2.7.3 X-ray Crystallographic Analysis

Samples of **27** and **64** were recrystallised to afford high quality crystals suitable for X-ray analysis in a further attempt to explain the differential reactivity of these two compounds.

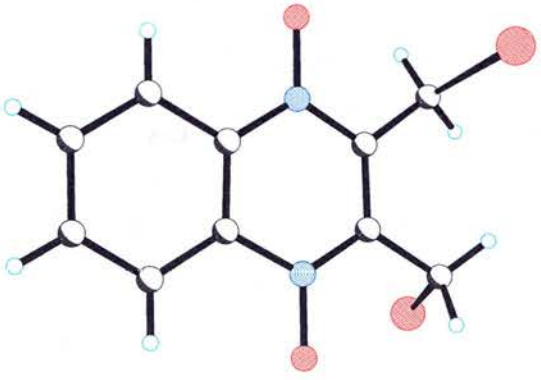

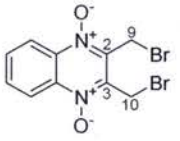

(27)

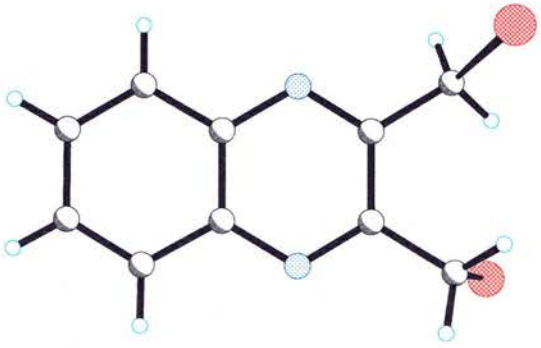

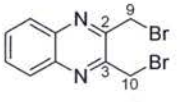

(64)

Figure 2.17. X-ray structure of **27** (top, yellow crystals) and **64** (bottom, colourless crystals). CDC numbers 255311 (**27**) and 255312 (**64**).

In both cases, in the solid state, the bromine atoms are located almost perpendicular to the plane of the quinoxaline ring system and on opposite faces. Based on the assumption that this is the preferred conformation in solution, the initial S_N2 displacement would result in both the secondary amine and the remaining bromomethylene group being on the same face. A rotation about the C(2)-C(9) and/or C(3)-C(10) bond must then occur as the transition state for cyclisation is approached (see later, Figure 1.8). To consider the possible influence of hydrogen-bonding capabilities from the solvent upon rotation, the studies were repeated in DMSO-d_6. The results showed that the major products and intermediates were as observed in $CDCl_3$ and no additional signals were observed, in particular that could correspond to the cyclised product **57**. It was concluded that hydrogen bonding interactions capable of restricting the required bond rotations are not important in determining the outcome of this reaction.[117]

It is interesting to note that the active site of an enzyme is often in a desolvated state. The exclusion of water means that a nucleophile in a desolvated environment would be more potent than its counterpart in aqueous solution. Organic reactions carried out in dipolar aprotic solvent such as DMSO or DMF provide an environment in which nucleophiles are not hydrogen bonded, close to that of an enzyme active site.[84] Consequently, the nucleophilic substitution was observed to occur more readily in DMSO-d_6 compared to $CDCl_3$.

2.7.4 Rationalisation Based on Computational Transition State Modelling

Computational modelling of the transition state (TS) in a reaction can provide structural information that is otherwise difficult to visualise. In a recent example TS modelling has been used in designing a catalyst that would stabilise the TS in an enolate forming reaction.[118]

To consider why, following the initial nucleophilic substitution reaction of **27** and **64** with *n*-butylamine to give **53** and **72** respectively, a different reaction pathway is observed, computational molecular modelling studies were carried out. These computational studies were therefore designed to visualise more effectively the transition states that would be required in order to undergo an S_N2-like cyclisation reaction for both

53 and **72**. In both cases a TS model was obtained (Figure 2.18). From the results of these studies several points of interest should be noted:

1. The electrostatic potential surface map for **53**‡ (Figure 5(b(ii))) illustrates the substantial build up of negative charge on the bromine atom, signifying a later TS (i.e. further along the reaction coordinate) compared to that for **72**.
2. The highly negatively charged bromine atom and the negatively charged *N*-oxide oxygen will repel one another.
3. For a cyclisation reaction to occur the approaching secondary amine in the TS is required to adopt an attack angle of greater than 160°. This is difficult in the case of **53**‡ (159.7° cf. 167.3° for **72**‡) because of the electrostatic repulsion and presumably a steric clash between the bromine and the *N*-oxide oxygen.
4. The repulsive forces between the bromine and the *N*-oxide oxygen result in significant puckering of the aromatic skeleton in **2a**‡ in which the bromine atom is forced to sit 57.8° out of the plane of the aromatic backbone. In contrast the aromatic backbone of **72**‡ is essentially planar and the leaving bromine atom lays only 29.6° out of the plane.
5. The envelope conformation adopted by the forming 5-membered ring is more distorted in **53**‡ than **72**‡. Evidence to support this is provided by the larger values for the dihedral angles in the envelope region for **53**‡.
6. As a result, the transition state for the cyclisation of **53** is more energetically demanding and hence disfavoured (and so, in reality, difficult to reach).[119] Consequently **53** prefers to undergo a second nucleophilic substitution reaction as opposed to the cyclisation mechanism observed for **72**.

Importantly, these calculations support the experimentally observed reactivity of **53** and **72**. Invoking an unfavorable electronic interaction between the *N*-oxide oxygen atom and the developing negative charge on the bromine atom in **53**‡ provides a concise explanation for the observed reaction paths (Scheme 2.15).

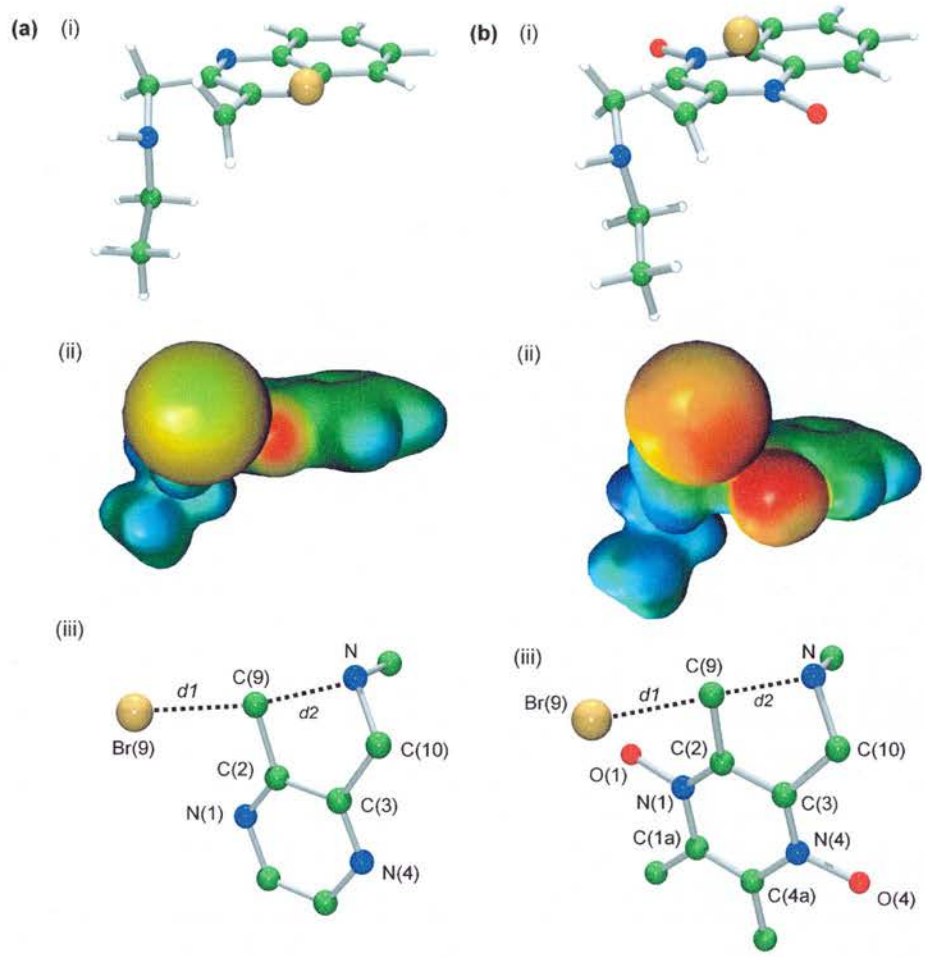

Bond length/angle	(a) $8^{\ddagger}$	(b) $2a^{\ddagger}$
Distance / Å		
d1	2.44	2.55
d2	2.08	2.11
Angle / °		
N-C(9)-Br(9) / °	167.3	159.7
Dihedral / °		
Envelope region		
C(9)-C(2)-C(3)-C(10)	-4.1	-13.1
N-C(9)-C(2)-C(3)	23.8	32.0
Br(9)-C(9)-C(2)-N	29.6	57.8
Ring system		
N(1)-C(2)-C(3)-N(4)	-2.6	-8.8
O(1)-N(1)-C(2)-C(9)	N/A	4.5
O(4)-N(4)-C(3)-C(10)	N/A	9.3

Figure 2.18. (HF/6-31G(d)), PCM Solvation model for $CHCl_3$ of (a) $\mathbf{72}^{\ddagger}$ and (b) $\mathbf{53}^{\ddagger}$. In each case, (i) illustrates the structure of the transition state for a cyclisation reaction, (ii) shows the electrostatic potential surface of the transition state (both (a) and (b) are plotted in the same scale) and (iii) provides a detailed view of the transition state geometry. Values of the parameters are provided in the table.

In summary, several possible explanations were investigated to rationalise the experimental differences in reactivity between **27** and **64** with amines. A conclusion was provided by a combination of NMR experiments, X-ray analysis and computational analysis of the relevant transition states. It was concluded that the presence of the *N*-oxide (**53**) determines the outcome of the reaction by forcing a structural distortion of the transition state relevant to an S_N2-like cyclisation reaction.

2.8 Reaction of 2,3-Bis(Bromomethyl)quinoxaline 1-oxide (69) with Diethylamine

An interesting prediction arises from our mechanistic explanation. Reaction of the unsymmetrical 2,3-bis(bromomethyl)quinoxaline 1-oxide (**69**) with diethylamine would be expected to proceed as follows: i) initial displacement of the bromine atom adjacent to the *N*-oxide functional group leads to product **102** via cyclisation; ii) initial displacement of the alternative bromine atom leads to the disubstituted product **104**. However, it is important to point out that that this prediction involves two assumptions: i) that formation of the mono-substituted intermediate **101** leads exclusively to **102** and ii) formation of the alternative intermediate **103** leads exclusively to **104**.

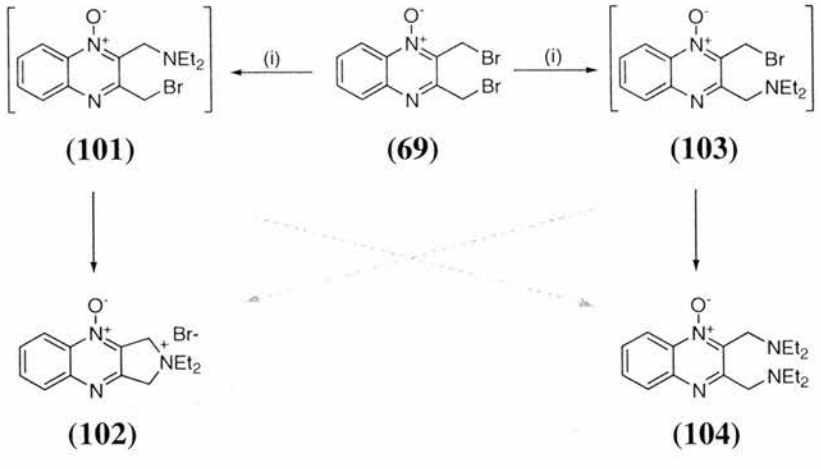

Scheme 2.20. The proposed reactivity of **69** with diethylamine.

To test this hypothesis, **69** was prepared from **64**, in an analogous manner to **27**, by favouring mono-*N*-oxidation using either 2.5 equivalents of *m*CPBA or decreasing reaction times (Section 2.1, Scheme 2.7). After purification by column chromatography **69** was isolated in 52% yield as a white crystalline solid. Mass spectrometric analysis of the

purified compound (**69**) showed the presence of a set of peaks consistent with the assignment for the mass plus sodium at *m/z* (ES) 357 [M^{81} + Na], 355 [$M^{81,79}$ + Na], and 353 [M^{79} + Na]. The ^{1}H NMR spectrum of **69** showed two signals, 5.02 and 4.77 ppm in $CDCl_3$, attributed to the non-equivalent CH_2Br moieties of which the lower field signal is assigned to the protons on C-9, adjacent to the *N*-oxide.

^{1}H NMR analysis of the reaction of **69** with diethylamine showed that two products, **102** and **104,** were formed (Scheme 2.21). The experimentally determined ratio of **102:104** was 63:37 based on ^{1}H NMR analysis of the reaction mixture. X-ray crystallographic analysis of **69** indicated that the carbon-bromine bond adjacent to the *N*-oxide functionality is the longer of the two (in the solid state, 1.976 Å vs 1.952 Å, Scheme 2.21) consistent with preferential nucleophilic attack adjacent to the *N*-oxide functionality (and hence preferential formation of **102**).

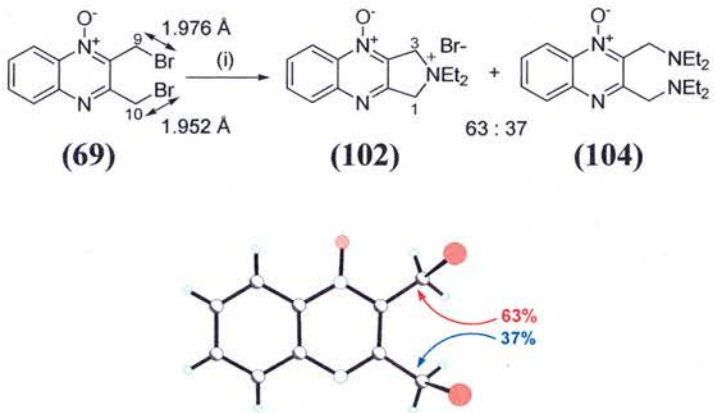

Scheme 2.21. Reaction of **69** (at 20 mM) with a secondary amine, diethylamine. *Reagents and conditions:* (i) diethylamine (4 equiv), $CDCl_3$, 25 °C, 50% yield (**101**). Insert: X-ray of **69** (colourless crystals). CDC number 255313. In contrast to **27** and **64**, **69** shows both bromine atoms aligned in the same plane.

^{1}H NMR of **102** was recorded in both $CDCl_3$ and D_2O. In an analogous manner to **87**, the signals corresponding to the benzylic methylene protons on C-1 and C-3 were no longer observed due to rapid proton-deuterium exchange. This was confirmed by the observation of two apparent quintets in the ^{13}C NMR acquired in D_2O coming into resonance at 62.0 and 65.7 ppm, corresponding to C-1 and C-3 respectively. The carbon shift was confirmed by a HSQC experiment in $CDCl_3$.

In light of the results for the reaction of 2,3-bis(bromomethyl)quinoxaline (**64**) with diethylamine, that showed that the disubstituted product **88** could be formed at high reaction concentrations, a concentration study for the reaction of **69** with diethylamine was also carried out. The results from this study were used to assess whether the initial assumptions used to predict the outcome for the reaction of **69** with diethylamine would hold. The reaction was performed at five different concentrations and the results are presented in Figure 2.19.

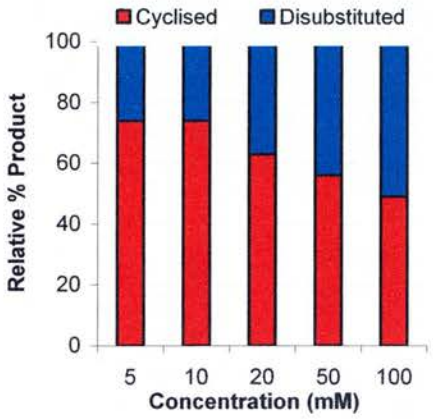

Figure 2.19. Concentration dependence observed for the reaction of **69** with diethylamine. *Reagents and conditions:* (i) **69** (1 equiv.), diethylamine (4 equiv), $CDCl_3$ (1 mL), 25 °C, 24 h.

In order to interpret the results from this study, one further assumption has been made. That is, the relative ratio of attack at C-9 and C-10 is independent of the reaction concentration. The results in Figure 2.19 then highlight three main points of interest.

1. At reaction concentrations of 20 mM and above, the formation of the disubstituted product (**104**) increases, in an analogous manner to that previously observed for **64**. This result argues that following an initial substitution reaction at C-9, intermediate **101**, can form either **102** or **104**. Therefore assumption i) does not hold at high reaction concentrations, i.e. the product ratio does not reflect the relative ratio of attack on C-9:C-10.
2. At 5 and 10 mM the ratio of products **102**:**104** was observed to be 76:24 in both cases. This plateau in the observed product ratio therefore indicates that the reaction is operating in a situation where both assumptions i) and ii) hold. To confirm further this result the reaction was carried out at 2 mM however incomplete reaction prevented adequate ^{1}H NMR analysis. However, it is believed that this product outcome is a true reflection of the preference for diethylamine to initially attack C-9 as opposed to C-10. Importantly, this suggests that there is no concentration at which

103 undergoes a cyclisation reaction. This observation further substantiates the results obtained from the previously discussed molecular modelling studies (Section 2.7.4) and is discussed further in Chapter 3.

3. These results highlighted that although the initial experiment at 20 mM indicated the correct preferred site of nucleophilic attack to be at C-9 the observed product ratio was not a true reflection of the ratio of initial attack of the nucleophile at C-9 and C-10. A more accurate value for this ratio would have been obtained if the reaction had been performed at a concentration of less than 10 mM, and would therefore be 76:24.

2.9 Reaction of 2,3-Bis(Bromomethyl)quinoxaline 1-oxide (69) with *n*-butylamine

Analogous results were obtained from the reaction of **69** with *n*-butylamine. In this case, four products were formed (Scheme 2.22). Compounds **105**, **106** and **107** probably result from initial attack at C-9, adjacent to the *N*-oxide functionality, by the amine nucleophile (Scheme 2.21). The remaining product **75** is the product resulting from initial displacement of the alternative bromine atom on C-10 via a mechanism analogous to path A, Scheme 2.4. The experimentally determined ratio of **75**:**105**:**106+107** was 35:51:14 giving a ratio of **105+106+107**:**75** of 65:35 which compares favourably with the observed ratio of **102**:**104** (63:37) formed on reaction of **69** with diethylamine at 20 mM (Scheme 2.21). The observed experimental data on the reaction of **69** with amines can therefore be rationalised based on our computational model findings (Section 2.7.4).

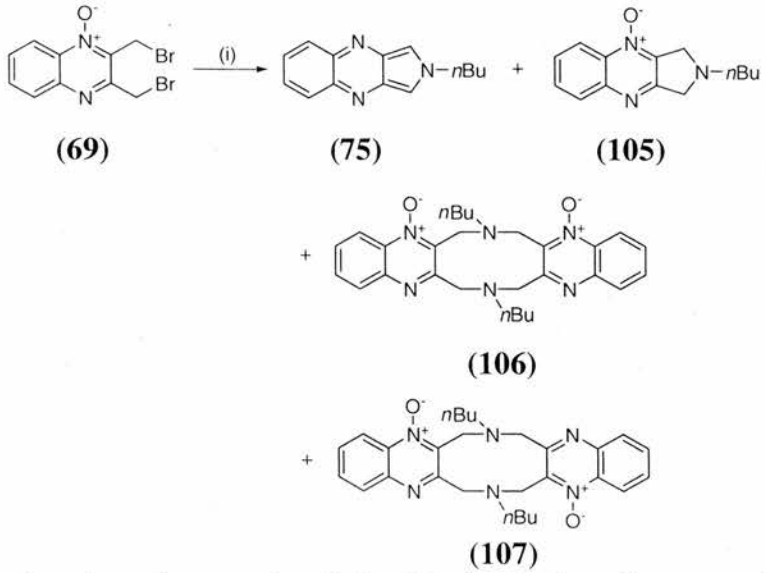

(69) **(75)** **(105)**

(106)

(107)

Scheme 2.22. Products formed on reaction of **69** with *n*-butylamine. Reagents and conditions: (i) *n*-butylamine (3 equiv.), $CDCl_3$, 25 °C.

2.10 THE REACTION OF 27 WITH A WATER-SOLUBLE PRIMARY AMINE

To assess the reaction of **27** with primary amines under more physiologically relevant conditions, an aqueous soluble analogue of **27** was required. However, attempts to synthesise a water-soluble derivative were unsuccessful (data not shown). A solution to this was to react **27** in 15% DMSO:D_2O with a water-soluble amine, 4-(3-aminopropyl)morpholine (**108**). **27** only had limited solubility in this solvent system preventing detailed analysis by ^1H NMR, however characteristic aromatic resonances corresponding to H-1 (7.88 ppm) and H-3 (7.99 ppm) in **109** were observed. Further analysis by LC-MS provided evidence for the formation of **109** (Figure 2.20).

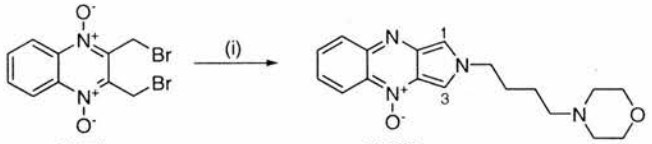

(27) **(109)**

Scheme 2.23. **27** was observed to form an analogous product to **56** when reacted with a water-soluble amine. *Reagents and conditions:* (i) 4-(3-aminopropyl)morpholine (**108**), 15% v/v DMSO:D_2O, RT.

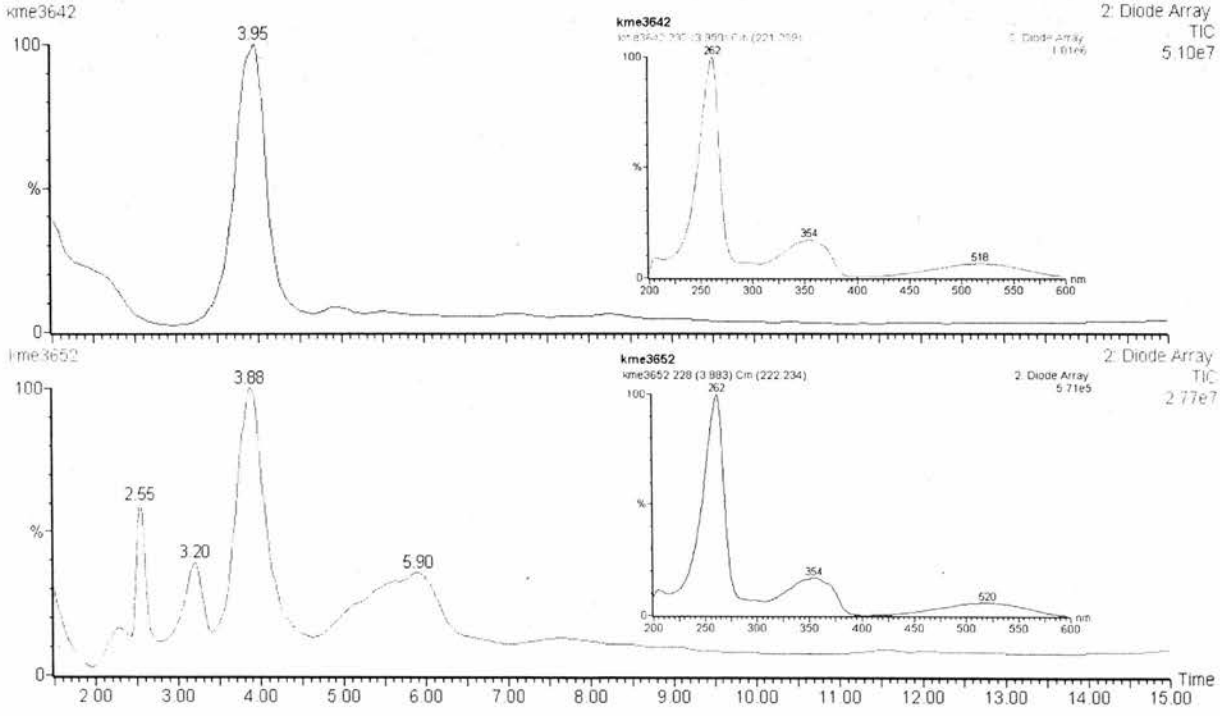

Figure 2.20. LC-MS trace resulting from reaction of **27** with 4-(3-aminopropyl)morpholine (**108**) performed in i) $CDCl_3$ and transferred into 15% DMSO:D_2O (top) and ii) 15% DMSO:D_2O (bottom). Insert UV spectrum of the major peak at 3.95 mins. (top) and 3.88 mins. (bottom). The peaks at 3.95 and 3.88 mins. correspond to the same compound by mass spectrometric and UV analysis.

3.0 CONCLUSION

This study was designed to clarify the mechanism of reaction of **27** with primary amines. The ^{1}H NMR studies using *n*-butylamine (a mimic of a nitrogen-based protein nucleophile) provide the first experimental evidence in support of a reaction pathway for **27** that involves two equivalents of the amine (Scheme 2.4, path A). In addition, computational techniques coupled with X-ray crystallographic studies have provided a rationalisation for the differential reactivity of **27**, **64** and **69** with amines. These studies also provide a clear explanation of the influence of the *N*-oxide functional group.

These studies also raise the intriguing possibility that two nucleophilic residues in close proximity are required for irreversible modification of a protein by **27**. Several examples already exist of small molecules that covalently modify two residues within the same protein.[120-122]

Whilst reaction of **27** with nitrogen-based protein nucleophiles may not ultimately prove to be the mechanism of action of **27** on *T. gondii* invasion, these studies clearly highlight one plausible mechanism. A deep understanding of the mechanism of action of **27** is necessary in an integrated approach towards protein target identification and unravelling its biological mode of action. Information extracted from these results has a direct inference in the design of a chemical proteomics probe based on **27**, which is the subject of Chapters 3 and 4.

CHAPTER 3

SUBSTITUENT EFFECTS UPON THE REACTIVITY OF 2,3-BIS(BROMOMETHYL)QUINOXALINE DERIVATIVES WITH AMINES

1.0 INTRODUCTION

As discussed in Chapter 2, the interesting chemical reactivity of **27** with primary amines may be related to the biological mechanism of action of **27**. In particular, the observation that **27** reacts with a water soluble primary amine in 15% DMSO:D_2O to form the heteroaromatic compound **109** (Scheme 2.23) suggests that the studies presented in $CDCl_3$ may well be of relevance to the mode of action. However, at this early stage of this long-term chemical biology project it is difficult to justify an explanation for the biological activity that focuses only on nitrogen-based protein nucleophiles as opposed to those based on sulfur. A decision was therefore taken to focus on the preparation of an affinity-based reagent based on **27** for its application towards identifying a protein target(s) for **27**. In the remainder of this thesis, the results from these studies have been split into two categories: i) the synthetic modification of **27** required to accommodate the required linker unit and tag for the preparation of an affinity reagent (see Chapter 1, Section 1.2.2) and what effect the necessary chemical modification has on the observed chemical reactivity with amines in $CDCl_3$ (Chapter 3) and ii) the synthesis and application of an affinity reagent based on **27** (Chapter 4). There is a deliberate effort to avoid linking the chemical results obtained from these studies to any speculation about the biological mode of action of **27** as at present there is insufficient experimental data to connect the two. Whilst Chapters 3 and 4 may be closely related, care has been taken to separate the two issues for the purpose of this thesis.

2.0 IDENTIFYING A SUITABLE ATTACHMENT SITE

Chemical probes that are of relevance to both target identification and chemical proteomics are usually comprised of a reactive functional group linked through a spacing unit to a label, tag or matrix (for use as part of the purification technique, Chapter 1). It is a well-known phenomenon that the attachment of a small molecule ligand to a solid support (e.g. an affinity matrix) or chemical derivatisation can result in its diminished biological activity.[123] Therefore, in order to prepare an affinity reagent based on **27** it was

necessary to identify a suitable attachment site in the original compound to enable incorporation of a marker, for example a biotin tag, without loss of the required biological activity. An additional challenge in this design is the fact that the chemistry used in conjunction with the attachment site must be orthogonal to all the chemical functionality present in the active compound.

The structure of **27** limits the choice of attachment site to the C-6/7 and C-5/8 positions, substitution at either of which renders the two electrophilic centres (C-9 and C-10) in the resulting analogue non-equivalent. In addition, the chemistry involved in attaching a chemical tag provides a significant challenge in the case of **27** due to the apparent incompatibility with a nitrogen nucleophile. Despite these concerns, compound **110** was selected as an initial synthetic target in order to assess whether attachment of a group at the C-6/7 position in **27** significantly reduced the activity of compounds of this type. Since aniline has been shown to be less reactive (less nucleophilic) towards benzylbromide than several amines, including *n*-butylamine (see later, Figure 3.13),[124] derivatisation following *N*-Boc deprotection, was planned through the moderately reactive aniline NH_2 group.

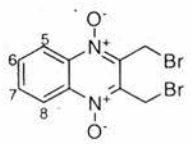

(27)

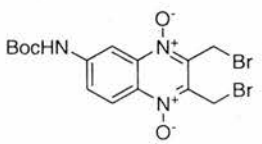

(110)

Figure 3.1. The chemical structure of **110**. **110** was selected as an initial synthetic target to assess whether attachment of a functional group in the C-6 position would retain biological activity.

2.1 SYNTHESIS OF *tert*-BUTYL 2,3-BIS(BROMOMETHYL)QUINOXALIN-6-YLCARBAMATE 1,4-DIOXIDE, (110)

Mono *N*-Boc protection of commercially available 2-nitro-*p*-phenylenediamine **(111)** occurred selectively at the 4-amino group in accordance with literature precedent.[125] **112** was obtained in quantitative yield without the requirement for flash column chromatography and the purity was confirmed by elemental analysis. The nitro functional group was then reduced using hydrogen in the presence of 10% palladium on charcoal to give diamine **113** in high yield (Scheme 3.1). A cyclocondensation reaction of **113** with 1,4-dibromo-2,3-butanedione resulted in formation of *N*-Boc-protected quinoxaline **114**,

which was subsequently converted to the desired di-*N*-oxide **110** using *m*CPBA as previously described (Chapter 2). Mass spectrometric analysis for **110** showed the presence of three peaks, consistent with the presence of two bromine atoms at *m/z* units 464, 462, and 460 corresponding to $[M - H]^-$ as is to be expected for the ^{81}Br and ^{79}Br isotope pattern in a dibrominated species.

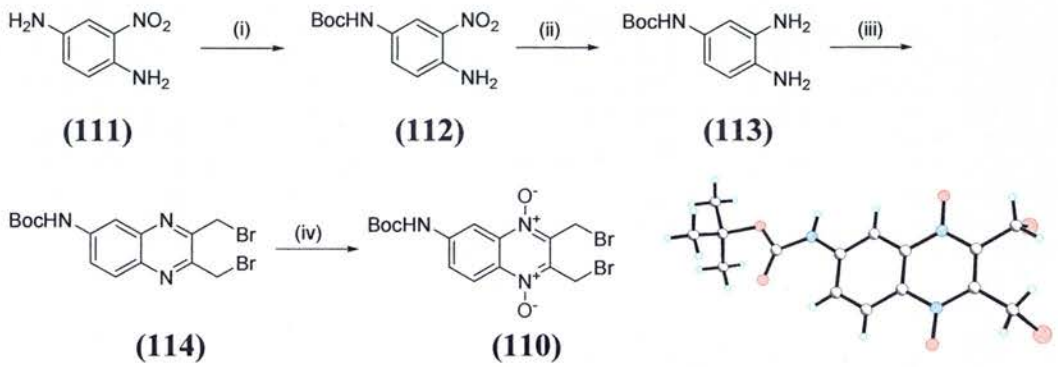

Scheme 3.1. Synthesis of an NHBoc containing derivative **110**. The NHBoc group is envisaged to provide a 'handle' for subsequent derivatisation. *Reagents and conditions:* (i) Boc anhydride (1.1 equiv.), DCM, RT, 2 d, quant.; (ii) H_2, 10% Pd/C, MeOH, RT, 24 h, 99%; (iii) 1,4-dibromo-2,3-butanedione (1.05 equiv.), THF, 0 °C to RT, 17 h, 89%; (iv) *m*CPBA (5.0 equiv.), DCM, RT, 42 h, 80%. Insert: X-ray crystal structure of **110** (bright yellow crystals).

Sufficiently high quality crystals of the 6-NHBoc-containing analogue **110** were successfully prepared to enable X-ray analysis (Figure 3.2). Figure 3.2 shows an intramolecular H-bond between the oxygen atom of the *N*-oxide functional group O(4A) and the hydrogen H(N6) of the NHBoc group of an adjacent molecule (in the solid state).

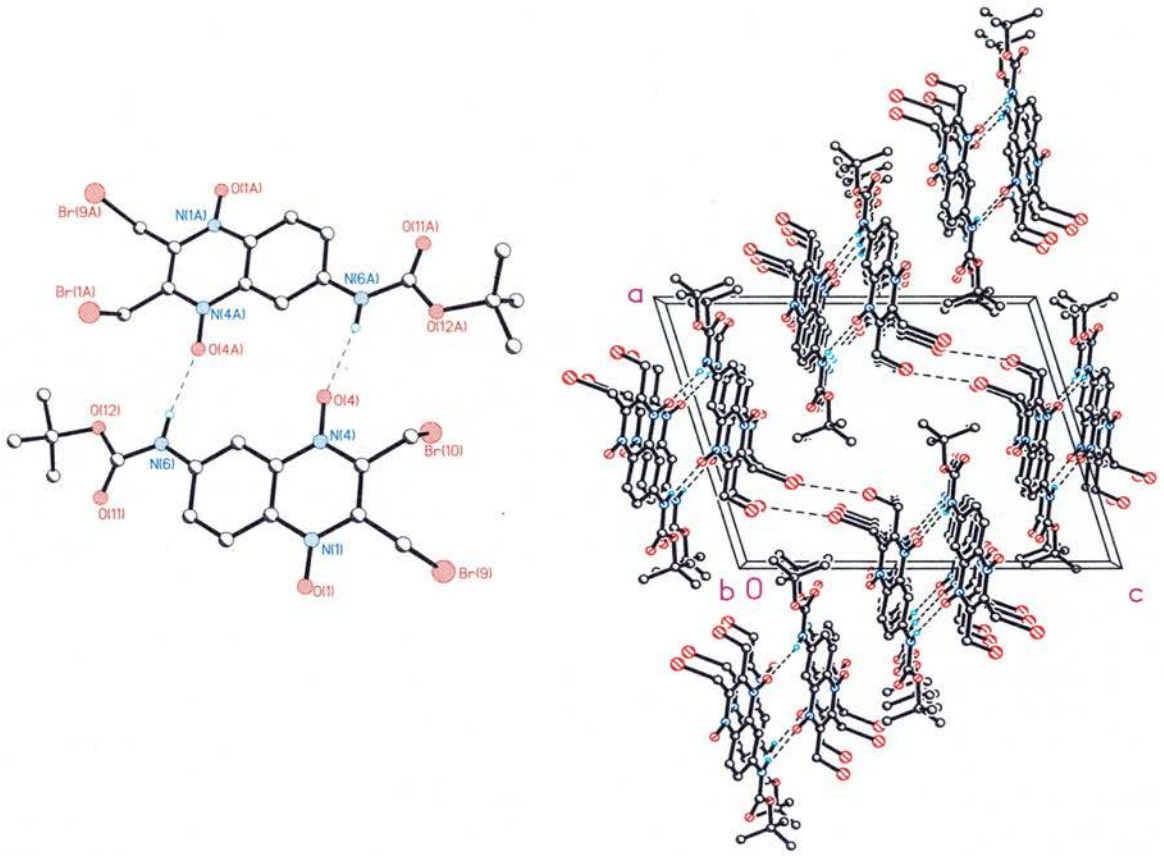

Figure 3.2. Intermolecular hydrogen-bonding between the hydrogen atoms from the 6-Nitrogen and the 4-Oxygen in **110**.

Assessment of the biological activity of **110** in the *T.gondii* invasion assay showed that whilst less active than **27**, **110** still retained the desired activity (LAC = 25 μM for **110** compared with 12.5 μM for **27**). Amongst several possible explanations (e.g. bioavailability), the observed difference in potency may result from a change in the chemical reactivity of **110** compared with **27**. Synthesis of **110** required modification of the initial bioactive compound **27** in such a way that rendered the two bromine atoms no longer equivalent. This was interesting because it introduced a regioisomeric question into our mechanistic studies. Close structural analogues of **27** (**115-120**, Figure 3.3), most of which are unsymmetrical, have also been reported in the literature to exhibit antibacterial activity.[126] In this study the authors observe "some dependence of the biological action of these compounds (quinoxaline 1,4-dioxides, **116** was not tested) on the type of substituent". It was also noted that only the derivatives with an unsymmetrical structure, having different substituents at the 6 and 7 positions (X and Y), exhibit activity against Gram-positive bacteria. However, no rationalisation as to why this was the case or reference to their biological mode of action was discussed. Therefore, it was decided to

compare the mechanism of reaction of **110** with *n*-butylamine using ^{1}H NMR techniques in an analogous manner to our previous studies using **27** (Chapter 2).[81] These studies were carried out using an initial concentration of **110** of 20 mM and *n*-butylamine 60 mM in neutral $CDCl_3$ at 25 °C. Spectra were acquired at regular time points over 17 hours using 500 MHz ^{1}H NMR spectroscopy.

Compound	X	Y
115	Cl	Cl
116	Cl	$N(CH_2CH_2)_2NMe$
117	Cl	$N(CH_2CH_2)_2O$
118	F	Cl
119	F	F
120	OEt	Cl

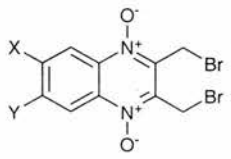

(27) X = Y = H

Figure 3.3. Structures of **27** and analogues **115**-**120** which are reported to show anti-bacterial activity.[126]

2.2 Reaction of *tert*-Butyl 2,3-bis(bromomethyl)quinoxalin-6-ylcarbamate 1,4-dioxide (110) with *n*-butylamine

The disappearance of ^{1}H NMR signals attributed to **110** occurred significantly faster (t = 7000 s, Figure 3.4) than for **27** (t = 28 000 s) consistent with an increase in the rate of the first nucleophilic displacement reaction (step 1, Scheme 3.2). The C(6)NHBoc substituent would be expected to promote nucleophilic attack at the C-9 position through increased stabilisation of any developing positive charge at C-9. However, attempts to provide evidence in support of an initial regioselective formation of **121** (cf. **122**, Figure 3.5) on reaction of *n*-butylamine with **110** proved difficult due to the complexity of the ^{1}H NMR spectrum at early time points.

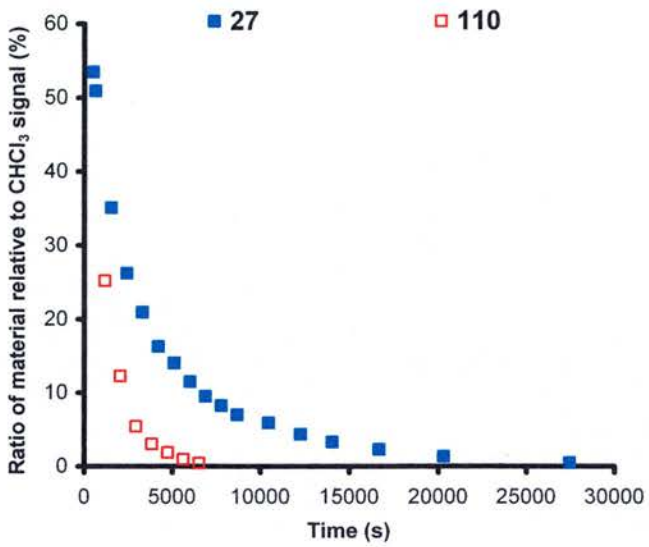

Figure 3.4. Comparison of the initial displacement reaction of **27** compared to **110** by *n*-butylamine. Data compared by extrapolation back to Y-axis when X = 0 to correct for $CHCl_3$.

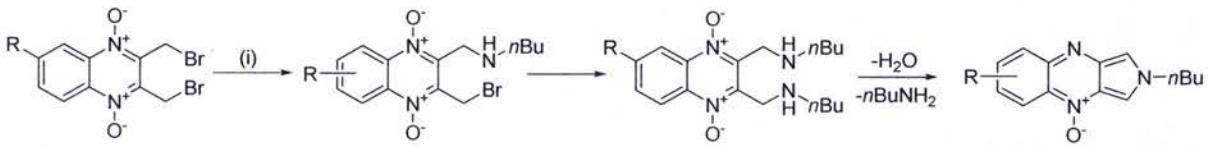

(27) **(110)** **(53)** **(121)/(122)** **(54)** **(123)** **(56)** **(124)/(125)**

Scheme 3.2. Reaction of **110** (R = H) and **27** (R = NHBoc) with an excess of a primary amine, *n*-butylamine. *Reagents and conditions:* *n*-butylamine (3 equiv.), $CDCl_3$, 25 °C.

The relatively fast consumption of **110** through reaction with *n*-butylamine results in a significantly different reaction profile for intermediate **121/122** compared with that for **53** (Figures 3.5 and 3.6). Whilst both curves reach maxima at approximately the same time (t = 1200 and 1500 s respectively), at t = 10 000 s intermediate **121/122** is present in only trace quantities whereas there remains a significant amount of **53**. This indicates that both the first and second displacement reactions are faster as a function of the electron-donating ability of the NHBoc substituent.

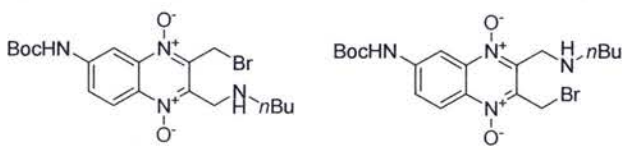

(121) **(122)**

Figure 3.5. The chemical structures resulting from regioselective attack by *n*-butylamine on either C-9 (**121**) or C-10 (**122**) of **110**.

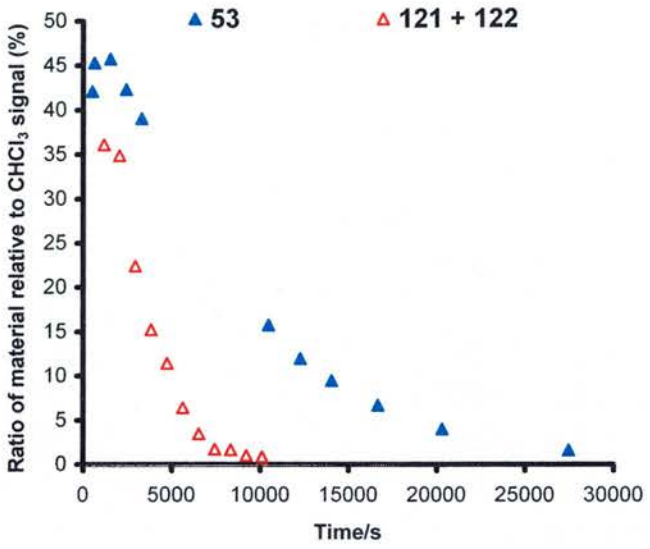

Figure 3.6. Comparison of the relative concentration of the monosubstituted intermediates in the reactions of **27** and **110** with *n*-butylamine. Data compared by extrapolation back to Y-axis when X = 0 to correct for $CHCl_3$.

The reaction profiles for **123** and **54** (Figure 3.7), whilst more difficult to interpret in detail, support another key difference between these two systems, the fact that **54** forms product **56** more rapidly than **123** forms products **124/125** (the sum of these two products is shown in Figure 3.8; see Scheme 3.4 for structures). For example, at t = 14 000s (Figure 3.8), the rate of production of **56** and **124/125** are approximately the same (see Appendix) despite the fact that the concentration of **54** is only 70% of that for **123**. The similarity in the overall rate of product formation suggests that the rate of imine formation for **54** is faster than that for **123**.

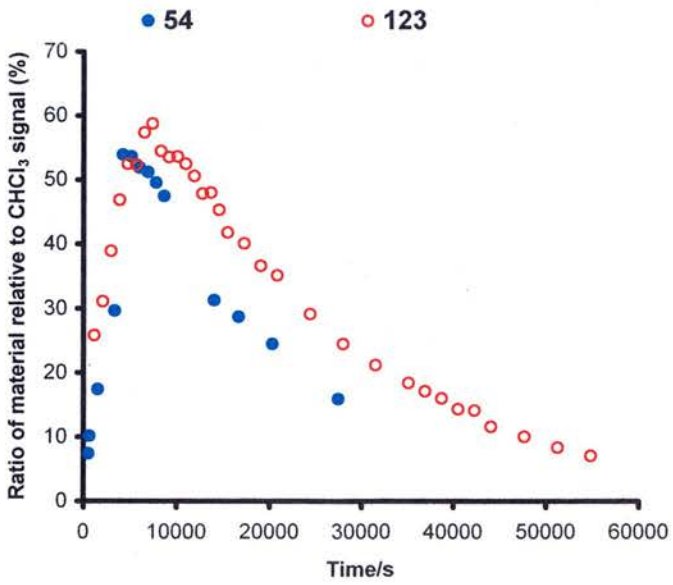

Figure 3.7. Comparison of the disappearance of the disubstituted intermediates **54** and **123**. Data compared by extrapolation back to Y-axis when X = 0 to correct for $CHCl_3$.

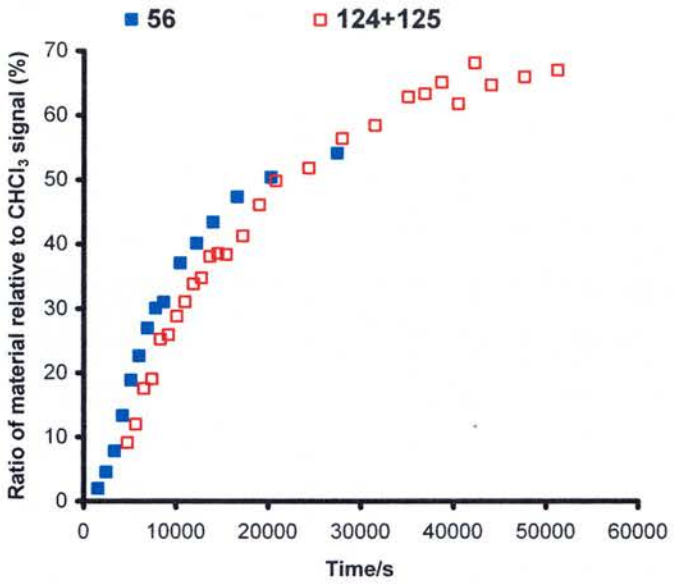

Figure 3.8. Total product formation in the reactions of **27** and **110** with *n*-butylamine. Between t = 7800 and 24 500 s the rate of total product formation is similar based on the calculated gradient (see Appendix). Data compared by extrapolation back to Y-axis when X = 0 to correct for $CHCl_3$.

In brief, whilst several differences between the reaction of **110** and **27** with *n*-butylamine in $CDCl_3$ have been identified, these ^1H NMR studies showed that the underlying reaction mechanism for both compounds is the same.

2.3 Diels Alder 1,3 cycloaddition reactions of pyrrolo[3,4-*b*]quinoxaline derivatives

As discussed above, the presence of a substituent at the C-6 position in **110** renders the two CH_2Br groups functionally distinct. In addition to the possibility of forming isomers **121** and **122** in the initial nucleophilic displacement reaction, two regioisomeric products, **124** and **125**, can also be formed (Scheme 3.4). Careful analysis of the ^1H NMR spectrum of the crude reaction mixture showed that the final ratio of **124**:**125** was 77:23. However, attempts to isolate **124** and **125** proved difficult due to their limited stability in the presence of air and light. This was not surprising in light of their extended *o*-quinonoidal structure.[106]

The *o*-quinonoidal system of isoindoles (bicyclic, benzo[*c*] heterocycles) and analogues containing a heteroatom are well known to undergo cycloadditions with dienophiles across the 1,3-positions.[127,128] This chemistry is also known for tricyclic

aromatic systems (naphtho[2,3-*c*] heterocycles, Scheme 3.3) for which the chemical behaviour is not significantly altered by insertion of a heteroatom (e.g. N) at the 4 and 9 positions (pyrrolo[3,4-*b*]quinoxalines, Scheme 3.3).[111] Haddadin *et al.* report the synthesis of the *endo* Diels Alder adduct **127** from reaction of **126** with *N*-phenylmaleimide (**130**). The electron withdrawing nature of the ring nitrogens on the diene was used to rationalise the observed sluggishness of the diene in the Diels Alder reaction (Scheme 3.3).[129] No analogous reaction is known for pyrrolo[3,4-*b*]quinoxaline derivatives containing an *N*-4/9-oxide. In order to provide further analytical evidence in support of the structures of **124** and **125**, it was decided to convert them to the corresponding Diels-Alder adducts by reaction with *N*-phenylmaleimide (**130**) (Scheme 3.4).

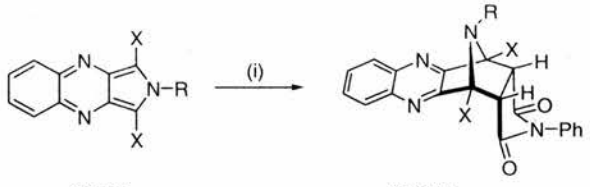

(126) **(127)**
(128) **(129)**

Scheme 3.3. Pyrrolo[3,4-*b*]quinoxaline heterocycles have previously been trapped as their corresponding *endo* Diels Alder adducts using *N*-phenylmaleimide (**130**). *Reagents and conditions:* **126/127** X = Ph, R = CH_3: **130** (1 equiv.), benzene, RT, 5h;[129] **128/129** X = H, R = *t*-butyl: **130**, RT.[111]

The dienophile, *N*-phenylmaleimide (**130**) (4 equiv.), was added to the reaction mixture in degassed $CHCl_3$ at 25 °C, at t = 12 600 seconds. This time point was selected as it corresponded to the point in the reaction profile at which **121/122** had been fully converted to **123** hence limiting the amount of *n*-butylamine available for undesired reaction with the dienophile (Figure 3.6).

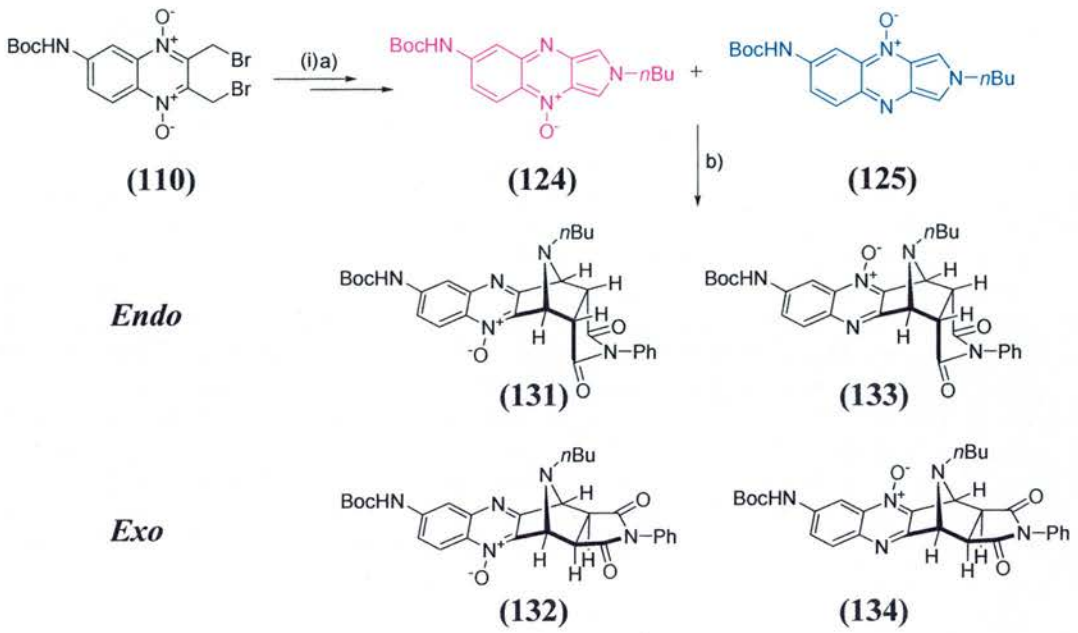

Scheme 3.4. Trapping of **124** and **125** in a Diels Alder reaction with *N*-phenylmaleimide. *Reagents and conditions:* (i) a) *n*-butylamine (3 equiv.), $CHCl_3$, RT, 3.5 h; b) *N*-phenylmaleimide (4 equiv.), RT, 14 h. Isolated 36% (**131/133**), 18% (**132/134**).

The reaction of **124/125** with *N*-phenylmaleimide led to the formation of the four possible isomers **131-134** (Scheme 3.4). The *endo*-adducts **131/133** were readily separated from the *exo*-adducts **132/134** by column chromatography. As expected, the *endo*-isomers were formed preferentially over the *exo*-isomers (*endo*:*exo* 36% yield:18% yield, a ratio of 67:33).

Endo and *exo* stereochemistry can be assigned based on the coupling constants of the bridgehead protons, H-9/H-15, to their *endo*/*exo* neighbouring protons H-10/H-14 respectively. The relationship between the dihedral angle (e.g. H–C9–C10–H) and the vicinal coupling coupling constant ^3J is given theoretically by the Karplus equation (Figure 3.9).[130,131] As expected, the ^{1}H NMR of the *endo* isomers ($\phi \sim 40°$) shows a coupled signal for H-9 and H-15 whereas the splitting observed in the signal corresponding to these protons in the *exo* isomers is reduced to a negligable value and the resonances appear as singlets (Figure 3.9). In all four isomers, the bridgehead protons, H-9/H-15, experience deshielding to different degrees by the quinoxaline ring (due to the presence of the single *N*-oxide) and therefore appear as two signals.

$$\text{Karplus equation}: {}^{3}J = \theta\cos^{2}\phi - 0.28$$

$$\theta = 8.5\ (0^{\circ} \leq \phi \leq 90^{\circ}) \text{ or } 9.5\ (90^{\circ} \leq \phi \leq 180^{\circ})$$

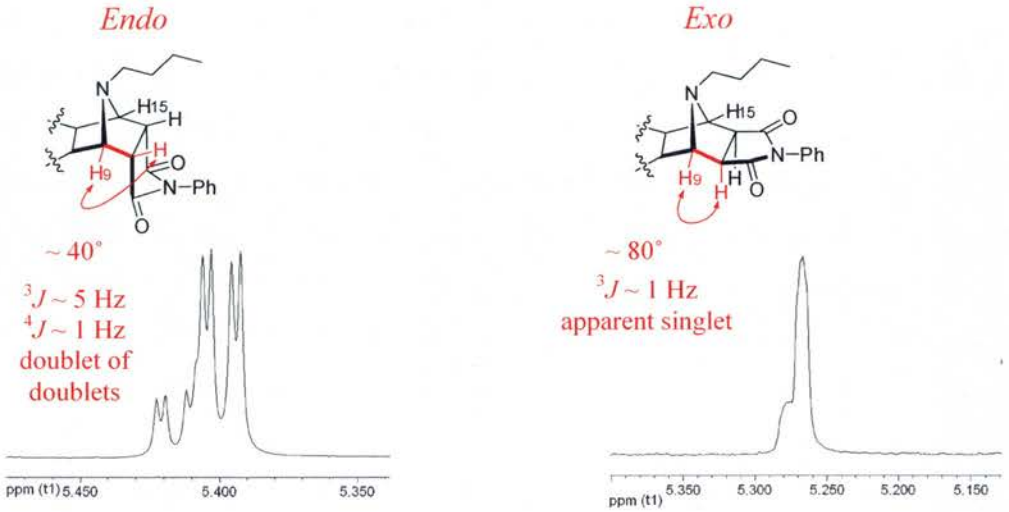

Figure 3.9. Karplus equation (top); *Endo* topology (left), ^{1}H NMR signals corresponding to H-9 of **131** (δ 5.40 ppm) and **133** (δ 5.42 ppm); *Exo* topology (right), ^{1}H NMR signals corresponding to H-9 of **132** (δ 5.27 ppm) and **134** (δ 5.28 ppm).

Although it was not possible to isolate pure samples of each isomer, analysis of the ^{1}H NMR spectra of the two sets of adducts allowed the structural assignment of each isomer. In addition, the ratio of **131** to **133** and **132** to **134** was similar (**131**:**133** 76:24; **132**:**134** 75:25) and consistent with the ratio obtained on analysis of the crude sample of **124**/**125** (see later Table 3.1, entry 1).

The observed product ratio (**124**:**125** 77:23) can be rationalised based on the preferential formation of imine **135** compared with imine **136** (Scheme 3.4). Formation of **135**/**136** occurs via initial tautomerisation of **123** to form either **137** or **138**. The relative ease of this key tautomerisation step depends on the acidity of the protons at C-9 and C-10. In the case of **123**, tautomersiation of the relatively more acidic protons at C-10 (cf. C-9) is expected to occur preferentially, hence leading to **124** as the major product.

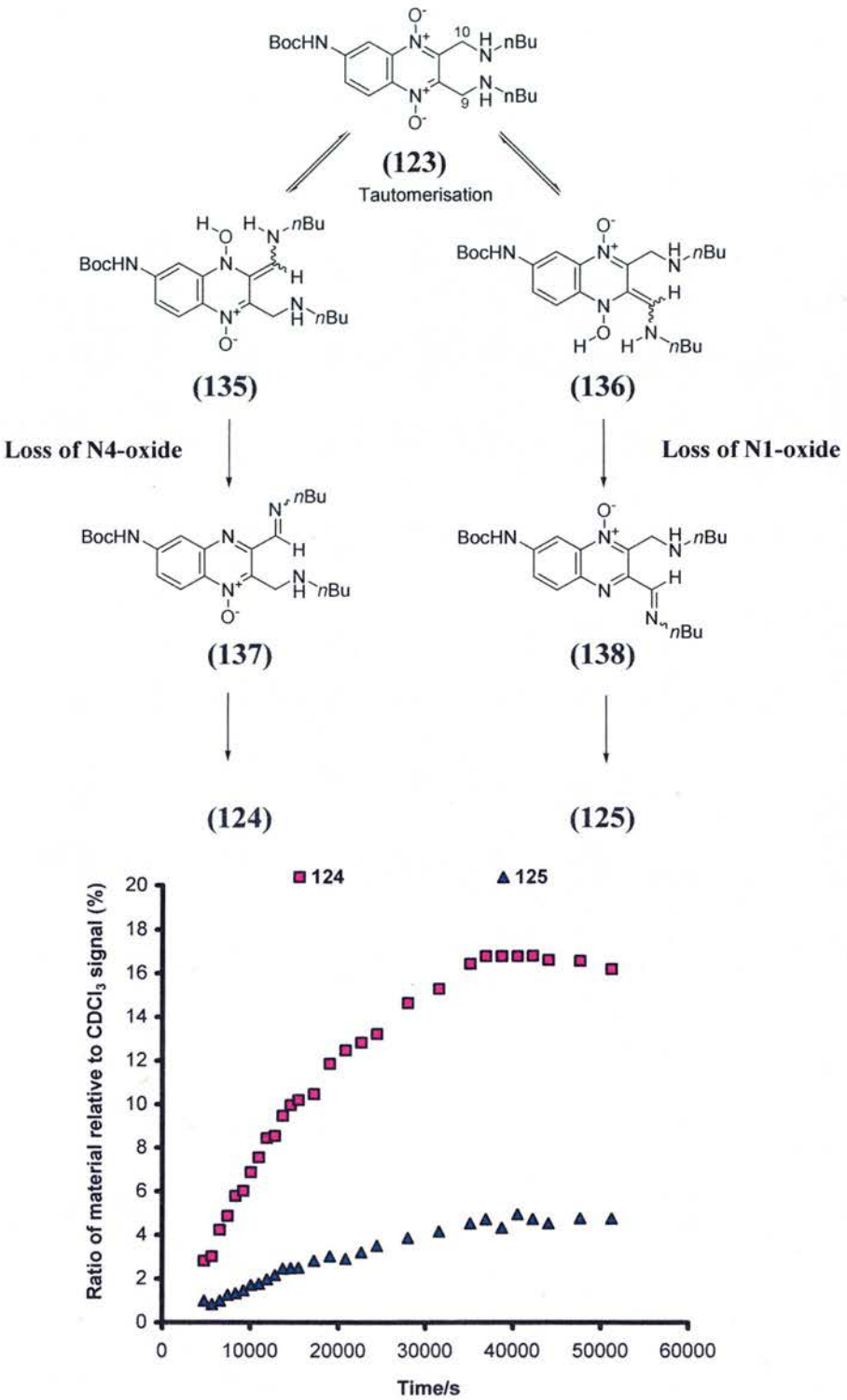

Scheme 3.4. Regioselective direction of tautomerisation gave a both regioisomeric products **124** and **125** in a 77:23 ratio.

Bunting has previously shown that the pK_a values of the single benzylic methylene in 3- and 4-(X-phenylacetyl) pyridines show a pronounced substituent dependence.[132] Typically pK_a values of the order OCH_3 > Cl > NO_2 (by 2-3 units) are reported. An electron donating NHBoc substituent has the effect of destabilising a forming negative

charge at the methylene carbon at C-9 upon deprotonation. In contrast, the electron withdrawing resonance effects of a nitro substituent on the para position (C-9) would be expected to stabilise a developing negative charge localised on C-9 during deprotonation. To provide further evidence in support of this explanation, ^{1}H NMR analysis of the reaction with *n*-butylamine was carried out using the C6-Br (**142**) and C6-NO_2 (**145**) derivatives.

3.0 Synthesis of C6-Bromo (142) and C6-Nitro (145) Quinoxaline Derivatives

A similar procedure to that used for **110** (Scheme 3.1) was used for the synthesis of **142** and **145** (Scheme 3.5). The only difference being for **142**, the reduction of the nitro group was carried out using stannous chloride dihydrate in ethanol with heating under reflux, as reported in the literature.[133] Reduction of the nitro group was not attempted using hydrogen and Pd/C since it was envisaged that this would result in replacement of the aromatic bromine with a hydrogen atom. In the case of **145**, 4-nitro-1,2-phenylenediamine (**143**) was commercially available, and therefore the first step was not required. The cyclocondensation reaction of (**143**) with 1,4-dibromo-2,3-butanedione (**68**) gave the quinoxaline derivative (**144**) in excellent yield of 95% compared to the previous literature synthesis of 28%.[134] The use of additional *m*CPBA (10 equiv) and heat was necessary to access sufficient quantities of **145**, presumably due to the strong electron withdrawing nature of the C-6 nitro substituent hindering *N*-oxidation. In the synthesis of **142** and **145**, the four possible products resulting from mono-oxidation were also isolated (see Section 4.0).

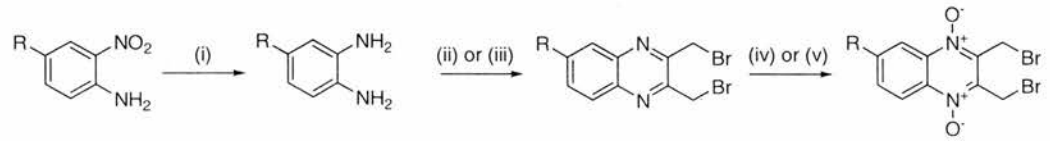

Scheme 3.5. Synthesis of C6–Br (**142**) and C6–NO_2 (**145**) derivatives. *Reagents and conditions*: (i) $SnCl_2.2H_2O$ (5 equiv.), EtOH, reflux, 23 h, 93%; (ii) R = Br, 1,4-dibromo-2,3-butanedione (**68**) (1.02 equiv), THF, 0 °C to RT, 27 h, 88%; (iii) R = NO_2, 1,4-dibromo-2,3-butanedione (**68**) (1.05 equiv), THF, 0 °C to RT, 12 h, 95%; (iv) R = Br, *m*CPBA (7.5 equiv.), DCM, RT, 34 h, 55% (**142**), 12% (**152**), 6% (**153**); (v) R = NO_2, *m*CPBA (10 equiv.), DCM, reflux, 48 h, 18% (**145**), 30% (**154**), 11% (**155**).

Mass spectrometric analysis of **145** showed molecular ion peaks at 396, 394, and 392 (ES) corresponding to $[M + H]^+$, whereas **142** showed molecular ion peaks consistent with a tribrominated species. The purity of **142** was confirmed by elemental analysis and sufficiently high quality crystals were obtained for X-ray crystallographic analysis (Figure 3.11). In the solid state **142** stacks in an offset arrangement stabilised by π-π interactions and efficient Br····Br interactions of approximately 3.6 Å.

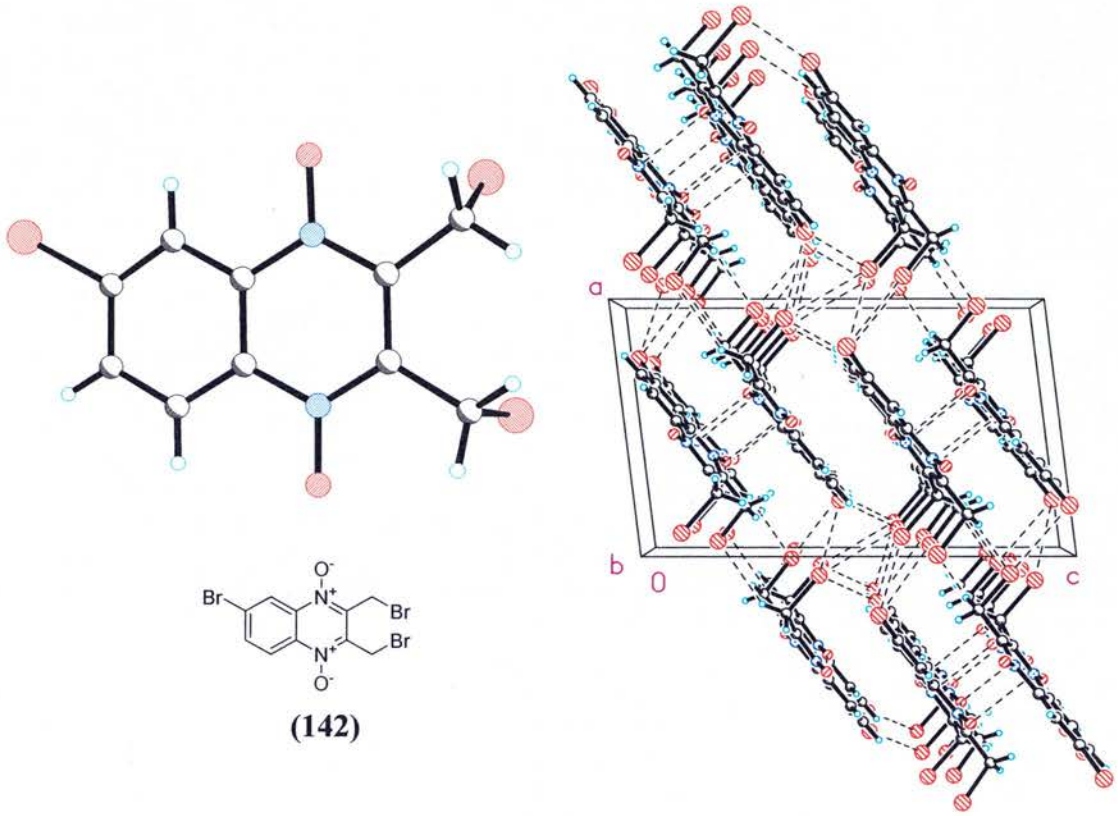

(142)

Figure 3.10. X-ray crystallographic analysis of **142** showed both C-9 and C-10 bromine atoms aligned in the same plane, perpendicular to the aromatic skeleton. An intricate network of attractive interactions between the aromatic bromines and the C-9/10 bromine atoms exists in the crystal packing to confer stability (mp > 180 °C dec.). Intermolecular Br6····Br9/10 interactions are approximately 3.6 Å.

3.1 REACTIONS OF 142 AND 145 WITH *n*-BUTYLAMINE

The ratio of the two regioisomeric products obtained on reaction of **142** and **145** with *n*-butylamine was in line with the effect of the corresponding C-6 substituent on the relative acidity of the C-9 and C-10 protons (Table 3.1). For example, in the case of **145**, where the electron-withdrawing nature of the nitro group would be expected to increase the acidity of the protons at C-9 (cf. C-10), the major product was **149** resulting from a change in the preferred site of tautomerisation compared with **123**. For **142**, the major product is

analogous to **146** (major product from **110**) although the degree of regioselectivity in the reaction is reduced, as expected.

Table 3.1. The relative product distribution changes as a function of the substituent effects in the reactions of 6-R 2,3-bis(bromomethyl)quinoxaline 1,4-dioxides with *n*-butylamine. When R = NHBoc, Br, or NO_2.

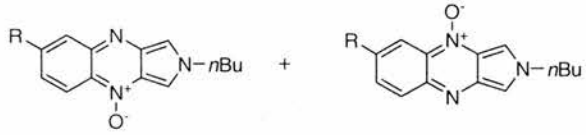

Results from loss of N4-oxide | Results from loss of N1-oxide

Entry	R	Starting material	% Product from loss of N4-oxide	% Product from loss of N1-oxide
1	NHBoc	**110**	77 **(124)**	23 **(125)**
2	Br	**142**	57 **(146)**	43 **(147)**
3	NO_2	**145**	28 **(148)**	72 **(149)**

When R = NO_2 a developing negative a charge on C-9 during deprotonation is stabilised better and therefore leads to preferential loss of the N1-oxide. In contrast, when R = NHBoc a partial negative charge on C-9 would be expected to be destabilised and hence loss of the N4-oxide dominates. For numbering see Scheme 3.4).

The ^{1}H NMR studies on the reaction of **142** and **145** with *n*-butylamine also led to the identification of several other differences compared with **110**. The relative rate of the initial substitution reaction was observed to be dependent on the substituent present in the starting material and was found to be of the order NHBoc > NO_2 ≥ Br > H (Figure 3.11). The faster rate observed for the reaction of **110** can be attributed to the 6-NHBoc substituent that provides electron donation by resonance thereby stabilising forming cationic charge on the benzylic carbon atom in the TS for the initial substitution reaction. The observation that **145** reacted faster than **27** or **142** was unexpected. The electron-withdrawing nature of the nitro substituent was expected to have the opposite effect upon the rate of the initial substitution reaction compared to **110**.

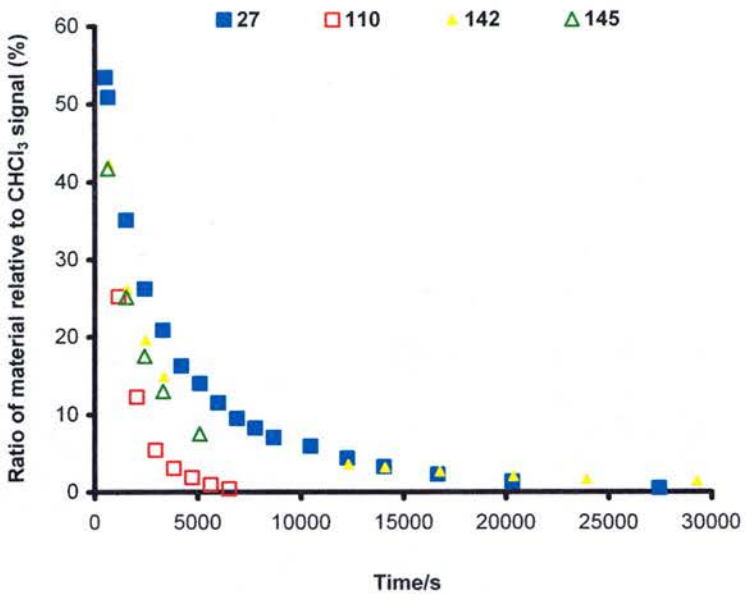

Figure 3.11. Comparison of the initial displacement reaction of substituted quinoxaline di-*N*-oxides **110** (R = NHBoc), **142** (R = Br), and **145** (R = NO_2) compared to **27** (R = H) by *n*-butylamine. Data compared by extrapolation back to Y-axis when X = 0 to correct for $CHCl_3$.

In fact, the relative rates are in accordance with literature reported by Shpan'ko and co-workers in their investigation of the substituent effects of benzyl bromide upon reaction with amines (Figure 3.12).[124]

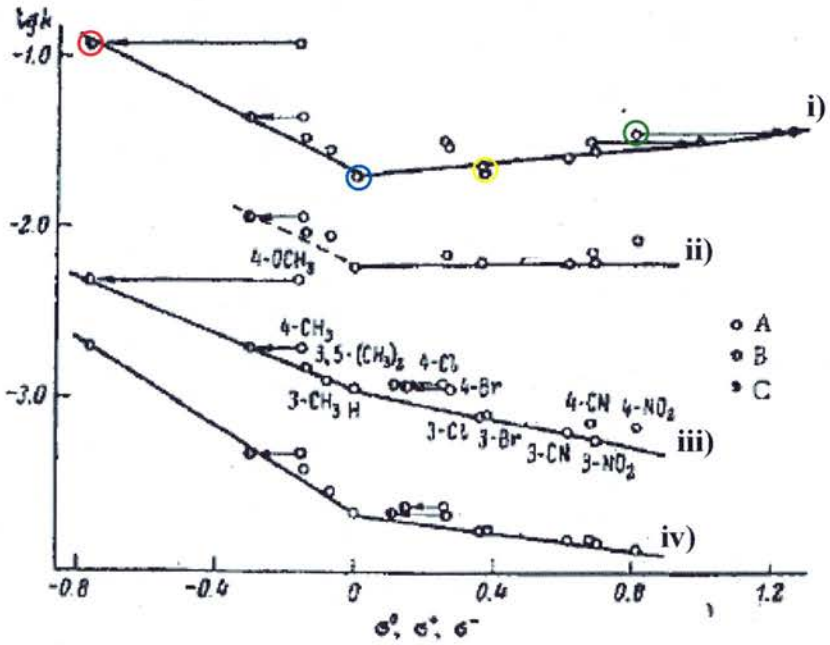

Figure 3.12. The dependence of log*k* on the Hammett constants σ^{o} (A), σ^{+} (B), and σ^{-} (C) for the reactions of benzyl bromides with i) butylamine, ii) benzylamine, iii) pyridine and iv) aniline in nitrobenzene at 40 °C. Highlighted points include OCH_3 (an example of an electron donating substituent, red), H (blue), Br (yellow), and 4-NO_2 (green) showing the observed rate of reaction to be of the order OCH_3 > NO_2 > Br > H. Image reproduced from I. V. Shpan'ko *et al. J. Org. Chem. USSR* **1984**, *20*, 1881-1888.

Shpan'ko *et al.* rationalised this behaviour to be the result of a change in the electronic demand within the scope of a single S_N2 mechanism. A change in mechanism from S_N2 (X = electron-withdrawing) to S_N1 (X = electron-donating) was ruled out, reasoning that the gradient of the line is smaller than would be expected for an S_N1 process.

Between t = 2400 and 7000 s, the rate of total product formation was observed to be of the order NO_2 > H > Br ≈ NHBoc (Figure 3.13). A significant decrease in the concentration of the disubstituted intermediate was observed when the substituent was a nitro group, consistent with an increase in conversion to the corresponding imine intermediate (data not shown). The net electron-withdrawing ability of the NO_2 functional group would be expected to lower the pK_a of the protons on C-9 and C-10 therefore increasing the rate of imine formation and hence conversion to products, relative to hydrogen.

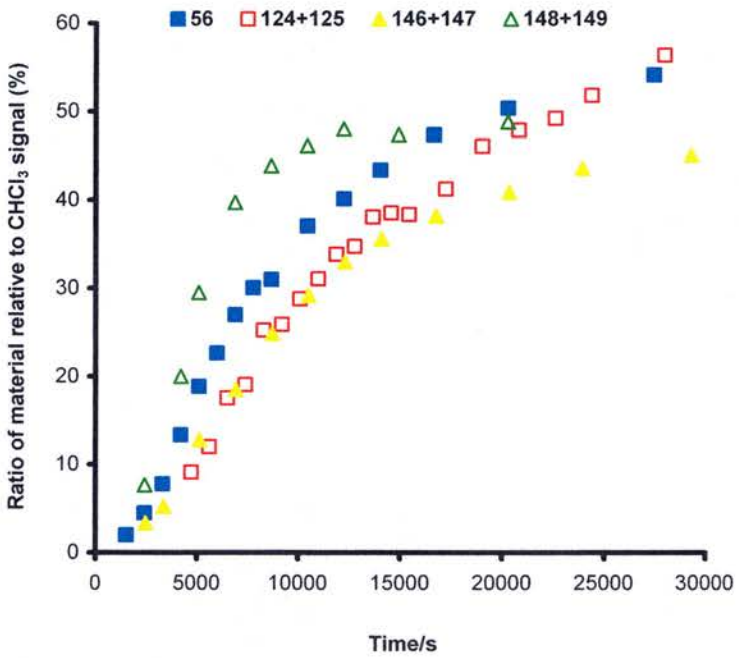

Figure 3.13. Comparison of the total product formation from the reaction of C6 substiuted 2,3-bis(bromomethyl)quinoxaline 1,4-dioxides. When the substituent was a nitro group the rate of product formation (**148**+**149**) was observed to faster compared to that for hydrogen (**56**), bromine (**146**+**147**), and NHBoc (**124**+**125**). Data compared by extrapolation back to Y-axis when X = 0 to correct for $CHCl_3$.

3.2 BIOLOGICAL ACTIVITY OF 110, 142 AND 145

The derivatives of **145** possessing a C(6)-substituent were sent to Prof. Gary Ward's laboratory (University of Vermont) in order to test their biological activity against the parasite *T. gondii*. All four derivatives (Table 3.2, entries 1-4) were assessed for their inhibitory activity in the established *T. gondii* invasion assay (see for more details Chapter 1, Section 3.3 and reference 66). In brief, the small molecules **27**, **110**, **142**, and **145** were dissolved to 40 μM concentration, stock solution, in DMSO and dose-response assays performed. The wells were then scored by "counting" the number of parasites that successfully invaded host cells. In all cases the experiment was repeated several times (at least, in duplicate) and the assay scoring carried out independently by at least two members of the Ward laboratory. The difference observed between 'test' and 'control' (DMSO treated only) wells led to the classification of the small molecules as strong (I(S)), medium (I(M)), and weak (I(W)) inhibitors. The values quoted are those for the lowest active concentration (LAC), defined as I(M) (medium level of inhibition of invasion was observed). The results from the invasion assays are shown in Table 3.2.

Table 3.2. Biological activities of C-6 substituted 2,3-bis(bromomethyl)quinoxaline 1,4-dioxides against invasion of the parasite *T. gondii* into host cells.

Entry	*Compound*	*R*	*Lowest Active Concentration (LAC) (μM)*
1	**27**	H	12.5
2	**110**	NHBoc	25
3	**142**	Br	6.25
4	**145**	NO_2	25

The relative order of biological activity was observed to be Br > H > NHBoc = NO_2. However, the LAC values observed for all four derivatives are within fourfold of one another. Given the qualitative nature of the assay it is believed that for a measurable difference in activity a fourfold difference in the level of inhibition is required. A twofold difference is not considered to be significant. This has been deduced through significant experimental experience in the Ward laboratory. Therefore, the only conclusion that can be drawn from Table 3.2 is that **142** is more active than both **110** and **145**. Despite this, two hypotheses have been considered:

i) if just forming an initial covalent adduct is important then the relative rates of the initial displacement reaction should correlate with the activity (Figure 3.11) and the expected order of reactivity would be NHBoc > Br ≈ NO_2 > H.

ii) if the only factor influencing biological activity is how fast final covalent adduct is formed then the order of biological activity should be as in Figure 3.13, i.e. **110** would be the most active derivative.

Neither of these points connects the relative order of observed inhibitory effect with the mechanistic studies presented herein. Comparing the biological activity with the observed experimental results presented for the reaction of **27**, **110**, **142**, and **145** in $CDCl_3$ does not provide a chemical explanation for the order of biological activity. This is not unsurprising since some target recognition factor(s) must also be involved and the reaction should arguably be studied in buffered media which has not been posssible.

In summary, incorporating a C-6 substituent affects the reactivity of **27** with *n*-butylamine. A tautomerisation step of the disubstituted intermediate on the reaction pathway is affected by the nature of the substituent. Additionally, the relative rate of the initial nucleophilic displacement reaction was increased in the substituted derivatives (NHBoc, Br, and NO_2) relative to **27**. However, it was not possible to obtain information about the regioselectivity involved in this step, this will be discussed further in the following section.

4.0 UNSYMMETRICAL SUBSTITUTED DERIVATIVES OF 27

In our previous work, Chapter 2, Section 2.8 in 2,3-bis(bromomethyl)quinoxaline 1-oxide (**69**) the presence of a single *N*-oxide was shown to impart differential reactivity at the methylene carbon atoms towards nucleophilic attack. Two possible products (**102** and **104**) arose from reaction of **69** with diethylamine depending upon which bromine was displaced first and the reaction concentration (minimal contributing factor at reaction concentrations of less than 20 mM). The results were rationalised based on the assumption that initial displacement of the bromine atom from the bromomethylene group opposite to the *N*-oxide functional group (C10–Br) afforded only disubstituted product (**104**) whereas displacement of the alternative bromine atom (C9–Br) led preferentially to formation of the cyclised product (**102**). At high reaction concentrations, it was shown that following initial attack at C-9 a second substitution reaction could occur. X-ray crystallographic analysis of

69 showed that the carbon-bromine bond adjacent to the *N*-oxide functionality was significantly longer providing evidence for favoured attack adjacent to the *N*-oxide and hence preferential formation of the cyclised product (**102**). However, it should be noted that at the time only ground-state parameters were used to provide this rationalisation. The product ratios obtained from the reaction of **69** with diethylamine in $CDCl_3$ and DMSO-d_6 were observed to be similar (Figure 3.14) therefore suggesting that hydrogen-bonding has an insignificant affect on the reaction outcome. Since ring-substituted mono-*N*1-oxides were readily available, we decided to examine the effect of a substituent (–NHBoc, –Br, $–NO_2$) on the product ratios in the reaction with diethylamine.

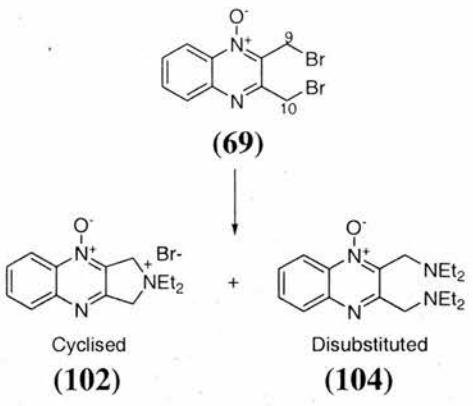

	Cyclised (102)	Disubstituted (104)
$CDCl_3$	63[a]	37[a]
d_6-DMSO	60 (±1)[b]	40 (±1)[b]

Figure 3.14. Reaction of **69** with a secondary amine. [a](from reference 81) [b]denotes over 8 data points (i.e. 4 integrations of 2 sets of peaks in the ^{1}H NMR spectrum). Error included in parentheses.

4.1 Reactions of the mono-*N*1-oxide substituted derivatives of 69 with Diethylamine

An analogous route to that presented in Section 3.0, allowed the preparation of the singly oxidised derivatives containing an NHBoc, Br, or NO_2 substituent at either C-6 or C-7. All six regioisomers have been synthesised and characterised. In the case of **150** and **151** (NHBoc) the two regioisomeric products could not be separated by column chromatography. However, analysis of the ^{1}H and ^{13}C NMR spectra (in combination with 2D ^{1}H–^{13}C HSQC and HMBC spectra) allowed the structural assignment of each regioisomer.

Reactions of all six isomers with diethylamine were performed in $CDCl_3$ in duplicate. In cases where the ^1H NMR signals were poorly resolved in $CDCl_3$, the final reaction mixture was carefully transferred into DMSO-d_6 to obtain clearer resolution for comparison. The results are presented in Table 3.3. In each case, a second sample was used to crystallise and collect the quaternary ammonium salt produced in the reaction for structural characterisation. Unfortunately, since the 6NBoc mono-*N*-oxides could not be separated by standard column chromatography techniques, a 2:1 mixture of regioisomers was reacted with diethylamine.

Table 3.3. The relative product distribution obtained from the reactions of the mono-*N*1-oxide 2,3-bis(bromomethyl)quinoxaline derivatives bearing a C-6/7 substituent with a secondary amine, diethylamine.

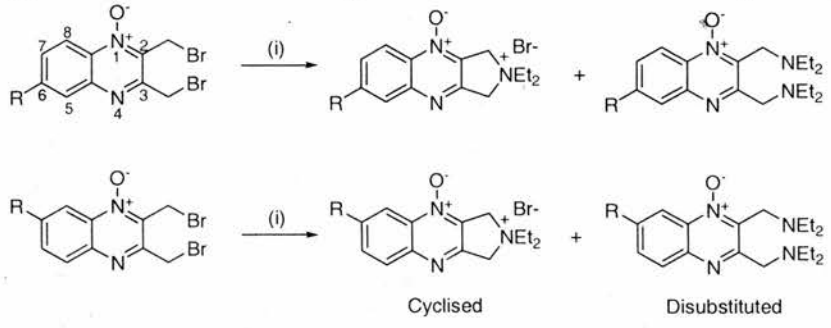

Entry	*Compound*	*R*	*Substituent Position*	*Cyclised*		*Disubstituted*	
1	**150**	NHBoc	6	61 (±2)[a] [71]	**(156)**	39 (±2)[a] [29]	**(157)**
2	**151**	NHBoc	7	68 (±1)[a] [70][b]	**(158)**	32 (±1)[a] [30][b]	**(159)**
3	**152**	Br	6	55.5 (±2)[c]	**(160)**	44.5 (±2)[c]	**(161)**
4	**153**	Br	7	57 (±2)[d]	**(162)**	43 (±2)[d]	**(163)**
5	**154**	NO_2	6	14 (±3)[e]	**(164)**	86 (±3)[e]	**(165)**
6	**155**	NO_2	7	12.5 (±2)[e]	**(166)**	87.5 (±2)[e]	**(167)**

Reagents and conditions: (i) diethylamine (4 equiv), $CDCl_3$, 25 °C. [a]denotes over 4 data points; [b]denote values obtained performing the experiment in DMSO-d_6; [c] denotes over 18 data points; [d] denotes over 16 data points; [e] denotes over 24 data points.

The results in Table 3.3 show two clear trends. First, the position of the substituent appears to have very little affect on the outcome of the reaction. Second, the substituent does have a pronounced influence on the product ratio, as expected. When the substituent is electron-donating (relative to H, i.e. NHBoc (**150** and **151**)) a preference for cyclised products (**156** and **158** respectively, Figure 3.15) was observed whereas, an electron-withdrawing substituent (i.e. NO_2 (**154** and **155**)) led almost exclusively to the disubstituted products **165** and **167** respectively. When the substituent was bromine (electron-withdrawing and mesomerically donating (**152** and **153**)) the experimental results fell in between the NHBoc and NO_2 extremes.

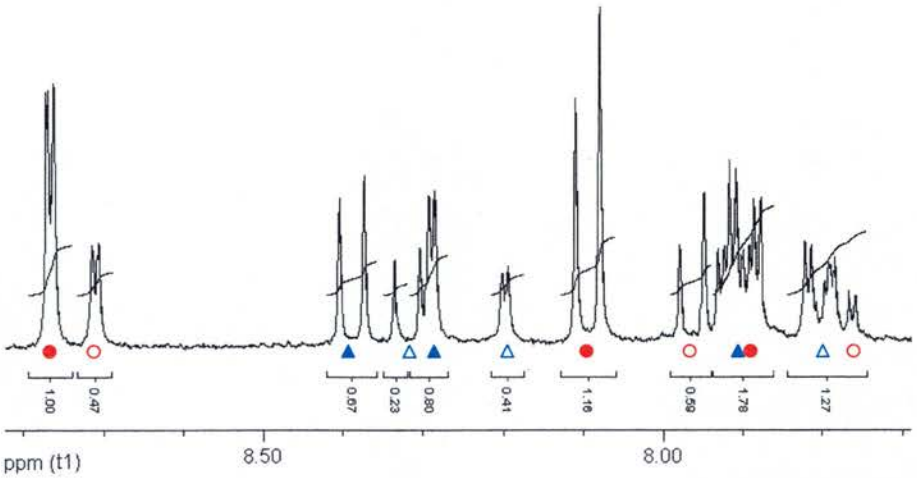

Figure 3.15. Aromatic region of the ^{1}H NMR in DMSO-d_6 of the four products resulting from reaction of a mixture of **150** and **151** with diethylamine. Cyclised products **158** (●) and **156** (▲) and disubstituted products **159** (○) and **157** (△).

4.2 RATIONALISATION OF THE EXPERIMENTAL DATA

In order to interpret this data, it was first necessary to reassess whether our previous assumption had been affected by the introduction of a substituent. Namely, initial attack by the nucleophile at C-9 (bromomethylene group adjacent to the *N*-oxide functional group) affords a cyclised product (depending upon the reaction concentration) while a displacement reaction on C-10 in the first instance leads to a monosubstituted intermediate that is unable to cyclise and gives exclusively a disubstituted product (Figure 3.16).

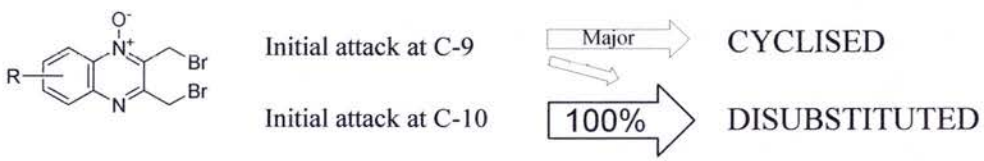

Figure 3.16. Summary of the product outcome available following an initial substitution reaction by a secondary amine, diethylamine, with a mono-*N*1-oxide derivative.

Owing to limited material and time constraints it was not possible to perform concentration dependence studies on these derivatives. However, computational analysis of the transition states that would be required to undergo an S_N2-like cyclisation reaction for the monosubstituted pairs of compounds containing either a 6-NHBoc (**168** and **169**) or a 6-NO_2 (**170** and **171**) substituent have been carried out. Figure 3.17 illustrates the TS models obtained for **170**‡ and **171**‡.

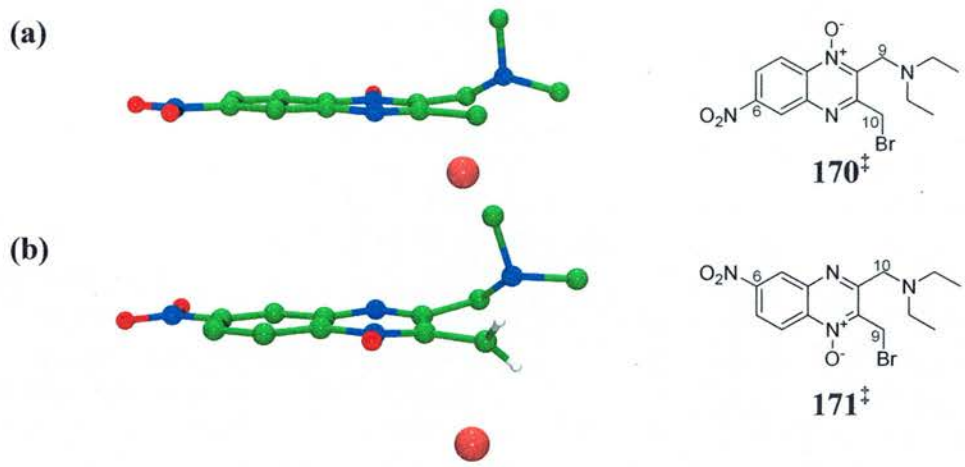

Figure 3.17. TS models of (a) $\mathbf{170}^{\ddagger}$ and (b) $\mathbf{171}^{\ddagger}$. The ethyl groups have been removed for clarity.

The TS models for $\mathbf{170}^{\ddagger}$ and $\mathbf{171}^{\ddagger}$ illustrate an analogous situation to that observed for $\mathbf{53}^{\ddagger}$ and $\mathbf{72}^{\ddagger}$ respectively (Chapter 2, Section 2.7.4) supporting our previous work.[81] In the case of $\mathbf{170}^{\ddagger}$ (Figure 3.17, (a)), which results from an initial displacement reaction at C-9, a favourable TS is easily reached in which the aromatic skeleton of $\mathbf{170}^{\ddagger}$ is essentially planar (therefore not energetically disfavoured) allowing an S_N2-like reaction to proceed. In contrast, in $\mathbf{171}^{\ddagger}$, which results from an initial displacement reaction at C-10, in order to position the nitrogen nucleophile at a suitable angle to carry out an S_N2-like displacement reaction, the aromatic skeleton suffers significant puckering caused predominantly by repulsion between the *N*-oxide oxygen and the bromine. Consequently, this orientation is energetically disfavoured, hindering cyclisation and forcing a second displacement reaction to occur instead. The results for $\mathbf{168}^{\ddagger}$ and $\mathbf{169}^{\ddagger}$ (NHBoc case) were in accordance with those presented for $\mathbf{170}^{\ddagger}$ and $\mathbf{171}^{\ddagger}$ (data not shown). Therefore, it was concluded that the product outcome is determined by the site of initial attack as previously discussed (Chapter 2, Section 2.8).

A key question revolves around why the position of initial attack varies across the series? In interpreting the effects of aromatic substitution on the outcome of the reaction of **150-155** with diethylamine both resonance and inductive effects require consideration. In this respect, the electron-donating ability of NHBoc in **150** and **151** would be expected to stabilise a forming positive charge on C-9 and C-10 respectively (ground state argument). Therefore in **150** the initial reaction would be expected to occur adjacent to the

N-oxide (C-9) and lead predominantly to cyclised product **156**, as observed. However, for **151** the preference for initial substitution would be predicted to be at C-10 resulting in **159** being the major product which is not in line with the experimental outcome. Similarly, for a nitro substituent that would be expected to pull electron density from C-9 and C-10 in **154** and **155** respectively, the observed experimental results are only consistent with the prediction based on "classical" resonance stabilisation, for **155**. Therefore, computational calculations have been performed to assess the relative electron density at C-9 and C-10 in the derivatives **150-155**. These calculations revealed that the difference in electron density of the two electrophilic centres in each pair of regioisomers (**150** and **151**, **152** and **153**, **154** and **155**) is only very slight. This indicates that the substituent effect is not translated through the aromatic system but is muted by the nitrogen atoms in the quinoxaline core. Interestingly, an alternative explanation for the observed change in initial nucleophilic attack is required. Several alternative parameters have been considered to try and explain the observed experimental results and will be discussed in the section that follows.

4.2.1 Rate of Cyclisation

Previous experiments have shown that an initial nucleophilic substitution on the carbon centre C-9, adjacent to the *N*-oxide can lead to either cyclised or disubstituted product, depending on the relative rates of the intramolecular cyclisation compared to a second nucleophilic substitution reaction. It was therefore considered whether the observed experimental results were a reflection of a change in the rate of the cyclisation reaction as a function of the substituent, as opposed to an effect on the preferred site of initial nucleophilic attack. In line with the experimental outcome for **155**, a decrease in the rate of cyclisation for intermediate **174** as a function of the nitro substituent would be expected to favour a second displacement reaction and therefore increase the yield of **167**. In order to investigate this scenario, a computational molecular modelling study was performed. The transition states **172**‡, **173**‡, and **174**‡ that would lead to cyclisation were calculated. Figure 3.18 shows the overlaid TS models **172**‡, **173**‡, and **174**‡ for the C7-substituted derivatives **172**, **173**, and **174** following an initial displacement at C-9.

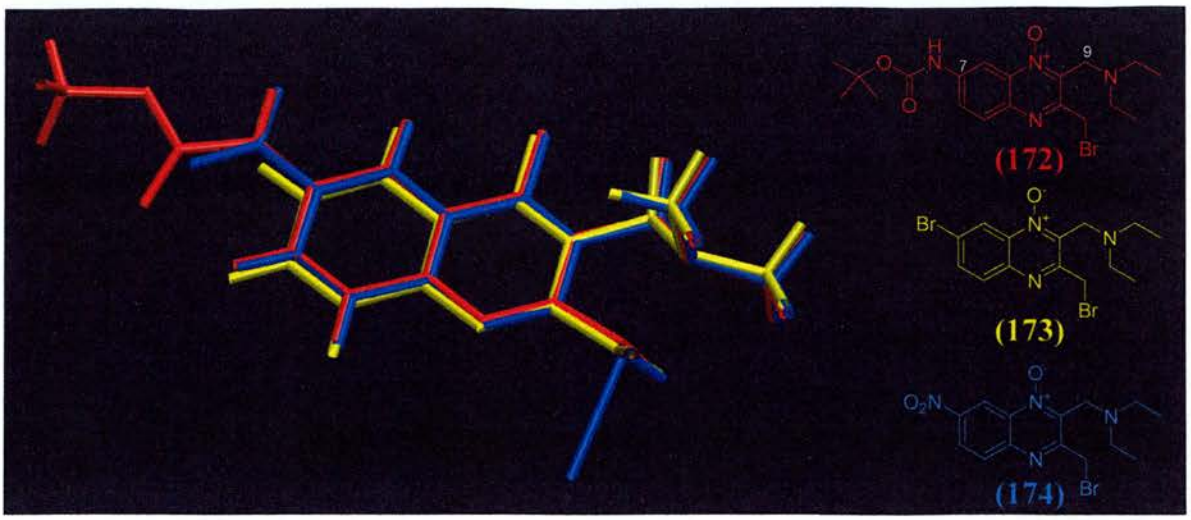

Figure 3.18. Calulated TS models for an S_N2-like cyclisation reaction for **172**, **173**, and **174**. The C–Br bond is only shown for **174**‡ for clarity.

When overlaid these models show that there is very little difference upon the structural orientation required for the cyclisation reaction to proceed. In all cases the aromatic skeleton shows minimal deviation from planarity and is only slightly affected by the substituent. Importantly, the calculated energy gap between the corresponding cyclised and disubstituted products across the series are all within 0.5 kcal of one another and hence the cyclisation reaction for all three intermediates (**172**, **173**, and **174**) would be expected to proceed at a similar rate. Therefore, these models do not support a hypothesis based on the energy required for cyclisation as an explanation for the differential product ratios across the series as they rule out the possibility of the rate of cyclisation being the source of the observed selectivity. Rather, they further support the alternative hypothesis that the effect observed experimentally is a reflection of the first step in the reaction.

However, these studies did highlight one difference in the TS structures of **172-174**. This is more clearly visualised in Figure 3.19.

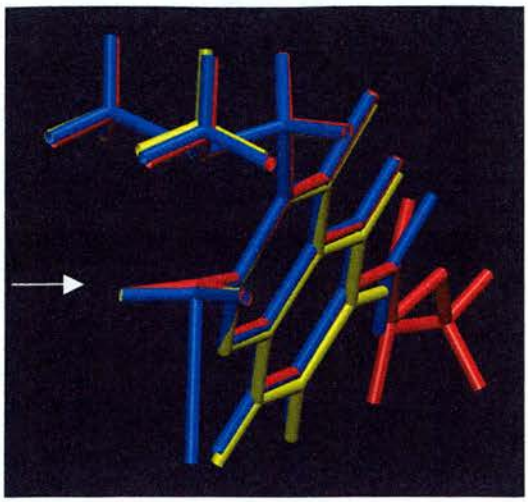

Figure 3.19. End view of the overlaid TS models for **172**‡ (NHBoc, red), **173**‡ (Br, yellow), and **174**‡ (NO_2, blue). In **172**‡ (red) C-10 is more cationic in character resulting from resonance stabilisation from the C7-NHBoc group and therefore more "S_N1-like". The longer C–Br bond due to C-10 being raised in comparison to **173**‡ and **174**‡ supports this conclusion.

In the case of **172**‡ (NHBoc), the electrophilic reaction centre C-10 is pyramidal therefore the C–Br bond is longer. The NHBoc substituent causes a net inductive charge at C-10 resulting in resonance stabilisation of positive charge at the transition state. Therefore, C–Br bond breaking is favoured and the observed TS is shifted in the direction of a carbocationic intermediate, becoming more "S_N1-like" in character but still within the scope of an S_N2 mechanism (Figure 3.19). In contrast, **174**‡ is more "S_N2 like". This can be further understood using the simplified 2D energy surface shown in Figure 3.20, in that **172**‡ would lie below the purple line (representing a perfect S_N2 mechanism), in the region of $c^{‡}$ (green line). **174**‡ would be predicted to fall above the purple line (in the region of $a^{‡}$ (blue line)) where C–N bond formation predominates over cleavage of the C–Br bond and there is a build up of negative charge at C-10 as the TS is approached.

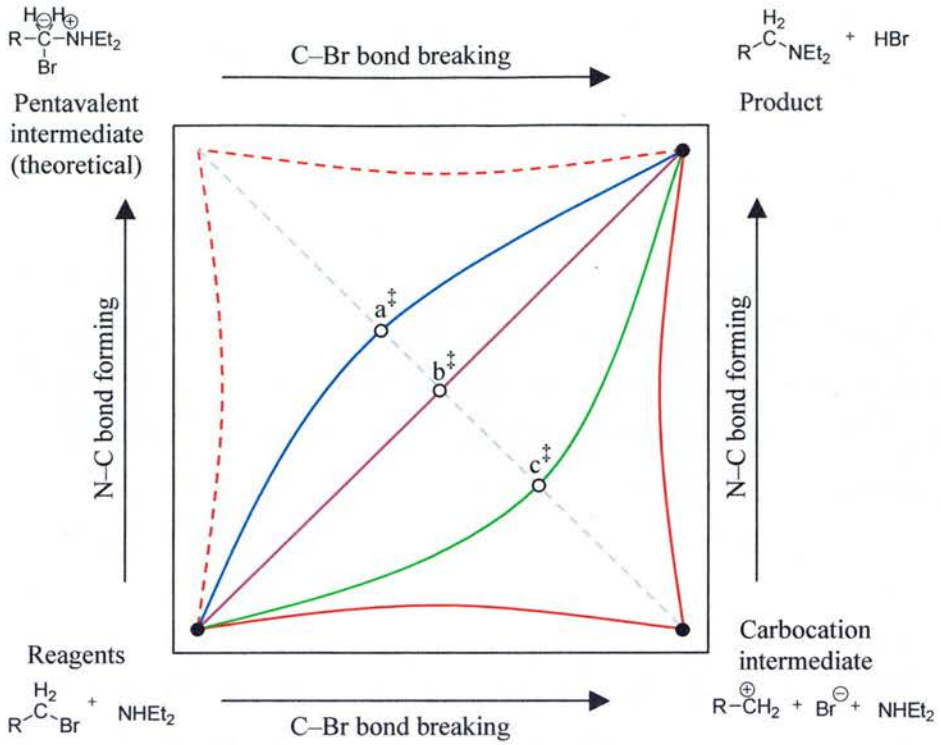

Figure 3.20. Simplified 2D energy surface diagram viewed from the top. Diagram illustrates the variation of the bond orders of the N–C and C–Br bonds in the reaction at a benzylic bromomethylene group with amines. The reaction coordinates are depicted for i) the S_N1 process (red solid line), ii) arbitrary reaction coordinates for the S_N2 process (green, purple and blue lines), and iii) the hypothetical limiting S_N2 process (red broken line). The transition states in the S_N2 reactions are labelled $a^{\ddagger}$ (N–C > C–Br), $b^{\ddagger}$ (N–C ≃ C–Br), and $c^{\ddagger}$ (N–C < C–Br). Image adapted from I. V. Shpan'ko *et al. J. Org. Chem. USSR* **1984**, *20*, 1881-1888 and 'Electron Flow in Organic Chemistry' P. H. Scudder **1992** John Wiley & Sons, Inc.

In summary, the calculated structures for the transition states across the series (**172**, **173**, and **174**) are all very similar. One slight difference was identified for **172**‡. However, whilst **172**‡ shows cationic character there is no overall change in mechanism from S_N2 to S_N1 on going from electron-donating to electron-withdrawing substituents, that is, all intermediates can undergo a cyclisation reaction within the scope of an S_N2 mechanism. The calculated differences in energy between the cyclisation compared to disubstitution products across the series are not large enough to significantly affect the rate of cyclisation and therefore this cannot be used to rationalise the observed selectivity.

4.2.2 X-ray Analysis

Since differences in the cyclisation reaction can be ruled out the experimentally observed ratios can be attributed to reflect selectivity between C-9 and C-10 in the initial nucleophilic displacement reaction. To investigate this further the C9–Br and C10–Br bond lengths for derivatives **150-155** were considered. Unfortunately in the case of **150** and **151**, suitably high-quality crystals could not be obtained for X-ray analysis. However, analogues **152-155** all afforded crystals of sufficient quality. The relevant bond lengths obtained for these derivatives are shown in Table 3.4.

Table 3.4. Comparison of the C9–Br and C10–Br bond lengths of substituted mono-*N*1-oxide 2,3-bis(bromomethyl)quinoxaline derivatives obtained from single crystal X-ray diffraction analysis. Numbers in parentheses denote the error.

Entry	Compound	R	Position	C9–Br	C10–Br
1	**69**	H	6/7	1.976 (4)	1.952 (4)
2	**152**	Br	6	1.979 (3)	1.967 (3)
3	**153**	Br	7	1.960 (18)	1.964 (15)
4	**154**	NO_2	6	1.967 (3)	1.961 (3)
5	**155**	NO_2	7	1.959 (3)	1.960 (3)

With the exception of entry 2, there is no significant difference between the C9–Br and the C10–Br bond lengths to suggest that either of these two sites favour attack by a nucleophile.

4.2.3 Electrophilicity of C-9 Compared to C-10 Centres Based on Their Corresponding ^{13}C NMR Shift

Measurement of the ^{13}C NMR shift that corresponds to C-9 and C-10 was also explored as a measure of electron density to estimate the electrophilicity of the two distinct reactive centres. ^{13}C NMR has previously been used to estimate the electrophilicity of carbon.[135,136]

Table 3.5. Comparison of the ^{13}C NMR shift (ppm) in $CDCl_3$ corresponding to C-9 and C-10 of substituted mono-*N*1-oxide 2,3-bis(bromomethyl)quinoxaline derivatives.

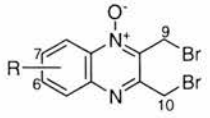

Entry	Compound	R	Position	C9	C10	ΔC10-C9
1	**69**	H	6/7	20.8	30.2	9.4
2	**150**	NHBoc	6	21.1	30.3	9.2
3	**151**	NHBoc	7	21.1	30.4	9.3
4	**152**	Br	6	20.5	29.9	9.4
5	**153**	Br	7	20.5	30.0	9.5
6	**154**	NO_2	6	20.0	29.5	9.5
7	**155**	NO_2	7	19.7	29.3	9.6

Three main points of interest can be extracted from Table 3.5.

1. ^{13}C NMR spectra showed that for all of the derivatives, C-10 comes into resonance at lower field compared to C-9 indicating an overall lower electron density on C-10. Therefore based on ^{13}C NMR, attack would be predicted to occur preferentially at C-10 and favour disubstituted products in all cases. The preferred site of attack based on ^{13}C NMR is not in agreement with the experimental results. However, this suggests that the electron density associated with the *N*-oxide functional group can be delocalised on C-9 better than C-10.
2. The ^{13}C NMR shift for the signals corresponding to C-9 and C-10 within each pair of regioisomers is very similar, supporting the previous observation that resonance effects based on the *position* of the substituent are not translated fully through the quinoxaline core.
3. Finally, a downfield shift from 19.7 – 21.1 ppm and 29.3 – 30.3 ppm for the signals corresponding to C-9 and C-10 respectively were observed, across the series from R = NO_2 (**154** and **155**) to NHBoc (**150** and **151**). The slightly higher shifts corresponding to both carbon centres observed for **150** and **151** (R = NHBoc) suggests that C-9 and C-10 are slightly more electrophilic and react faster in the initial displacement reaction compared to **154** and **155** (R = NO_2, cf. Figure 3.11).

In summary, ^{13}C NMR and X-ray analysis provides structural information for derivatives **150-155** but does not provide a rationalisation for the observed experimental data, as expected due to the fact that these are ground state observations.

4.2.4 Directing Effect of the *N*-oxide Functional Group

The ability of the *N*-oxide functional group to influence the site of attack has also been considered based on previous literature.[137,138] Given that the *N*-oxide lies in the plane of the quinoxaline ring, it is relatively difficult to envisage how an interaction can be formed with an incoming nucleophile that could favour/disfavour attack by an incoming nucleophile. One possibility is presented in Figure 3.21. However, since the experimental results show that the product outcome is similar in $CDCl_3$ compared to DMSO-d_6 (Figure 3.14 and entries 1 and 2, Table 3.3) hydrogen bonding interactions are not thought to play a role in directing in an attacking nucleophile.[119]

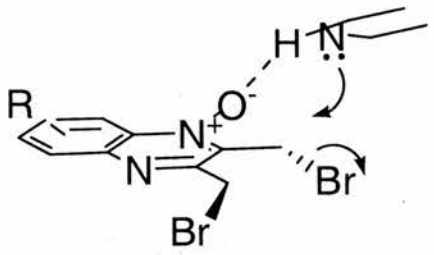

Figure 3.21. One possible approach of the nucleophile, directed in by hydrogen-bonding to the *N*-oxide functional group. However, it is difficult to envisage how this could be a source for the observed regioselectivity in the initial displacement reaction.

4.2.5 Rationalisation Based on Cation Stabilisation

When the substituent was NHBoc, the TS for the cyclisation reaction revealed evidence of S_N1-like character. Therefore it was reasonable to calculate the relative energies of the two isomeric cations resulting from cleavage of the C9–Br and the C10–Br bonds respectively in the NHBoc case (Figure 3.22). These calculations showed that the cation that gives rise to the major product is more stable than that leading to the minor product by > 3 kcalmol^{-1}.

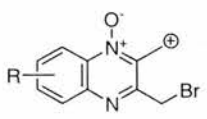

(175)

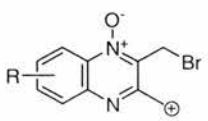

(176)

Figure 3.22. When the substituent is NHBoc the cation **175** resulting from C9–Br bond breaking has been shown to be more stable than cation **176**, which results from C10–Br bond breaking. Stabilisation of the positive charge by the electron donating *N*-oxide functional group occurs when the reaction proceeds via a TS that is more S_N1-like in character.

Whilst this energy difference is larger than would be expected to reflect the product ratio the stability order has proven to be insensitive to basis set effects. Therefore although the absolute magnitude of the stability may not be correct there is no doubt that cation **175** is more stable than **176**. This is consistent with the preference for cyclised product when the substituent is electron donating and the reaction proceeds via a more S_N1-like TS. In this case the *N*-oxide functional group can stabilise a forming positive charge on C-9 better than C-10 in the TS by resonance.

In summary, the results from the computational analysis support the conclusion that the experimentally observed product ratios result from the initial substitution reaction. They argue against the possibility that it could be due to a difference in rate of the cyclisation reaction, based on the fact that the energy gap between the transition states for formation of the cyclised and disubstituted products across the series are almost equal. Several considerations have been investigated in order to explain the selectivity observed, including C-9 and C-10 bond lengths and relative electrophilicity. However these routes provided no clear rationalisation. Computational analysis also indicated that when the substituent was electron donating (i.e. NHBoc) the TS for cyclisation was more S_N1-like in character. Therefore it was reasonable to assume that an analogous situation exists for the TS for the initial substitution reaction. Calculations of the relative stability of a full cationic intermediate (that would exist in an S_N1 mechanism) have shown that the C-9 cation (**175**) is more stable better than that at C-10 (**176**), as a result of the *N*-oxide functional group. This supports the observation that attack is favoured at C-9, which leads preferentially to formation of cyclised product. It therefore seems reasonable to conclude that when the substituent is electron-withdrawing (i.e. NO_2) a developing negative charge at C-10 is stabilised more by this system than at C-9. Initial nucleophilic attack is therefore favoured at C-10 leading to the disubstituted product.

5.0 CONCLUSION

Incorporation of a substituent at the C-6 position renders 2,3-bis(bromomethyl)quinoxaline 1,4-dioxide derivatives unsymmetrical. Therefore, the two methylene carbons become functionally distinct. Whilst this does not change the fundamental mechanism of their reaction with *n*-butylamine, it introduces interesting regioisomeric questions, in particular, two regioisomeric products become possible. Their

relative ratios of formation have been shown to be dependent upon the nature of the substituent. The key product-determining step is believed to be the ease of tautomerisation at either C-9 or C-10 of the disubstituted intermediate on the pathway. The product ratio can be tailored by varying the substituent.

The singly oxidised derivatives containing either a C-6/7 substituent show a clear trend upon reaction with diethylamine. The position of the substituent has been shown to have only subtle effects on the reaction outcome. The product distribution is reversed from cyclised product to that resulting from a second substitution reaction in shifting from an electron-donating to an electron-withdrawing substituent. When the substituent is electron-donating (i.e. NHBoc) the selectivity can be rationalised based on the ability of the electron rich *N*-oxide functional group to stabilise inductively the developing cationic charge on the C-9 carbon centre in the transition state.

Integration of the *N*6-protected functional group into **27** has been shown to retain the desired biological activity. The successful synthesis of **110** therefore provided a precursor relevant to the preparation of an affinity reagent. The synthesis towards a chemical probe based on **27** will therefore be the focus of Chapter 4.

MECHANISM SUMMARY

In 1969, Anderson and Fleming proposed a mechanism for the conversion of **27** to **51** on reaction with methylamine (Scheme 3.6) based on the characterisation of **51** at that time. Following this publication no further evidence has been available in support of this mechanism. The work presented within this thesis provides the first experimental evidence in support of the mechanism proposed by Anderson and Fleming involving the reaction of **27** with two equivalents of an amine nucleophile. The mono- and disubstituted intermediates (**53** and **54**) from reaction of **27** with *n*-butylamine have been observed by ^{1}H NMR analysis.

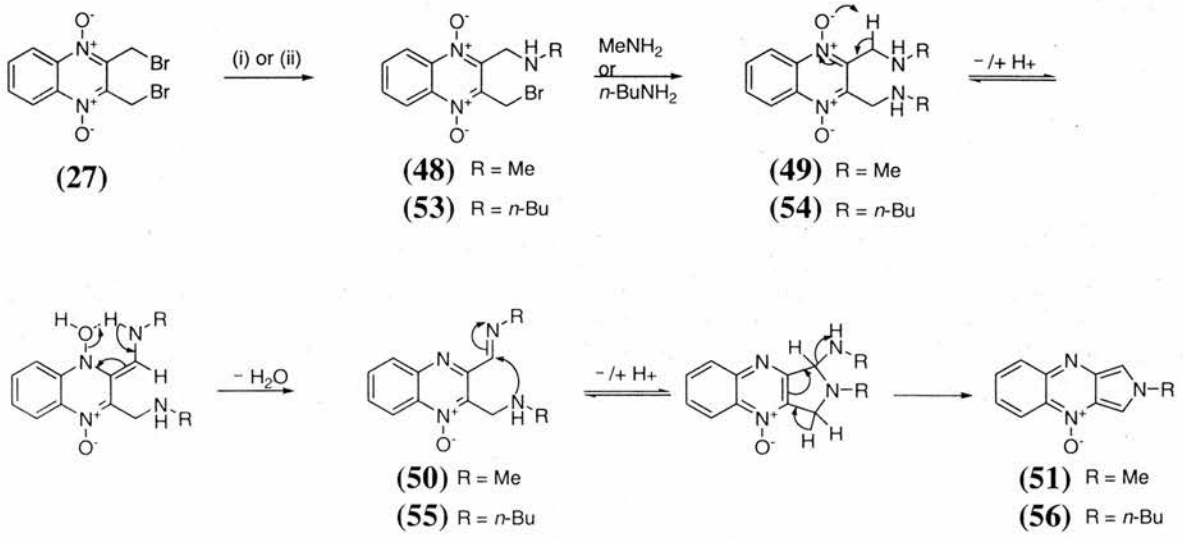

Scheme 3.6. The reaction mechanism proposed by Anderson and Fleming for the conversion of **27** to **51** with methylamine.[101] Evidence for intermediates **53** and **54** has been shown to provide credence to the above mechanism.[81] *Reagents and conditions:* (i) methylamine, -80 °C;[101] (ii) *n*-butylamine, 25 °C.

In addition to providing no experimental evidence to support their mechanism, Anderson and Fleming also provided no rationalisation of the reaction pathway. This area has been significantly developed in this thesis.

The presence of the *N*-oxide functional groups in **27** has been shown to limit the reaction of **27** to an intermolecular pathway. Computational molecular modelling has shown that the competing intramolecular cyclisation pathway is prevented because of the electrostatic repulsion between the *N*-oxide oxygen and the leaving bromine atom in the TS for cyclisation of the monosubstituted intermediate **53**.

Further investigations into the above mechanistic transformation involved the incorporation of a substituent at the C-6/7 position of 2,3-bis(bromomethyl)quinoxaline 1,4-dioxides. ^{1}H NMR analysis of the reaction of the substituted derivatives of **27** with *n*-butylamine showed an affect on two key steps in the mechanism. Firstly, the relative rate of the initial S_N2 displacement reaction at C-9/10 was dependent upon the substituent, NHBoc > NO_2 ≥ Br > H. The order of reactivity has been rationalised by the ability of the substituent to stabilise the TS for nucleophilic substitution. Switching substituent from NO_2 to NHBoc involved a change in the electronic demand at C-9/10 of the TS (from S_N2 to an "S_N1-like" mechanism, respectively) within the scope of an S_N2 mechanism. However, information regarding the possibility of favoured initial regioselective substitution at either C-9 or C-10 (e.g. in the 6-NHBoc case, Figure 3.23) could not be gained from the ^{1}H NMR data.

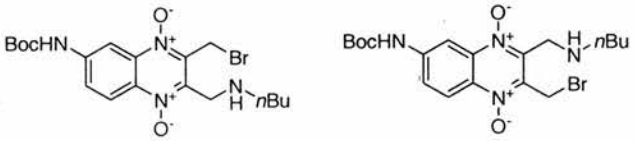

(121) **(122)**

Figure 3.23. The two possible isomers resulting from regioselective attack at either C-9 or C-10, shown in the 6-NHBoc case.

Secondly, the incorporation of a substituent has provided insight into the transformation of the disubstituted intermediate (cf. **54**) through to product(s) (e.g. **124** and **125**). The ratio of regioisomeric products reflects the relative acidity of the protons at C-9 and C-10 and hence the relative ease of tautomerisation. The product ratio observed has been shown to be dependent upon the nature of the substituent.

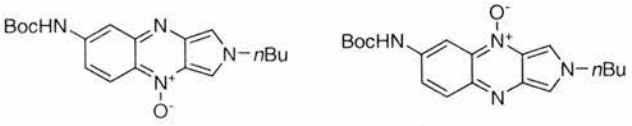

(124) **(125)**

Figure 3.24. The two regioisomeric products formed upon reaction of the C-6 substituted derivative of **27** with *n*-butylamine, shown in the 6-NHBoc case.

Following formation of the disubstituted intermediate **54**, the intermediates drawn on the pathway by Anderson and Fleming were not visible in the ^{1}H NMR studies discussed herein. It remains uncertain as to whether conversion of the disubstituted

intermediate to the corresponding imine occurs via a concerted electrocyclic mechanism (as shown in Scheme 3.6) or an alternative acid-catalysed process.

It is believed that information provided by the detailed mechanistic study discussed in Chapters 2 and 3 provides substantial information relating to the chemical framework that is possibly involved in the biological mode of action of 2,3-bis(bromomethyl)quinoxaline 1,4-dioxide derivatives. As biological studies continue (see Chapter 4) the information obtained here will prove essential in fully explaining how this type of compounds inhibit processes of relevance to parasitic and bacterial disease.

The detailed understanding gained in the first part of this study also enabled predictions of the behaviour of mono-*N*-oxide derivatives to be developed. These predictions were subsequently tested and a detailed understanding of the mono-*N*-oxide systems was developed using substituent effects.

CHAPTER 4

DEVELOPING A CHEMICAL PROBE BASED ON 27

1.0 INTRODUCTION

As discussed in Chapters 1 and 2, the small molecule **27** produces the desired phenotype, inhibition of invasion of the parasite *T. gondii* into host cells. However, the cellular target(s), within the parasite, to which **27** binds is currently unknown. As pointed out in chapters 2 and 3 detailed analysis of chemical reactivity of **27** is possible but its relevance to the biological system is unclear. In order to try and address this problem, we set about establishing the methodology necessary to identify protein-binding partners of **27**. The selected approach first requires the synthesis of a range of chemical probes with which to carry out *in vitro* and *in vivo* labelling studies. Chapter 4 therefore focuses on the synthesis and characterisation of analogues of **27** as suitable reagents for affinity-based methods of protein target identification. Within this chapter preliminary biological data is also presented resulting from the use of a successfully synthesised chemical probe.

2.0 COVALENT PROTEIN MODIFIERS IN AFFINITY CHROMATOGRAPHY

The first approach towards target identification involved affinity chromatography (see Chapter 1, Section 1.2.1). A resin bound analogue of **27** compatible with traditional affinity chromatography techniques was investigated. However, since **27** was considered a covalent modifier of proteins several changes were required compared to conventional affinity chromatography approaches with small molecules that form non-covalent bonds to proteins.

Covalent modifiers are generally considered unfavourable in affinity chromatography applications because of the difficulty in removing intact binding proteins from the matrix. The affinity approach usually relies upon a *reversible* interaction between the small molecule and protein-binding partners. If the small molecule forms a covalent bond to the target protein or has a very strong interaction with a complementary protein (e.g. nanomolar affinity) it cannot be eluted from the affinity column for identification and further studies (see Chapter 1, Figure 1.2). For this reason, the affinity chromatography approach is not usually the method of choice for the application of a known covalent modifier.

However, covalent affinity chromatography has long been exploited for the purification of thiol-containing proteins based on disulfide-exchange. Incubation of a matrix loaded with a disulfide ligand facilitates binding of a thiol protein by disulfide exchange. After thorough washing of the affinity column the covalently bound proteins are released by a second disulfide exchange reaction with cystamine.[89]

Tryptic digestion of resin-bound protein(s) and subsequent mass analysis of the tryptic peptides is the generally accepted method for identifying the unknown covalently-bound proteins (Figure 4.1).

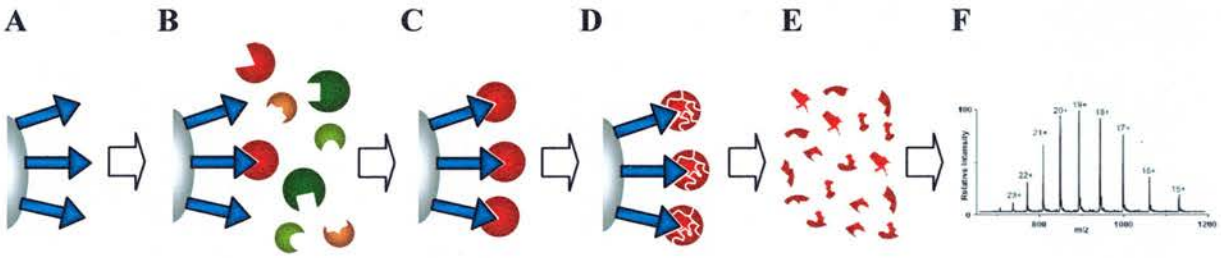

Figure 4.1. Schematic representation of the affinity chromatography approach when the immobilised small molecule covalently binds to proteins of interest on the resin. **A.** Affinity resin loaded with an immobilised small molecule covalent modifier (depicted as a blue triangle) via a linker unit (blue rectangle) **B.** Affinity matrix is incubated with crude cell extracts and stringently washed to remove non-specific binding proteins **C.** Protein-small molecule (red sphere-blue triangle) complex covalently bound to an affinity matrix **D.** Digestion of the bound protein by incubation of the affinity resin with trypsin **E.** Trypsin cleaves the proteins at the carboxyl site of Arg and Lys residues into peptides of suitable size for MS analysis **F.** MS/MS analysis to identify the bound protein(s).

One of the drawbacks associated with tryptic digestion is that it produces short peptides that can make it difficult to assign correctly which proteins have been retained on the matrix. For example, tryptic digestion can form identical –GG signature peptides for ubiquitin as well as NEDD8 and ISG15.[139] In addition, fragmentation efficiency of MALDI generated tryptic peptide ions is often poor.[140,141] If covalent modification occurs on a residue at a potential cleavage site, labelling can also go undetected. Other disadvantages include the fact that proteins of low abundance can be difficult to assign and in the context of **27**, the genome sequence of *T. gondii* is currently incomplete.[142] If the affinity resin is < 100% loaded there is the potential for covalent non-specific binding to any unblocked sites on the resin and these proteins are subsequently digested by trypsin. It would therefore be beneficial if an alternative technique were available to release covalently bound proteins, ideally in a more intact state.

2.1 THE NEED FOR A CLEAVABLE LINKER

One solution to the elution problem, caused by high-affinity or covalent inhibitor-protein interactions is the use of an alkali sensitive linker to the affinity matrix.[143] In Jahng's study, an alkali cleavable, irreversible affinity reagent containing a biotin tag was used to identify retinoid binding proteins (Figure 4.2). In theory, cleavage at either alkali labile ester linkage (C-3 or C-15) releases covalently bound protein(s).

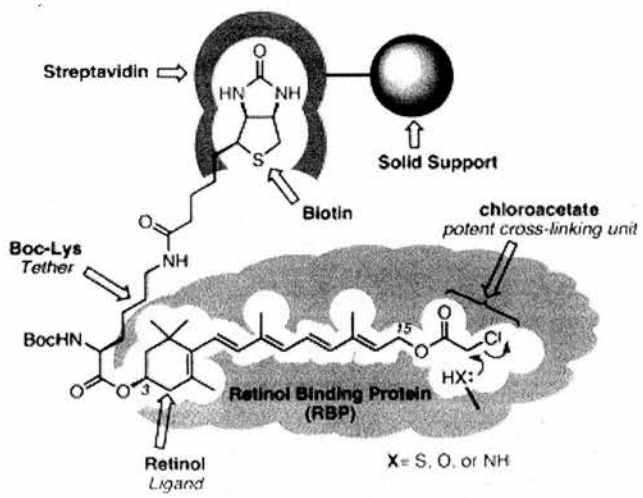

Figure 4.2. A biotinylated affinity-labelling agent for retinoid binding proteins incorporating a cleavable linker. Treatment of the beads at pH 11 can cleave the linker at C-3 and/or C-15. Image reproduced from W. J. Jahng *et al. Biochemistry* **2003**, *42*, 6159-6168.

Treatment of retinal pigment epithelium (RPE) membranes, labelled with the biotinylated reagent, with neutravidin beads allowed the capture of biotinylated proteins onto the beads. The high affinity of tetrameric avidin for biotinylated proteins can make the elution exceedingly difficult. However, treatment of the beads at pH 11 cleaved the linker, allowing for the elution and subsequent identification of the proteins RPE65 and lecithin retinol acyltransferase (LRAT). This cleavage left the labelled proteins tagged with a $-CH_2COOH$ group and hence provided a handle in mass spectroscopy studies i.e. the labelled peptide had an increment of 58 Da over the unlabelled species. MS/MS revealed that RPE65 was covalently modified at two cysteine residues, Cys-231 and Cys-448.

Concisely, from perhaps thousands of RPE membrane proteins, labelling with the affinity reagent above, at low concentrations, allowed for the specific labelling of RPE65 and LRAT. Importantly, this study demonstrated that RPE65 is a retinoid binding protein.

In summary, additional considerations are required in the design of an affinity chromatography approach when the immobilised small molecule can covalently bind proteins. Two methods are known to retrieve covalently bound proteins for identification when using an affinity approach. These involve either tryptic digestion or the incorporation of an alkali cleavable linker. For an affinity chromatography reagent based on **27** the development of a novel cleavable linker has been explored and will be the topic of the section that follows.

2.2 DESIGNING A COVALENT AFFINITY CHROMATOGRAPHY REAGENT BASED ON 27

Cleavage of a linker unit would release the small molecule-protein complex and the molecular weight of the bound complex could then be identified using mass spectrometry. In this way, if the binding mode of the small molecule were known, this approach would provide access to the mass of the whole protein, reinstating the importance of the mechanistic studies for **27** presented in Chapter 2. The whole protein-small molecule complex could be analysed further by MS/MS to provide identification and information on the amino acid(s) modified by the small molecule. (Figure 4.3).

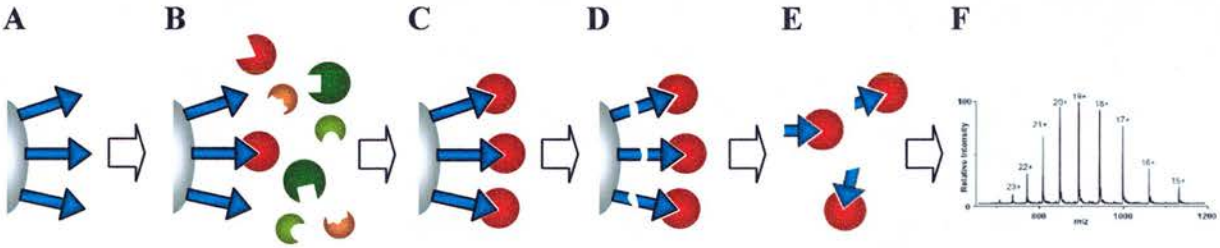

Figure 4.3. Schematic representation of the affinity chromatography approach incorporating a cleavable linker for release of covalent binding partners of an immobilised small molecule. **A-C.** Affinity resin loaded with an immobilised small molecule via a linker unit, which covalently modifies a protein binding partner upon incubation with a crude cell lysate. **D.** Cleavage of the linker unit to release captured proteins. **E.** Proteins released bound to the small-molecule inhibitor (in part or full). **F.** MS/MS analysis to ascertain protein mass and subsequent identification. The labelled residues can be identified with prior knowledge of the mechanism of binding of the small molecule and/or comparison with unlabelled protein following identification.

The proposed method of attachment of **27** onto an affinity resin, through a linker unit, was through an NH_2 functional group on C-6. Linkers commonly employed for such applications are based on polyethylene glycol as it is felt that a simple poly-CH_2 linker unit, such as $(CH_2)_8$, may suffer from hydrophobic collapse and therefore be unable to interact selectively with proteins in a cell extract resulting in non-specific interactions with

proteins. However, incorporating more than four CH_2CH_2O units has been proposed to facilitate linker collapse because of chelation by calcium and magnesium ions.

The linker unit chosen for this study is based on (*E*)-hex-3-ene-1,6-diol (**179**), the key component being the olefin (Scheme 4.1). The placement of the double bond was based on literature precedent by Barrett *et al.* and will be discussed in more depth in Part II of this thesis. It is envisaged that cleavage of the linker could be achieved by oxidation of the alkene bond. The use of a six carbon chain was considered the maximum for an alkyl unit and the oxygen atoms were placed at either end to minimise hydrophobic collapse and provide a functional group with which to attach to a resin. However, the length of the linker unit could be subject to modification at a late stage if required to decrease non-specific binding of proteins.

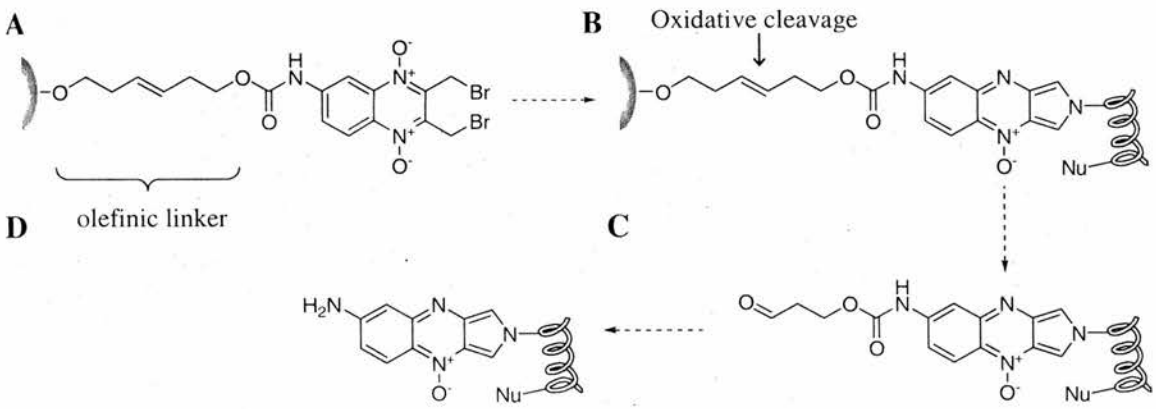

Scheme 4.1. Scheme representing the approach to affinity chromatography using an immobilised derivative of **27**. **A.** The derivative of **27** proposed for attachment to an affinity resin. **B.** One possible state for the covalent modification of a binding partner to **27**. **C.** Oxidative cleavage to release the small molecule-protein complex from the resin. **D.** Remainder of the linker chain cleaved. Mass spectrometric analysis can be used to identify the molecular weight of the small molecule-protein complex. If the binding mode of the small molecule is known the mass of the protein can be deduced.

Oxidative cleavage of the olefin requires mild, selective conditions that can preferably be applied in aqueous conditions. Possible reagents for chemoselective oxidation of C=C include ozone, osmium tetroxide (followed by periodate cleavage), and peracids (RCO_3H). However, one potential drawback associated with this mode of cleavage is the possible sensitivity of amino acids to oxidation. Sutherland and Hall have previously reported oxidation of sulfide to the corresponding sulfoxide and sulfone during ozonolysis for the release of resin-bound tripeptides by cleavage of an olefin.[144]

2.2.1 SYNTHESIS OF THE LINKER UNIT: (*E*)-6-Triisopropylsilanyloxy-hex-3-en-1-ol, 180

Our initial target linker was a simple hexene 1,6-diol (**179**) with one of the primary hydroxyl groups selectively protected. In fact, previous studies by Koert and co-workers report the synthesis of a similar compound to **180** in which the TIPS group is substituted for TBDMS.[145] Their synthesis was implemented in our system.

The starting point in the synthesis of the linker was commercially available (*E*)-hex-3-enedioic acid (**177**) (Scheme 4.2), which was converted to the corresponding dimethyl ester **178** using TMSCl in methanol in an excellent yield of 98%. The crude product was shown to be clean by ^{1}H NMR spectroscopy without the need for purification by column chromatography. Reduction of the ester groups in **178** to give the primary alcohols was achieved by reaction of **178** with lithium aluminium hydride in THF. The diol **179** was obtained in near quantitative yield (98%) after filtration through Celite®, evaporation of the solvent and column chromatography. Subsequent monosilylation of the diol gave **180** using Koert's conditions that employ one equivalent of sodium hydride.[145] **180** was obtained in a modest yield of 53% comparable to that of Koert *et al.* of 54% for mono TBDMS protection of the diol **179**. NMR analysis is consistent with the inclusion of only one silyl group owing to the compound becoming unsymmetrical.

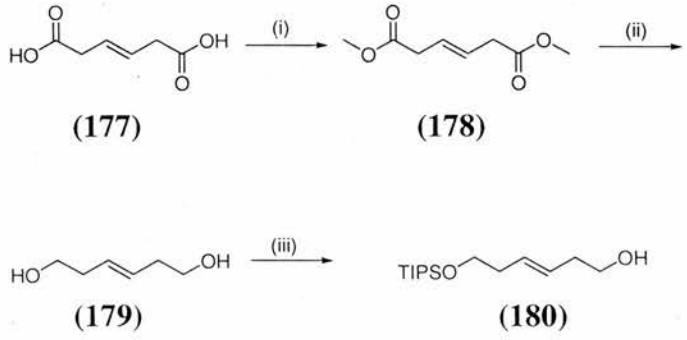

Scheme 4.2. Synthesis of (*E*)-6-triisopropylsilanyloxy-hex-3-en-1-ol, (**180**) linker unit. *Reagents and conditions:* (i) TMSCl (2 equiv.), MeOH, 0 °C, 48 h, 98%. (ii) $LiAlH_4$ (3 equiv.), THF, 0 °C – RT, 2 h, 98%. (iii) a) NaH (1 equiv.), THF, 0 °C – RT, 45 mins. b) TIPSCl (2 equiv.), RT, 15 h, 53%. TMS = trimethylsilyl, TIPS = triisopropylsilyl.

The mono-*O*-protected linker unit (**180**) can be easily accessed through this three-step synthesis on a multi-gram scale. The alkene unit in **180** (Scheme 4.2) was assumed to

be *E* configured, based on the geometry of the starting acid **177**, in line with literature precedent and a coupling constant (approximately ^{3}J = 15-16 Hz, inaccuracy due to the complexity of the signal) consistent with *E* geometry.

2.2.2 Towards Immobilisation of 27

With multi-gram quantities of the linker unit **180** in hand, the coupling of **180** to **27** was investigated, Scheme 4.3. We envisaged that an acylation reaction using an activated form of **180**, **182**, would be an efficient route for coupling through the C-6 nucleophilic nitrogen that can be generated from the hydrobromide salt, **184** (Schemes 4.3 and 4.4).

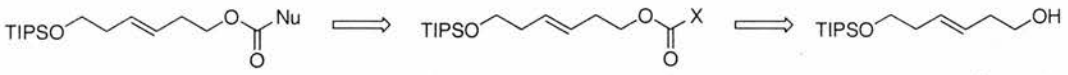

(181) **(182)** **(180)**

Scheme 4.3. Reterosynthetic analysis for coupling to the linker unit **180** (where X = an activating group, imidazole or halo and Nu = a nucleophilic functionality in a small molecule).

The activation of **180** was carried out using triphosgene in the presence of pyridine to afford the corresponding chloroformate intermediate **183** (Scheme 4.4). By-product pyridine salts were removed from the reaction by extraction. Subsequent addition of the hydrobromide salt **184** to the chloroformate **183** under solvent-free conditions, prior to the addition of base and solvation in THF, was found to be crucial to the successful formation of **185**. Dissolving **184** in THF before the addition of **183** resulted in an intractable mixture of products and no evidence for the formation of **185**, as judged by ^{1}H NMR and TLC analysis, was obtained. The successful synthesis of **185** was judged by ^{1}H and ^{13}C NMR, however, later efforts to resynthesise **185** for further analysis were unsuccessful.

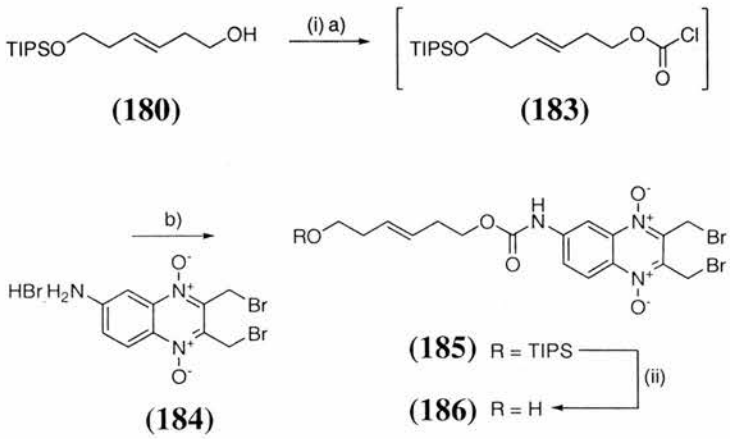

Scheme 4.4. Synthesis of an affinity reagent based on the covalent modifier **27** for application in affinity chromatography experiments. *Reagents and conditions:* (i) a) Triphosgene (0.6 equiv.), Py (1.0 equiv.), 30 mins. 0 °C; 2 h, RT; b) HBr salt (**21**) (0.1 equiv.), Py (1.0 equiv.), THF, 0 °C, 2 h; 10 h, RT, 40%; (ii) HF.Py, THF, RT, 1 h.

Removal of the TIPS group on a small-scale was carried out using HF.Py. The reaction gave a compound that by ^{1}H NMR analysis showed peaks resembling the starting material in which the signal corresponding to the protons of the TIPS group (1.06-1.04 ppm) were absent. The product was observed to be more polar by TLC analysis as would be expected for the free alcohol (**186**). Following purification by column chromatography, subsequent ^{1}H NMR in CD_3OD was consistent with the assignment of **186** however exposure to methanol resulted in degradation (see Section 3.12 for discussion).

Coupling of **186** to an affinity matrix was planned via the alcohol. A number of companies offer a selection of affinity chromatography resins (see reference [146] for an extensive list). However, the reactive functional groups available on the resins for loading are limited. With this in mind, loading of **186** was envisaged by activation of the alcohol functional group using triphosgene and coupling to an aniline based resin (prepared in house). Model studies using a β–lactam compound tethered to the linker have been carried out to assess cleavability of the linker unit (data not shown). However, due to the difficulty in the preparation of **186** and its limited stability in hydroxyl-containing solvent, this approach was abandoned and other target identification approaches were investigated.

3.0 LABELLING METHODS FOR TARGET IDENTIFICATION STUDIES

As previously discussed, there are several different labelling methods available that facilitate target identification studies (Chapter 1). These approaches fall into one of two categories, *in vitro* or *in vivo* methods. Traditionally, the protein targets of small molecules have been identified using *in vitro* methods such as affinity chromatography or photoaffinity labelling.[46] *In vitro* methods involve incubation of a modified version of the small molecule with a crude cell lysate. One of the disadvantages of working with cell lysates is that often large levels of non-specific binding of proteins are observed. In addition, these methods are often labour intensive and sensitive to low protein expression levels or protein degradation during cell lysis.[46] More importantly however, an argument against the *in vitro* approach is the fact that an isolated target *in vitro* may not be the *in vivo* target. Both *in vitro* and *in vivo* approaches have been considered in relation to **27** and will be discussed in turn in the remainder of this chapter.

3.1 DEVELOPMENT OF A BIOTIN-LABELLED PROBE

Biotin is usually the tagging method of choice, as previously discussed (see Chapter 1, Section 1.2.2). However, the presence of the bulky biotin reporter tag can result in poor cellular uptake and/or unduly influence probe distribution within the cell.[147] For this reason studies using biotinylated probes are often performed using cell extracts. However, several examples exist in the literature where biotin has been successfully used as a chemical tag *in vivo* (see Chapter 1).

A biotinylated probe was selected as a target since both *in vitro* and *in vivo* techniques are possible using a biotin tag. Derivatives synthesised as chemical probes require the incorporation of a functional group as a "handle" or attachment point with which to append a tag. Selecting the position of attachment of the chemical tag is key since the derivative must retain the biological activity observed for the original small molecule.

Whilst several differences between the reaction of **110** and **27** with *n*-butylamine in $CDCl_3$ have been identified, the ^1H NMR studies detailed in Chapter 3 (see Section 2.2) showed that the underlying reaction mechanism for both compounds is similar in $CDCl_3$.

This conclusion coupled with the preliminary biological data that showed that **110** retained the desired activity led us to prepare a biotinylated analogue **187** in which the Boc group of **110** was exchanged for a biotin group (Scheme 4.5).

3.1.1 Synthesis of a Biotinylated Derivative of 27

The treatment of **110** under standard Boc deprotection conditions, for example TFA, gave an intractable mixture of products. Clean removal of the Boc group was achieved using HBr in acetic acid presumably due to the fact that the hydrobromide salt, **184**, precipitated from the reaction mixture.[148] Commercially available D-(+)-Biotin (**188**) (5 equiv.) was then converted to the corresponding acid chloride using thionyl chloride and reacted with **184** in the presence of pyridine in DMF to give **187** in moderate yield following purification by column chromatography.

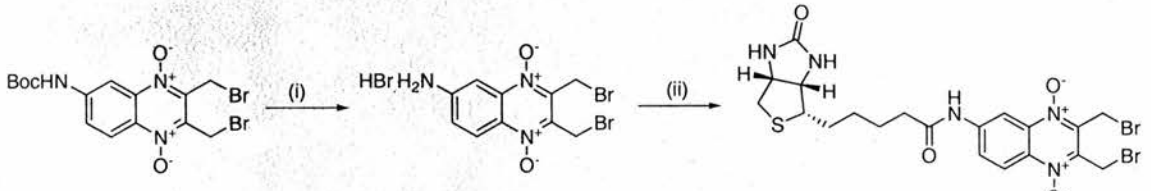

(110) **(184)** **(187)**

Scheme 4.5. Synthesis of the biotinylated analogue **187**. *Reagents and conditions:* (i) 45% HBr in AcOH, AcOH, 10 mins., 94%; (ii) a) D-(+)-Biotin (**188**) (5 equiv.), $SOCl_2$ (xs), 30 mins.; b) **184** (1 equiv.), Py (1 equiv.), DMF, 5 h, 24%.

3.1.2 Evidence of Attachment of Biotin

The biotinylated derivative **187** was found to be insoluble in many organic solvents, including $CDCl_3$, and had only limited solubility in CD_3OD. NMR experiments were performed in CD_3OD (since the material would be difficult to retrieve from DMSO), however because of the low solubility of **187**, the signal:noise ratio was relatively low. The analysis of **187** by ^1H NMR spectroscopy, in comparison to D-(+)-biotin (**188**), is illustrated in Figure 4.4.

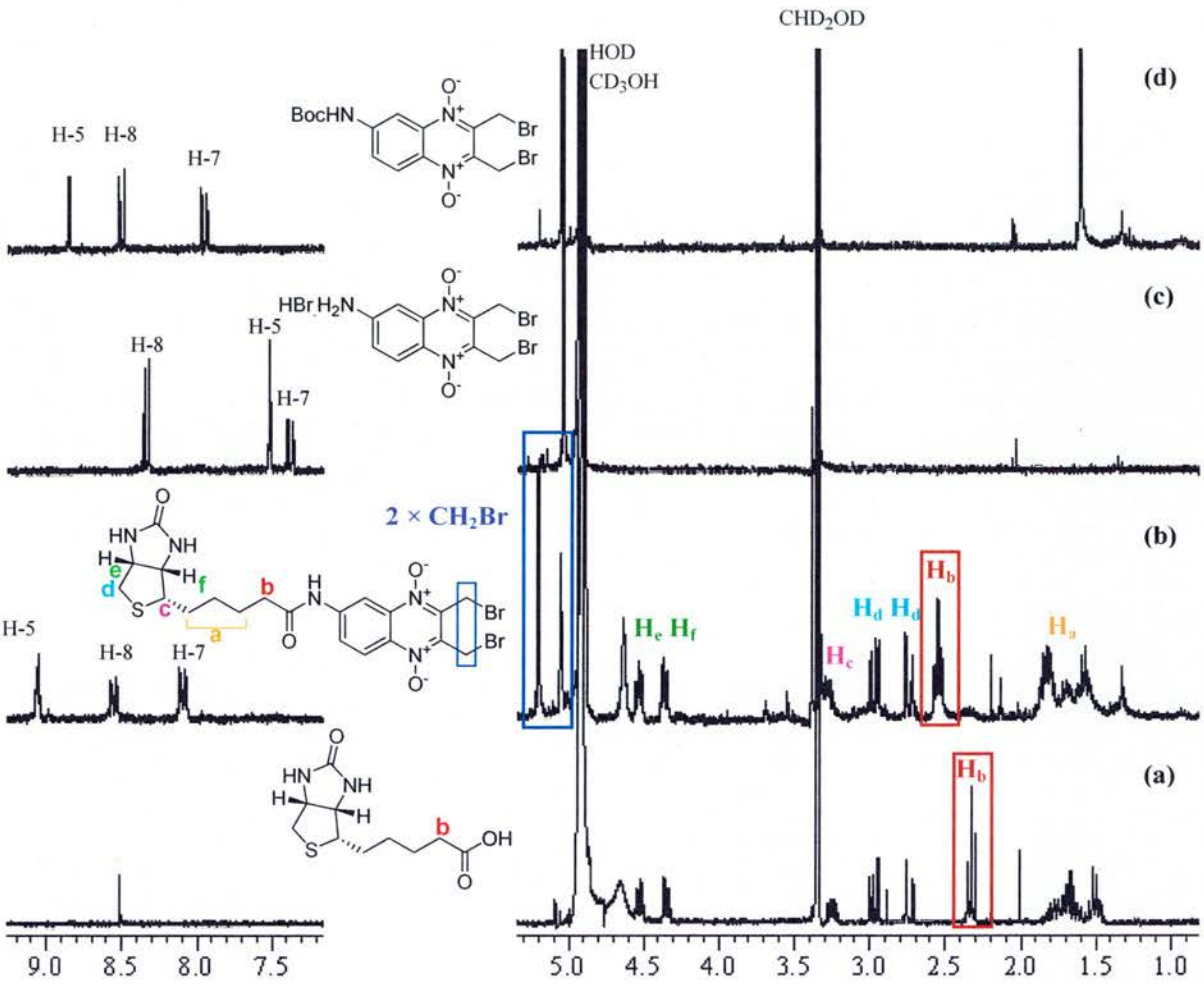

Figure 4.4. ^{1}H NMR spectra of (a) D-(+)-biotin (**188**) and (b) biotinylated derivative **187** (c) hydrobromide salt **184**, and (d) NHBoc compound **110** in CD_3OD. Appendage of the biotin group at C-6 in **187** produces analogous shifts for the signals corresponding to the aromatic protons of the quinoxaline ring, H-5, H-8, and H-7 as observed for **110**.

Evidence in support of the formation of **187** came from several observations. The ^{1}H NMR spectrum of **187** showed a triplet observed at 2.48 ppm that can be assigned to the methylene group labelled as H_b, and is shifted downfield from 2.24 ppm in D-(+)-biotin (**188**) consistent with the transformation from an acid to an amide functional group. Further evidence comes from the appearance of three resonances in the aromatic region belonging to H-5, H-8, and H-7 of the quinoxaline ring with similar shifts to the analogous signals in **110** (Figure 4.4, (b) and (d)). Two further resonances are observed which are assigned to the non-equivalent CH_2Br groups in **187** at 5.14 ppm (CH_2-9) and 4.99 ppm (CH_2-10). The assignment of **187** has been further substantiated by comparison with the NMR and IR data reported by Qi *et al.* for the biotin-component of **189** (Figure 4.5).[149]

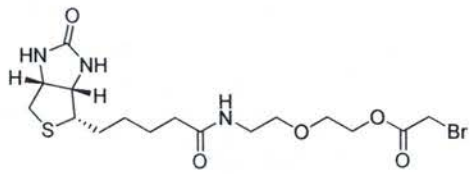

(189)

Figure 4.5. The chemical structure of the biotinylated derivative (**189**) prepared by Qi *et al.* in the preparation of biotin conjugated nanoparticles.[149]

Despite the limited solubility, HSQC and HMBC data were acquired to aid identification and assignment of the carbon signals, in particular the quaternary carbons, by ^{1}H–^{13}C correlations. Several observations were key to allow complete assignment and are summarised in Figure 4.6.

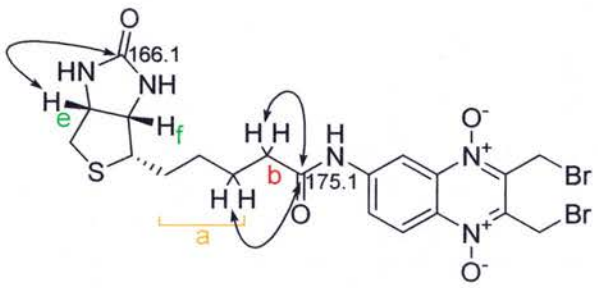

Figure 4.6. Selected key correlations were observed in the HMBC spectra of **187** to identify and allow assignment of the ^{13}C NMR and ^{1}H NMR signals. In particular, the carbonyl carbon of the biotin unit was assigned based on observed correlation to H_e and assignment of H_e and H_f was achieved in combination with HSQC data.

All seven quaternary carbon signals were observed by HMBC correlations. In particular, the carbonyl carbon of the biotin unit was difficult to identify. Assignment was possible based on an observed correlation of a carbon signal at 166.1 ppm to a proton signal at 4.49-4.44 ppm, assigned to the proton labelled H_e (Figure 4.6). The second carbonyl carbon shift was assigned based on an observed correlation of a resonance at 175.1 ppm to signals in the proton spectrum corresponding to the methylene protons labelled H_b and H_a.

Mass spectrometric analysis for **187** was consistent with the assigned structure with peaks at *m/z* 614, 612, and 610 corresponding to the triplet isotope pattern expected for $[M + Na]^+$ due to the presence of two Br atoms per molecule. The successful synthesis of **187** from the hydrobromide salt **184** not only provides a valuable reagent but the precursor **184**

can, in theory, be used in several conjugation approaches to provide a variety of chemical probes (see Sections 3.2 and 3.3).

187 has been observed to undergo significant decomposition upon storage in CD_3OD with exposure to daylight whereas only a small amount of degradation was observed by LC-MS upon storage of the solid at –20 °C in the absence of light. Inspection of the literature highlighted a paper by Elina *et al.* reporting the photochemical degradation reactions of **27** and related quinoxaline *N*-oxides in hydroxyl-containing solvents (water, methanol, and ethanol) on exposure to light.[150] The authors identified a series of degradation products however, the associated mechanism for conversion remains unclear. The implication of this degradation was that any biological experiments using the biotinylated analogue **187** or derivatives of **27** required the use of freshly dissolved material in anhydrous DMSO and careful storage at –20° C with minimal exposure to light.

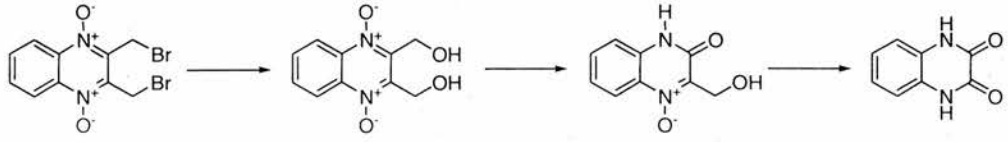

(27) **(34)** **(190)** **(191)**

Scheme 4.6. Degradation of **27** observed by Elina *et al.*[150] **27** was observed by chromatographic separation to hydrolyse to **34** followed by photochemical degradation to **191** via **190** after preparation of a solution of **27** in EtOH with heating. Without the use of heat in the preparation of the sample peaks corresponding to **191** only were observed.

In fact, the activity of **27** (and derivatives **110** (NHBoc) **142** (Br), and **145** (NO_2), Chapter 3) was observed to decrease upon storage over 8-10 weeks. This observation indicates that the biologically active compound in the invasion assay is not a degradation product of **27**. In light of Elina's study it is reasonable to suggest that the observed decrease in biological activity is the result of degradation of the parent compound to the corresponding dihydroxyl analogues (cf. **34**) known to be inactive.[11]

3.13 Biological Activity of the Biotinylated Analogue 187

Unfortunately, **187** was found to be inactive in the *T. gondii* invasion assay (carried out in the lab of Prof. G. E. Ward) and was shown to have no effect at the highest concentration assayed (100 μM, using a fresh sample). The fact that **187** was inactive was

postulated to be the result of the biotin moiety rendering **187** membrane impermeant, for which there exists literature precedent.[151] Therefore, despite the associated disadvantages, performing biological experiments using parasite cell extracts has been explored in Prof. Ward's laboratory. Initial results from these experiments will be discussed in Section 4.0. Since the use of **187** was not optional attempts to prepare alternative chemical probes based on **27** were also carried out, aimed at preparing a cell permeable analogue.

3.2 DEVELOPING AN AZIDE-CONTAINING CHEMICAL PROBE

Alternative *in vivo* labelling strategies have recently appeared in the literature and have already been briefly introduced (see Chapter 1). These methods require the appendage of a tag or reactive functional group that doesn't compromise the pharmacokinetics of the original small molecule. The synthesis of an azide-containing derivative **195** was explored as a means of accessing a potentially cell permeable analogue of **27** which could be later applied in an *in vivo* two-step labelling approach towards target identification.

3.2.1 Attempted Synthesis of a 6*N*-phenyl-azido Analogue 195

The proposed synthetic route for incorporation of an azido functional group took advantage of the previously prepared hydrobromide salt **184** (Scheme 4.7). This approach involved the synthesis of the precursor 4-azidobenzoic acid (**193**), which was achieved in excellent yield using a literature procedure involving reaction with a combination of sodium nitrite and sodium azide.[152,153] Subsequent conversion of **193** to the corresponding acid chloride **194** using thionyl chloride was then achieved in excellent yield. The successful formation of **194** was confirmed by comparison of its melting point with the literature value.[153] The coupling of **194** with the hydrobromide salt **184** was attempted under analogous conditions to those used in the preparation of **187** and was expected to yield **195**. However, this reaction proved extremely difficult, producing an intractable mixture of products. None of the desired product was obtained and attempts to isolate any product or related material proved unsuccessful. Due to time restrictions further attempts to successfully prepare **195** were not undertaken.

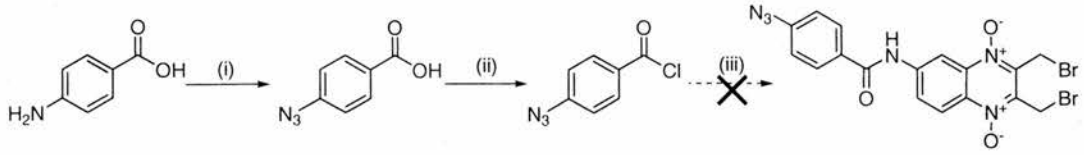

(192) **(193)** **(194)** **(195)**

Scheme 4.7. Two step coupling attempted towards the preparation of 6*N*-phenyl-azido analogue **195**. *Reagents and conditions:* (i) a) $NaNO_2$ (1.2 equiv.), 10% aq. HCl, 0-5 °C, 30 mins.; b) NaN_3 (1.2 equiv.), H_2O, 0-5 °C, 1 h; RT, 12 h, 98% (ii) $SOCl_2$ (xs), reflux, 45 mins. 99% (iii) HBr salt **184**, pyridine, THF, 12h.

3.3 LABELLING WITH A CELL PERMEABLE FLUOROPHORE

Another approach that was considered involved the synthesis of a molecular probe based on **27**, containing a fluorescent tag, specifically BODIPY (**196**, Figure 4.7). BODIPY fluorophores are a relatively new class of probes whose chromophore (shown in Figure 4.7) can be modified by substitutions particularly at the 1, 3, 5, 7, and 8 positions to generate an attachment site and alter the fluorescent characteristics.[27] BODIPY fluorescent conjugates of low molecular weight molecules are commonly cell permeable (due to the absence of ionisable groups) and therefore make ideal tools for imaging in live cells.[154] A range of BODIPY derivatives can be purchased from Molecular Probes, however these are relatively expensive (typically, 5 mg costs > £100).

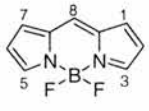

(196)

Figure 4.7. The basic structure of BODIPY fluorophores, based on 4,4-difluoro-4-bora-3a,4a-diaza-s-indacene. BODIPY is a registered trademark of Molecular Probes; U.S. Patent 4,774,339.

3.3.1 Designing a BODIPY Fluorescent Probe

The proposed synthesis of a BODIPY derivative **199** is outlined in Scheme 4.8. Incorporation of the BODIPY moiety is required in a limited number of steps since only small-scale reactions would be feasible based on cost. Therefore an analogous coupling procedure to that for the synthesis of **187** was chosen, again utilising the hydrobromide salt **184**. However, based on the poor performance of the coupling chemistry in the case of **187** and the attempted synthesis of **195**, and the requirement of a large excess of the labelling reagent it was felt that this option was not possible given expense.

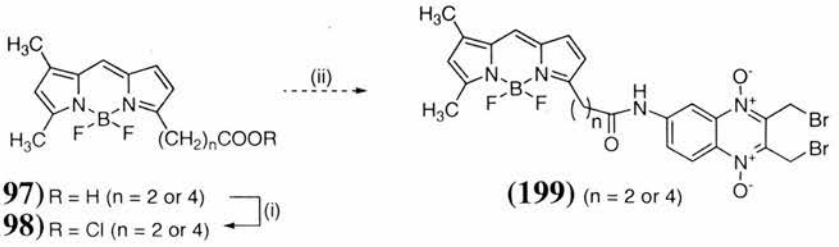

Scheme 4.8. Proposed synthesis of a BODIPY derivative **199**. **197** when n = 2, BODIPY® FL 5 mg, £136.30; n = 4, BODIPY® FL C_5 1 mg, £68.70 (Cost as of 9th March 2006, Molecular Probes). *Reagents and conditions:* (i) $SOCl_2$, RT/reflux; (ii) HBr salt **184**, pyridine, DMF, RT.

3.4 SUMMARY

A biotinylated derivative of **27**, **187**, has been successfully synthesised. **187** could only be used in target identification approaches involving the use of cell lysates due to its inactivity in the cell-based assay (presumably as a result of its poor cell permeability). The synthesis of the hydrobromide salt analogue **184** in theory provides a modifiable derivative from which a variety of reagents can be synthesised. Compounds have been designed to allow fluorescent (**199**) and two-step labelling (**195**). Once an optimised coupling procedure has been established these can be used in conjunction with **184** to provide a very useful and potentially powerful set of reagents.

4.0 BIOLOGICAL APPLICATION OF THE BIOTINYLATED AFFINITY REAGENT 187

The biological experiments presented in this chapter were carried out in the laboratory of Prof. Gary E. Ward at the University of Vermont by Dr. Jeralyn Haraldsen. The goal of these experiments was to try and identify the protein binding partners of **27** in *T. gondii*.

4.1 SEARCHING FOR PROTEIN BINDING PARTNERS OF 27 IN PARASITE EXTRACTS

The first experiment examined whether incubation of **187** with parasite cell extracts would result in biotinylation of any proteins. Following incubation of **187** (100 μM) with a total *T. gondii* protein extract the proteins were acetone precipitated and separated by 1D SDS-PAGE. Labelled proteins were detected by western blot using streptavidin-HRP conjugate and enhanced chemiluminescent (ECL) reagents. Prior to

loading, the proteins are resuspended in SDS buffer containing β-mercaptoethanol and heated, therefore the only proteins to be observed would be those *covalently* bound to **187**. Any non-covalent interactions would be expected to be disrupted by this treatment and **187** itself is of low molecular weight so runs off the gel and is undetectable.

Examining the western blot (Figure 4.8, A) showed strong labelling of multiple bands, even at the lowest concentration of parasite proteins loaded. Such a high number of protein bands was extremely disappointing since it suggested that **27** was extremely unselective in binding to proteins in cell extracts. Further evidence in support of this assumption was obtained following incubation with decreasing amounts of **187** to try and distinguish a specifically labelled protein. This resulted in a decreased level of labelling (i.e. the intensity of the biotin signal) but the pattern of bands labelled remained the same (Figure 4.8, B). Furthermore, the pattern of biotinylated proteins is in fact similar to that of the total protein profile of the extract (data not shown, revealed by staining with Sypro Ruby).

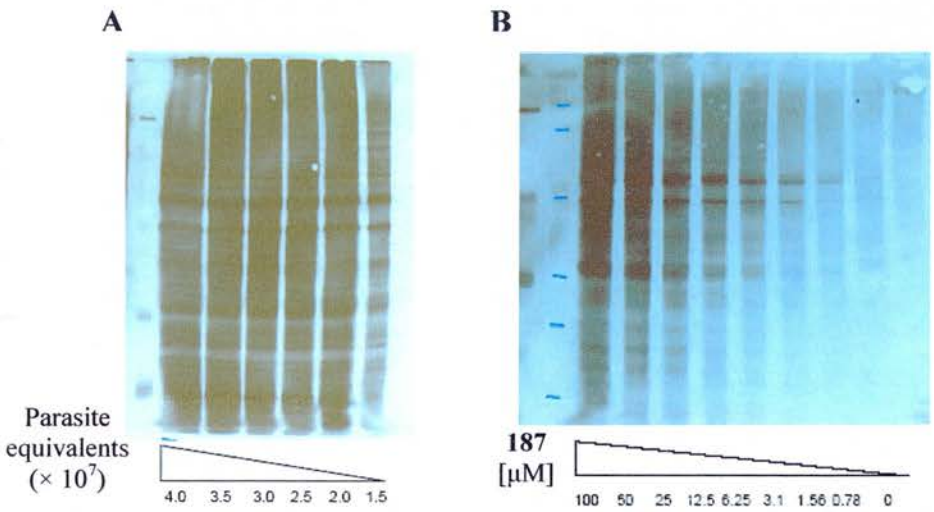

Figure 4.8. Detection of blotted biotinylated proteins using streptavidin-horseradish peroxidase (HRP) conjugate to produce a chemiluminescent read-out. Biotinylation of parasite proteins shows high levels of binding (**A** + **B**). Decreasing the concentration of **187** decreased the amount of biotinylated proteins but the pattern remains the same (**B**). The biotinylation profile is similar to that of the total protein profile (data not shown).

In conclusion, this result implies that **27** is capable of covalent modification of a large number of proteins, as would be expected for a non-selective alkylating agent. However, **27** was previously observed to possess a level of selectivity in the secondary biological assays (see Chapter 1, Section 3.3). This led to the hypothesis that the large

"background" level of proteins labelled by **187** was a result of labelling of proteins that would usually be inaccessible to **27** in live parasites.

4.2 INTERACTION OF PROTEIN-BASED THIOL GROUPS WITH 187

One likely explanation was that **27** could irreversibly interact with free SH groups, one of which could likely be the target protein. However, it remains difficult to explain how this could elicit the selective biological profile given the relatively simple structure of **27**.

In order to test whether any of the biotinlyated protein bands are a result of labelling by sulfur the parasite extract was pre-treated with iodoacetamide (a known sulfur alkylating reagent) before incubation with **187** (50 μM). Iodoacetamide was proposed to block labelling of available sulfur containing residues and hence only labelling by other protein nucleophiles might be expected to be observed.[155]

Figure 4.9. Pretreatment of a parasite cell lysate with iodoacetamide greatly reduced the amount of biotinylated proteins (right) observed compared to the biotinylation profile resulting from untreated parasite cell lysate (left).

Pretreatment of the parasite cell extract with iodoacetamide greatly reduced the overall amount of biotinylated protein bands (Figure 4.9). This result provided evidence in support of the assumption that **187** is able to label sulfur-based protein nucleophiles. Moreover, protein bands were still labelled by **187** after iodoacetamide treatment. This indicated the possibility of **187** being able to bind to proteins through a non-sulfur based nucleophile such as nitrogen.

Assuming that binding through nitrogen nucleophiles is possible then the scenario presented in Chapter 2 may well be of relevance. Two mechanistic possibilities can be presented for binding through a protein-based nitrogen nucleophile resulting in either irreversible covalent modification (Figure 4.10, A) or reversible binding (Figure 4.10, B).

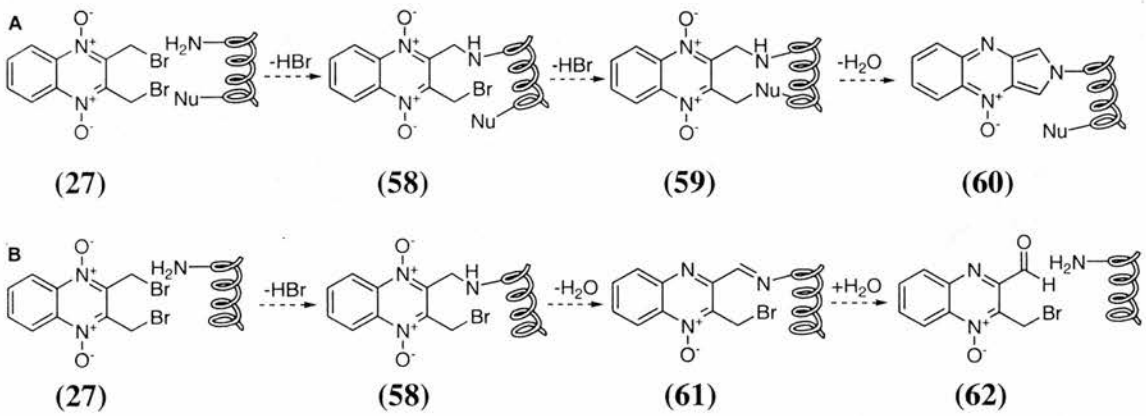

Figure 4.10. A schematic representation of one method for covalent protein modification of a protein by **27**. **A.** Covalent modification by a 'double-hit' nucleophilic displacement reaction to form a protein-inhibitor complex **27**. **B.** Involvement of only a single nucleophile is predicted to be reversible. If a second nucleophile is unavailable hydrolysis of an imine intermediate is proposed leading to turnover of **27** and reformation of native enzyme that is available for reaction with a competitive inhibitor.

Three interesting protein bands were reproducibly prominently labelled (Figure 4.11, A + B). Two of these bands, at ~50 and ~66 kDa, could not be competed off by addition of **27** after incubation indicating that binding of **187** was irreversible. Identification of these protein bands is therefore interesting to try and assess whether the mechanistic studies are of relevance.

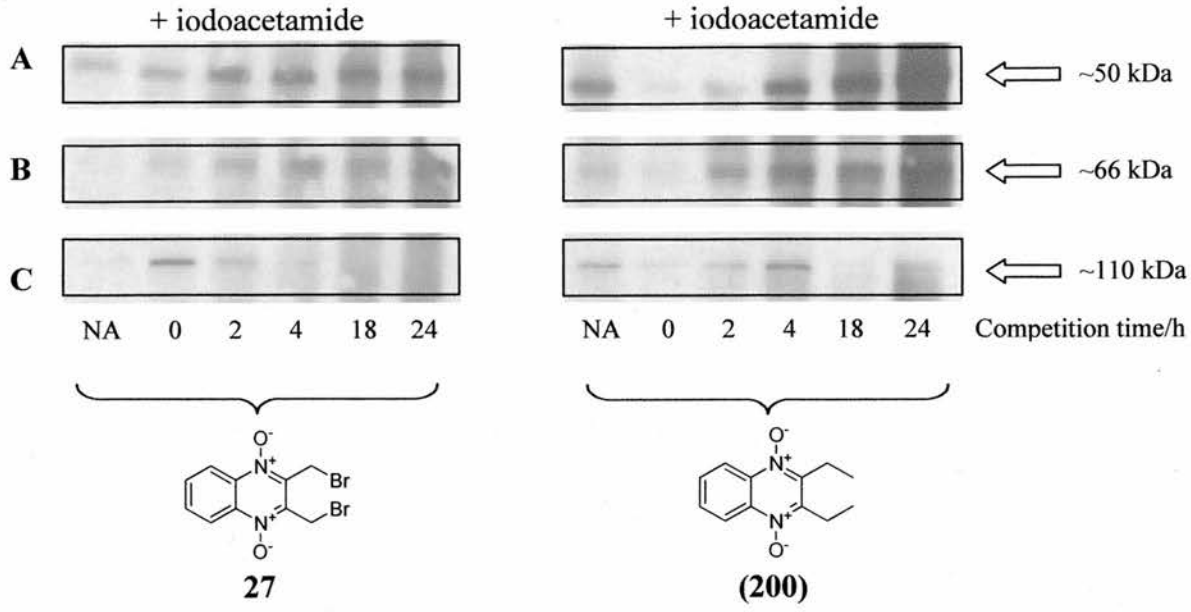

Figure 4.11. Selected enlarged images of the interesting protein bands observed from incubation of **187** with *T. gondii* protein extract pre-treated with iodoacetamide. Addition of either **27** or **200** and incubation for varying lengths of time was investigated to determine if the binding proteins to **187** could be competitively displaced. 2,3-diethylquinoxaline 1,4-dioxide (**200**) has previously been shown to be inactive against invasion of *T. gondii* parasites into host cells. **200** was therefore used as a control in biological experiments involving **187**. Two bands at ~50 and ~66 kDa were irreversibly labelled by **187**. A third band at ~110 kDa appeared to be successfully competed by **27**. One possible explanation for the observed reversible binding is through a nitrogen-based nucleophile. Slow hydolysis of an imine intermediate would allow for subsequent binding of a target protein to **27**. NA = none added.

A third band was also revealed at ~110 kDa (Figure 4.11, C). This band appeared to be successfully competed off by **27** in a time dependent manner and after only 4 hours incubation with **27** was still present when competed off by the inactive analogue **200**. One possible explanation for this observation is that this protein is labelled by a single nitrogen-based nucleophile and would therefore be expected to be reversible. Hence, **187** can be replaced by **27** (Figure 4.11, B).

In comparison to the competition experiment with **27**, when binding was competed with **200**, after 18 hours the band at ~110 kDa appears absent i.e. no longer biotinylated. This suggests that **187** has been depleted from the extract and after dissociation is unable to reform a covalent bond with the protein. Nonetheless, the inference that a nitrogen-based protein nucleophile can bind to **27** is a pleasing result in the context of the mechanistic studies presented in Chapter 2. Identification of this particular protein is therefore a high priority.

In summary, the fact that the level of proteins labelled by **187** was reduced when the parasite extract was pre-treated with iodoacetamide indicates that **27** has a clear

capability for binding sulfur-based protein nucleophiles. However, as previously alluded to, the high levels of binding proteins observed suggest that this is mostly due to non-specific binding and is likely to be a reflection of exposure to a large number of proteins in the cell lysate that would normally be inaccessible to **27** in live parasites. This large number of binding proteins means that identifying a single protein that may bind specifically is extremely difficult since it will almost certainly be hidden. These results therefore highlighted one of the problems associated with in vitro target identification studies and further studies using **187** were to be abandoned. However, the implication of **187** binding to nitrogen-based nucleophiles is an exciting result based on the mechanistic studies presented in Chapter 2. One further experiment was carried out that involved labelling in live parasites.

4.3 LABELLING EXPERIMENTS USING LIVE PARASITES

To overcome the problem of large amounts of protein labelling in cell lysates a further experiment was designed and carried out by the Ward group (Figure 4.13). The biotinylation protein profile of cell extracts was compared for parasites that were pre-treated with either **27** or an inactive derivative (**200**, **201**, **202**, or **64**, Figure 4.12).

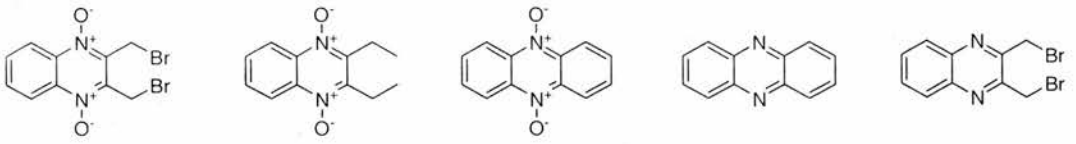

(27) **(200)** **(201)** **(202)** **(64)**

Figure 4.12. The chemical structures of the small molecules used in the live parasite blocking experiment. Compounds **64** and **200-202** have previously been shown to be inactive against invasion of *T. gondii* parasites into host cells and are therefore used as controls.

The rationale predicted that incubation of the live parasites with **27** would allow **27** to bind its *in vivo* protein target(s). Treatment of the protein extract, generated from these preincubated parasites, with **187** (50 μM) should then result in the loss of a biotinylated band(s) corresponding to the *in vivo* labelled protein(s).

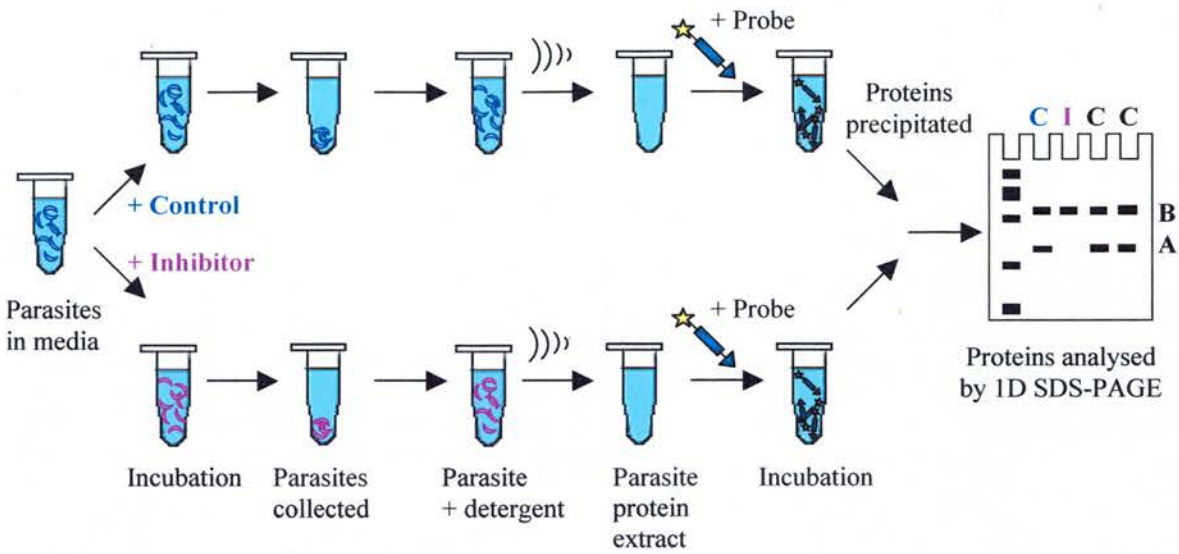

Figure 4.13. Schematic describing the experimental procedure for the live parasite blocking experiments. Live parasites were pre-treated with either a control (C) or inhibitor (I) before preparing the parasite cell lysate. The biotinylated probe **187** was added and following incubation the biotinylated proteins in the lysates compared by 1D SDS-PAGE and western analysis. If a protein was covalently bound *in vivo* by the inhibitor it would be unavailable to bind to the biotinylated probe and the band on the gel corresponding to this protein would be absent when compared to the controls (band A). Any proteins which are labelled non-specifically in the cell lysate would show no difference compared to the controls (band B).

Figure 4.14 shows the resulting western blots from two independently performed experiments, stained with ECL Streptavidin-HRP to visualise biotinylated proteins. Unfortunately, both blots contain patches where labelling could not be observed and therefore two sets of data are shown where these appear in different locations on each blot. Despite this, comparison of the biotinylation profile from parasites pre-treated with **27** prior to extraction revealed, excitingly, two bands that are clearly absent (Figure 4.14, lane 2) but are present in all of the samples treated with either DMSO (control, lane 1) or inactive derivatives (lanes 3-6). These bands are reproducibly observed at ~25 kDa and ~110 kDa, with a third, more subtle difference within the triplet of bands at ~45 kDa that cannot be seen from the images reproduced here. These proteins could be possible *in vivo* targets for **27** capable of mediating the inhibitory invasion effect of *T. gondii* into host cells and for this reason are worthwhile pursuing for the purposes of identification.

Interestingly, the protein band at ~110 kDa is of a similar molecular weight to the band that has been previously identified from the experiments discussed using iodoacetamide (Section 4.2). This reinforces the importance of obtaining identification of this protein as a possible target for **27**, as it is both biologically and chemically interesting. The bands that were previously labelled at ~50 and ~66 kDa in the iodoacetamide experiment are again labelled following pre-treatment of the live parasites with **27**.

Therefore, since these proteins are not labelled following incubation of **27** with whole parasites and only bind *in vitro*, this indicates that these proteins are unlikely to be mediating the inhibitory invasion effect on the parasites. From a chemical perspective they remain, of course, of interest.

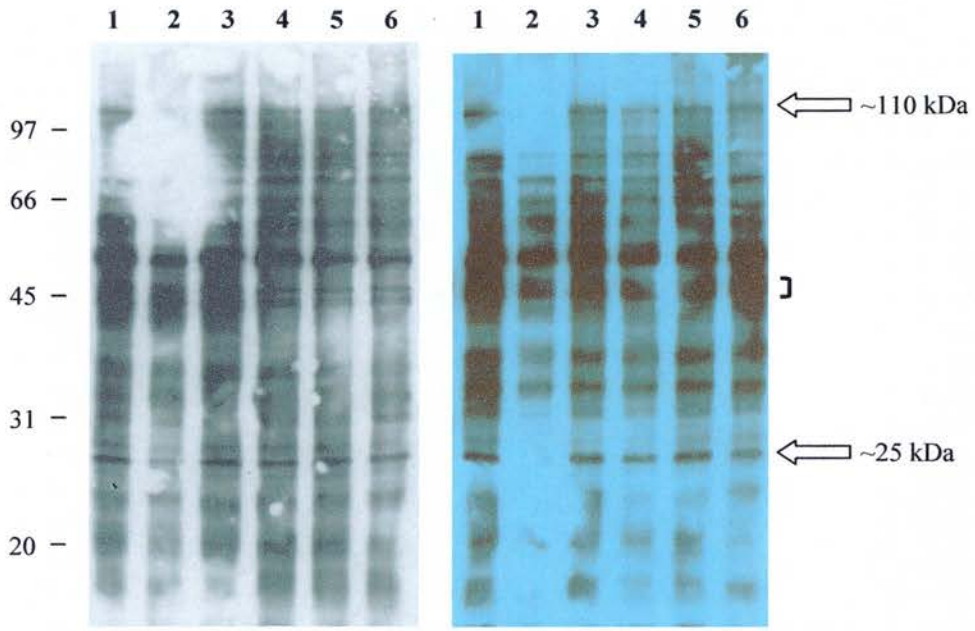

Figure 4.14. The biotinylation profile of the parasite extract following pre-treatment of the live parasites with reagents **1.** DMSO; **2. 27** (active); **3. 200**, **4. 201**, **5.** phenazine (**202**), and **6. 64** (inactive). Western blots shown from two independently performed experiments. Excitingly, there appears to be two protein bands missing, ~25 kDa and ~110 kDa, and a third, more subtle, difference within the triplet of bands at ~40kDa. It is possible that these proteins could be responsible for mediating the inhibition of *T. gondii* into host cells.

Unfortunately, due to time restrictions, analysis of these protein bands has not been possible in time to be included in this thesis. The biological results presented are extremely promising, in particular the two protein bands (at ~110 kDa and ~25 kDa) are considered a first priority in the context of this project. It is hoped that use of 2D SDS-PAGE will highlight resolved protein bands more clearly for subsequent identification by LC-MS/MS analysis.

5.0 Conclusion

In conclusion, the successful development of a chemical probe based on **27** has been achieved with the synthesis of the biotinylated derivative **187**. Isolation of the key compound **184** enabled access to **187**, as well as providing a potential starting point for the future development of other chemical probes based on **27**. Preliminary biological

experiments involving incubation of **187** with *T. gondii* cell lysates have been initiated in the laboratory of Prof. Gary E. Ward. These experiments have indicated that a large number of proteins were labelled by **187** *in vitro* and the number of binding proteins was dramatically reduced following pretreatment of the cell lysate with iodoacetamide. Proteins at ~50, ~66 and ~110 kDa were observed to bind to **187** following iodoacetamide treatment and it is proposed that these are bound through non-sulfur based residues with interesting implications for the chemistry of labelling of these proteins by **27**. Competition experiments, involving live parasites, identified two exciting proteins at ~25 kDa and ~ 110 kDa (previously identified in the iodoacetamide experiment) as protein binding partners of **187** and **27**. Further experiments are now required to identify and ultimately validate these proteins as the cellular target of **27**.

The high level of proteins that have been observed to bind unselectively to **187** suggests that the usual approach to affinity chromatography using a covalent modifier involving trypsin digestion would not be an appropriate target identification method for **27**. However, future development of **180** remains a key approach to the design of a cleavable linker for affinity chromatography applications using covalent modifiers. Studies concerning the development of the cleavage chemistry will be presented in Part II.

CHAPTER 5

EXPERIMENTAL

1.1 General procedures

Chemicals and solvents were purchased from Acros Organics, Alfa Aesar-Avocado/Lancaster, Bamford Laboratories, Fisher Scientific or Sigma-Aldrich and were used as received unless otherwise stated. All reactions were performed in flame or oven-dried glassware under a positive pressure of nitrogen or argon unless otherwise stated. Diethyl ether (Et_2O) and tetrahydrofuran (THF) were dried by refluxing with sodium-benzophenone under an atmosphere of N_2 and collected by distillation. Dichloromethane (DCM) was dried by heating under reflux over calcium hydride and distilled under an atmosphere of nitrogen. Pyridine and triethylamine were dried over KOH pellets. Thionyl chloride was freshly distilled under an atmosphere of nitrogen before use. PE 40-60 refers to the fraction of light PE 40-60 boiling in the range 40-60 °C. *m*CPBA was purified by dissolving in DCM and washing with KH_2PO_4 (1.0 M solution, pH 7.4 – 7.5). The DCM phase was then treated as for a separation. 2,6-Lutidine was distilled from CaH_2 under an N_2 atmosphere.

Analytical thin-layer chromatography (TLC) was performed on pre-coated TLC plates SIL G-25 UV_{254} (layer 0.25 mm silica gel with fluorescent indicator UV_{254}) (Aldrich). Developed plates were air dried and analysed under a UV lamp, Model UVGL-58 (Mineralight LAMP, Multiband $UV_{254/365}$ nm) and where necessary stained with iodine on silica, a solution of ceric ammonium molybdate (CAM), potassium permanganate, or *p*-dimethyaminocinnamaldehyde (DACA) to aid identification. Flash column chromatography was performed using silica gel (40-63 μm, Fluorochem).

Melting points were recorded using an Electrothermal 9100 capillary melting point apparatus. Values are quoted to the nearest 0.5 °C and are uncorrected.

Fourier Transform Infra-red (FT IR) spectra were recorded on a Perkin Elmer Paragon 1000 FT spectrometer. Absorption maxima are reported in wavenumbers (cm^{-1}) and intensities are quoted as strong (s), medium (m), weak (w), and broad (br).

Microanalyses for carbon, hydrogen and nitrogen were performed by Mrs. Sylvia Williamson, using EA 1110 CHNS Instruments elemental analyser, at the University of St. Andrews.

Ozone was generated using a Fischer Ozon-Generator 500 using commercial-grade oxygen as a source.

1.2 NMR Spectroscopy

^{1}H Nuclear magnetic resonance (NMR) spectra were recorded either on a Brüker Advance 300 (300.1 MHz), Brüker Advance 500 (499.9 MHz), or a Varian Gemini 2000 (300.0 MHz). ^{13}C NMR spectra using the PENDANT sequence were recorded on a Bruker Advance 300 (75.5 MHz) or a Bruker Advance 500 (125.7 MHz) spectrometer. All other ^{13}C spectra were recorded on a Varian Gemini 2000 (75.5 MHz) spectrometer using composite pulse ^{1}H decoupling. All NMR samples were acquired using the deuterated solvent as the lock and the residual solvent as the internal reference. The chemical shift data for each signal are given as (δ) in units of parts per million (ppm). Coupling constants (J) are quoted in Hz and are recorded to the nearest 0.1 Hz. The multiplicity used in the assignment of ^{1}H NMR spectra is indicated by the following abbreviations: s, singlet; d, doublet; dd, doublet of doublets; ddd, doublet of doublets of doublets; dt, doublet of triplets; t, triplet; q, quartet, m, multiplet and br, broad. Signals were assigned by means of two-dimensional (2D) NMR spectroscopy (^{1}H-^{1}H COSY (Correlated Spectroscopy), ^{1}H-^{13}C COSY (HSQC: Heteronuclear Single Quantum Coherence) and long-range ^{1}H-^{13}C COSY spectra (HMBC: Heteronuclear Multiple Bond Correlation).

1.3 Mass Spectrometry

Low and high-resolution mass spectral analysis (EI and CI) were recorded using a VG AUTOSPEC mass spectrometer or a Micromass GCT (Time-of-Flight), high performance, orthogonal acceleration spectrometer coupled to an Aglient Technologies 6890N GC system. Electrospray mass spectrometry (ES) was recorded on a high performance orthogonal acceleration reflecting TOF mass spectrometer operating in positive or negative ion mode, coupled to a Waters 2975 HPLC. Major peaks only are reported and intensities and assignments are given in parantheses.

1.4 Determining Enantiomeric Purity

Enantiomeric excesses (*ee*) were measured using chiral high performance liquid chromatography (HPLC); HPLC system which includes a Waters 2996 photodiode array detector, Waters 2795 Alliance HT Seperations Module, Micromass LCT, Thinkcenter

IBM running MassLynx™ 4.0 Global. Separations were performed using a Daicel® Chiralpak AD-RH HPLC analytical chiral column (150 × 4.6 mm, 5 μm).

Optical rotations were measured on an Optical Activity AA-1000 automatic polarimeter (Optical Activity Ltd. Polarimeter millidegree-autoranging), operating at 589 nm using a 2 mL solution cell with a 20 cm path length. The concentration (c) is expressed in g/100 mL (equivalent to g/0.1 dm^3). Specific rotations are denoted $[\alpha]_D^T$ and are given in units of 10^{-1} deg cm^2 g^{-1} (T = ambient temperature in °C).

1.5 X-Ray Crystallography

X-Ray crystallographic analysis was performed at the University of St. Andrews by Professor Alexandra Slawin. X-Ray Crystallography data were recorded on: a) Brüker SMART diffractometer with graphite-monochromated Mo-Kα radiation (λ = 0.71073 Å), sealed tube and CCD detector, b) Mer-Rigaku, mercury detector 007 with Mo-Kα radiation (λ = 0.71073 Å) generator (rotating anode), or c) Cop-Saturn 92 detector 007, Cu-Kα radiation with rotation.

1.6 Electronic Structure Calculations

Electronic structure calculations were performed at the University of St. Andrews by Dr. Douglas Philp. Transition states for the formation of compounds **53** and **72** by an intramolecular S_N2 mechanism were calculated using GAMESS[156] (Version 19 May 2004 R4). Initial transition state guesses were generated from calculations at the HF/3-21G level of theory and these structures were used as the starting point for calculations at the HF/6-31G(d) level of theory. These calculations also included corrections for the solvent ($CHCl_3$) using the PCM solvation[157,158] model. Transition state structures were characterised by vibrational frequency analysis, ensuring that there was only one imaginary frequency and that the imaginary vibration corresponded to the reaction coordinate.

1.7 General kinetic NMR procedure (NMR scale reactions): Method A

Quinoxaline derivative (**27**, **64**, **69**, **94**, **110**, **142**, or **145**) (0.5 mL of a 40 mM solution in $CDCl_3$ equilibrated to 25 °C) and *n*-butylamine (0.5 mL of a 120 mM solution

in $CDCl_3$ equilibrated to 25 °C) were mixed together in an NMR tube at 25 °C and then monitored by 500 MHz ^{1}H NMR over a 17 h period by a Varian UNITYplus 500 MHz NMR spectrometer. An initial concentration of 20 mM was chosen based on solubility and NMR sensitivity limits required to track reaction intermediates. The same protocol was performed at a five-fold dilution (4 mM) for **27**. The raw data were analysed, relative to the $CHCl_3$ signal using the deconvolution tool available within 1D WINNMR. Peaks representing starting material, reaction intermediates and products were normalised once correctly assigned. In a limited number of situations where the benzylic methylene signal was obscured, by the signal assigned to the NH_2 in unreacted *n*-butylamine, a best fit data point (relative to the ratio of material before and after that specific time point) is included for clarity.

1.8 General Procedure for Reactions of Quinoxaline Derivatives With Diethylamine: Method B

To a solution of the quinoxaline derivative (0.5 mL of a 40 mM solution in $CDCl_3$) was added a solution of diethylamine (0.5 mL of a 120 mM solution in $CDCl_3$) in an NMR tube at 25 °C and then monitored by 300 MHz ^{1}H NMR. The excess of diethylamine was used to drive the reactions to completion, in order to assist interpretation of the ^{1}H NMR spectra.

2,3-Bis(bromomethyl)quinoxaline, 64[107]

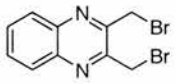

A solution of 1,2-phenylene diamine (6.81 g, 63.0 mmol) in anhydrous THF (40.0 mL) was added to 1,4 dibromo-2,3-butanedione (14.6 g, 60.0 mmol) in anhydrous THF (80.0 mL) at 0 °C over 15 mins. with stirring. The reaction was warmed to room temperature and stirred for a further 17 h. After concentration *in vacuo*, the crude material was partitioned between 10% w/v aqueous sodium hydrogen carbonate solution (150 mL) and DCM (200 mL). The organic phase was washed with brine (100 mL), dried ($MgSO_4$) and concentrated *in vacuo* to give a dark brown solid. Purification by flash column chromatography on silica gel (EA:PE 40-60, 1:9) gave **64** as a white crystalline solid (16.7 g, 52.9 mmol, 88%); mp 153.0 °C, (sharp, recrystallised from EA:PE 40-60) (lit. 150.0-151.0 °C, acetone/ethanol).[107] **IR** (NaCl, Nujol) ν_{max}: 774 (s) (ArC–H), 696 (m) (C–Br) cm^{-1}; **^{1}H NMR** (300 MHz, $CDCl_3$): δ 8.10-8.04 (m, AA′ part of the AA′XX′ system, 2H, H-5 and H-8), 7.82-7.76 (m, XX′ part of the AA′XX′ system, 2H, H-6 and H-7), 4.93 (s, 4H, 2 × $C\underline{H}_2$); **^{13}C NMR** (75.5 MHz, $CDCl_3$): δ 150.8 (C2 and C3), 141.5 (C4a and C8a), 130.9 (C6 and C7), 129.0 (C5 and C8), 30.5 (2 × $\underline{C}H_2$); **MS-EI+** (*m/z*) 318 ($[M]^{+\bullet}$, 2 × ^{81}Br, 20%), 316 ($[M]^{+\bullet}$, ^{79}Br + ^{81}Br, 40), 314 ($[M]^{+\bullet}$, 2 × ^{79}Br, 20), 237 ($[M - Br]^{+\bullet}$, ^{81}Br, 100), 235 ($[M - Br]^{+\bullet}$, ^{79}Br, 100), 156 ($[M - 2Br]^{+\bullet}$, 65); **HRMS-EI+** (*m/z*) Calcd for $C_{10}H_8N_2Br_2$ $[M]^{+\bullet}$: 315.9034, found 315.9035; **Anal.** Calcd for $C_{10}H_8N_2Br_2$: C, 38.01; H, 2.55; N, 8.87. Found: C, 37.87; H, 2.27; N, 8.72. Structure also confirmed by X-ray crystallographic analysis.

2,3-Bis(bromomethyl)quinoxaline 1,4-dioxide, 27

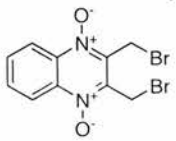

Purified *m*CPBA (13.8 g, 80.0 mmol) was added to a solution of **64** (5.06 g, 16.0 mmol) in anhydrous DCM (160 mL) with stirring at room temperature. After 42 h the reaction mixture was diluted with DCM (1.00 L) and washed with 10% w/v aqueous sodium carbonate solution (2 × 250 mL). The organic phase was dried ($MgSO_4$) and concentrated *in vacuo* to give a yellow solid. Purification by flash column chromatography on silica gel (EA:PE 40-60, 1:4) gave **27** as a bright yellow crystalline solid (3.64 g, 10.5

mmol, 65%); mp 178.5-179.0 °C (recrystallised from EA) (lit. 188.0-189.0 °C, dioxane).[100] **IR** (NaCl, Nujol) ν_{max}: 1341 (m) (N–O), 1036 (w), 774 (w) (ArC–H), 643 (m) (C–Br) cm^{-1}; **^{1}H NMR** (300 MHz, $CDCl_3$): δ 8.69-8.63 (m, AA' part of the AA'XX' system, 2H, H-5 and H-8), 7.92-7.86 (m, XX' part of the AA'XX' system, 2H, H-6 and H-7), 4.94 (s, 4H, 2 × CH_2); **^{13}C NMR** (75.5 MHz, $CDCl_3$): δ 139.8 (C2 and C3), 137.6 (C4a and C8a), 132.5 (C6 and C7), 120.7 (C5 and C8), 20.5 (C9 and C10); **MS-ES+** (*m/z*) 373 ($[M + Na]^+$, 2 × ^{81}Br, 18%), 371 ($[M + Na]^+$, ^{79}Br + ^{81}Br, 100), 369 ($[M + Na]^+$, 2 × ^{79}Br, 20); **HRMS-EI+** (*m/z*) Calcd for $C_{10}H_8Br_2N_2O_2$ $[M]^{+\bullet}$: 345.8952, found 345.8949; **Anal.** Calcd for $C_{10}H_8Br_2N_2O_2$: C, 34.51; H, 2.32; N, 8.05. Found: C, 34.25; H, 1.95; N, 7.70. In addition **69** was isolated as a white crystalline solid (0.930 g, 2.8 mmol, 18%). Structure also confirmed by X-ray crystallographic analysis.

(3-(Bromomethyl)quinoxalin-2-ylmethyl)butylamine 1,4-dioxide, intermediate 53 and **Butyl(3-(butylaminomethyl)quinoxalin-2-ylmethyl)amine 1,4-dioxide, intermediate 54**

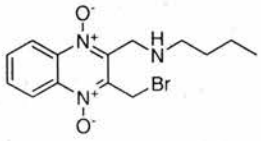

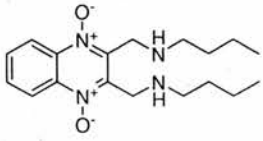

Prepared according to the general kinetic NMR procedure (Method A) using **27** with *n*-butylamine. After 522 s formation of intermediate **53** was observed in the presence of *n*-butylamine. Attempts to isolate **53** proved unsuccessful. Intermediate **53**: **^{1}H NMR** (500 MHz, $CDCl_3$): δ 8.67-8.60 (m, 2H, H-5 and H-8), 7.90-7.82 (m, 2H, H-6 and H-7), 4.99 (s, 2H, CH_2Br), 4.26 (s, 2H, CH_2NH), 2.77-2.67 (m, 2H, NCH_2 of *n*Bu) 1.54-1.48 (m, 2H, NCH_2CH_2 of *n*Bu), 1.39-1.33 (m, 2H, CH_2CH_3), 0.92-0.89 (m, 3H, CH_3). After 54572 s intermediate **54** was observed in the presence of **56** and excess *n*-butylamine. Attempts to isolate **54** proved unsuccessful. Intermediate **54**: ^{1}H NMR (500 MHz, $CDCl_3$): δ 8.62-8.60 (m, AA' part of the AA'XX' system, 2H, H-5 and H-8), 7.85-7.83 (m, XX' part of the AA'XX' system, 2H, H-6 and H-7), 4.28 (s, 4H, 2 × CH_2NH), 2.70 (t, ^3J = 7.2 Hz, 4H, 2 × NCH_2 of *n*Bu), 1.54-1.34 (m, 8H, 2 × $NCH_2CH_2CH_2$), 0.91 (t, ^3J = 7.4 Hz, 6H, 2 × CH_3).

2-Butyl-2*H*-pyrrolo[3,4-*b*]quinoxaline 4-oxide, 56

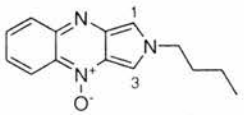

Prepared according to the general kinetic NMR procedure (Method A) using **27** and *n*-butylamine. Also, on preparative scale: A solution of *n*-butylamine (27 mg, 0.37 mmol) in $CDCl_3$ (3.00 mL) was added to a solution of **27** (40 mg, 0.12 mmol) in $CDCl_3$ (2.86 mL) with stirring at room temperature. After 20 h the reaction mixture was quenched with silica and the solvent removed *in vacuo*. Purification by flash column chromatography on silica gel (EA:PE 40-60, 1:9 to 1:4) yielded an unstable dark red oil (25 mg, 0.10 mmol, 90%). **56** was observed to decompose rapidly in the absence of solvent. **IR** (NaCl, Nujol) ν_{max}: 1578 (w), 1544 (w), 1326 (m) (N–O), 745 (m) (ArC–H) cm^{-1}; **^{1}H NMR** (500 MHz, $CDCl_3$): δ 8.55 (d, ^3J = 8.5 Hz, 1H, H-5), 8.00 (d, ^3J = 8.8 Hz, 1H, H-8), 7.67 (d, ^4J = 2.3 Hz, 1H, H-3), 7.61 (d, ^4J = 2.3 Hz, 1H, H-1), 7.59-7.56 (m, 1H, H-6 or H-7), 7.53-7.50 (m, 1H, H-6 or H-7), 4.39 (t, ^3J = 7.1 Hz, 2H, NCH_2 of *n*Bu), 2.02-1.98 (m, 2H, NCH_2CH_2), 1.46-1.34 (m, 2H, CH_2CH_3), 0.97 (t, ^3J = 7.4 Hz, 3H, CH_3); **^{13}C NMR** (75.5 MHz, $CDCl_3$): δ 145.0 (C8a), 137.9 (C9a), 133.5 (C4a), 130.0 (C8), 129.0 (C7), 127.9 (C6), 125.2 (C3a), 118.3 (C5), 111.4 (C1), 103.6 (C3), 53.0 (NCH_2 of *n*Bu), 33.4 (NCH_2CH_2), 19.7 (CH_2CH_3), 13.4 (CH_3); **MS-CI+** (*m/z*) 242 ($[M + H]^+$, 100%); **HRMS-EI+** (*m/z*) Calcd for $C_{14}H_{15}N_3O$ $[M]^{+\bullet}$: 241.1215, found 241.1215.

2-(Bromomethyl)quinoxaline-3-carbaldehyde 1-oxide, 62

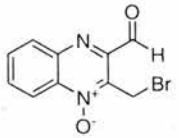

n-Butylamine (202 mg, 2.76 mmol) was added to a solution of **27** (320 mg, 0.92 mmol) in $CHCl_3$ (200 mL) with stirring at room temperature under nitrogen. After 1 h the reaction mixture was quenched by addition of silica and the solvent removed *in vacuo*. Purification by column chromatography on silica (EA:PE 40-60, 1:1 to 1:0) gave **62** as an off-white solid (24 mg, 0.09 mmol, 10%); mp > 150 °C dec. **IR** (NaCl, Nujol) ν_{max}: 1713 (s) (C=O), 1571 (m) (ArC–C), 1351(s) (N–O), 816 (m), 778 (m) (ArC–H), 638 (C–Br) cm^{-1}; **^{1}H NMR** (300 MHz, $CDCl_3$): δ 10.20 (s, 1H, CHO), 8.66-8.61 (m, 1H, H-8), 8.30-8.24 (m, 1H, H-5), 7.97-7.89 (m, 2H, H-6 and H-7), 5.36 (s, 2H, CH_2); **^{13}C NMR** (75 MHz, $CDCl_3$): δ 192.1 (C=O), 146.0 (C3), 143.5 (C4a), 139.2 (C2), 137.3 (C8a), 133.2

(C6 or C7), 132.6 (C6 or C7), 131.1 (C5), 119.4 (C8), 19.5 (CH_2); **MS-EI+** (*m/z*) 268 ($[M]^{+\bullet}$, ^{81}Br, 28%), 266 ($[M]^{+\bullet}$, ^{79}Br, 28), 187 ($[M]^{+\bullet}$ – Br, 100); **HRMS-EI+** (*m/z*) Calcd for $C_{10}H_7{}^{79}BrN_2O_2$ $[M]^{+\bullet}$: 265.9691, found 265.9691. **MS-ES+** (*m/z*) 291 ($[M + Na]^+$, ^{81}Br, 92%), 289 ($[M + Na]^+$, ^{79}Br, 100); **HRMS-ES+** (*m/z*) Calcd for $C_{10}H_7{}^{81}BrN_2O_2Na$ $[M + Na]^+$: 290.9568, found 290.9562; **HRMS-ES+** (*m/z*) Calcd for $C_{10}H_7{}^{79}BrN_2O_2Na$ $[M + Na]^+$: 288.9589, found 288.9583. In addition, **27** (0.194 g, 0.56 mmol, 61%) was recovered.

2,3-Bis(bromomethyl)quinoxaline 1-oxide, 69

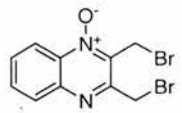

Purified *m*CPBA (0.57 g, 3.30 mmol) was added to a solution of **64** (1.01 g, 3.20 mmol) in anhydrous DCM (20.0 mL) at room temperature. After 20 h the reaction mixture was washed with 10% w/v aqueous sodium carbonate (2 × 20 mL) and the combined aqueous washings extracted with DCM (3 × 50 mL). The combined organic phase was dried ($MgSO_4$) and concentrated *in vacuo* to give a pale yellow solid. Purification by flash column chromatography on silica gel (EA:PE 40-60, 1:9 to 1:4) gave **69** as a white crystalline solid (0.55 g, 1.65 mmol, 52%); mp 168.5-169.0 °C (recrystallised from EA:PE 40-60) (lit. 167.0-168.0 °C).[100] **IR** (NaCl, Nujol) ν_{max}: 1564 (w), 1481 (m), 1357 (m) (N–O), 1060 (w), 769 (m) (ArC–H), 675 (m) and 662 (m) (C–Br) cm^{-1}; **^{1}H NMR** (300 MHz, $CDCl_3$): δ 8.57 (dd, ^3J = 8.5, ^4J = 1.5 Hz, 1H, H-8), 8.07 (dd, ^3J = 8.4, ^4J = 1.5 Hz, 1H, H-5), 7.87-7.73 (m, 2H, H-6 and H-7), 5.02 (s, 2H, CH_2-9), 4.77 (s, 2H, CH_2-10); **^{13}C NMR** (75.5 MHz, $CDCl_3$): δ 152.6 (C3), 143.4 (C4a), 138.5 (C2), 136.3 (C8a), 132.2 (C6), 130.9 (C7), 130.1 (C5), 119.2 (C8), 30.2 (C10), 20.8 (C9); **MS-ES+** (*m/z*) 357 ($[M + Na]^+$, 2 × ^{81}Br, 19%), 355 ($[M + Na]^+$, ^{79}Br + ^{81}Br, 100), 353 ($[M + Na]^+$, 2 × ^{79}Br, 23); **HRMS-EI+** (*m/z*) Calcd for $C_{10}H_8Br_2N_2O$ $[M]^{+\bullet}$: 329.9003, found 329.9002; **Anal.** Calcd for $C_{10}H_8Br_2N_2O$: C, 36.18; H, 2.43; N, 8.44. Found: C, 36.18; H, 2.07; N, 8.14. Structure also confirmed by X-ray crystallographic analysis. Compounds **27** (52 mg, 0.15 mmol, 5%) and **64** (0.41 g, 1.3 mmol, 41%) were also isolated.

2-Butyl-2,3-dihydro-1*H*-pyrrolo[3,4-*b*]quinoxaline, 73 [102] and

7,16-Di-*n*-butyl[1,6]diazecino[3,4-*b*;8,9-*b*´]diquinoxaline, 74

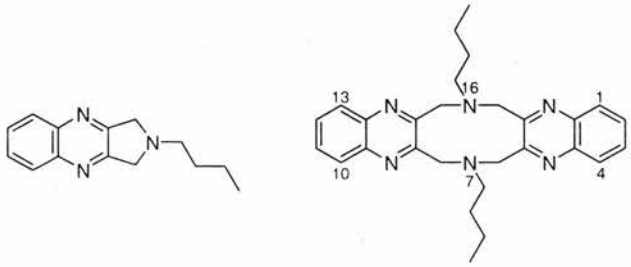

Prepared according to the general kinetic NMR procedure using **64** and *n*-butylamine. Also, on a preparative scale: *n*-butylamine (312 mg, 4.26 mmol) was added to a solution of **64** (449 mg, 1.42 mmol) in $CHCl_3$ (40.0 mL) at room temperature under nitrogen. After 20 h the reaction mixture was concentrated *in vacuo*. Purification by flash column chromatography on silica gel (EA:PE 40-60, 1:3) gave **73** as a pink solid (200 mg, 0.88 mmol, 62%), **74** as a yellow oil (26 mg, 0.06 mmol, 8%) and **75** (trace amounts) as an unstable red oil.

Compound **73**: mp 54.5 °C dec.; **^{1}H NMR** (300 MHz, $CDCl_3$): δ 8.07-8.01 (m, AA´ part of the AA´XX´ system, 2H, H-5 and H-8), 7.75-7.69 (m, XX´ part of the AA´XX´ system, 2H, H-6 and H-7), 4.13 (s, 4H 2 × CH_2N), 2.85 (t, ^3J = 7.5 Hz, 2H, NCH_2 of *n*Bu), 1.70-1.60 (m, 2H, NCH_2CH_2), 1.52-1.39 (m, 2H, CH_2CH_3), 0.99 (t, ^3J = 7.3 Hz, 3H, CH_3); **^{13}C NMR** (75.5 MHz, $CDCl_3$): δ 156.9 (C3a and C9a), 141.7 (C4a and C8a), 129.1 (Ar-C), 128.9 (Ar-C), 57.9 (2 × CH_2N), 56.3 (NCH_2 of *n*Bu), 30.3 (NCH_2CH_2), 20.5 (CH_2CH_3), 14.0 (CH_3); **MS-APCI+** (*m/z*) 270 ([M + H + CH_3CN]$^+$, 20%), 269 ([M + CH_3CN]$^+$, 100), 229 ([M + H]$^+$, 15), 228 ([M]$^+$, 90); **HRMS-CI+** (*m/z*) Calcd for $C_{14}H_{18}N_3$ [M]$^+$: 228.1501, found 228.1497.

Compound **74**: **^{1}H NMR** (300 MHz, $CDCl_3$): δ 8.05-8.00 (m, AA´ part of the AA´XX´ system, 4H, H-1, 4, 10, and 13), 7.72-7.66 (m, XX´ part of the AA´XX´ system, 4H, H-2, 3, 11, and 12), 4.37 (s, 8H, 4 × CH_2N), 2.60 (t, ^3J = 7.7 Hz, 4H, 2 × NCH_2 of *n*Bu), 1.37-1.27 (m, 4H, 2 × NCH_2CH_2), 1.07-0.95 (m, 4H, 2 × CH_2CH_3), 0.64 (t, ^3J = 7.3 Hz, 6H, 2 × CH_3); **^{13}C NMR** (75.5 MHz, $CDCl_3$): δ 154.5 (C5a, 8a, 14a, 17a), 140.7 (C4a, 9a, 13a, 18a), 129.3 (Ar-C), 128.5 (Ar-C), 63.1 (CH_2N), 54.4 (NCH_2 of *n*Bu), 28.9 (NCH_2CH_2), 20.5 (CH_2CH_3), 13.7 (CH_3); **MS-APCI+** (*m/z*) 456 ([M + H]$^+$, 28%), 455 ([M]$^+$, 100); **HRMS-CI+** (*m/z*) Calcd for $C_{28}H_{35}N_6$ [M]$^+$: 455.2923, found 455.2915.

2-Butyl-2*H*-pyrrolo[3,4-*b*]quinoxaline, 75

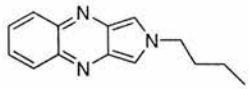

Compound **75**: crude isolation afforded a red oil, **^{1}H NMR** (500 MHz, $CDCl_3$): δ 7.99-7.96 (m, AA' part of the AA'XX' system, 2H, H-5 and H-8), 7.61 (s, 2H, H-1 and H-3), 7.55-7.52 (m, XX' part of the AA'XX' system, 2H, H-6 and H-7), 4.47 (t, ^3J = 7.2 Hz, 2H, NCH_2), 2.03 (m, 2H, $NCHCH_2$), 1.65-1.20 (contains m, 2H, CH_2CH_3), 0.97 (t, ^3J = 7.4 Hz, 3H, CH_3); **MS-EI+** (*m/z*) 225 ($[M]^{+\bullet}$, 33%), 183 (100), 156 (26); **HRMS-EI+** (*m/z*) Calcd for $C_{14}H_{15}N_3$ $[M]^{+\bullet}$: 225.1266, found 225.1276.

2,2-Diethyl-2,3-dihydro-1*H*-pyrrolo[3,4-*b*]quinoxalin-2-ium bromide, 87 [26]

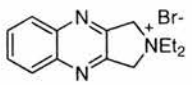

Prepared according to the general procedure: Method B using **64** and diethylamine. Reaction was scaled up 30-fold for full analysis. **87** was collected following crystallisation from chloroform to yield a white crystalline solid (0.138 g, 0.45 mmol, 74%); mp 195.5-196.0 °C dec. (lit. 195.0 °C).[159159] **IR** (KBr) ν_{max}: 3461 (s), 3394 (s), 2974 (m), 2936 (m), 1503 (m), 1465 (s), 1030 (m), 763 (s) (ArC–H) cm^{-1}; **^{1}H NMR** (300 MHz, D_2O): δ 8.10-8.04 (m, AA' part of the AA'XX' system, 2H, H-5 and H-8), 7.93-7.87 (m, XX' part of the AA'XX' system, 2H, H-6 and H-7), 3.80 (q, ^3J = 7.2 Hz, 4H, 2 × CH_2 of Et), 1.42 (t, ^3J = 7.2 Hz, 6H, 2 × CH_3 of Et); **^{1}H NMR** (300 MHz, $CDCl_3$): δ 8.14-8.08 (m, AA' part of the AA'XX' system, 2H, H-5 and H-8), 7.84-7.79 (m, XX' part of the AA'XX' system, 2H, H-6 and H-7), 5.59 (s, 4H, 2 × CH_2N), 4.15 (q, ^3J = 7.2 Hz, 4H, 2 × CH_2 of Et), 1.44 (t, ^3J = 7.2 Hz, 6H, 2 × CH_3 of Et); **^{13}C NMR** (75.5 MHz, D_2O, referenced to dioxane): δ 149.6 (C3a and C9a), 142.2 (C4a and C8a), 132.4 (C6 and C7), 129.0 (C5 and C8), (65.2, 64.9, 64.6, 64.3, 64.0) (2 × CH_2N), 59.3 (2 × CH_2 of Et), 8.8 (2 × CH_3 of Et); **MS-ES+** (*m/z*) 229 ($[M + H]^+$ 14%), 228 ($[M]^+$, 100%); **HRMS-CI+** (*m/z*) Calcd for $C_{14}H_{18}N_3$ $[M]^+$: 228.1501, found 228.1497.

(*E/Z*)-*N*-((2-(Bromomethyl)quinoxalin-3-yl)methylene)butan-1-amine 1-oxide, 90

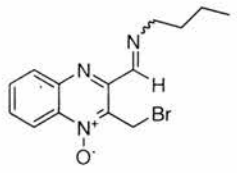

Intermediate **90**: ^{1}H NMR (300 MHz, $CDCl_3$): δ 8.63-8.59 (m, 1H, H-8), 8.55-8.54 (m, 1H, H-10), 8.14-8.10 (m, 1H, H-5), 7.88-7.76 (m, 2H, H-6 and H-7), 5.64 (s, 2H, CH_2-9), 3.79 (td, ^3J = 6.9 Hz, ^4J = 1.3 Hz, 2H, NCH_2 of *n*Bu), 1.83-1.73 (m, 2H, NCH_2CH_2), 1.55-1.42 (m, 2H, CH_2CH_3), 0.91 (t, ^3J = 7.4 Hz, 6H, 2 × CH_3).

7,16-Di-*n*-butyl[1,6]diazecino[3,4-*b*;8,9-*b*´]diquinoxaline 5,9,14,18-tetraoxide, 91

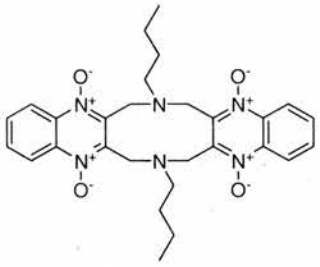

Prepared according to the general kinetic NMR procedure (Method A) using **27** and *n*-butylamine. Attempts to isolate **91** by column chromatography yielded an unstable red oil (1.5 mg, 3.0 μmol, 5%). **^{1}H NMR** (500 MHz, $CDCl_3$): δ 8.67-8.53 (m, 4H, H-1, 4, 10 and 13), 7.90-7.71 (m, 4H, H-2, 3, 11 and 12), 4.71 (s, 8H, 4 × NCH_2), 2.77-2.67 (m, 4H, 2 × NCH_2 of *n*Bu) 1.54-1.48 (m, 4H, 2 × NCH_2CH_2), 1.39-1.33 (m, 4H, 2 × CH_2CH_3), 0.92-0.89 (m, 6H, 2 × CH_3); **MS-ES+** (*m/z*) 541 ([M + Na]$^+$, 100%), 519 ([M + H]$^+$, 35); **HRMS-ES+** (*m/z*) Calcd for $C_{28}H_{35}N_6O_4$ [M + H]$^+$: 519.2720, found 519.2711.

(3-(Diethylaminomethyl)quinoxalin-2-ylmethyl)diethylamine 1,4-dioxide, 93

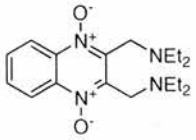

Prepared according to the general procedure: Method B using **27** and diethylamine. Attempts to isolate **93** on a preparative scale were unsuccessful due to rapid decomposition. **^{1}H NMR** (300 MHz, $CDCl_3$): δ 8.68-8.62 (m, AA´ part of the AA´XX´ system, 2H, H-5 and H-8), 7.84-7.78 (m, XX´ part of the AA´XX´ system, 2H, H-6 and H-7), 4.35 (s, 4H, 2 × CH_2N), 2.64 (q, ^3J = 7.1 Hz, 8H, 4 × CH_2 of Et), 1.03 (t, ^3J = 7.1 Hz, 12H, 4 × CH_3 of Et); **^{13}C NMR** (75.5 MHz, $CDCl_3$): δ 144.1 (C2 and C3), 137.2 (C4a and

C8a), 131.4 (C6 and C7), 120.7 (C5 and C8), 47.8 (2 × $\underline{C}H_2N$), 42.7 ($\underline{C}H_2$ of Et), 12.1 (CH_3); **MS-ES+** (*m/z*) 355 ($[M + Na]^+$, 20%), 260 ($[M - N(CH_2CH_3)_2]^+$, 100), 214 (14), 198 (84); **HRMS-ES+** (*m/z*) Calcd for $C_{18}H_{29}N_4O_2$ $[M + H]^+$: 333.2291, found 333.2294.

1-Bromobutane-2,3-dione, 99

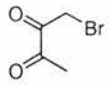

Butane-2,3-dione (5.00 g, 58.1 mmol) in $CHCl_3$ (10 mL) was added to a solution of copper (II) bromide (12.98 g, 58.1 mmol) in $CHCl_3$ (10 mL). To this was added a catalytic amount of 18-crown-6 (0.04 g, 0.15 mmol) and the reaction mixture heated to reflux with stirring for 2.5 d. After cooling to room temperature the reaction mixture was filtered to remove residual copper salts. The filtrate was then decolourised over activated charcoal and filtered over celite washing with $CHCl_3$. After removal of the solvent the residue was purified by distillation under vacuum. The desired product **99** was collected as a bright yellow oil (3.53 g, 21.4 mmol, 37%). **IR** (NaCl, Nujol) ν_{max}: 1732 (m) (C=O), 1717 (s) (C=O) cm^{-1}; **^{1}H NMR** (300 MHz, $CDCl_3$): δ 4.30 (s, 2H, $C\underline{H}_2$), 2.43 (s, 3H, $C\underline{H}_3$); **^{13}C NMR** (75.5 MHz, $CDCl_3$): δ 195.7 (C2), 189.2 (C3), 28.7 (C1), 24.3 (C4). Data are in agreement with literature values.[114]

2-(Bromomethyl)-3-methylquinoxaline, 100

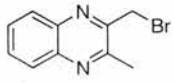

A solution of 1-bromo-2,3-butanedione (3.45 g, 20.9 mmol) in anhydrous THF (10.0 mL) was added to a solution of 1,2-phenylene diamine (2.37 g, 22.0 mmol) in anhydrous THF (35.0 mL) at 0 °C over 15 mins. with stirring. The reaction was warmed to room temperature and stirred for a further 17 h. After concentration *in vacuo*, the crude material was partitioned between 10% w/v sodium hydrogen carbonate solution (50 mL) and DCM (100 mL). The organic phase was washed with brine (50 mL), dried ($MgSO_4$) and concentrated *in vacuo* to give a brown solid. Purification by flash column chromatography on silica gel (EA:PE 40-60, 1:9) gave **100** as a white crystalline solid (1.82 g, 7.83 mmol, 37%); mp 120.5-121.0 °C; (lit. 119.0-120.0 °C, ethanol).[160] **IR** (NaCl, Nujol) ν_{max}: 1560 (w), 769 (m) (ArC–H), 673 (m) (C–Br) cm^{-1}; **^{1}H NMR** (300 MHz, $CDCl_3$): δ 7.98-7.91 (m, AA' part of the AA'XX' system, 2H, $\underline{H}$-5 and $\underline{H}$-8), 7.69-

7.60 (m, XX' part of the AA'XX' system, 2H, H-6 and H-7), 4.67 (s, 2H, CH_2), 2.80 (s, 3H, CH_3); **^{13}C NMR** (75.5 MHz, $CDCl_3$): δ 152.9 (C2 or C3), 150.6 (C2 or C3), 141.7 (C4a or C8a), 140.6 (C4a or C8a), 130.2 (C6 or C7), 129.2 (C6 or C7), 128.8 (C5 or C8), 128.2 (C5 or C8), 31.7 (CH_2), 22.3 (CH_3); **MS-EI+** (*m/z*) 238 ($[M]^{+\bullet}$, ^{81}Br, 20%), 236 ($[M]^{+\bullet}$, ^{79}Br, 21), 157 ($[M - Br]^{+\bullet}$, 100); **HRMS-EI+** (*m/z*) Calcd for $C_{10}H_9BrN_2$ $[M]^{+\bullet}$: 235.9949, found 235.9961; **Anal.** Calcd for $C_{10}H_9BrN_2$: C, 50.66; H, 3.83; N, 11.82. Found: C, 50.56; H, 3.52; N, 11.88.

2-(Bromomethyl)-3-methylquinoxaline 1,4-dioxide, 94

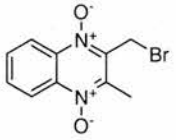

Purified *m*CPBA (1.86 g, 10.8 mmol) was added to a solution of **100** (0.50 g, 2.15 mmol) in anhydrous DCM (20 mL) with stirring at room temperature. After 20 h the reaction mixture was diluted with DCM (20 mL) and washed with 10% w/v aqueous sodium carbonate solution (2 × 20 mL). Following extraction into DCM (2 × 20 mL) the organic phase was dried ($MgSO_4$) and concentrated *in vacuo* to give a yellow solid. Purification by flash column chromatography on silica gel (EA:PE 40-60, 1:1 to 1:0) gave **94** as a bright yellow crystalline solid (0.29 g, 1.08 mmol, 50%); mp 171.0-172.0 °C (recrystallised from EA to give bright yellow needles) (lit. 172-173 °C, methanol).[161] **IR** (NaCl, Nujol) ν_{max}: 1506 (w), 1341 (m) (N–O), 1328 (m) (N–O), 1065 (m), 774 (m) (ArC–H), 629 (m) (C–Br) cm^{-1}; **^{1}H NMR** (300 MHz, $CDCl_3$): δ 8.64-8.61 (m, 2H, H-5 and H-8)), 7.89-7.80 (m, 2H, H-6 and H-7), 4.89 (s, 2H, CH_2), 2.78 (s, 3H, CH_3); **^{13}C NMR** (75 MHz, $CDCl_3$): δ 141.2 (C2 or C3), 140.0 (C2 or C3), 137.4 (C4a or C8), 136.8 (C4a or C8), 132.2 (C6 or C7), 131.5 (C6 or C7), 120.5 (C5 or C8), 120.2 (C5 or C8), 22.0 (C9), 14.2 (C10); **MS-ES+** (*m/z*) 293 ($[M + Na]^+$, ^{81}Br, 93%), 291 ($[M + Na]^+$, ^{79}Br , 100); **HRMS-EI+** (*m/z*) Calcd for $C_{10}H_9BrN_2O_2$ $[M]^{+\bullet}$: 267.9847, found 267.9854; **Anal.** Calcd for $C_{10}H_9BrN_2O_2$: C, 44.63; H, 3.37; N, 10.41. Found: C, 44.49; H, 3.07; N, 10.43.

2-Methylquinoxaline-3-carbaldehyde 1-oxide, 97

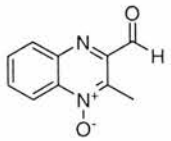

n-Butylamine (27 mg, 37 μL, 0.37 mmol) was added to a solution of **94** (100 mg, 0.37 mmol) in $CHCl_3$ (4.0 mL) with stirring at room temperature under nitrogen. After 1 h the reaction mixture was quenched by addition of silica and the solvent removed *in vacuo*. Purification by column chromatography on silica (EA:PE 40-60, 1:1 to 1:0) gave **97** as an off-white solid (30 mg, 0.16 mmol, 42%); mp 160.0-162.0 °C dec. (lit 167.0-169.0 °C, acetone).[162] **IR** (NaCl, Nujol) ν_{max}: 1719 (s) (C=O), 1570 (m), 1328 (N–O), 1095 (w), 743 (ArC–H) cm^{-1}; **^{1}H NMR** (300 MHz, $CDCl_3$): δ 10.23 (s, 1H, C<u>H</u>O), 8.67-8.60 (m, 1H, <u>H</u>-5), 8.28-8.21 (m, 1H, <u>H</u>-5), 7.92-7.84 (m, 2H, <u>H</u>-6 and <u>H</u>-7), 2.98 (s, 3H, C<u>H</u>$_3$); **^{13}C NMR** (75.5 MHz, $CDCl_3$): δ 192.8 (<u>C</u>HO), 147.2 (C3), 142.8 (C4a), 140.8 (C2), 137.1 (C8a), 132.8 (C6 or C7), 131.4 (C6 or C7), 130.8 (C5), 119.0 (C8), 12.1 (<u>C</u>H$_3$); **MS-CI+** (*m/z*) 189 ($[M + H]^+$, 100%), 173 ($[M + H - O]^+$, 95); **HRMS-EI+** (*m/z*) Calcd for $C_{10}H_8N_2O_2$ $[M]^{+\bullet}$: 188.0586, found 188.0587.

2,2-Diethyl-2,3-dihydro-1*H*-pyrrolo[3,4-*b*]quinoxalin-2-ium bromide, 4-oxide, 102 and **(3-(Diethylaminomethyl)quinoxalin-2-ylmethyl)diethylamine 4-oxide, 104**

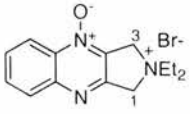

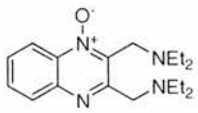

Prepared according to the general procedure (Method B) using **69** and diethylamine. Reaction was scaled up 30-fold for full analysis. Compound **102** was collected following crystallisation to yield a white crystalline solid (98 mg, 0.30 mmol, 50%). Compound **104** was recovered from the filtrate in the presence of diethylamine. Compound **102**: mp 203.0-204.0 °C dec; **IR** (KBr) ν_{max}: 3490 (s), 3423 (s), 2984 (m), 2917 (m), 1589 (m), 1565 (s), 1498 (s), 1369 (s) (N–O), 1097 (s), 1011 (w), 772 (s) (ArC–H) cm^{-1}; **^{1}H NMR** (500 MHz, D_2O): δ 8.46 (dd, ^3J = 8.7 Hz, ^4J = 1.3 Hz, 1H, <u>H</u>-5), 8.16 (dd, ^3J = 8.4 Hz, ^4J = 1.3 Hz, 1H, <u>H</u>-8), 8.01-7.92 (m, 2H, <u>H</u>-6 and <u>H</u>-7), 3.81 (q, ^3J = 7.2 Hz, 4H, 2 × C<u>H</u>$_2$ of Et), 1.42 (t, ^3J = 7.2 Hz, 6H, 2 × C<u>H</u>$_3$ of Et); **^{1}H NMR** (500 MHz, $CDCl_3$): δ 8.54-8.52 (m, 1H, <u>H</u>-5), 8.16-8.14 (m, 1H, <u>H</u>-8), 7.91-7.80 (m, 2H, <u>H</u>-6 and <u>H</u>-7), 5.65 (s, 2H, C<u>H</u>$_2$-3), 5.56 (s, 2H, C<u>H</u>$_2$-1), 4.22-4.11 (m, 4H, 2 × C<u>H</u>$_2$ of Et) 1.50 (t, ^3J =

7.1 Hz, 6H, 2 × C<u>H</u>$_3$ of Et); **^{13}C NMR** (125.7 MHz, D_2O, reference to dioxane): δ 151.6 (C9a), 146.3 (C8a), 136.7 (C4a), 133.9 (C7), 133.9 (C3a), 132.7 (C6), 129.9 (C8), 118.2 (C5), ((66.0, 65.8, 65.7, 65.5, 65.3) (C3), (62.4, 62.2, 62.0, 61.8, 61.5) (C1)), 59.8 (CH_2 of Et), 8.8 (CH_3 of Et); **MS-ES+** (*m/z*) 244 ([M – Br]$^+$, 100%), 198 (81); **HRMS-ES+** (*m/z*) Calcd for $C_{14}H_{18}N_3O$ [M – Br]$^+$ 244.1450, found 244.1456.

Compound **104**: **^{1}H NMR** (300 MHz, $CDCl_3$): δ 8.60-8.56 (m, 1H, <u>H</u>-5), 8.10-8.06 (m, 1H, <u>H</u>-8), 7.78-7.65 (m, 2H, <u>H</u>-6 and <u>H</u>-7), 4.34 (s, 2H, C<u>H</u>$_2$-9), 4.13 (s, 2H, C<u>H</u>$_2$N-10), 2.69-2.59 (m, 8H, 4 × NC<u>H</u>$_2$ of Et) 1.06-1.00 (m, 12H, 4 × C<u>H</u>$_3$ of Et); **MS-ES+** (*m/z*) 339 ([M + Na]$^+$, 32%), 317 ([M + H]$^+$, 17), 299 ([M – OH]$^+$, 24), 244 ([M]$^+$, compound **102,** 94), 228 ([M – O]$^+$, compound **102**, 100); **HRMS-ES+** (*m/z*) Calcd for $C_{18}H_{29}N_4O$ [M + H]$^+$: 317.2341, found 317.2354.

2-Butyl-2,3-dihydro-1*H*-pyrrolo[3,4-*b*]quinoxaline 4-oxide, 105

7,16-Di-*n*-butyl[1,6]diazecino[3,4-*b*;8,9-*b*´]diquinoxaline 5,9-dioxide, 106 and **7,16-Di-*n*-butyl[1,6]diazecino[3,4-*b*;8,9-*b*´]diquinoxaline 5,14-dioxide, 107.**

Prepared according to the general kinetic NMR procedure using **69** with *n*-butylamine. Attempts to cleanly isolate the title compounds proved unsuccessful due to their inherent instability.

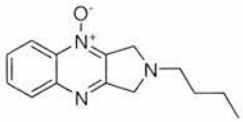

Compound **105**, crude isolation afforded a pink oil; ^{1}H NMR (500 MHz, $CDCl_3$): δ 8.58 (dd, ^3J = 8.5 Hz, ^4J = 1.3 Hz, 1H, <u>H</u>-5), 8.07 (dd, ^3J = 8.4, ^4J = 1.0 Hz, 1H, <u>H</u>-8), 7.80-7.69 (m, 2H, <u>H</u>-6 and <u>H</u>-7), 4.28 (s, 2H, C<u>H</u>$_2$-3), 4.16 (s, 2H, C<u>H</u>$_2$-1), 2.81 (t, ^3J = 7.4 Hz, 2H), 1.65-1.20 (m, 4H, NCH$_2$C<u>H</u>$_2$C<u>H</u>$_2$), 0.98 (t, ^3J = 7.4 Hz, 3H, C<u>H</u>$_3$); **MS-ES+** (*m/z*) 487 ([M + H]$^+$, **28** + **29**, 50%), 244 ([M + H]$^+$, 100); **HRMS-ES+** (*m/z*) Calcd for $C_{14}H_{18}N_3O$ [M]$^+$: 244.1450, found 244.1458.

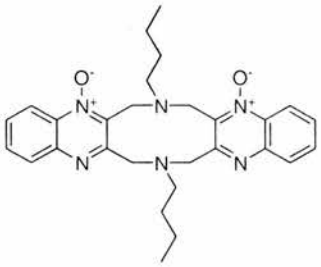

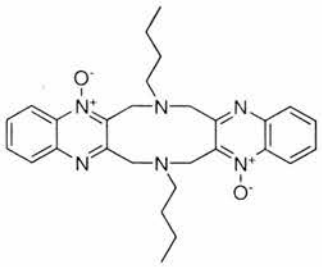

Compounds **106** and **107**: crude isolation afforded a red oil; **^{1}H NMR** (500 MHz, $CDCl_3$): δ 8.43 (dd, ^3J = 8.3 Hz, ^4J = 1.5 Hz, 2H, Ar-H adjacent to *N*-oxide), 8.39 (dd, ^3J = 8.5, ^4J = 1.3 Hz, 2H, Ar-H adjacent to *N*-oxide), 7.89 (dd, ^3J = 8.5, ^4J = 1.5 Hz, 2H, Ar-H opposite to *N*-oxide), 7.85 (dd, ^3J = 8.3, ^4J = 1.2 Hz, 2H, Ar-H opposite to *N*-oxide), 7.60-7.52 (m, 8H, H-2, 3, 11, and 12), 4.59 (s, 4H, CH_2N adjacent to *N*-oxide), 4.58 (s, 4H, CH_2N adjacent to *N*-oxide), 4.29 (s, 4H, CH_2N opposite to *N*-oxide), 4.28 (s, 4H, CH_2N opposite to *N*-oxide), 2.79-2.71 (m, 8H, NCH_2 of *n*Bu), 1.65-1.20 (contains m, 16H, 4 × $NCH_2CH_2CH_2$), 0.81 (t, ^3J = 7.4 Hz, 12H, 4 × CH_3); **MS-ES+** (*m/z*) 487 ($[M + H]^+$, 100%); **HRMS-ES+** (*m/z*) Calcd for $C_{28}H_{35}N_6O_2$ $[M + H]^+$: 487.2821, found 487.2829.

tert-Butyl 4-amino-3-nitrophenylcarbamate, 112

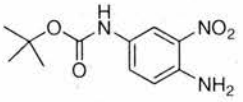

Di-*tert*-butyl-dicarbonate (48.0 g, 0.22 mol) was added to a solution of 2-nitro-*p*-phenylenediamine (30.6 g, 0.20 mol) in anhydrous DCM (1.00 L) at room temperature, under nitrogen. After stirring for 2 d the reaction mixture was diluted with DCM (1.00 L) and washed with 10% w/v aqueous sodium hydrogen carbonate solution (2 × 500 mL). The organic phase was washed with brine (500 mL) and the combined aqueous phases extracted with DCM (2 × 500 mL). The combined organic phases were dried ($MgSO_4$) and concentrated *in vacuo*. Drying under vacuum at 50 °C gave **112** as a bright orange solid, (50.7 g, 0.20 mol, quant.); mp 135.0–137.0 °C. **IR** (NaCl, Nujol) ν_{max}: 3500 (s), 3381 (s), 3335 (s), 1691 (s) (C=O), 1531 (s) (NO_2), 1252 (m), 1218 (m), 1161 (s), 887 (w), 822 (w), 747 (w) (ArC–H) cm^{-1} **^{1}H NMR** (300 MHz, DMSO-d_6): δ 9.28 (br s, 1H, NH), 8.20 (br s, 1H, H-2), 7.40 (dd, ^3J = 9.1 Hz, ^4J = 2.5 Hz, 1H, H-6), 7.25 (s, 2H, NH_2), 6.95 (d, ^3J = 9.1 Hz, 1H, H-5), 1.46 (s, 9H, 3 × CH_3); **^{13}C NMR** (75.5 MHz, $CDCl_3$): δ 152.8 (C=O), 142.3 (C4), 129.3 (C3), 128.5 (C6), 128.2 (C1), 119.4 (C5), 112.6 (C2), 79.0 (CCH_3), 28.0 (3 × CH_3); **MS-EI+** (*m/z*) 253 ($[M]^{+\bullet}$, 4%), 197 (45), 153 (25); **HRMS-EI+** (*m/z*) Calcd

for $C_{11}H_{15}N_3O_4$ $[M]^{+\bullet}$ 253.1063, found 253.1063 **Anal.** Calcd for $C_{11}H_{15}N_3O_4$: C, 52.17; H, 5.97; N, 16.59. Found: C, 52.39; H, 6.07; N, 16.35.

tert-Butyl 3,4-diaminophenylcarbamate, 113

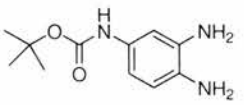

A 250 mL round-bottomed flask equipped with **112** (4.00 g, 15.8 mmol) and 10% Pd/C (0.80 g) was purged with nitrogen. Anhydrous methanol (60.0 mL) was added with stirring and the flask covered in foil. The flask was then purged with hydrogen and a hydrogen balloon introduced that was replaced a further 3 times. After 24 h stirring at room temperature the reaction mixture was filtered over Celite® washing with MeOH (300 mL). Removal of the solvent *in vacuo* afforded the desired product **113** as an off-white crystalline solid (3.50 g, 15.7 mmol, 99%) and used without any further purification. **IR** (NaCl, Nujol) ν_{max}: 3410-3215 (s) (NH_2), 1725 (m), 1700 (s), 1610 (m), 1521 (s), 1243 (s), 1166 (s), 1059 (w), 850 (w), 810-720 (w) (ArC–H) cm^{-1}; **^{1}H NMR** (300 MHz, $CDCl_3$): δ 6.92 (br s, 1H, H-2), 6.59 (d, ^3J = 8.2 Hz, 1H, H-5), 6.50 (dd, ^3J = 8.2, ^4J = 2.3 Hz, 1H, H-6), 6.37 (br s, 1H, NH), 3.23 (br s, 4H, 2 × NH_2), 1.49 (s, 9H, 3 × CH_3); **^{13}C NMR** (75.5 MHz, $CDCl_3$): δ 153.1 (C=O), 135.7 (C3), 131.5 (C1), 129.9 (C4), 117.2 (C5), 110.5 (C6), 108.0 (C2), 80.0 (CCH_3), 28.3 (3 × CH_3).

tert-Butyl 2,3-bis(bromomethyl)quinoxalin-6-ylcarbamate, 114

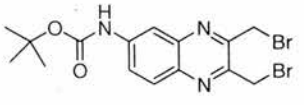

A solution of 1,4-dibromo-2,3-butanedione (2.00 g, 8.20 mmol) in anhydrous THF (40.0 mL) was added dropwise to a solution of **113**, (1.74 g, 7.79 mmol) in anhydrous THF (40.0 mL) at 0 °C over 15 minutes with stirring. The reaction was warmed to room temperature and stirred for a further 17 h. After concentration *in vacuo*, the crude material was redissolved in DCM (100 mL) and partitioned between 10% w/v aqueous sodium hydrogen carbonate solution (200 mL) and DCM (300 mL). The organic phase was washed with brine (100 mL), dried ($MgSO_4$), filtered and concentrated *in vacuo* to give a dark brown solid. Purification by flash column chromatography on silica gel (EA:PE 40-60, 1:4) gave **114** as a yellow glassy crystalline solid (2.98 g, 6.90 mmol, 89%); mp 54.0-56.0 °C. **IR** (NaCl, Nujol) ν_{max}: 3317 (s), 1723 (m), 1702 (s), 1623 (w), 1572 (m), 1535

(s), 1496 (w), 1309 (w), 1246 (s), 1153 (s) 1055 (w), 839 (ArC–H) cm^{-1}; **^{1}H NMR** (300 MHz, $CDCl_3$): δ 8.04 (d, ^4J = 2.4 Hz, 1H, H-5), 7.96 (d, ^3J = 9.1 Hz, 1H, H-8), 7.85 (dd, ^3J = 9.1, ^4J = 2.4 Hz, 1H, H-7), 6.98 (br s, 1H, NH), 4.89 (s, 2H, CH_2-9 or 10), 4.87 (s, 2H, CH_2-9 or 10), 1.55 (s, 9H, 3 × CH_3); **^{13}C NMR** (75.5 MHz, $CDCl_3$) δ; 152.1 (N(6)C=O), 151.2 (C2 or C3), 148.8 (C2 or C3), 142.5 (C4a or C6), 140.8 (C4a or C6), 138.2 (C8a), 129.6 (C8), 123.7 (C7), 114.3 (C5), 81.6 (CCH_3), 30.7 (C9 or C10), 30.5 (C9 or C10), 28.2 (3 × CH_3); **MS-ES–** (*m/z*) 432 ([M – H]$^-$, 2 × ^{81}Br, 9%), 430 ([M – H]$^-$, ^{79}Br + ^{81}Br, 100), 428 ([M – H]$^-$, 2 × ^{79}Br, 12); **HRMS-ES–** (*m/z*) Calcd for $C_{15}H_{16}{}^{79}Br^{81}BrN_3O_2$ [M – H]$^-$: 429.9589, found 429.9586.

tert-Butyl 2,3-bis(bromomethyl)quinoxalin-6-ylcarbamate 1,4-dioxide, 110

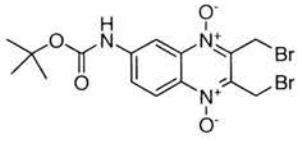

Purified *m*CPBA (2.07 g, 12.0 mmol) was added to a solution of **114** (1.04 g, 2.40 mmol) in anhydrous DCM (80 mL) with stirring at room temperature. After 42 h the reaction mixture was diluted with DCM (250 mL) and washed with 10% w/v aqueous sodium carbonate solution (2 × 250 mL). The organic phase was dried ($MgSO_4$) and concentrated *in vacuo* to give a yellow solid. Purification by flash column chromatography on silica gel (EA:PE 40-60, 1:4) gave **110** as a bright yellow crystalline solid (0.89 g, 1.91 mmol, 80%); mp >180 °C dec. (recrystallised from EA : PE 40-60 1:3). **IR** (KBr) ν_{max}: 3313 (s), 1737 (s) (C=O), 1611 (s), 1546 (s), 1480 (m), 1369 (m) (N–O), 1237 (s), 1145 (s), 1030 (m), 881-730 (m) (ArC–H), 635 (s) (C–Br) cm^{-1}; **^{1}H NMR** (300 MHz, $CDCl_3$): δ 8.56 (d, ^3J = 9.4 Hz, 1H, H-8), 8.51 (d, ^4J = 2.3 Hz, 1H, H-5), 8.23 (br d, ^3J = 9.4 Hz, 1H, H-7), 7.37 (br s, 1H, NH), 4.93 (s, 2H, CH_2Br), 4.92 (s, 2H, CH_2Br), 1.57 (s, 9H, 3 × CH_3); **^{13}C NMR** (75.5 MHz, $CDCl_3$): δ 151.8 (C=O), 143.5 (C4a), 140.1 (C2 or C3), 138.1 (C6), 137.9 (C2 or C3), 133.2 (C8a), 124.0 (C7), 121.8 (C8), 106.2 (C5), 82.4 (CCH_3), 28.2 (3 × CH_3), 20.7 (CH_2), 20.6 (CH_2); **MS-ES–** (*m/z*) 464 ([M – H]$^-$, 2 × ^{81}Br, 21%), 462 ([M – H]$^-$, ^{79}Br + ^{81}Br, 100), 460 ([M – H]$^-$, 2 × ^{79}Br, 22); **HRMS-ES–** (*m/z*) Calcd for $C_{15}H_{16}{}^{79}Br^{81}BrN_3O_4$ [M – H]$^-$: 461.9487, found 461.9494; **Anal.** Calcd for $C_{15}H_{17}Br_2N_3O_4$: C, 38.90; H, 3.70; N, 9.07. Found: C, 38.76; H, 3.54; N, 8.77. Structure also confirmed by X-ray crystallographic analysis.

***tert*-Butyl-2-Butyl-2*H*-pyrrolo[3,4-*b*]quinoxalin-7-ylcarbamate 4-oxide, 124** and ***tert*-Butyl-2-Butyl-2*H*-pyrrolo[3,4-*b*]quinoxalin-6-ylcarbamate 4-oxide, 125**

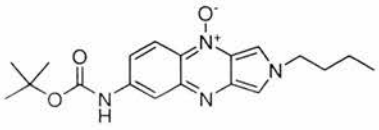

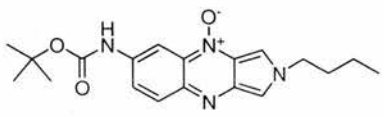

Prepared according to the general kinetic NMR procedure (Method A) using **110** and *n*-butylamine. Also, on preparative scale: A solution of *n*-butylamine (53 mg, 0.73 mmol) in $CDCl_3$ (6 mL) was added to a solution of **110** (112 mg, 0.24 mmol) in $CDCl_3$ (6 mL) with stirring at room temperature. After 15 h the reaction mixture was quenched with silica and the solvent removed *in vacuo*. Purification by flash column chromatography on silica gel (EA) gave **124** and **125** as a mixture of regioisomers. **124** and **125** were collected as an unstable dark red oil (35 mg, 0.10 mmol, 41%). **124** and **125** were observed to decompose rapidly in the absence of solvent. Compounds **124 + 125**: **MS-ES+** (*m/z*) 357 ($[M + H]^+$, 100), 301 (56); **HRMS-ES+** (*m/z*) Calcd for $C_{19}H_{25}N_4O_3$ $[M + H]^+$: 357.1927, found 357.1925.

Compound **124**: **^{1}H NMR** (500 MHz, $CDCl_3$): δ 8.48 (d, ^3J = 9.8 Hz, 1H, H-5), 7.91 (d, ^4J = 2.1 Hz, 1H, H-8), 7.69 (dd, ^3J = 9.8 Hz, ^4J = 2.1 Hz, 1H, H-6), 7.61 (d, ^4J = 2.5 Hz, 1H, H-3), 7.51 (d, ^4J = 2.5 Hz, 1H, H-1), 6.83 (br s, 1H, NH), 4.35 (t, ^3J = 7.1 Hz, 2H, NCH_2 of *n*Bu), 2.04-1.94 (m, 2H, NCH_2CH_2), 1.55 (s, 9H, 3 × CH_3 of Boc), 1.41-1.28 (m, 2H, CH_2CH_3), 0.97 (t, ^3J = 7.4 Hz, 2H, CH_3 of *n*Bu).

Compound **125**: **^{1}H NMR** (500 MHz, $CDCl_3$): δ 8.41 (d, ^4J = 2.5 Hz, 1H, H-5), 8.18 (d, ^3J = 9.5 Hz, H-8), 7.79 (dd, ^3J = 9.5 Hz, ^4J = 2.5 Hz, 1H, H-7), 7.61 (d, ^4J = 2.5 Hz, 1H, H-3), 7.58 (d, ^4J = 2.5 Hz, 1H, H-1), 6.97 (br s, 1H, NH), 4.42 (t, ^3J = 7.1 Hz, 2H, NCH_2 of *n*Bu), 2.06-2.00 (m, 2H, NCH_2CH_2), 1.47-1.36 (m, 2H, CH_2CH_3), 0.99 (t, ^3J = 7.4 Hz, 2H, CH_3).

Diels-Alder adducts with *N*-phenylmaleimide

n-Butylamine (0.26 g, 0.36 mL, 3.60 mmol) was added to a solution of **110** (0.56 g, 1.20 mmol) in degassed $CHCl_3$ (60.0 mL) with stirring at room temperature. After 3.5 h, *N*-phenylmaleimide (0.83 g, 4.80 mmol) was added and the reaction continued stirring at room temperature for 14 h. The solvent was removed *in vacuo* to give a brown solid, which by ^{1}H NMR analysis of the crude reaction contained *endo*:*exo* products in a ratio of 71:29 and showed four regioisomeric products. Purification by flash column

chromatography on silica gel (EA:PE 40-60, 1:1) gave the desired compounds, **131/133** as a pink crystalline solid (0.23 g, 0.43 mmol, 36%); and **132/134** as a yellowy brown solid (0.12 g, 0.22 mmol, 18%).

ENDO regioisomers, 131 and **133**

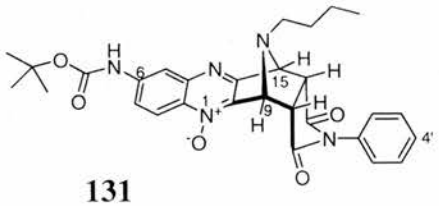

131

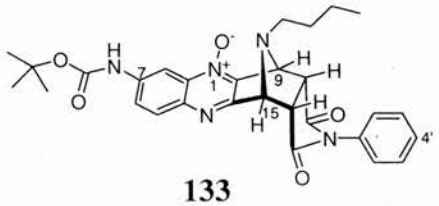

133

Compounds **131** and **133**: mixed mp > 80 °C dec. to red crystals; **IR** (NaCl, Nujol) ν_{max}: 1776 (w), 1717 (s) (C=O), 1239 (m), 1156 (s), 1052 (m), 833 (w), 734 (w) (ArC–H), 690 (w) cm^{-1}; **MS-ES+** (*m/z*) 1081 ($[2M + Na]^+$, 53%), 552 ($[M + Na]^+$, 7), 530 ($[M + H]^+$, 40), 411 (8), 379 (100), 357 (36), 247 (24); **MS-ES–** (*m/z*) 528 ($[M - H]^-$, 100%), 355 (24); **HRMS-ES–** (*m/z*) Calcd for $C_{29}H_{30}N_5O_5$ $[M - H]^-$: 528.2247, found 528.2232. Major regioisomer **131**: **^{1}H NMR** (500 MHz, $CDCl_3$): δ 8.47 (d, ^3J = 9.3 Hz, 1H, H-8), 8.08 (d, ^4J = 2.3 Hz, 1H, H-5), 7.84 (dd, ^3J = 9.3 Hz, ^4J = 2.3 Hz, 1H, H-7), 7.14-7.05 (m, 4H, H-3′, H-5′, NH and H-4′), 6.37-6.32 (m, 2H, XX′ H-2′ and H-6′), 5.40 (dd, ^3J = 5.3 Hz, ^4J = 1.6 Hz, 1H, H-9), 4.82 (dd, ^3J = 5.6 Hz, ^4J = 1.6 Hz, 1H, H-15), 4.13-4.08 (m, 1H, H-10), 4.08-4.04 (m, 1H, H-14), 2.37 (t, ^3J = 7.5 Hz, 2H, NCH_2 of *n*Bu), 1.54 (s, 9H, 3 × CCH_3), 1.50-1.43 (m, 2H, NCH_2CH_2), 1.32-1.24 (m, 2H, CH_2CH_3), 0.87 (t, ^3J = 7.3 Hz, 3H, CH_3); **^{13}C NMR** (125.5 MHz, $CDCl_3$) δ; 172.5 (C13), 172.0 (C11), 160.5 (C3), 152.0 (C=O of Boc), 146.0 (C4a), 141.8 (C6), 136.9 (C2), 132.5 (C8a), 130.5 (C1′), 128.9 (C3′ and C5′), 128.5 (C4′), 125.7 (C2′ and C6′), 121.5 (C7), 119.6 (C8), 115.8 (C5), 81.7 (CCH_3), 67.7 (C15), 63.2 (C9), 48.2 (NCH_2), 47.1 (C10), 47.0 (C14), 30.5 (NCH_2CH), 28.2 (CH_3 of Boc), 20.3 (CH_2CH_3), 13.8 (CH_3 of *n*Bu).

Minor regioisomer **133**: **^{1}H NMR** (500 MHz, $CDCl_3$): δ 8.38 (d, ^4J = 2.4 Hz, 1H, H-5), 8.15 (br m, 1H, H-7), 8.02 (d, ^3J = 9.1 Hz, 1H, H-8), 7.14-7.05 (m, 4H, H-3′, H5′, NH and H-4′), 6.37-6.32 (m, 2H, H-2′ and H-6′), 5.42 (dd, ^3J = 5.3 Hz, ^4J = 1.6 Hz,1H, H-9), 4.83 (dd, ^3J = 5.6 Hz, ^4J = 1.6 Hz, 1H, H-15), 4.13-4.08 (m, 1H, H-10), 4.08-4.04 (m, 1H, H-14), 2.37 (t, ^3J = 7.5 Hz, 2H, NCH_2), 1.54 (s, 9H, 3 × CCH_3), 1.50-1.43 (m, 2H, NCH_2CH_2), 1.32-1.24 (m, 2H, CH_2CH_3), 0.87 (t, ^3J = 7.3 Hz, 3H, CH_3 of *n*Bu); **^{13}C NMR** (125.5 MHz, $CDCl_3$) δ; 172.6 (C13), 171.9 (C11), 157.7 (C3), 152.1 (C=O of Boc), 141.0 (C4a or C8a), 140.8 (C4a or C8a), 138.4 (C2), 137.3 (C6), 130.5 (C1′), 130.7 (C8), 128.9

(C3′ and C5′), 128.5 (C4′), 125.7 (C2′ and C6′), 123.3 (C7), 105.2 (C5), 81.7 ($\underline{C}CH_3$), 67.6 (C9), 63.3 (C15), 48.2 ($N\underline{C}H_2$), 47.1 (C10 or C14), 47.0 (C10 or C14), 30.5 ($NCH_2\underline{C}H_2$), 28.2 ($\underline{C}H_3$ of Boc), 20.3 ($\underline{C}H_2CH_3$), 13.8 ($\underline{C}H_3$).

EXO regioisomers, 132 and **134**

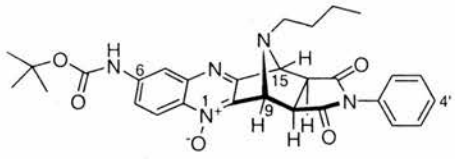

132

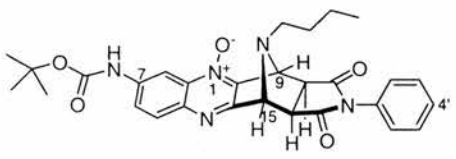

134

Compounds **132** and **134**: mixed mp 113.0-115.0 °C dec.; **IR** (NaCl, Nujol) ν_{max}: 1779 (w), 1712 (s) (C=O), 1238 (m), 1154 (s), 1052 (m), 840 (w), 757 (w) (ArC–H), 692 (w) cm^{-1}; **MS-ES+** (*m/z*) 552 ($[M + Na]^+$, 6%), 379 (100), 269 (59), 247 (14); **MS-ES–** (*m/z*) 528 ($[M - H]^-$, 100%), 355 (14); **HRMS-ES–** (*m/z*) Calcd for $C_{29}H_{30}N_5O_5$ $[M - H]^-$: 528.2247, found 528.2259.

Major regioisomer **132**: **^{1}H NMR** (300 MHz, $CDCl_3$): δ 8.51 (d, ^3J = 9.3 Hz, 1H, $\underline{H}$-8), 8.07 (d, ^4J = 2.3 Hz, 1H, $\underline{H}$-5), 7.84 (dd, ^3J = 9.3 Hz, ^4J = 2.3 Hz, 1H, $\underline{H}$-7), 7.53-7.40 (m, 3H, $\underline{H}$-3′, $\underline{H}$-5′and $\underline{H}$-4′), 7.32-7.29 (m, 2H, $\underline{H}$-2′ and $\underline{H}$-6′), 6.93 (br s, 1H, N$\underline{H}$), 5.27 (s, 1H, $\underline{H}$-9), 4.76 (s, 1H, $\underline{H}$-15), 3.32 (d, ^3J = 7.1 Hz, 1H, $\underline{H}$-14), 3.22 (d, ^3J = 7.1 Hz, 1H, $\underline{H}$-10), 2.33 (t, ^3J = 7.0 Hz, 2H, $NC\underline{H}_2$), 1.56 (s, 9H, 3 × $CC\underline{H}_3$), 1.46-1.34 (m, 2H, $NCH_2C\underline{H}_2$), 1.34-1.20 (m, 2H, $C\underline{H}_2CH_3$), 0.85 (t, ^3J = 7.3 Hz, 3H, $C\underline{H}_3$); **^{13}C NMR** (75.5 MHz, $CDCl_3$) δ: 174.7 (C13), 174.2 (C11), 163.0 (C3), 152.0 (C=O, Boc), 146.1 (C4a), 141.6 (C6), 138.4 (C2), 132.6 (C8a), 131.9 (C1′), 129.3(C3′ and C5′), 128.9 (C4′), 126.4 (C2′ and C6′), 121.4 (C7), 119.5 (C8), 115.8 (C5), 81.8 ($\underline{C}CH_3$), 68.8 (C15), 63.8 (C9), 47.4 (C10), 47.0 ($N\underline{C}H_2$), 46.9 (C14), 30.5 ($N\underline{C}H_2CH_2$), 28.2 ($\underline{C}H_3$ of Boc), 20.0 ($\underline{C}H_2CH_3$), 13.7 ($\underline{C}H_3$).

Minor isomer **134**: **^{1}H NMR** (300 MHz, $CDCl_3$): δ 8.43 (d, ^4J = 2.3 Hz, 1H, $\underline{H}$-5), 8.07 (br d, ^3J = 9.1 Hz, 1H, $\underline{H}$-7) 8.02 (d, ^3J = 9.1 Hz, 1H, $\underline{H}$-8), 7.53-7.40 (m, 3H, $\underline{H}$-3′, $\underline{H}$-5′and $\underline{H}$-4′), 7.30 (m, 2H, $\underline{H}$-2′ and $\underline{H}$-6′), 7.06 (br s, 1H, N$\underline{H}$), 5.28 (s, 1H, $\underline{H}$-9), 4.76 (s, 1H, $\underline{H}$-15), 3.32 (d, ^3J = 7.1 Hz, 1H, $\underline{H}$-10 or $\underline{H}$-14), 3.22 (d, ^3J = 7.1 Hz, 1H, $\underline{H}$-10 or $\underline{H}$-14), 2.33 (t, ^3J = 7.0 Hz, 2H, $NC\underline{H}_2$), 1.56 (s, 9H, 3 × $CC\underline{H}_3$), 1.46-1.34 (m, 2H, $NCH_2C\underline{H}_2$), 1.34-1.20 (m, 2H, $C\underline{H}_2CH_3$), 0.85 (t, ^3J = 7.3 Hz, 3H, $\underline{C}H_3$);

4-Bromo-1,2-phenylenediamine, 140 [163]

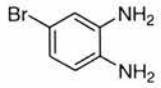

To a solution of 4-bromo-2-nitroaniline (500 mg, 2.30 mmol) in ethanol (25 mL) was added stannous chloride dihydrate (2.60 g, 11.5 mmol) with stirring. The reaction was then heated to reflux. After 23 h the reaction was cooled and the solvent was removed *in vacuo*. The crude material was redissolved in 2 M NaOH (100 mL) and extracted with diethyl ether (3 × 75 mL). The organic phase was washed with distilled water (50 mL), dried ($MgSO_4$), filtered and concentrated *in vacuo* to give **140** as a yellow solid (398 mg, 2.13 mmol, 93%) which was used without any further purification; mp 57.5-60.0 °C (lit. 66 °C).[164] **^{1}H NMR** (300 MHz, $CDCl_3$): δ 6.83-6.78 (m, 2H, H-3 and H-5), 6.57 (d, ^3J = 8.0 Hz, 1H, H-6), 3.33 (br s, 4H, 2 × NH_2); **^{13}C NMR** (75.5 MHz, $CDCl_3$): δ 136.3 (C2), 133.7 (C1), 122.5 (C5), 119.0 (C3), 117.8 (C6), 111.8 (C4); **MS-ES+** (*m/z*) 213 (100%), 211 (98), 189 ($[M + H]^+$, ^{81}Br, 52), 187 ($[M + H]^+$, ^{79}Br, 57).

2,3-Bis(bromomethyl)-6-bromoquinoxaline, 141

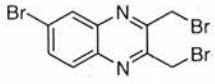

A solution of 1,4-dibromo-2,3-butanedione (529 mg, 2.17 mmol) in anhydrous THF (20 mL) was added dropwise to a solution of **140** (398 mg, 2.13 mmol) in anhydrous THF (20 mL) at 0 °C over 15 mins. with stirring. The reaction was warmed to room temperature and stirred for a further 27 h. After concentration *in vacuo*, the crude material was redissolved in DCM (100 mL) and partitioned between 10% w/v aqueous sodium hydrogen carbonate solution (200 mL) and DCM (300 mL). The organic phase was washed with brine (100 mL), dried ($MgSO_4$), filtered and concentrated *in vacuo* to give a pale brown solid. Purification by flash column chromatography on silica gel (EA:PE 40-60, 1:9) gave **141** as a white crystalline solid (736 mg, 1.86 mmol, 88%); mp 143.0–144.0 °C. **IR** (KBr) ν_{max}: 3090 (w), 3027 (m), 2968 (w), 1597 (s), 1476 (s), 1419 (m), 1357 (m), 1211 (m), 939 (m), 833 (s), 799 (s), 722 (s), 638 (m), 603 (w), 569 (m), 426 (s) cm^{-1}; **^{1}H NMR** (300 MHz, $CDCl_3$): δ 8.24 (d, ^4J = 2.1 Hz, 1H, H-5), 7.92 (d, ^3J = 8.9 Hz, 1H, H-8), 7.85 (dd, ^3J = 8.9, ^4J = 2.1 Hz, 1H, H-7), 4.89 (s, 4H, 2 × CH_2Br); **^{13}C NMR** (75 MHz, $CDCl_3$): δ 151.8 (C2 or C3), 151.1 (C2 or C3), 142.0 (C4a), 140.2 (C8a), 134.4 (C7), 131.3 (C5), 130.2 (C8), 125.1 (C6), 30.2 (CH_2), 30.1 (CH_2); **MS-ES+** (*m/z*) 399 ([M +

H]$^+$, 3 × ^{81}Br, 23%), 397 ([M + H]$^+$, 2 × ^{81}Br + ^{79}Br, 95), 395 ([M + H]$^+$, 2 × ^{79}Br + ^{81}Br, 100), 393 ([M + H]$^+$, 3 × ^{79}Br, 25); **Anal.** Calcd for $C_{10}H_7Br_3N_2$: C, 30.42; H, 1.79; N, 7.09. Found: C, 30.50; H, 1.60; N, 6.94.

2,3-Bis(bromomethyl)-6-bromoquinoxaline 1,4-dioxide, 142

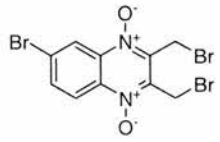

To a solution of **141** (312 g, 0.79 mmol) in anhydrous DCM (20.0 mL) was added purified *m*CPBA (1.02 g, 5.93 mmol) with stirring. The reaction was then allowed to stir at room temperature. After 34 h the reaction mixture was diluted with DCM (20.0 mL) and washed with 10% w/v sodium carbonate solution (3 × 20 mL). The organic phase was dried ($MgSO_4$), filtered and concentrated *in vacuo* to give a yellow solid. Purification by flash column chromatography on silica gel (EA:PE 40-60, 1:19 to 1:9) gave **142** as a bright yellow crystalline solid (184 mg, 0.43 mmol, 55%); mp >180 °C dec. (recrystallised from EA : PE 40-60 1:9) (lit. 203-204 °C, acetic acid).[165] **IR** (KBr) ν_{max}: 3096 (w), 3066 (m), 2974 (w), 1590 (m) and 1495 (m) (ArC–C), 1421 (m), 1329 (s) (N–O), 1162 (s), 1031 (s), 823 (m) and 705 (w), 669 (s) and 646 (s) (C–Br) cm^{-1}; **^{1}H NMR** (300 MHz, DMSO-d_6): δ 8.65 (d, ^4J = 2.1 Hz, 1H, H-5), 8.43 (d, ^3J = 9.1 Hz, 1H, H-8), 8.16 (dd, ^3J = 9.1, ^4J = 2.1 Hz, 1H, H-7), 5.04 (s, 2H, CH_2), 5.03 (s, 2H, CH_2); **^{1}H NMR** (300 MHz, $CDCl_3$): δ 8.82 (d, ^4J = 2.0 Hz, 1H, H-5), 8.50 (d, ^3J = 9.1 Hz, 1H, H-8), 7.95 (dd, ^3J = 9.1, ^4J = 2.0 Hz, 1H, H-7), 4.90 (s, 2H, CH_2), 4.89 (s, 2H, CH_2); **^{13}C NMR** (75.5 MHz, $CDCl_3$) δ; 140.7 (C2 or C3), 140.0 (C2 or C3), 137.9 (C4a), 136.4 (C8a), 136.0 (C7), 127.7 (C6), 123.3 (C5), 122.2 (C8), 20.24 (CH_2), 20.20 (CH_2); **MS-ES+** (*m/z*) 431 ([M + H]$^+$, 3 × ^{81}Br, 27%), 429 ([M + H]$^+$, 2 × ^{81}Br + ^{79}Br, 96), 427 ([M + H]$^+$, 2 × ^{79}Br + ^{81}Br, 100), 425 ([M + H]$^+$, 3 × ^{79}Br, 29); **MS-ES+** (*m/z*) 453 ([M + Na]$^+$, 3 × ^{81}Br, 3%), 451 ([M + Na]$^+$, 2 × ^{81}Br + ^{79}Br, 88), 449 ([M + Na]$^+$, 2 × ^{79}Br + ^{81}Br, 100), 447 ([M + Na]$^+$, 3 × ^{79}Br, 4); **Anal.** Calcd for $C_{10}H_7Br_3N_2O_2$: C, 28.14; H, 1.65; N, 6.56. Found: C, 28.15; H, 1.40; N, 6.48. Compounds **152** (0.039 g, 0.095 mmol, 12%) and **153** (0.021 g, 0.050 mmol, 6%) were also isolated.

2,3-Bis(bromomethyl)-6-nitroquinoxaline, 144

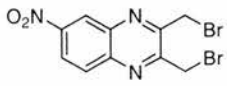

A solution of 1,4-dibromo-2,3-butanedione (2.00 g, 8.20 mmol) in anhydrous THF (40 mL) was added dropwise to a solution of 4-nitro-1,2-phenylenediamine (1.19 g, 7.80 mmol) in anhydrous THF (40 mL) at 0 °C over 15 mins. with stirring. The reaction was warmed to room temperature and stirred for a further 12 h. After concentration *in vacuo*, the crude material was redissolved in DCM (100 mL) and partitioned between 10% w/v aqueous sodium carbonate solution (200 mL) and DCM (300 mL). The organic phase was washed with brine (100 mL), dried ($MgSO_4$), filtered and concentrated *in vacuo* to give a pale brown solid. Purification by flash column chromatography on silica gel (EA:PE 40-60, 1:9) gave **144** as an off-white crystalline solid (2.66 g, 7.38 mmol, 95%) which was recrystallised (from EA:PE 40-60 1:3) to give colourless crystals; mp 115.0-115.5 °C (lit. 108-109 °C).[134] **IR** (Nujol, NaCl) ν_{max}: 3550 (br w), 1536 (s) (NO_2), 1364 (s) (NO_2), 1332 (m), 896 (w), 851 (w), 809 (m), 720 (m) ; **^{1}H NMR** (300 MHz, $CDCl_3$): δ 8.97 (d, ^4J = 2.5 Hz, 1H, H-5), 8.55 (dd, ^3J = 9.2 Hz, ^4J = 2.5 Hz, 1H, H-7), 8.22 (d, ^3J = 9.2 Hz, 1H, H-8), 4.94 (s, 2H, CH_2), 4.93 (s, 2H, CH_2); **^{13}C NMR** (75.5 MHz, $CDCl_3$) δ; 154.1 (C2 or C3), 153.4 (C2 or C3), 148.4 (C6), 143.8 (C8a), 140.4 (C4a), 130.7 (C8), 125.3 (C5), 124.2 (C7), 29.7 (CH_2), 29.6 (CH_2); **MS-ES–** (*m/z*) 362 ([M – H]$^-$, 2 × ^{81}Br, 12%), 360 ([M – H]$^-$, ^{79}Br + ^{81}Br, 100), 358 ([M – H]$^-$, 2 × ^{79}Br, 10) **HRMS-ES–** (*m/z*) Calcd for $C_{10}H_6{}^{81}Br^{79}BrN_3O_2$ [M – H]$^-$: 359.8806, found 359.8806; **Anal.** Calcd for $C_{10}H_7Br_2N_3O_2$: C, 33.27; H, 1.95; N, 11.64. Found: C, 33.27; H, 1.64; N, 11.49.

2,3-Bis(bromomethyl)-6-nitroquinoxaline 1,4-dioxide, 145

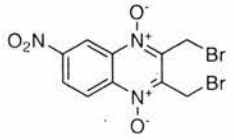

To a solution of **144** (610 mg, 1.70 mmol) in anhydrous DCM (50 mL) was added purified *m*CPBA (2.93 g, 17.0 mmol) with stirring. The reaction was then heated to reflux. After 48 h the reaction mixture was allowed to cool, diluted with DCM (100 mL) and washed with 10% w/v sodium carbonate solution (3 × 200 mL). The organic phase was dried ($MgSO_4$), filtered and concentrated *in vacuo* to give an orange solid. Purification by flash column chromatography on silica gel (EA:PE 40-60, 1:9 to 2:3) gave **145** as a bright

orange crystalline solid (120 mg, 0.31 mmol, 18%); mp 85.0-87.0 °C. **IR** (KBr) ν_{max}: 3103 (w), 1619 (w), 1542 (s) (NO_2), 1337 (s) (N–O), 1171 (w), 1031 (m), 838 (m), 798 (w), 741 (m), 676 (s) (C–Br) cm^{-1}; **^{1}H NMR** (300 MHz, $CDCl_3$); δ 9.51 (dd, ^4J = 2.4, ^5J = 0.4 Hz, 1H, H5), 8.85 (dd, ^3J = 9.3, ^5J = 0.4 Hz, 1H, H8), 8.64 (dd, ^3J = 9.3, ^4J = 2.4 Hz, 1H, H7), 4.91 (s, 4H, 2 × CH_2); **^{13}C NMR** (75.5 MHz, $CDCl_3$): δ 149.4 (C6), 142.5 (C2 or C3), 141.7 (C2 or C3), 139.6 (C8a), 137.4 (C4a), 125.9 (C7), 123.2 (C8), 117.6 (C5), 19.9 (CH_2), 19.9 (CH_2); **MS-ES+** (*m/z*) 396 ([M + H]$^+$, 2 × ^{81}Br, 40%), 394 ([M + H]$^+$, ^{79}Br + ^{81}Br, 100), 392 ([M + H]$^+$, 2 × ^{79}Br, 44); **MS-CI+** (*m/z*) 396 ([M + H]$^+$, 2 × ^{81}Br, 6%), 394 ([M + H]$^+$, ^{79}Br + ^{81}Br, 12), 392 ([M + H]$^+$, 2 × ^{79}Br, 7), 380 ([M – O]$^+$, 2 × ^{81}Br, 9), 378 ([M – O]$^+$, ^{79}Br + ^{81}Br, 17), 376 ([M – O]$^+$, 2 × ^{79}Br, 10); 316 ([M – ^{79}Br]$^+$, ^{81}Br, 6), 314 ([M – Br]$^+$, 16), 312 ([M – Br]$^+$, 8), 300 ([M – O – Br]$^+$, 78), 298 ([M – O – Br]$^+$, 77), 284 ([M – 2 × O – ^{79}Br]$^+$, ^{81}Br, 28), 282 ([M - 2 × O – Br]$^+$, 26), 236 (12), 234 (22), 232 (8), 220 (100), 218 (32), 204 (39) 202 (14); **HRMS-CI+** (*m/z*) Calcd for $C_{10}H_8{}^{81}Br_2N_3O_4$ [M + H]$^+$: 395.8841, found 395.8842; **HRMS-CI+** (*m/z*) Calcd for $C_{10}H_8{}^{81}Br^{79}BrN_3O_4$ [M + H]$^+$: 393.8874, found 393.8874; **HRMS-CI+** (*m/z*) Calcd for $C_{10}H_8{}^{79}Br_2N_3O_4$ [M + H]$^+$: 391.8882, found 391.8882. Compounds **148** (195 mg, 0.52 mmol, 30%) and **149** (68 mg, 0.18 mmol, 11%) were also isolated.

2-Butyl-7-bromo-2*H*-pyrrolo[3,4-*b*]quinoxaline 4-oxide, 146 and **2-Butyl-6-bromo-2*H*-pyrrolo[3,4-*b*]quinoxaline 4-oxide, 147**

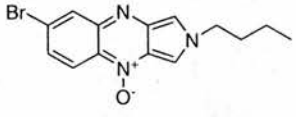

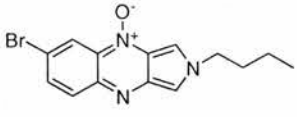

Prepared according to the general kinetic NMR procedure (Method A) using **142** (6.5 mg, 0.02 mmol) and *n*-butylamine (4 mg, 6 μL, 0.05). After 20 h the reaction mixture was quenched with silica and the solvent removed *in vacuo*. Purification by flash column chromatography on silica gel (EA:PE 40-60, 1:1 to 1:0) gave the desired products **146** and **147** as a mixture of regioisomers. **146** and **147** were collected as an unstable dark red oil (3 mg, 0.10 mmol, 50%). The mixture of **146** and **147** was observed to decompose rapidly in the absence of solvent. Compounds **146** and **147**: **MS-ES+** (*m/z*) 322 ([M + H]$^+$, ^{81}Br, 96%), 320 ([M + H]$^+$, ^{79}Br, 100); **HRMS-ES+** (*m/z*) Calcd for $C_{14}H_{15}{}^{81}BrN_3O$ [M + H]$^+$: 322.0378, found 322.0390; **HRMS-ES+** (*m/z*) Calcd for $C_{14}H_{15}{}^{79}BrN_3O$ [M + H]$^+$: 320.0398, found 320.0393.

Major regioisomer **146**: **^{1}H NMR** (500 MHz, $CDCl_3$): δ 8.42 (d, ^3J = 9.6 Hz, 1H, H-5), 8.20 (d, ^4J = 2.0 Hz, H-8), 7.65 (d, ^4J = 2.5 Hz, 1H, H-3), 7.61-7.60 (m, contains 1H, H-1), 7.54 (dd, ^3J = 9.6 Hz, ^4J = 2.0 Hz, 1H, H-6), 4.38 (t, ^3J = 7.1 Hz, 2H, CH_2-1′), 2.03-1.97 (m, 2H, CH_2-2′), 1.42-1.34 (m, 2H, CH_2-3′), 0.99 (t, ^3J = 7.4 Hz, 2H, CH_3).

Minor regioisomer **147**: **^{1}H NMR** (500 MHz, $CDCl_3$): δ 8.75 (d, ^4J = 2.2 Hz, 1H, H-5), 7.87 (d, ^3J = 9.4 Hz, H-8), 7.66 (d, ^4J = 2.5 Hz, 1H, H-3), 7.61 (dd, ^3J = 9.4 Hz, ^4J = 2.2 Hz, 1H, H-6), 7.61-7.60 (m, contains 1H, H-1), 4.39 (t, ^3J = 7.1 Hz, 2H, CH_2-1′), 2.03-1.97 (m, 2H, CH_2-2′), 1.42-1.34 (m, 2H, CH_2-3′), 0.99 (t, ^3J = 7.4 Hz, 2H, CH_3).

2-Butyl-7-nitro-2*H*-pyrrolo[3,4-*b*]quinoxaline 4-oxide, 148 and **2-Butyl-6-nitro-2*H*-pyrrolo[3,4-*b*]quinoxaline 4-oxide, 149**

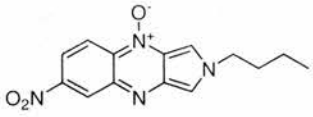

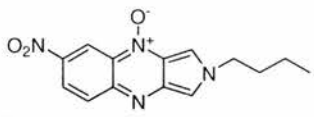

Prepared according to the general kinetic NMR procedure (Method A) using **145** and *n*-butylamine. Also, on preparative scale: A solution of *n*-butylamine (26.5 mg, 36 μL, 0.36 mmol) in $CDCl_3$ (3.0 mL) was added to a solution of **145** (47.5 mg, 0.12 mmol) in $CDCl_3$ (3.0 mL) with stirring at room temperature. After 20 h the reaction mixture was quenched with silica and the solvent removed *in vacuo*. Purification by flash column chromatography on silica gel (EA:PE 40-60, 1:1) gave **148** and **149**. **148** was collected as an unstable violet oil (4 mg, 0.01 mmol, 12%). **149** was collected as an unstable indigo oil (10 mg, 0.03 mmol, 29%). **148** and **149** were observed to decompose rapidly in the absence of solvent. Compounds **148** + **149**: **MS-ES+** (*m/z*) 287 ([M + H]$^+$, 100); **HRMS-ES+** (*m/z*) Calcd for $C_{14}H_{15}N_4O_3$ [M + H]$^+$: 287.1144, found 287.1146.

Compound **148**: **IR** (PTFE, $CDCl_3$) ν_{max}: 3102 (w), 1719 (w), 1529 (s) (NO_2), 1343 (s) (N–O), 771 (w) and 739 (m) (ArC–H) cm^{-1}; **^{1}H NMR** (500 MHz, $CDCl_3$): δ 8.98 (d, ^4J = 2.3 Hz, 1H, H-8), 8.68 (d, ^3J = 9.9 Hz, 1H, H-5), 8.20 (dd, ^3J = 9.9 Hz, ^4J = 2.3 Hz, 1H, H-6), 7.74 (d, ^4J = 2.5 Hz, 1H, H-3), 7.71 (d, ^4J = 2.5 Hz, 1H, H-1), 4.43 (t, ^3J = 7.1 Hz, 2H, NCH_2 of *n*Bu), 2.06-2.00 (m, 2H, NCH_2CH_2), 1.47-1.36 (m, 2H, CH_2CH_3), 0.99 (t, ^3J = 7.4 Hz, 2H, CH_3).

Compound **149**: **IR** (PTFE, $CDCl_3$) ν_{max}: 3099 (w), 1619 (w), 1559 (m) (NO_2), 1517 (w), 1498 (w), 1432 (m), 1346 (s), 1312 (s), 784 (w) and 741 (m) (ArC–H) cm^{-1}; **^{1}H NMR** (500 MHz, $CDCl_3$): δ 9.49 (d, ^4J = 2.5 Hz, 1H, H-5), 8.28 (dd, ^3J = 9.6 Hz, ^4J = 2.5 Hz,

H-7), 8.11 (d, ^3J = 9.6 Hz, 1H, H-8), 7.74 (d, ^4J = 2.5 Hz, 1H, H-3), 7.65 (d, ^4J = 2.5 Hz, 1H, H-1), 4.42 (t, ^3J = 7.1 Hz, 2H, NCH_2 of *n*Bu), 2.06-2.00 (m, 2H, NCH_2CH_2), 1.47-1.36 (m, 2H, CH_2CH_3), 0.99 (t, ^3J = 7.4 Hz, 2H, CH_3); **^{13}C NMR** (75.5 MHz, $CDCl_3$) δ: 150.9 (C6), 145.9 (C8a), 145.7 (C4a), 138.9 (C3a), 132.0 (C8), 125.8 (C9a), 122.0 (C7), 116.8 (C5), 112.3 (C1), 104.9 (C3), 53.4 (NCH_2 of *n*Bu), 33.3 (NCH_2CH_2), 19.7 (CH_2CH_3), 13.4 (CH_3).

tert-Butyl 2,3-bis(bromomethyl)quinoxalin-6-ylcarbamate 1-oxide, 150 and **_tert_-Butyl 2,3-bis(bromomethyl)quinoxalin-7-ylcarbamate 1-oxide, 151**

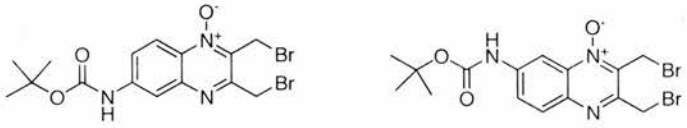

Prepared from **114** (1.00 g, 2.32 mmol) and purified *m*CPBA (3.00 g, 17.4 mmol) using the method described for **110** with a reaction time of 24 h. The desired products **150** and **151** were isolated as a mixture of regioisomers, collected as a yellow crystalline solid (0.71 g, 1.58 mmol, 68%); Compounds **150** and **151**: mixed mp 92.0-95.0 °C; **IR** (NaCl, Nujol) ν_{max}: 1732 (s) (C=O), 1620 (m), 1583 (m),1351 (s) (N–O), 1240 (m), 1153 (s), 1060 (m), 835 (w) (ArC–H) cm^{-1}; **MS-ES–** (*m/z*) 448 ([M – H]$^-$, 2 × ^{81}Br, 9%), 446 ([M – H]$^-$, ^{79}Br + ^{81}Br, 100), 444 ([M – H]$^-$, 2 × ^{79}Br, 12); **HRMS-ES–** (*m/z*) Calcd for $C_{15}H_{16}{}^{79}Br^{81}BrN_3O_3$ [M – H]$^-$: 445.9538, found 445.9532.

Compound **150**: **^{1}H NMR** (300 MHz, $CDCl_3$): δ 8.46 (d, ^3J = 9.4 Hz, 1H, H-8), 8.09 (d, ^4J = 2.3 Hz, 1H, H-5), 7.79 (dd, ^3J = 9.4 Hz, ^4J = 2.3 Hz, 1H, H-7), 6.95 (br s, 1H, NH), 5.00 (s, 2H, CH_2-9), 4.73 (s, 2H, CH_2-10), 1.55 (s, 9H, 3 × CH_3); **^{13}C NMR** (75.5 MHz, $CDCl_3$): δ 153.1 (C3), 152.1 (C=O), 144.5 (C4a or C6), 142.3 (C4a or C6), 137.0 (C2), 132.3 (C8a), 123.2 (C7), 120.0 (C8), 115.1 (C5), 81.9 (CCH_3), 30.3 (C10), 28.2 (3 × CH_3), 21.1 (C9).

Compound **151**: **^{1}H NMR** (300 MHz, $CDCl_3$): δ 8.43 (d, ^3J = 2.4 Hz, 1H, H-8), 8.19 (br d, ^3J = 9.2 Hz, 1H, H-6), 7.99 (d, ^3J = 9.2 Hz, 1H, H-5), 7.27 (br s, 1H, NH), 5.02 (s, 2H, CH_2-9), 4.76 (s, 2H, CH_2-10), 1.57 (s, 9H, 3 × CH_3); **^{13}C NMR** (75.5 MHz, $CDCl_3$): δ 152.3 (C=O), 150.1 (C3), 142.1 (C7), 139.8 (C4a), 138.7 (C2), 136.7 (C8a), 130.9 (C5), 124.5 (C6), 105.0 (C8), 82.0 (CCH_3), 30.4 (C10), 28.2 (3 × CH_3), 21.1 (C9).

In addition **110** was isolated as a yellow crystalline solid (164 mg, 0.35 mmol, 15%).

2,3-Bis(bromomethyl)-6-bromoquinoxaline 4-oxide, 152 and **2,3-Bis(bromomethyl)-7-bromoquinoxaline 1-oxide, 153**

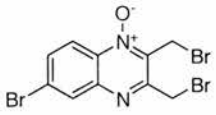
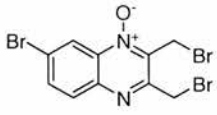

Prepared from **141** (0.20 g, 0.51 mmol) and purified *m*CPBA (0.16 g, 0.94 mmol) using the method described for **142**. Compound **152** was collected as a pale yellow solid (37 mg, 0.09 mmol, 18%); Compound **153** was collected as a white crystalline solid (30 mg, 0.07 mmol, 14%). Compound **152**: mp 144.5-146.0 °C; **IR** (NaCl, Nujol) ν_{max}: 3450 (br s), 1595 (w), 1567 (s), 1351 (s) (N–O), 1204 (w), 1168 (m), 1107 (w), 1057 (w), 823 (m) and 774 (w) (ArC–H), 683 and 670 (m) (C–Br) cm^{-1}; **^{1}H NMR** (300 MHz, DMSO-d_6): δ 8.40 (d, ^4J = 2.1 Hz, 1 H, H-5), 8.36 (d, ^3J = 9.2 Hz, 1 H, H-8), 8.02 (dd, ^3J = 9.2, ^4J = 2.1 Hz, 1 H, H-7), 5.00 (s, 2 H, CH_2), 4.99 (s, 2 H, CH_2); **^{1}H NMR** (300 MHz, $CDCl_3$): δ 8.39 (d, ^3J = 9.2 Hz, 1 H, H-8), 8.23 (d, ^4J = 2.0 Hz, 1 H, H-5), 7.80 (dd, ^3J = 9.2, ^4J = 2.0 Hz, 1 H, H-7), 4.96 (s, 2 H, CH_2-9), 4.73 (s, 2 H, CH_2-10); **^{13}C NMR** (75.5 MHz, $CDCl_3$): δ 153.8 (C3), 143.8 (C4a), 138.8 (C2), 135.3 (C8a), 134.2 (C7), 132.2 (C5), 126.8 (C6), 120.6 (C8), 29.9 (C10), 20.5 (C9); **MS-ES+** (*m/z*) 435 ($[M + Na]^+$, 2 × ^{81}Br + ^{79}Br, 79), 433 ($[M + Na]^+$, 2 × ^{79}Br + ^{81}Br, 100); **HRMS-ES+** (*m/z*) Calcd for $C_{10}H_7{}^{79}Br^{81}Br_2N_2ONa$ $[M + Na]^+$: 434.7965, found 434.7953. **HRMS-ES+** (*m/z*) Calcd for $C_{10}H_7{}^{79}Br_2{}^{81}BrN_2ONa$ $[M + Na]^+$: 432.7986, found 432.7975; Structure also confirmed by X-ray crystallographic analysis.

Compound **153**: mp > 180 °C dec.; **IR** (NaCl, Nujol) ν_{max}: 3450 (br s), 1597 (w), 1561 (w), 1355 (s) (N–O), 830 (m) and 74 (w) (ArC–H), 672 (m) (C–Br) cm^{-1}; **^{1}H NMR** (300 MHz, $CDCl_3$): δ 8.73 (br d, ^4J = 1.8 Hz, 1H, H-8), 7.92 (m, 2H, H-5 and H-6), 4.98 (s, 2H, CH_2-9), 4.74 (s, 2H, CH_2-10); **^{13}C NMR** (75.5 MHz, $CDCl_3$) δ; 152.9 (C3), 142.1 (C4a), 139.1 (C2), 136.7 (C8a), 135.9 (C6), 131.4 (C5), 125.6 (C7), 122.0 (C8), 30.0 (C10), 20.5 (C9); **MS-ES+** (*m/z*) 435 ($[M + Na]^+$, 2 × ^{81}Br + ^{79}Br, 74), 433 ($[M + Na]^+$, 2 × ^{79}Br + ^{81}Br, 100); **HRMS-ES+** (*m/z*) Calcd for $C_{10}H_7{}^{79}Br^{81}Br_2N_2ONa$ $[M + Na]^+$: 434.7965, found 434.7955. **HRMS-ES+** (*m/z*) Calcd for $C_{10}H_7{}^{79}Br_2{}^{81}BrN_2ONa$ $[M + Na]^+$: 432.7986, found 432.7980; **Anal.** Calcd for $C_{10}H_7Br_3N_2O$: C, 29.23; H, 1.72; N, 6.82. Found: C, 29.49; H, 1.43; N, 6.60. Structure also confirmed by X-ray crystallographic analysis.

2,3-Bis(bromomethyl)-6-nitroquinoxaline 1-oxide, 154 and **2,3-Bis(bromomethyl)-7-nitroquinoxaline 1-oxide 155**

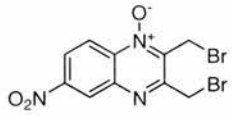
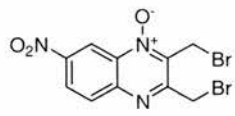

154 and **155** were isolated in the synthesis of **145**. Prepared from **144** (610 mg, 1.70 mmol) and purified *m*CPBA (2.93 g, 17.0 mmol). Compound **154** was collected as a pale yellow solid (195 mg, 0.52 mmol, 30%). Compound **155** was collected as beige solid (68 mg, 0.18 mmol, 11%).

Compound **154**: mp 126.5-127.5 °C; **IR** (NaCl, Nujol) ν_{max}: 3420 (br s), 1540 (s) (NO_2), 1349 (s) (N–O and NO_2), 1233 (m), 1208 (m), 1058 (m), 956 (s), 923 (s), 842 (m), 828 (m), 742 (s) and 723 (s) (ArC–H), 670 (m) (C–Br) cm^{-1}; **^{1}H NMR** (300 MHz, $CDCl_3$) δ 8.97 (d, ^4J = 2.4 Hz, 1H, H-5), 8.74 (d, ^3J = 9.4 Hz, 1H, H-8), 8.51 (dd, ^3J = 9.4, ^4J = 2.4 Hz, 1H, H-7), 4.99 (s, 2H, CH_2-9), 4.79 (s, 2H, CH_2-10); **^{13}C NMR** (75 MHz, $CDCl_3$) δ 155.3 (C3), 149.5 (C6), 142.8 (C4a), 140.9 (C2), 138.9 (C8a), 126.3 (C5), 124.0 (C7), 121.5 (C8), 29.5 (C10), 20.0 (C9); **MS-CI+** (*m/z*) 380 ($[M + H]^+$, 2 × ^{81}Br, 34%), 378 ($[M + H]^+$, ^{79}Br + ^{81}Br, 74), 376 ($[M + H]^+$, 2 × ^{79}Br, 37), 300 ($[M - {}^{79}Br]^+$, ^{81}Br, 57), 298 ($[M - Br]^+$, 100), 296 ($[M - Br]^+$, 42); **HRMS-CI+** (*m/z*) Calcd for $C_{10}H_8{}^{81}Br_2N_3O_3$ $[M + H]^+$: 379.8891, found 379.8885; **HRMS-CI+** (*m/z*) Calcd for $C_{10}H_8{}^{79}Br^{81}BrN_3O_3$ $[M + H]^+$: 377.8912, found 377.8904; **HRMS-CI+** (*m/z*) Calcd for $C_{10}H_8N_3O_3{}^{79}Br_2$ $[M + H]^+$: 375.8932, found 375.8938. Structure also confirmed by X-ray crystallographic analysis.

Compound **155**: mp 134.5-135.5 °C; **IR** (NaCl, Nujol) ν_{max}: 3423 (br s), 1593 (m), 1524 (s) (NO_2), 1486 (s), 1363 (s) (NO_2), 1342 (s) (N–O), 1051 (w), 842 (w), 821 (w), 748 (m) and 736 (w) (ArC–H), 679 (m) (C–Br) cm^{-1}; **^{1}H NMR** (300 MHz, $CDCl_3$) δ 9.42 (d, ^4J = 2.5 Hz, 1H, H-8), 8.60 (dd, ^3J = 9.2, ^4J = 2.5 Hz, 1H, H-6), 8.25 (d, ^3J = 9.2 Hz, 1H, H-5), 4.99 (s, 2H, CH_2-9), 4.78 (s, 2H, CH_2-10); **^{13}C NMR** (75 MHz, $CDCl_3$) δ 155.9 (C3), 148.0 (C7), 145.4 (C4a), 140.0 (C2), 135.8 (C8a), 131.8 (C5), 125.5 (C6), 116.2 (C8), 29.3 (C10), 19.7 (C9); **MS-ES+** (*m/z*) 402 ($[M + Na]^+$, 2 × ^{81}Br, 6%), 400 ($[M + Na]^+$, ^{79}Br + ^{81}Br, 88), 398 ($[M + Na]^+$, 2 × ^{79}Br, 8%), 236 ($[M - {}^{81}Br - NO_3]^+$, 100); **HRMS-ES+** (*m/z*) Calcd for $C_{10}H_7{}^{81}Br_2N_3O_3Na$ $[M + Na]^+$ 401.8711 found 401.8696; **HRMS-ES+** (*m/z*) Calcd for $C_{10}H_7{}^{79}Br^{81}BrN_3O_3Na$ $[M + Na]^+$: 399.8731, found 399.8729; **HRMS-ES+** (*m/z*) Calcd for $C_{10}H_7{}^{79}Br_2N_3O_3Na$ $[M + Na]^+$: 397.8752, found 397.8743. Structure also confirmed by X-ray crystallographic analysis.

tert-Butyl 2,2-diethyl-2,3-dihydro-1*H*-pyrrolo[3,4-*b*]quinoxalin-7-ylcarbamate-2-ium bromide 4-oxide, 156 and **_tert_-Butyl 2,2-diethyl-2,3-dihydro-1*H*-pyrrolo[3,4-*b*]quinoxalin-6-ylcarbamate-2-ium bromide 4-oxide, 158**

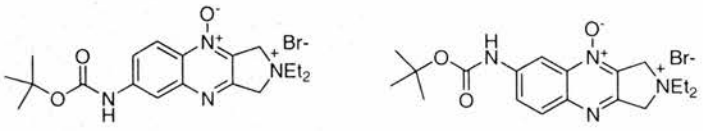

Prepared according to the general procedure (Method B) using a 1:2 mixture of **150**:**151** and diethylamine. Reaction was scaled up 5-fold for full analysis. Compounds **156** and **158** were collected as a mixture of regioisomers following crystallisation to yield a pale yellow crystalline solid (7 mg, 0.06 mmol, 17%). Compounds **157** and **159** were recovered from the filtrate in the presence of diethylamine.

Compounds **156** and **158**: mixed mp > 190.0 °C dec.; **MS-ES+** (*m/z*) 359 ([M – Br]$^+$, 100%); **HRMS-ES+** (*m/z*) Calcd for $C_{19}H_{27}N_4O_3$ [M – Br]$^+$: 359.2083, found 359.2078. Minor regioisomer **156**: **^{1}H NMR** (300 MHz, DMSO-d_6): δ 10.15 (br s, 1H, NH), 8.39 (d, ^3J = 9.4 Hz, 1H, H-5), 8.29 (d, ^4J = 2.1 Hz, 1H, H-8), 7.93-7.88 (m, contains 1H, H-6), 5.20 (s, 2H, CH_2-3), 5.19 (s, 2H, CH_2-1), 3.75-3.69 (m, 4H, 2 × CH_2 of Et), 1.31 (t, ^3J = 7.1 Hz, 6H, 2 × CH_3 of Et). Major regioisomer **158**: **^{1}H NMR** (300 MHz, DMSO-d_6): δ 10.22 (br s, 1H, NH), 8.77 (d, ^4J = 2.3 Hz, 1H, H-5), 8.10 (d, ^3J = 9.1 Hz, 1H, H-8), 7.93-7.88 (m, contains 1H, H-7), 5.24 (s, 2H, CH_2-3), 5.19 (s, 2H, CH_2-1), 3.75-3.69 (m, 4H, 2 × CH_2 of Et), 1.31 (t, ^3J = 7.1 Hz, 6H, 2 × CH_3 of Et).

(3-(Diethylaminomethyl)-6-ylcarbamatequinoxalin-2-ylmethyl)diethylamine 1-oxide, 157 and **(3-(Diethylaminomethyl)-7-ylcarbamatequinoxalin-2-ylmethyl)diethylamine 1-oxide, 159**

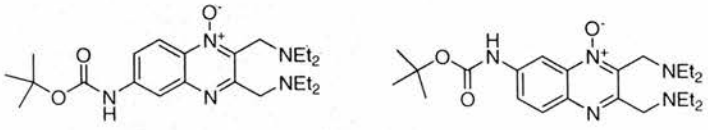

Minor regioisomer **157**: **^{1}H NMR** (300 MHz, DMSO-d_6): δ 10.02 (br s, 1H, NH), 8.32 (d, ^3J = 9.4 Hz, 1H, H-8), 8.20 (d, ^4J = 2.3 Hz, 1H, H-5), 7.91 (dd, ^3J = 9.4 Hz, ^4J = 2.3 Hz, 1H, H-6), 4.22 (s, 2H, CH_2-9), 4.01 (s, 2H, CH_2-10), 2.60-2.49 (m, 8H, 4 × CH_2 of Et), 1.94 (t, ^3J = 7.1 Hz, 6H, 4 × CH_3 of Et). Major regioisomer **159**: **^{1}H NMR** (300 MHz, DMSO-d_6): δ 10.08 (br s, 1H, NH), 8.71 (d, ^4J = 2.5 Hz, 1H, H-8), 7.97 (d, ^3J = 9.1 Hz, 1H, H-5), 7.90 (dd, ^3J = 9.1 Hz, ^4J = 2.5 Hz, 1H, H-6), 4.25 (s, 2H, CH_2-9), 4.00 (s, 2H, CH_2-10), 2.60-2.49 (m, 8H, 4 × CH_2 of Et), 1.94 (t, ^3J = 7.1 Hz, 6H, 4 × CH_3 of Et).

2,2-Diethyl-2,3-dihydro-1*H*-pyrrolo[3,4-*b*]-7-bromoquinoxalin-2-ium bromide 4-oxide, 160 and **(3-(Diethylaminomethyl)-6-bromoquinoxalin-2-ylmethyl)diethylamine 1-oxide, 161**

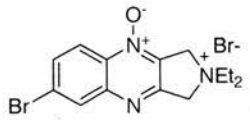

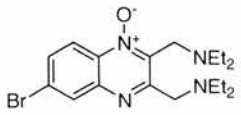

Prepared according to the general procedure (Method B) using **152** and diethylamine. Reaction was scaled up 6-fold for full analysis. Compound **160** was collected following crystallisation to yield a white crystalline solid (16 mg, 0.04 mmol, 35%). Compound **161** was recovered from the filtrate in the presence of diethylamine. Compound **160**: mp >195 °C dec.; **IR** (NaCl, Nujol) ν_{max}: 3458 (br s), 1597 (m), 1571 (s), 1368 (s) (N–O), 1107 (m), 820 (m), 743 (m) and 723 (m) (ArC–H) cm^{-1}; **^{1}H NMR** (300 MHz, DMSO-d_6): δ 8.49 (d, ^4J = 2.1 Hz, 1H, H-8), 8.42 (d, ^3J = 9.2 Hz, 1H, H-5), 8.06 (dd, ^3J = 9.2 Hz, ^4J = 2.1 Hz, 1H, H-6), 5.26 (s, 2H, CH_2-3), 5.23 (s, 2H, CH_2-1), 3.72 (q, ^3J = 7.1 Hz, 4H, 2 × CH_2 of Et), 1.31 (t, ^3J = 7.1 Hz, 6H, 2 × CH_3 of Et); **^{13}C NMR** (75.5 MHz, DMSO-d_6): δ 153.8 (C9a), 146.1 (C8a), 135.6 (C3a), 133.4 (C4a), 133.4 (C6) 131.6 (C8), 125.6 (C7), 119.8 (C5), 65.4 (C1), 62.0 (C3), 57.7 (CH_2 of Et), 8.4 (CH_3 of Et); **MS-ES+** (*m/z*) 324 ([M – Br]$^+$, ^{81}Br, 87%), 322 ([M – Br]$^+$, ^{79}Br, 100); **HRMS-ES+** (*m/z*) Calcd for $C_{14}H_{18}{}^{81}BrN_3O$ [M – Br]$^+$: 324.0535, found 324.0538; **HRMS-ES+** (*m/z*) Calcd for $C_{14}H_{18}{}^{79}BrN_3O$ [M – Br]$^+$: 322.0555, found 322.0552.

Compound **161**: **^{1}H NMR** (300 MHz, DMSO-d_6): δ 8.36 (d, ^3J = 9.2 Hz, 1 H, H-8), 8.32 (d, ^4J = 2.1 Hz, 1 H, H-5), 7.94 (dd, ^3J = 9.2, ^4J = 2.1 Hz, 1 H, H-7), 4.24 (s, 2 H, CH_2-9), 4.06 (s, 2 H, CH_2-10), 2.63-2.49 (m, 8 H, 4 × CH_2 of Et), 0.95 (t, 12 H, 4 × CH_3 of Et); **^{1}H NMR** (300 MHz, $CDCl_3$): δ 8.40 (d, ^3J = 9.2 Hz, 1 H, H-8), 8.23 (d, ^4J = 2.1 Hz, 1 H, H-5), 7.72 (dd, ^3J = 9.2, ^4J = 2.1 Hz, 1 H, H-7), 4.26 (s, 2 H, CH_2-9), 4.10 (s, 2 H, CH_2-10), 2.65-2.54 (m, 8 H, 4 × CH_2 of Et), 1.02-0.97 (m, 12 H, 4 × CH_3 of Et); **^{13}C NMR** (75.5 MHz, $CDCl_3$): δ 158.9 (C3),143.6 (C4a), 141.7 (C2), 134.7 (C8a), 132.7 (C7), 131.9 (C5), 125.0 (C6), 121.0 (C8), 57.6 (C10), 47.2 (C9), 47.0 (CH_2 of Et), 46.5 (CH_2 of Et), 11.3 (CH_3 of Et), 11.0 (CH_3 of Et); **MS-ES+** (*m/z*) 397 ([M + H]$^+$, ^{81}Br, 79%), 395 ([M + H]$^+$, ^{79}Br, 100), 379 ([M – OH]$^+$, ^{81}Br, 54), 395 ([M – OH]$^+$, ^{79}Br, 55), 324 ([M – NEt_2]$^+$, ^{81}Br, 28), 322 ([M – NEt_2]$^+$, ^{79}Br, 32), 308 ([M – O – NEt_2]$^+$, ^{81}Br, 56), 306 ([M – O – NEt_2]$^+$, ^{79}Br, 83); **HRMS-ES+** (*m/z*) Calcd for $C_{18}H_{27}{}^{81}BrN_4ONa$ [M + Na]$^+$: 419.1245, found 419.1262; **HRMS-ES+** (*m/z*) Calcd for $C_{18}H_{27}{}^{79}BrN_4ONa$ [M + Na]$^+$: 417.1266, found 417.1264.

2,2-Diethyl-2,3-dihydro-1*H*-pyrrolo[3,4-*b*]-6-bromoquinoxalin-2-ium bromide 4-oxide, 162 and **(3-(Diethylaminomethyl)-7-bromoquinoxalin-2-ylmethyl)diethylamine 1-oxide, 163**

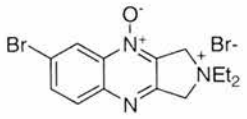

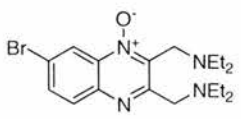

Prepared according to the general procedure (Method B) using **153** and diethylamine. Compound **162** was collected following crystallisation to yield a white crystalline solid (3 mg, 0.01 mmol, 37%). Compound **163** was recovered from the filtrate in the presence of diethylamine.

Compound **162**: mp >185 °C dec.; **IR** (NaCl, Nujol) ν_{max}: 3423 (br m), 1591 (w), 1561 (m), 1491(m), 1369 (s) (N–O), 1110 (w), 898 (m) and 723 (w) (ArC–H) cm^{-1}; **^{1}H NMR** (300 MHz, DMSO-d_6): δ 8.65-8.64 (m, 1H, H-5), 8.17-8.16 (m, 2H, H-7 and H-8), 5.28 (s, 2H, CH_2-3), 5.24 (s, 2H, CH_2-1), 3.72 (q, ^3J = 7.1 Hz, 4H, 2 × CH_2 of Et), 1.32 (t, ^3J = 7.1, 6 H, 2 × CH_3 of Et); **^{13}C NMR** (75.5 MHz, DMSO-d_6): δ 153.0 (C9a), 144.3 (C8a), 136.9 (C3a), 135.4 (C7), 133.7 (C4a) 131.6 (C8), 123.7 (C6), 120.1 (C5), 65.4 (C1), 61.9 (C3), 57.7 (CH_2 of Et), 8.4 (CH_3 of Et); **MS-ES+** (*m/z*) 324 ([M – Br]$^+$, ^{81}Br, 87%), 322 ([M – Br]$^+$, ^{79}Br, 100); **HRMS-ES+** (*m/z*) Calcd for $C_{14}H_{18}{}^{81}BrN_3O$ [M – Br]$^+$: 324.0535, found 324.0544; **HRMS-ES+** (*m/z*) Calcd for $C_{14}H_{18}{}^{79}BrN_3O$ [M – Br]$^+$: 322.0555, found 322.0545.

Compound **163**: **^{1}H NMR** (300 MHz, $CDCl_3$): δ 8.76 (d, ^3J = 8.8 Hz, 1H, H-8), 7.94 (d, ^4J = 2.0 Hz, 1H, H-5), 7.81 (dd, ^3J = 8.8, ^4J = 2.0 Hz, 1 H, H-7), 4.31 (s, 2H, CH_2N), 4.09 (s, 2H, CH_2N opp N-ox), 2.68-2.56 (m, 8H, 4 × CH_2 of Et), 1.04-0.99 (m, 12H, 4 × CH_3 of Et); **^{1}H NMR** (300 MHz, DMSO-d_6): δ 8.59-8.58 (m, 1 H, H-8), 8.02-8.03 (m, 2 H, H-5 and H-6), 4.25 (s, 2 H, CH_2N), 4.05 (s, 2 H, CH_2N opp N-ox), 2.62-2.49 (m, 8 H, 4 × CH_2 of Et), 0.95 (t, 12 H, ^3J = 7.1 Hz, 4 × CH_3 of Et); **MS-ES+** (*m/z*) 397 ([M + H]$^+$, ^{81}Br, 82%), 395 ([M + H]$^+$, ^{79}Br, 100), 379 ([M – OH]$^+$, ^{81}Br, 22), 395 ([M – OH]$^+$, ^{79}Br, 25), **HRMS-ES+** (*m/z*) Calcd for $C_{18}H_{28}{}^{81}BrN_4O$ [M + H]$^+$: 397.1426, found 397.1440; **HRMS-ES+** (*m/z*) Calcd for $C_{18}H_{28}{}^{79}BrN_4O$ [M + H]$^+$: 395.1446, found 395.1435.

2,2-Diethyl-2,3-dihydro-1*H*-pyrrolo[3,4-*b*]-7-nitroquinoxalin-2-ium bromide 4-oxide, 164 and **(3-(Diethylaminomethyl)-6-nitroquinoxalin-2-ylmethyl)diethylamine 1-oxide, 165**

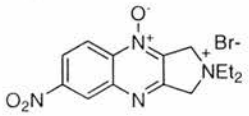
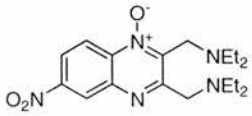

Prepared according to the general procedure (Method B) using **154** and diethylamine. Isolation of **164** was not possible due to low yield. Compound **165** was recovered from the filtrate in the presence of diethylamine.

Compound **164**: **^{1}H NMR** (300 MHz, $CDCl_3$): δ 8.99 (d, 1H, ^4J = 2.5 Hz, H-8), 8.74 (d, ^3J = 9.4 Hz, 1H, H-5), 8.53-8.46 (m, contains 1H, H-6), 5.14 (s, 2H, CH_2-3), 5.10 (s, 2H, CH_2-1), 3.16 (br q, 4H, 2 × CH_2 of Et), 1.58 (t, ^3J = 7.2 Hz, 6H, 2 × CH_3 of Et).

Compound **165**: **^{1}H NMR** (300 MHz, $CDCl_3$): δ 8.97 (d, ^4J = 2.4 Hz, 1 H, H-5), 8.72 (d, ^3J = 9.4 Hz, 1H, H-8), 8.42 (dd, ^3J = 9.4, ^4J = 2.4 Hz, 1H, H-7), 4.31 (s, 2 H, CH_2-9), 4.16 (s, 2H, CH_2-10), 2.70-2.58 (m, 8H, 4 × CH_2 of Et), 1.04 (t, ^3J = 7.1 Hz, 12H, 4 × CH_3 of Et); **MS-ES+** (*m/z*) 362 ($[M + H]^+$, 6%), 344 ($[M - OH]^+$, 33), 229 (92), 227 ($[M - NO_3]^+$, 100).

2,2-Diethyl-2,3-dihydro-1*H*-pyrrolo[3,4-*b*]-6-nitroquinoxalin-2-ium bromide 4-oxide, 166 and **(3-(Diethylaminomethyl)-7-nitroquinoxalin-2-ylmethyl)diethylamine 1-oxide, 167**

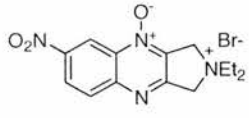
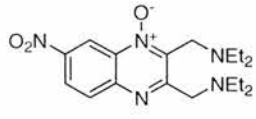

Prepared according to the general procedure (Method B) using **155** and diethylamine. Isolation of **166** was not possible due to low yield. Compound **167** was recovered from the filtrate in the presence of diethylamine.

Compound **166**: **^{1}H NMR** (300 MHz, $CDCl_3$): δ 9.47 (d, ^4J = 2.6 Hz, 1H, H-5), 8.57-8.53 (m, 1H, H-6), 8.24-8.20 (m, 1H, H-7), 5.29 (s, 2H, CH_2-3), 5.14 (s, 2H, CH_2-1), 3.51-3.37 (m, 4H, 2 × CH_2 of Et), 1.60 (t, ^3J = 7.2, 6H, 2 × CH_3 of Et).

Compound **167**: **^{1}H NMR** (300 MHz, $CDCl_3$): δ 9.45 (d, ^4J = 2.6 Hz, 1H, H-8), 8.51 (dd, ^3J = 9.1, ^4J = 2.6 Hz, 1H, H-6), 8.24 (d, ^3J = 9.1 Hz, 1H, H-5), 4.31 (s, 2H, CH_2-9), 4.16 (s, 2H, CH_2-10), 2.71-2.58 (m, 8H, 4 × CH_2 of Et), 1.03 (t, ^3J = 7.1 Hz, 12H, 4 × CH_3 of Et); **MS-ES+** (*m/z*) 362 ($[M + H]^+$, 10%), 344 ($[M - OH]^+$, 100), 273 ($[M - O]^+$, compound **166**, 10), 229 (64), 227 ($[M - NO_3]^+$, 68).

(*E*)-Dimethyl hex-3-enedioate, 178 [145]

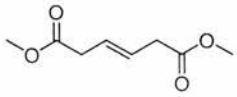

Trimethylsilyl chloride (8.56 g, 10.0 mL, 78.8 mmol) was added to a solution of (*E*)-hex-3-enedioic acid (5.60 g, 38.9 mmol) in anhydrous MeOH (105 mL) with stirring at 0 °C. The reaction was stirred for 48 h at 0 °C. The solvent was removed *in vacuo* and the residue partitioned between Et_2O (4 × 100 mL) and water. The combined organic layers were washed with 10% w/v aqueous sodium hydrogen carbonate solution (100 mL) and brine (100 mL). The organic phase was dried ($MgSO_4$) and concentrated *in vacuo* to afford **178** as a colourless oil (6.57 g, 38.2 mmol, 98%) and used without any further purification. **IR** (NaCl, Nujol) ν_{max}: 3358 (b), 1742 (s) (C=O), 1281 (w), 1201 (w), 1165 (m), 1045 (m), 971 (m) cm^{-1}; **^{1}H NMR** (300 MHz, $CDCl_3$): δ 5.69-5.65 (m, 2H, H-3 and H-4), 3.67 (s, 6H, 2 × CH_3), 3.08 (dd, ^3J = 3.8 Hz, ^4J = 1.6 Hz, 4H, 2 × CH_2-2, 5); **^{13}C NMR** (75.5 MHz, $CDCl_3$): δ 171.9 (2 × C=O), 125.9 (C3 and C4), 51.8 (2 × CH_3), 37.6 (C2 and 5). Data are in agreement with literature values.[145]

(*E*)-hex-3-ene-1,6-diol, 179 [145]

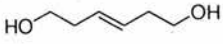

To a suspension of lithium aluminium hydride (1.32 g, 34.8 mmol) in anhydrous THF (80 mL) was added a solution of **178** (2.00 g, 11.6 mmol) in anhydrous THF (20 mL) dropwise at 0 °C. The reaction mixture was then allowed to warm to room temperature. After stirring for 2 h the reaction was quenched by slow addition of distilled water (15 mL). The resulting suspension was filtered through Celite® washing with THF (100 mL). The filtrate was concentrated *in vacuo* to give a yellow oil. Purification by flash column chromatography on silica gel (EA:Et_2O, 1:1) gave **179** as a pale yellow oil (1.32 g, 11.4 mmol, 98%). **IR** (film) ν_{max}: 3343 (b) (OH), 2929 (s), 1427 (m), 1045 (s), 969 (s) cm^{-1}; **^{1}H NMR** (300 MHz, $CDCl_3$): δ 5.54-5.50 (m, 2H, H-3 and H-4), 3.64 (t, ^3J = 6.1 Hz, 4H, CH_2-1, 6), 2.31-2.25 (m, 4H, 2 × CH_2-2, 5), 2.11 (br s, 2H, OH); **^{13}C NMR** (75.5 MHz, $CDCl_3$): δ 129.6 (C3 and C4), 61.7 (C1 and C6), 35.9 (C2 and C5). Data are in agreement with literature values.[145]

(*E*)-6-Triisopropylsilanyloxy-hex-3-en-1-ol, 180

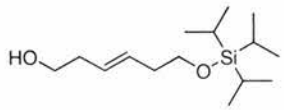

To a suspension of hexane-washed sodium hydride (0.24 g, 60% in mineral oil, 6.0 mmol,) in anhydrous THF (20 mL) was added a solution of **179** (0.70 g, 6.0 mmol) in anhydrous THF (10 mL) dropwise at 0 °C. The reaction mixture was then allowed to warm to room temperature. After stirring for 45 mins. triisopropylsilyl chloride (2.34 g, 2.60 mL, 12.2 mmol) was added dropwise and stirring continued. After 15 h 10% w/v aqueous sodium hydrogen carbonate (100 mL) was added and the reaction extracted with Et_2O (3 × 100 mL). The combined organic layers were washed with brine (100 mL). The resulting organic phase was dried ($MgSO_4$), filtered and the solvent removed *in vacuo* to give a yellow oil. Purification by flash column chromatography on silica gel (Et_2O:Hexane, 1:9 to 1:4) gave **180** as a pale yellow oil (0.87 g, 3.20 mmol, 53%). **IR** (film) ν_{max}: 3357 (br s) (OH), 2943 (s), 2866 (s), 1463 (s), 1383 (s), 1248 (m), 1106 (s), 1046 (s), 969 (s), 883 (s), 775 (m), 681 (s) cm^{-1}; **^{1}H NMR** (300 MHz, $CDCl_3$): δ 5.64-5.54 (m, 1H, H-3 or H-4), 5.50-5.40 (m, 1H, H-3 or H-4), 3.70 (t, ^3J = 6.7 Hz, 2H, CH_2-6), 3.62 (t, ^3J = 6.1 Hz, 2H, CH_2-1), 2.31-2.24 (m, 4H, CH_2-2,5), 1.77 (br s, 1H, OH), 1.06-1.04 (m, 21H, Si(CH(CH_3)$_2$)$_3$); **^{13}C NMR** (75.5 MHz, $CDCl_3$): δ 130.7 (C3 or C4), 127.9 (C3 or C4), 63.1 (C6), 61.8 (C1), 36.5 (C2 or C5), 36.0 (C2 or C5), 18.0 (SiCCH_3), 12.0 (SiCCH$_3$); **MS-ES+** (*m/z*) 295 ([M + Na]$^+$, 100%); **MS-CI+** (*m/z*) 273 ([M + H]$^+$, 82%), 229 (45), 175 (22), 99 (100), 81 (31); **HRMS-CI+** (*m/z*) Calcd for $C_{15}H_{33}O_2Si$ [M + H]$^+$: 273.2250, found 273.2256.

2,3-Bis(bromomethyl)quinoxalin-6-ylamine 1,4-dioxide hydrobromide, 184

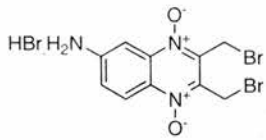

A solution of 45% HBr in AcOH (4.0 mL) was added to a solution of **110** (580 mg, 1.25 mmol) in AcOH (5.0 mL) and the reaction mixture was stirred at room temperature for 10 mins. The resulting solution was added dropwise to cold dry diethyl ether (20.0 mL) with stirring. The precipitate was collected by suction filtration washing with diethyl ether (20.0 mL). The desired product **184** was collected as a pink solid (521 mg, 1.17 mmol, 94%); mp > 200 °C dec. **IR** (NaCl, Nujol) ν_{max}: 3387 (br) (NH_2), 2576 (m), 1329

(s) (N–O), 1159 (w), 1026 (m), 834 (w) and 736 (w) (ArC–H) cm^{-1}; **^{1}H NMR** (300 MHz, CD_3OD): δ 8.24 (d, ^3J = 9.4 Hz, 1H, H-8), 7.42 (d, ^4J = 2.4 Hz, 1H, H-5), 7.28 (dd, ^3J = 9.4 Hz, ^4J = 2.4 Hz, 1H, H-7), 4.94 (s, 2H, CH_2), 4.93 (s, 2H, CH_2); **MS-ES+** (*m/z*) 366 ([M – Br]$^+$, 2 × ^{81}Br, 39%), 364 ([M – Br]$^+$, ^{79}Br + ^{81}Br, 100), 362 ([M – Br]$^+$, 2 × ^{79}Br, 44), 316 (55), 314 (54), 300 (14), 298 (13); **HRMS-ES+** (*m/z*) Calcd for $C_{10}H_{10}{}^{79}Br^{81}BrN_3O_2$ [M – Br]$^+$: 363.9119, found 363.9124; **HRMS-ES+** (*m/z*) Calcd for $C_{10}H_{10}{}^{79}Br_2N_3O_2$ [M – Br]$^+$: 361.9140, found 361.9139; **Anal.** Calcd for 1.03HBr.$C_{10}H_9Br_2N_3O_2$: C, 27.87; H, 2.34; N, 9.75. Found: C, 27.88; H, 2.06; N, 9.41.

(*E*)-6-(triisopropylsilyloxy)hex-3-enyl 2,3-bis(bromomethyl)quinoxalin-6-ylcarbamate 1,4-dioxide, 185

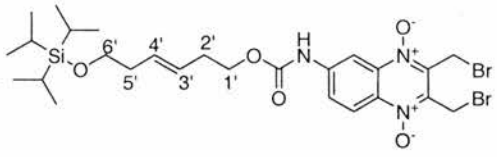

To a solution of **180** (442 mg, 1.62 mmol) in anhydrous DCM (30 mL) were added triphosgene (290 mg, 0.97 mmol) and pyridine (128 mg, 130 μL, 1.62 mmol) with stirring at 0 °C. The reaction was stirred for 30 mins. at 0 °C and then a further 2 h at room temperature. After concentration *in vacuo*, the crude material was partitioned between distilled water (60 mL) and ethyl acetate (60 mL). The organic phase was washed with brine (20 mL), dried ($MgSO_4$) and concentrated *in vacuo* to give a pale yellow oil which was then used without any further purification. To the residue was added the hydrobromide salt **184** (60.0 mg, 0.14 mmol), pyridine (128 mg, 130 μL, 1.62 mmol) and anhydrous THF (8.0 mL) with stirring at 0 °C. The reaction was stirred for 2 h at 0 °C and then a further 10 h at room temperature. The solvent was removed *in vacuo*. Purification by flash column chromatography on silica gel (EA:Hexane, 2:3) gave a pale yellow solid (20 mg, 0.03 mmol, 22%). **^{1}H NMR** (300 MHz, $CDCl_3$): δ 8.59 (d, ^3J = 9.4 Hz, 1H, H-8), 8.54 (d, ^4J = 2.2 Hz, 1H, H-5), 8.29 (dd, ^3J = 9.4 Hz, ^4J = 2.2 Hz, 1H, H-7), 7.65 (br s, 1H, NH), 5.68-5.58 (m, 1H, H-4), 5.54-5.45 (m, 1H, H-3), 5.12 (s, 2H, CH_2-9 or 10), 5.10 (s, 2H, CH_2-9 or 10), 4.26 (t, ^3J = 6.9 Hz, 2H, CH_2-1), 3.70 (t, ^3J = 6.7 Hz, 2H, CH_2-6), 2.53-2.34 (m, 2H, CH_2-2), 2.33-2.24 (m, 2H, CH_2-5), 1.06-1.04 (m, 21H, Si(CH(CH_3)$_2$)$_3$); **^{13}C NMR** (75.5 MHz, $CDCl_3$): δ 152.9 (N(6)C=O carbamate), 143.5 (C4a or C6), 140.1 (C2 or C3), 138.1 (C4a or C6), 138.0 (C2 or C3), 133.5 (C8a), 130.5 (C4′), 126.5 (C3′), 124.1 (C7), 122.0 (C8), 106.5 (C5), 65.7 (C1′), 63.2 (C6′), 36.4 (C2), 35.12 (C9 or C10), 35.08 (C9 or C10), 32.2 (C5), 18.0 (SiCCH_3),12.0 (SiCCH$_3$).

_N_-(2,3-bis(bromomethyl)quinoxalin-6-yl 1,4-dioxide)-5-((3a_S_,4_S_,6a_R_)-2-oxo-hexahydro-1_H_-thieno[3,4-_d_]imidazol-4-yl)pentanamide, 187

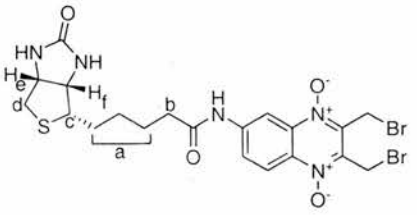

D-(+)-Biotin (500 mg, 2.05 mmol) and thionyl chloride (10.0 mL) were stirred together under nitrogen. The biotin dissolved and gave a homogeneous yellow solution after stirring at room temperature for 15 mins. After a further 15 mins. at room temperature the excess thionyl chloride was removed *in vacuo*. DMF (8.0 mL) was added to the residue followed by pyridine (32 mg, 33 μL, 0.41 mmol) with stirring under nitrogen. **184** (182 mg, 0.41 mmol) was added and the reaction mixture stirred at room temperature for 5 h. The solvent was removed *in vacuo*. Purification by flash column chromatography on silica gel (DCM:MeOH 1:19) gave **187** as a yellow solid (58 mg, 0.10 mmol, 24 %); mp >180 °C dec. **IR** (thin film, DCM) ν_{max}: 3500-2800, 1745 (w), 1718 (m) (C=O amide), 1688 (s), 1654 (s) (C=O urea), 1561 (CNH δ), 1539 (CNH δ), 1459, 1433, 1332 (s) (N–O), 1264, 1037, 733 (w) and 699 (w) (ArC–H) cm^{-1}; **^{1}H NMR** (300 MHz, CD_3OD): δ 9.01-8.96 (m, 1H, H-5), 8.51-8.46 (m, 1H, H-8), 8.06-7.99 (m, 1H, H-7), 5.14 (s, 2H, CH_2Br), 4.99 (s, 2H, CH_2Br), 4.56 (s, 2H), 4.49-4.44 (m, 1H, $CHCH_2S$ of biotin unit H-e), 4.31-4.27 (m, 1H, CHCHS of biotin unit H-f), 3.24-3.18 (m, 1H, CHS of biotin unit H-c), 2.90 (dd, ^2J = 12.7 Hz, ^3J = 4.9 Hz, 1H, one of the CH_2S of biotin unit H-d), 2.67 (d, ^2J = 12.7 Hz, 1H, one of the CH_2S of biotin unit H-d), 2.48 (t, ^3J = 7.2 Hz, 2H, CH_2CON H-b), 1.84-1.43 (m, 6H, $(CH_2)_3CH_2ON$, H-a); **^{13}C NMR** (125.5 MHz, $CDCl_3$) δ 175.1 (C=O amide), 166.1 (C=O of biotin unit), 144.6 (C4a), 142.3 (C2 or C3), 139.9 (C2 or C3), 139.7 (C6), 135.3 (C8a), 126.6 (C8), 122.1 (C7), 108.4 (C5), 63.4 (CH-f), 61.8 CH-e), 57.1 (CH-c), 41.0 (CH_2-d), 37.8 (CH-b), 36.6 (CH_2Br), 27.8 (CH_2-a), 29.6 (CH_2-a), 26.5 (CH_2-a), 21.9 (CH_2Br); **MS-ES+** (*m/z*) 614 ([M + Na]$^+$, 2 × ^{81}Br, 5%), 612 ([M + Na]$^+$, ^{79}Br + ^{81}Br, 31), 610 ([M + Na]$^+$, 2 × ^{79}Br, 4), 570 ([M – $CONH_2$ + Na]$^+$, 2 × ^{81}Br, 3), 568 ([M – $CONH_2$ + Na]$^+$, ^{79}Br + ^{81}Br, 100), 566 ([M – $CONH_2$ + Na]$^+$, 2 × ^{79}Br, 49); **HRMS-ES+** (*m/z*) Calcd for $C_{20}H_{23}{}^{79}Br^{81}BrN_5O_4NaS$ [M + Na]$^+$: 611.9715, found 611.9731; **HRMS-ES+** (*m/z*) Calcd for $C_{20}H_{23}{}^{79}Br_2N_5O_4NaS$ [M + Na]$^+$: 609.9735, found 609.9717.

4-Azidobenzoic acid, 193

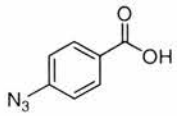

A solution of 4-aminobenzoic acid (2.00 g, 14.6 mmol) in 10% aqueous hydrochloric acid (130 mL) was added to a solution sodium nitrite (1.21 g, 17.5 mmol) in distilled water (8.0 mL) at 0-5 °C in an open flask, with vigorous stirring. The reaction was stirred for 30 mins. A solution of sodium azide (1.14 g, 17.5 mmol) was added and the reaction stirred for 1 h. The temperature was maintained below 5 °C throughout. The reaction was warmed to room temperature and stirred for 12 h. The crude reaction was extracted with Et_2O (3 × 250 mL). The organic phase was dried ($MgSO_4$), filtered and concentrated *in vacuo* to yield **193** as an off-white solid (2.33 g, 14.3 mmol, 98%): mp >180 °C dec. (lit. 179.0-180.0 dec.)[153] which was used without any further purification. **IR** (Nujol, NaCl) ν_{max}: 3500-3300 (br w) (OH), 2104 (s), 1601 (s) (C=O), 1377 (m) 1286 (s), 860 (w) and 767 (w) (ArC–H); **^{1}H NMR** (300 MHz, CD_3OD): δ 8.05-8.01 (m, AA′ part of the AA′XX′ system, 2H, H-2 and H-6), 7.17-7.12 (m, XX′ part of the AA′XX′ system, 2H, H-3 and H-5); **^{13}C NMR** (75.5 MHz, $CDCl_3$): δ 169.1 (C=O), 146.2 (C4), 132.7 (C2 and C6), 128.6 (C1), 119.9 (C3 and C5).

4-Azidobenzoyl chloride, 194

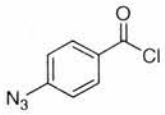

A suspension of **193** (400 mg, 2.45 mmol) in thionyl chloride (10.0 mL) was heated to reflux for 45 mins. to give a homogeneous yellow solution. After cooling, the excess thionyl chloride was removed *in vacuo* and the final traces removed by co-evaporation with hexane (2 × 20 mL) to yield **194** as an off white solid (442 mg, 2.43 mmol, 99%) and used without any further purification; mp 55.0 – 56.0 °C (lit. 56.0-57.0 °C).[157]

REFERENCES

REFERENCES

1. Venter, J. C.; Adams, M. D.; Myers, E. W.; Li, P. W.; Mural, R. J.; *et al. Science* **2001**, *291*, 1304-1351.
2. Westwood, N. J. *Phil. Trans. R. Soc. Lond. A* **2004**, *362*, 2761-2774.
3. Schreiber, S. L.; *Chemical and Engineering News* **2003**, Mar. 3, 51-61.
4. Haggarty, S. J.; Mayer, T. U.; Miyamoto, D. T.; Fathi, R.; King, R. W.; Mitchison, T. J.; Schreiber S. L. *Chem. Biol.* **2000**, *7*, 275-286.
5. Kuruvilla, F.G.; Shamji, A. F.; Sternson, S. M.; Hergenrother, P. J.; Schreiber, S. L. *Nature* **2002**, *416*, 653-657.
6. Ward, G. E.; Carey, K. L.; Westwood, N. J. *Cell. Microbiol.* **2002**, *4*, 471-482.
7. Blackwell, H. E.; Zhao, Y. *Plant Physiol.* **2003**, *133*, 448-455.
8. Mayer, T. U.; Kapoor, T. M.; Haggarty, S. J.; King, R. W.; Schreiber, S. L.; Mitchison, T. J. *Science* **1999**, *286*, 971-974.
9. Straight, A. F.; Cheung, A.; Limouze, J.; Chen, I.; Westwood, N. J.; Sellers, J. R.; Mitchison, T. J. *Science* **2003**, *299*, 1743-1747.
10. Schreiber, S. L. *Bioorg. Med. Chem.* **1998**, *6*, 1127-1153.
11. Carey, K. L.; Westwood, N. J.; Mitchison, T. J.; Ward, G. E. *Proc. Natl. Acad. Sci. USA* **2004**, *101*, 7434-7438.
12. Stockwell, B. R. *Nat. Rev. Genet.* **2000**, *1*, 116-125.
13. Kim, T. K. *J. Biochem. Mol. Biol.* **2004**, *37*, 53-58.
14. Strausberg R.; Schreiber, S. L. *Science* **2003**, *300*, 294-295.
15. Kim, T. K.; *Mol. Biol. News* **2000**, *1*, 30
16. King, R. W. *Chem. Biol.* **1999**, *6*, R327–R333
17. Burdine, L.; Kodadek, T. *Chem. Biol.* **2004**, *11*, 593-597.
18. Tochtrop, G. P.; King, R. W. *Comb. Chem. High Throughput Screening* **2004**, *7*, 677-688.
19. Spring, D. R. *Chem. Soc. Rev.* **2005**, *34*, 472-482.
20. Morgan, R. E.; Westwood, N. J. *Parasitology* **2004**, *128*, S71-S79.
21. Brown, E. J.; Albers, M. W.; Shin, T. B.; Ichikawa, K.; Keith, C. T.; Lane, W. S.; Schreiber, S. L. *Nature* **1994**, *369*, 756-758.
22. Harding, M. W.; Galat, A.; Uehling, D. E.; Schreiber, S. L. *Nature* **1989**, *341*, 758-760.
23. Taunton, J.; Hassig, C. A.; Schreiber, S. L. *Science* **1996**, *272*, 408-411.

24. Knockaert, M.; Gray, N.; Damiens, E.; Chang, Y. T.; Grellier, P.; Grant, K.; Fergusson, D.; Mottram, J.; Soete, M.; Dubremetz, J. F.; Le Roch, K.; Doerig, C.; Schultz, P.; Meijer, L. *Chem. Biol.* **2000**, *7*, 411-422.

25. Gray, N. S. *Curr. Opin. Neurobiol.* **2001**, *11*, 608-614.

26. Jeffery, D. A.; Bogyo, M. *Curr. Opin. Biotechnol.* **2003**, *14*, 87-95.

27. Hermanson, G. T. *Bioconjugate Techniques* Academic Press **1996**, 341-354.

28. Miller, D. K.; Gillard, J. W.; Vickers, P. J. Sadowski, S.; Leveille, C.; Mancini, J. A.; Charleson, P.; Dixon, R. A. F.; Ford-Hutchinson, A. W. Fortin, R.; Gauthier, J. Y.; Rodkey, J.; Rosen, R.; Rouzer, C.; Sigal, I. S.; Strader, C. D.; Evans, J. F. *Nature* **1990**, *343*, 278-281.

29. Gurnett, A. M.; Liberator, P. A.; Dulski, P. M.; Salowe, S. P.; Donald, R. G. K.; Anderson, J. W.; Wiltsie, J.; Diaz, C. A.; Blum, P. S.; Misura, A. S.; Tamas, T.; Sardana, M. K.; Yuan, J.; Biftu, T.; Schmatz, D. M. *J. Biol. Chem.* **2002**, *277*, 15913-15922.

30. Wilchek, M.; Bayer, E. A. Methods Enzymol. **1990**, *184*, 5-13.

31. Tomohiro, T.; Hashimoto, M.; Hatanaka, Y. *Chem. Rec.* **2005**, *5*, 385-395.

32. Rosania, G. R.; Chang, Y-T.; Perez, O.; Sutherlin, D.; Dong, H.; Lockhart, D. J.; Schultz, P. G. *Nature Biotechnol.* **2000**, *18*, 304-308.

33. Sin, N.; Meng, L.; Wang, M. Q. W.; Wen, J. J.; Bornmann, W. G.; Crews, C. M. *Proc. Natl. Acad. Sci. USA* **1997**, *94*, 6099-6103.

34. Kim, K. B.; Myung, J.; Sin, N.; Crews, C. M. *Bioorg. Med. Chem. Lett.* **1999**, *9*, 3335-3340.

35. Dormán, G.; Prestwich, G. D. *Trends Biotechnol.* **2000**, *18*, 64-77.

36. Hatanaka, Y.; Sadakane, Y.; *Curr. Topics Med. Chem.* **2002**, *2*, 271-288.

37. Konoki, K.; Sugiyama, N.; Murata, M.; Tachibana, K.; Hatanaka, Y. *Tetrahedron* **2000**, *56*, 9003-9014.

38. Hatanaka, Y.; Kempin, U.; Jong-Jip, P.; *J. Org. Chem.* **2000**, *65*, 5639-5643.

39. Van Sweiten, P. F.; Leeuwen*n*Burgh, M. A.; Kessler, B. M.; Overkleeft, H. S. *Org. Biomol. Chem.* **2005**, *3*, 20-27.

40. Agard, N. J.; Prescher, J. A.; Bertozzi, C. R. *J. Am. Chem. Soc.* **2004**, *126*, 15046-15047.

41. Prescher, J. A.; Bertozzi, C. R. *Nat. Chem. Biol.* **2005**, *1*, 13-21.

42. Vocaldo, D. J.; Hang, H. C.; Kim, E. J.; Hanover, J. A.; Bertozzi, C. R. *Proc. Natl. Acad. Sci. USA* **2003**, *100*, 9116-9121.

43. Vocaldo, D. J.; Bertozzi, C. R. *Angew. Chem. Int. Ed.* **2004**, *43*, 5338-5342.

44. Huisgen, R. *Angew. Chem. Int. Ed.* **1963**, *2*, 565-598.

45. Rostovtsev, V. V.; Green, L. G.; Fokin, W.; Sharpless, K. B. *Angew. Chem. Int. Ed.* **2002**, *41*, 2596-2599.

46. Lefurgy, S.; Cornish, V. *Chem. Biol.* **2004**, *11*, 151-152.

47. Licitra, E. J.; Liu, J. O. *Proc. Natl. Acad. Sci. USA* **1996**, *93*, 12817.

48. Becker, F.; Murthi, K.; Smith, C.; Come, J.; Costa-Roldan, N.; Kaufmann, C.; Hanke, U.; Degenhart C.; Baumann, S.; Wallner, W.; Huber, A.; Dedier, S.; Dill, S.; Kinsman D.; Hediger, M.; Bockovich, N.; Meier-Ewert, S.; Kluge, A. F.; Kley, N. *Chem. Biol.* **2004**, *11*, 211-223.

49. Drahl, C.; Cravatt, B. F.; Sorenson, E. J. *Angew. Chem. Int. Ed.* **2005**, *44*, 5788-5809.

50. Zhou, S *J. Chromatogr. B* **2003**, *767*, 63-90.

51. Robertson, J.G. *Biochemistry* **2005**, *44*, 5561-5571.

52. Roux, M. V.; Jiménez, P.; Dávalos, J. Z.; Castaño, O.; Molina, M. T.; Notario, R.; Herreros, M.; Abboud, J.-L. M. *J. Am. Chem. Soc.* **1996**, *118*, 12735-12737.

53. Wu, K. K. *Circulation* **2000**, *102*, 2022-2023 and references therein.

54. Thomas, A. M.; Ginj, C.; Jelesarov, I.; Amrhein, N.; Macheroux, P. *Eur. J. Biochem.* **2004**, *271*, 2682-2690.

55. Silverman, R. B.; *The Organic Chemistry of Drug Design and Drug Action*, Academic Press: London, **1992**.

56. Yabe, Y.; Guillaume, D.; Rich, D. H. *J. Am. Chem. Soc.* **1988**, *110*, 4043-4044.

57. Kudo, N.; Matsumori, N.; Taoka, H.; Fujiwara, D.; Schreiner, E. P.; Wolff, B.; Yoshida, M.; Horinouchi, S. *Proc. Natl. Acad. Sci. USA* **1999**, *96*, 9112-9117.

58. Kijima, M.; Yoshida, M.; Sugita, K.; Horinouchi, S.; Beppu, T. *J. Biol. Chem.* **1993**, *268*, 22429-22435.

59. Kidd, D.; Liu, Y.; Cravatt, B. F. *Biochemistry* **2001**, *40*, 4005-4015.

60. Campbell, D. A.; Szardenings, A. K. *Curr. Opin. Chem. Biol.* **2003**, *7*, 296-303.

61. Speers, A. E.; Cravatt, B. F. *Chem. Biol.* **2004**, *11*, 535-546.

62. Greenbaum, D. C.; Baruch, A.; Grainger, M.; Bozdech, Z.; Medzihradszky, K. F.; Engel, J.; DeRisi, J.; Holder, A. A.; Bogyo, M. *Science* **2002**, *298*, 2002-2006.

63. Speers, A. E.; Adam, G. C.; Cravatt, B. F. *J. Am. Chem. Soc.* **2003**, *125*, 4686-4687.

64. Ovaa, H.; van Sweieten, P. F.; Leeuwe*n*Burgh, M. A.; Fiebiger, E.; van der Nieuwendijk, A. M.; Galardy, P. J.; van der Marel, G. A.; Ploegh, H. L.; Overkleeft, H. S. *Angew Chem. Int. Ed. Engl.* **2003**, *42*, 3626-3629.

65. Speers, A.E.; Cravatt, B. F. *ChemBioChem* **2004**, *5*, 41-47.

66. Nichols, B. A.; Chiappino, M. L. *J. Protozool.* **1987**, *34*, 217-226.

67. Russell, D. G.; Burns, R. G. *J. Cell Sci.* **1984**, *65*, 193-207.

68. Hu, K.; Roos, D. S.; Murray, J. M. *J. Cell Biol.* **2002**, *156*, 1039-1050.

69. Morrissette, N. S.; Sibly, L. D. *Microbiol. Mol. Biol. Res.* **2002**, *66*, 21-38.

70. Swedlow, J. R.; Hu, K.; Andrews, P. D.; Roos, D. S.; Murray, J. M. Proc. Natl. Acad. Sci. USA **2002**, *99*, 2014-2019.

71. Pfefferkorn, E. R. Cell Biology of *Toxoplasma gondii*, in *Modern Parasite Biology*, Ed. David J. Wyler, W.H. Freeman and Company **1990**, Chapter 2, 26-50.

72. Keely, A.; Soldati, D. *Trends Cell Biol.* **2004**, *14*, 528-532.

73. Håkansson, S.; Charron, A. J.; Sibley, L. D. *EMBO J* **2001**, *20*, 3132-3144.

74. Monteiro, V. G.; de Melo, E. J. T.; Attias, M.; de Souza, W. *J. Struct. Biol.* **2001**, *136*, 181-189.

75. Mondragon, R.; Frixione, E. *J. Eukaryotic Microbiol.* **1996**, *4*, 120-127.

76. Firestone, R. A.; Barker, P. L.; Pisano, J. M.; Ashe, B. M.; Dahlgren, M. E. *Tetrahedron* **1990**, *46*, 2255-2262.

77. Knight, W. B.; Chabin, R.; Green, B. *Arch. Biochem. Biophys.* **1992**, *296*, 704-708.

78. Knight, W. B.; Swiderek, K. M.; Sakuma, T.; Calaycay, J.; Shively, J. E.; Lee T. D.; Covey, T. R.; Shushan, B.; Green, B. G.; Chabin, R.; Shah, S, Mumford, R.; Dickinson, T. A.; Griffin, P. R. *Biochemistry* **1993**, *32*, 2031-2035.

79. Wilmouth, R. C.; Westwood, N. J.; Anderson, K.; Brownlee, W.; Claridge, T. D. W.; Clifton, I. J.; Pritchard, G. J.; Aplin, R. T.; Schofield, C. J. *Biochemistry* **1998**, *37*, 17506-17513.

80. Yarrow, J. C.; Totsukawa, G.; Charras, G. T.; Mitchison, T. J. *Chem. Biol.* **2005**, *12*, 385-395.

81. Pearson, R. J.; Evans, K. M.; Slawin, A. M. Z.; Philp, D.; Westwood, N. J. *J. Org. Chem.* **2005**, *70*, 5055-5061.

82. Antonini, I.; Lin, T-S.; Cosby, L. A.; Dai, Y-R.; Sartorelli, A. C. *J. Med. Chem.* **1982**, *25*, 730-735.

83. Lin, A. J.; Lillis, B. J.; Sartorelli, A. C. *J. Med. Chem.* **1975**, *18*, 917-921.

84. Bugg, T. D. H. *Introduction to Enzyme and Coenzyme Chemistry*, 2nd Ed., Blackwell Publishing **2004**.

85. Stryer, L. *Biochemistry*, 4th Ed., W. H. Freeman and Company: New York, **1995**.

86. Bunnett, J. F. *Annu. Rev. Phys. Chem.* **1963**, *14*, 271-290.

87. Leichert, L. I.; Jakob, U. *PloS Biol.* **2004**, *2*, 1723-1737.

88. Pe'er, I.; Felder, C. E.; Man, O.; Silman, I.; Sussman, J. L.; et al *Proteins* **2004**, *54*, 20-40.

89. Rich, D.H. *Inhibitors of Cysteine Proteases in Proteinase Inhibitors*, Ed. Barrett, A. J.; Salvesen, G., Elsevier **1986**, Chapter 4, 153-178.

90. Shaw, E.; Green, G. D. L.; *Methods Enzymol.* **1981**, *80*, 820-826.

91. Leary, R.; Shaw, E. *Biochem. Biophys. Res. Comm.* **1977**, *79*, 926-931.

92. Hempel, J.; Nicholas, H.; Lindahl, R. *Protein Sci.* **1993**, *2*, 1890-1900.

93. Mori, M.; Niwa, T.; Hirata, R.; Furata, K.; Ishikawa, T.; Noyori, R. *J. Am. Chem. Soc.* **1997**, *119*, 2376-2385.

94. McCaldon, P.; Argos, P. *Proteins* **1988**, *4*, 99-122.

95. Klapper, M. H. *Biochem. Biophys. Res. Commun.* **1977**, *78*, 1018-1024.

96. Powers, J. C.; Asgian, J. L.; Ekici, Ö. D.; James, K. E. *Chem. Rev.* **2002**, *102*, 4639-4750.

97. Aplin, R. T.; Robinson, C. A.; Schofield, C. J.; Westwood, N. J. *J. Chem. Soc. Chem. Commun.* **1992**, 1650-1652.

98. Aplin, R. T.; Robinson, C. V.; Schofield, C. J.; Westwood, N. J. *Tetrahedron*, **1993**, *49*, 10903-10912.

99. Wilmouth, R. C.; Kassamally, S.; Westwood, N. J.; Sheppard, R. J.; Claridge, T. D. W.; Aplin, R. T.; Wright, P. A.; Pritchard, G. J.; Schofield, C. J. *Biochemistry*, **1999**, *38*, 7989-7998.

100. Landquist, J. K.; Silk, J. A. *J. Chem. Soc.* **1956**, 2052-2063.

101. Anderson, R. C.; Fleming, R. H. *Tetrahedron Lett.* **1969**, 1581-1584.

102. Ried, W.; Grabosch J. *Chem. Ber.* **1958**, 2485-2495.

103. Katritzky, A. R.; Lagowski, J. M. Chapter 4, Reactions of Substituents on Heterocyclic *N*-oxides, Blomquist, A. T. *Chemistry of the heterocyclic N-oxides*, 1st edition, Academic Press, London and New York, **1971**, 389.
104. Shields, J. E.; Bornstein, J. *Chem. Industr.* **1967**, 1404-1405.
105. Morgan, R. E.; Evans, K. M.; Catti, F.; Patterson, S.; Ward, G. E.; Westwood, N. J. *Current Drug Targets*, **2006**, *in press*.
106. Haddadin M. J.; Samaha, M. S; Hajj-Ubayd, A. B. *Heterocycles* **1992**, *33*, 541-544.
107. Moriconi, E. J.; Fritsch, A. J. *J. Org. Chem.* **1965**, *30*, 1542-1547.
108. Deady, L. W.; Desneves, J.; Ross, A. C. *Tetrahedron* **1993**, *49*, 9823-9828.
109. Barbieri, G.; Benassi, R.; Lazzeretti, P.; Schenetti, L.; Taddei, F. *Org. Mag. Res.* **1975**, *7*, 451-454.
110. Kluge, A. F.; Maddox, M. L.; Lewis, G. S. *J. Org. Chem.* **1980**, *45*, 1909-1914.
111. Kreher, R.; Use, G. *Tetrahedron Lett.* **1978**, 4671-4674.
112. King, J. F.; Tsang, G. T. Y. *J. Chem. Soc. Chem. Comm.* **1979**, 1131-1132.
113. Gottlieb, H. E.;, Kotlayar, V.; Nudelman, A. *J. Org. Chem.* **1997**, *62*, 7512-7515.
114. Engel, W.; Schieberle, P. *J. Agric. Food Chem.* **2002**, *50*, 5394-5399.
115. King, L. C.; Ostrum, G. K. *J. Org. Chem.* **1964**, *29*, 3459.
116. Okonya, J. F.; Hoffman, R. V.; Johnson, M. C. *J. Org. Chem.* **2002**, *67*, 1102-1108.
117. Hunter, C. A. *Angew. Chem. Int. Ed.* **2004**, *43*, 5310-5324.
118. Zhu, Y.; Drueckhammer, D. G. *J. Org. Chem.* **2005**, *70*, 7755-7760.
119. Raposo, C.; Wilcox, C. S. *Tetrahedron Lett.* **1999**, *40*, 1285-1288.
120. Hartman, F. C.; Wold, F. *J. Am. Chem. Soc.* **1966**, *88*, 3890-3891.
121. Navia, M. A.; Springer, J. P; Lin, T-Y.; Williams, H. R.; Firestone, R. A.; Pisano, J. M.; Doherty, J. B.; Finke, P. E.; Hoogsteen, K. *Nature* **1987**, *327*, 79-82.
122. Bode, W.; Turk, D.; Karshikov, A. *Protein Sci.* **1992**, *1*, 426-471.
123. Chen. J. K.; Lane, W.S.; Schreiber, S. L. *Chem. Biol.* **1999**, *6*, 221-235.
124. Shpan'ko, I. V.; Korostylev, A. P.; Rusu, L. N. *J. Org. Chem. USSR (Transl)* **1984**, *20*, 1881-1888.
125. Smith, D. M.; McFarlane, M. D.; Moody, D. J. *J. Chem. Soc. Perkin Trans. I* **1988**, 691-696 and therein.
126. Glushkov, R. G.; Vozyakova, T. I.; Adamskaya, E. V.; Aleinikova, S.A.; Radkevich, T. P.; Shepilova, L. D.; Padeiskaya, E. N.; Gus'kova, T.A. *Pharmaceutical Chemistry Journal (Engl. Trans)*, **1994**, *28*, 17-20.

127. Bonnett, R,; North, S. A *Tetrahedron* **1983**, *39*, 1401-1405.

128. Kreher, R. P.; Seubert, J.; Schmitt, D.; Use, G.; Kohl, N.; Muleta, T. *Chem. Ber.* **1990**, *123*, 381-390.

129. Haddadin, M. J.; Chelhot, N. C.; Pieridou, M. *J. Org. Chem.* **1974**, *39*, 3278-3281.

130. Karplus, M. *J. Am. Chem. Soc.* **1963**, *85*, 2870-2871.

131. Cooley, J. H.; Williams R. V. *J. Chem. Educ.* **1997**, *74*, 582-585.

132. Bunting, J. W.; Stefanidis, D. J. Am. Chem. Soc. 1988, 110, 4008-4017.

133. Rangarajan, M.; Kim, J. S.; Sim, S-P.; Liu, A.; Liu, L. F.; La Voie, E. J. *Bioorg. Med. Chem.* **2000**, *8*, 2591-2600.

134. Krajewski, J. J.; Kotz, P. J.; Traxler, J. T.; Ristich,S. S.; Huffman, C. W. *J. Agric. Food Chem.* **1971**, *19*, 298-301.

135. Cusack, K. P.; Arnold, L. D.; Barberis, C. E.; Chen, Haipeng, Ericsson, A. M.; Gaza-Bulseco, G.S; Gordon, T. D.; Grinnell, C. M.; Harsch, A.; Pellegrini, M.; Tarcsa, E. *Bioorg. Med. Chem. Lett.* **2004**, *14*, 5503-5507.

136. Spencer, S. R.; Xue, L. A.; Klenz, E. M.; Talalay, P. *Biochem. J.* **1991**, *273*, 711-717.

137. Tominaga, M.; Konishi, K.; Aida, T. *J. Am. Chem. Soc.* **1999**, *121*, 7704-7705.

138. Ashton, P. R.; Calcagno, P.; Spencer, N.; Harris, K. D. M.; Philp, D. *Org. Lett.* **2000**, *2*, 1365-1368.

139. Kirkpatrick, D. S.; Denison, C.; Gygi, S. P. *Nature Cell Biol.* **2005**, *7*, 750-757.

140. Openshaw, M. E.; Connelly, J. B. *Am. Soc. Mass Spectrom. Conference* **2005**, Technical Seminar Poster.

141. Wysocki, V. H.; Tsprailis, G.; Smith, L. L.; Breci, L. A. *J. Mass Spectrom.* **2000**, *35*, 1399-1406.

142. Kissinger, J. C.; Gajria, B.; Li, L.; Paulsen, I. T.; Roos, D. S. *Nucleic Acids Res.* **2003**, *31*, 234-236.

143. Jahng, W. J.; David, C.; Nesnas, N.; Nakanishi, K.; Rando, R. R. *Biochemistry* **2003**, *42*, 6159-6168.

144. Hall, B. J.; Sutherland, J. D. *Tetrahedron Lett.* **1998**, *39*, 6593-6596.

145. Hoppen, S.; Bäurle, S.; Koert, U. *Chem. Eur. J.* **2000**, *6*, 2382-2396.

146. Lesney, M. S. *Modern Drug Discovery* **2002**, 5(12), 27-29.

147. Speers, A.E.; Adam, G. C.; Cravatt, B. F. *J. Am. Chem. Soc.* **2003**, *125*, 4686-4687.

148. Niculescu-Duvaz, D.; Niculescu-Duvaz, I.; Freidlos, F.; Martin, J.; Lehouritis, P.; Marais, R.; Springer, C. J. *J. Med. Chem.* **2003**, *46*, 1690-1705 and references therein.

149. Qi, K.; Ma, Q.; Remsen, E.; Clark, C. G., Jr.; Wooley, K. *J. Am. Chem. Soc.* **2004**, *126*, 6599-6607.

150. Dvoryantseva, G. G.; Tetenchuk, K. P.; Pol'shakov, V. I.; Elina, A. S. *Pharm. Chem. J. (Engl. Transl.)* **1986**, *20*, 227-235.

151. Kessler, B. M.; Tortorella, D.; Altun, M.; Kisselev, A. F.; Fiebinger, E.; Hekking, B. G.; Ploegh, H. L.; Overkleeft, H. S. *Chem. Biol.* **2001**, *8*, 913-929.

152. Stauffer, S.R.; Sun, J.; Katzenellenbogen, B. S.; Katzenellenbogen, J. A. *Bioorg. Med. Chem.* **2000**, *8*, 1293-1316.

153. Pinney, K. G.; Katzenellenbogen, J. A. *J. Org. Chem.* **1991**, *56*, 3125-3133.

154. Greenbaum, D.; Baruch, A.; Hayrapetian, L.; Darula, Z.; Burlingame, A.; Medzihradszky, K. F.; Bogyo, M. *Mol. Cell. Proteomics* **2002**, *1*, 60-68.

155. Creighton, T. E. *Protein Structure a Practical Approach*, Oxford University Press **1989**

156. Schmidt, M. W.; Baldridge, K. K.; Boatz, J. A.; Elbert, S. T.; Gordon, M. S.; Jensen, J. H.; Koseki, S.; Matsunaga, N.; Nguyen, K. A.; Su, S.; Windus, T. L.; Dupuis, M.; Montgomery Jr, J. A. *J. Comput. Chem.* **1993**, *14*, 1347-1363.

157. Tomasi, J.; Persico, *M. Chem. Rev.* **1994**, *94*, 2027-2094.

158. Li, H.; Jensen, J. H. *J. Comput. Chem. 2004, 25,*1449-1462.

159. Hahn, W. E.; Lesiak, J. Z. *Soc. Sci. Lodz., Acta Chim.* **1972**, *17*, 201-205.

160. Simon, H.; Heubach, G.; Bitterlich, W.; Gleinig, H. *Chem. Ber.* **1965**, *98*, 3692-3702.

161. Elina, A. S.; Titkoua, R. M.; Tsyrulnikova, L.G.; Filipenko, T. Ya *Pharm. Chem. J. Engl. Transl.* **1976**, *10*, 38-41.

162. Cue, B. W. Jr.; Czuba, L. J.; Dirlam, J. P. *J. Org. Chem.* **1978**, *43*, 4125-4127.

163. Rangarajan, M.; Kim, J. S.; Sim, S-P.; Liu, A.; Liu, L. F.; La Voie, E. J. *Bioorg. Med. Chem.* **2000**, *8*, 2591-2600.

164. Hűbner, H. *Justus, Liebigs Ann. Chem.* **1881**, *209*, 328-396.

165. Musatova, I. S.; Elina, A. S.; Solov'eva, N. P.; Polukhina, L. M.; Moskalenko, N. Y.; Pershin, G. N. *Pharm. Chem. J. Engl. Transl.* **1983**, *17*, 779-784.

PART II

CHAPTER 1

PART II
OZONOLYTIC CLEAVAGE OF THE BUTENYL FUNCTIONAL GROUP

1.0 INTRODUCTION

The previous chapter described preliminary results towards the development of a cleavable linker for application in affinity chromatography studies (Chapter 4, Section 2.2). The chemistry at the heart of the cleavable linker system is also relevant to other applications. Part II of this thesis is concerned with the extension of the existing chemical methods required. This includes an expansion of protecting group methodology and provides a novel solid-phase linker system.

2.0 A PROTECTING GROUP FOR PHENOLS

2.1 PROTECTING GROUP METHODOLOGY

Protecting groups are frequently necessary in synthetic organic chemistry to allow selective transformation at one reactive site, in the presence of other such groups or other reactive functionality in a molecule. Undesired activation or reaction, leading to unwanted side reactions and by-products, is prevented by temporarily blocking another reactive site(s) during a chemical reaction. In selecting a protecting group, the chemist must take into account many factors, such as reactants, reaction conditions and functionality. A good protecting group must react selectively in high yield and be stable to the subsequent reaction conditions. It should then be removable in high yield, without attacking the regenerated functionality. The reagents involved should ideally be readily available and non-toxic.

In compound library design, or natural product synthesis it often remains necessary to use protecting group chemistry, when ideally it would be avoided to reduce the number of synthetic steps. This is emphasised more so for a targeted compound collection in which the core product is defined. So, in practice, expanding protecting group chemistry that is compatible with both solution and solid phase approaches is of undeniable importance.

2.2 PHENOL PROTECTING GROUPS

A plethora of protecting groups are available for phenol protection, of which ethers are the most widely used.[1] The use of allylic protecting groups such as the allyl ether are typically employed and can be cleaved under Pd-mediated conditions. Protection as the *tert*-butyl ether is also common and is typically cleaved using acid. This class also includes the methoxymethyl ether (MOM), the methoxyethoxymethyl ether (MEM), and the ethoxyethyl ether (EE) to name but a few. Two other standard classes of protecting groups applicable to phenols are the benzyl and to a lesser extent, silyl ethers.[1,2] The benzyl (Bn) protecting group, and its most common relation, the *para*-methoxybenzyl (PMB) group have been in use for many years but this class also includes for example, the more recent *para*-SEM (2-triethylsilyl)ethoxymethoxybenzyl group. Esters are also important protective groups for phenols, such as an acetate (Ac) or benzoate (Bz) group for which cleavage can occur under either acid or basic conditions. Listed above are only select examples of each class. For an in-depth overview several texts are available to which the reader is referred.[1,3-5]

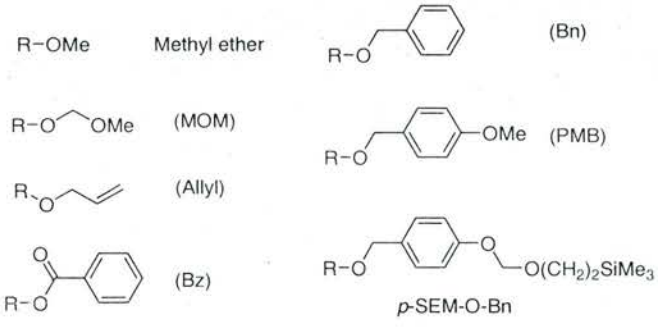

Figure 1.1. Selected examples of phenol protecting groups.

2.3 AN ORTHOGONAL PROTECTING GROUP FOR SOLUTION AND SOLID PHASE SYNTHESIS

The protecting groups discussed above typically perform well and can be employed in solid-phase synthesis. One example of this is the use of the allyl group in the galanthamine-based diversity-oriented synthesis (DOS)[6] library prepared by Shair and co-workers (Scheme 1.1).[7] Here, the use of a silyl based resin ruled out the use of acid labile phenol protecting groups (such as *tert*-butyl) and the conditions used to cleave a methyl

group are incompatible with the resin. However, a better application of the library design would have taken advantage of the aromatic bromine substituent in C–C bond forming reactions as a diversity-incorporating handle. This was not possible due to the use of the allyl groups that are deprotected under Pd-mediated conditions.

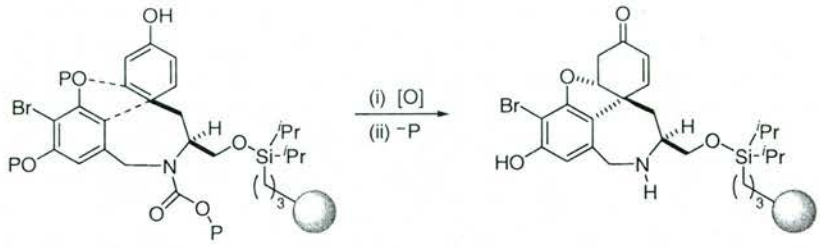

Scheme 1.1. DOS of a library of Galanthamine-like small molecules. Diversity-generating reactions did not include a Pd-catalysed C–C bond forming strategy since the design involved a Pd-mediated deprotection step. P = allyl.

Orthogonality of the protecting group(s) with the chemistry within a library design is difficult and therefore, another protecting group amenable to solid phase synthesis would be useful. The methodology presented within this chapter is based on a protecting group designed by Barrett, currently only applied to carboxylic acids but has the scope to be extended to other functional groups and to be orthogonal to other protecting groups. This is particularly useful in DOS libraries where a silyl linkage is employed.

2.4 BARRETT'S METHOD

We identified Barrett's butenyl protecting group for carboxylic acids as a potentially excellent candidate for phenol protection.[8] Barrett developed this protecting group due to the requirement in the total synthesis of Nikkomycin B for an ester protecting group that could be converted to the corresponding acid under non-aqueous conditions.[9] Barrett *et al.* successfully protected a range of carboxylic acids as their corresponding 3-butenyl esters (**203**).[8] Deprotection was achieved via ozonolysis and subsequent β–elimination of the resultant 3-acyloxypropanal (**204**) derivative regenerating the initial carboxylic acid (**205**, Scheme 1.2). Indirect precedent for Barrett's protection strategy was in the use of 2-methylthioethyl esters, deprotection of which had been achieved by S-oxidation to the corresponding sulfone and base-induced β–elimination.[10] Since protons

to sulfones are less acidic than those α to aldehydes it was reasonable to expect that the aldehyde intermediate could be removed by an $E1_{CB}$ mechanism.

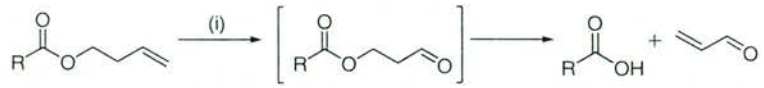

(203) **(204)** **(205)** **(206)**

Scheme 1.2. Barrett's use of 3-butenyl esters as convenient protecting groups for carboxylic acids.[8] *Reagents and conditions:* (i) O_3, DCM/MeOH 1/1 v/v, –78 °C; $(CH_3)_2S$, –78 °C to RT; Et_3N, RT; 79-99%.

Barrett's butenyl protecting group has subsequently been utilised in the masking of the C-4 carboxylic acid functionality in the synthesis of monocyclic azetidin-2-one derivatives (Scheme 1.3).[11] In accord with the literature precedent the free acid (**208**) was obtained as the major component following deprotection of **207**. It was also noted by the author that the products corresponding to methanolysis (**209**) and hydrolysis (**210**) of the *β*–lactam were also observed. Repetition of the deprotection reaction in the absence of methanol avoided the formation of **209**.

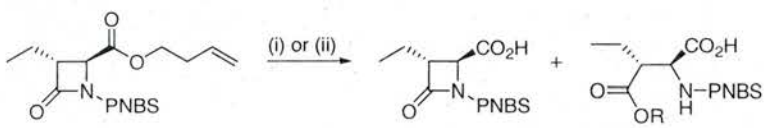

(207) **(208)** **(209)** $R = CH_3$

(210) R = H

Scheme 1.3. Ozonolytic deprotection of the butenyl group masking the C-4 carboxylic acid. *Reagents and conditions:* (i) O_3, DCM/MeOH 1/1 v/v, –78 °C; $(CH_3)_2S$, –78 °C to RT; Et_3N, RT. (ii) O_3, DCM, –78 °C; $(CH_3)_2S$, –78 °C to RT; Et_3N, RT.

2.5 OZONOLYSIS – A LEVEL OF SELECTIVITY CAN BE ACHIEVED

Ozonolysis is a method for oxidative cleavage of carbon-carbon double bonds using ozone. Ozone is an electrophilic reagent and so reacts preferentially with electron-rich alkenes and is (relatively) specific for carbon-carbon double bonds. Ozonolysis can be performed in the presence of other functional groups (e.g. alcohols, aromatic rings) without fear of their oxidation. The oxidation of an alkyl-substituted alkene in the presence of an *α,β*-unsaturated carbonyl system demonstrates that selectivity is achievable (Scheme 1.4).[12] Selective oxidation of an exocyclic double bond rather than an endocyclic double bond via ozonolysis can also be enhanced by the presence of pyridine.[13]

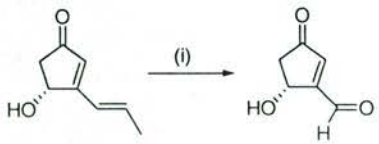

(211) **(212)**

Scheme 1.4. An example of selective ozonolysis.[12] *Reagents and conditions:* (i) O_3, EtOH, Solvent Red 19, –78 °C; $(CH_3)_2S$, –78 °C to RT; 90%.

The mechanism for ozonolysis (Scheme 1.5)[14,15] is driven by the instability of the ozonides formed. The primary ozonide (1,2,3-trioxolane) is unstable and collapses to the secondary ozonide. This is decomposed *in situ*, typically by the addition of a reducing agent, such as dimethylsulfide ($(CH_3)_2S$)[16] or triphenylphoshine (PPh_3) to give the two corresponding carbonyl compounds. Alternatively, lithium aluminium hydride or sodium borohydride reduce the ozonide to give alcohols whereas hydrogen peroxide oxidises the ozonide to form carboxylic acids.

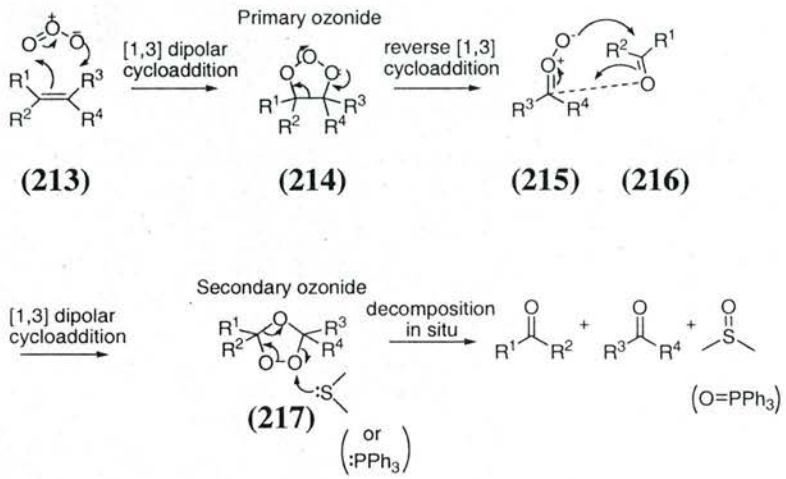

(213) **(214)** **(215)** **(216)** **(217)**

Scheme 1.5. Mechanism of ozonolytic cleavage of a C–C double bond.[14] The primary ozonide is unstable and cleaves to an aldehyde (**216**) and an intermediate (**215**). A second [1,3] dipolar cycloaddition reaction of **215** and **216** occurs to form the secondary ozonide **217**. *In situ* reduction of **217** using DMS or PPh_3 affords the product aldehydes.

2.6 Extension of Barrett's Butenyl Protecting Group

The aim of this section was to develop the butenyl protecting group introduced by Barrett *et al.* In brief, by extending the scope of Barrett's methodology we aimed to add a versatile protecting group to solution and solid phase chemistry, that is of particular relevance due to its mild deprotection protocol.

2.7 PHENOL PROTECTION

A series of phenol 3-butenyl ethers were efficiently prepared by reaction of the appropriate phenol with 3-buten-1-ol under conventional Mitsunobu conditions using DEAD in combination with triphenylphosphine (Table 1.1).[17] The four derivatives (**222-225**) were synthesised in parallel and each allowed to react for 24 hours. In the case of entries 3 and 4 the yields were lower than expected and residual phenol starting material was observed in both cases by TLC analysis. The synthesis of **224** (R = 4-OMe) was repeated and achieved in 99% yield under similar experimental conditions but over a longer time.

An alternate set of conditions has also been tested using 4-bromobut-1-ene (**226**) and potassium carbonate in DMF, also resulting in moderate to high yields. Under alkylation conditions in DMF, comparative product yields were observed for **223** (R = 4-NO_2) and **225** (R = 4-CHO) however this method resulted in a lower yield in the case of **222** (R = 3-NO_2).

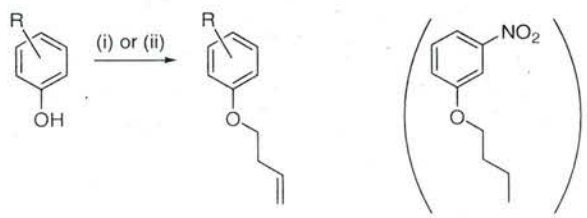

(227)

Scheme 1.6. Phenol protection. *Reagents and conditions:* (i) 3-buten-1-ol (1.2 equiv.), PPh_3 1.2 equiv.), DEAD (1.2 equiv.), toluene, 80 °C, 24 h; or (ii) 4-bromobut-1-ene (2 – 4 equiv.), DMF, RT, 48-60 h. Where R = 3-NO_2, 4-NO_2, 4-OMe, 4-CHO.

Table 1.1. Phenol protection under Mitsunobu [a] or Alkylation [a/d] conditions.

Entry	R	Product	% yield [b]	% yield [c]
1	3-NO_2 **(218)**	**222**	90	52 [d]
2	4-NO_2 **(219)**	**223**	82	87 [d]
3	4-OMe **(220)**	**224**	67 (99)[e]	ND
4	4-CHO **(221)**	**225**	51	67 [a]

[a] All reactions at 0.2 M in SM. [b] Isolated yields from Mitsunobu conditions. [c] Isolated yields from Alkylation conditions. [d] Reactions at 0.14 M in SM. [e]Yield in parentheses for the reaction performed at 0.11 M in **220** over 36 h. ND = not done.

Interestingly, a by-product was isolated from preliminary deprotection reactions using **222** and **223** in the range 4–9%. The by-product was assigned as the saturated counterpart (e.g. **227**) based on NMR data, consistent with the literature.[18] The use of commercially available 4-bromobut-1-ene (**226**) was attributed to be the source of the saturated impurity and so **226** was freshly prepared in accordance with the literature.[19] When 4-bromobut-1-ene (**226**) prepared by this route was used, **227** was not observed.

2.8 PHENOL DEPROTECTION

The four protected phenols were then deprotected using an ozonolysis protocol. The results are presented in Table 1.2.

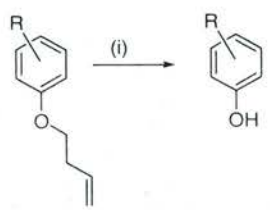

Scheme 1.7. Phenol deprotection. *Reagents and conditions:* (i) O_3, DCM, –78 °C; $(CH_3)_2S$ (2 equiv), 2 h, –78 °C to RT; Et_3N (2 equiv), RT, 3 h. Where R = 3-NO_2, 4-NO_2, 4-OMe, 4-CHO.

Table 1.2. Phenol deprotection [a].

Entry	R	Product	% yield[b]
1	3-NO_2 **(222)**	**218**	92 (90)[c]
2	4-NO_2 **(223)**	**219**	87
3	4-OMe **(224)**	**220**	99
4	4-CHO **(225)**	**221**	66

[a] All reactions at 0.2 M in SM. [b] Isolated yields. [c] Reaction at 0.25 M in SM under Barrett conditions ((i) O_3, DCM:MeOH 9:1 v/v, –78 °C; $(CH_3)_2S$, –78 °C to RT; Et_3N, RT; 10% aqueous HCl workup).[8]

Deprotection involved bubbling ozone through a solution of the butenyl-protected phenol (*c.* 200 mg in 10 mL of DCM) at –78 °C, until a blue end-point. Dimethylsulfide was employed as the reductant and the reaction mixture was warmed to room temperature and stirred for 2 h. In a one-pot protocol, treatment with triethylamine then regenerated the phenol starting material. The cleavage resulted in the formation of the volatile by-product, acrolein, which was readily removed *in vacuo*. The crude reaction mixtures were applied to a silica column, to remove residual triethylamine. On one occasion the reaction mixture

was subjected to an acidic workup without a detrimental effect on the yield (entry 1, Table 1.2).

Analogous deprotection conditions were used for **222–225**, affording the respective phenols **218–221** in high yields (87-99%, for entries 1-3), whereas a moderate yield was obtained in the deprotection of **225** (entry 4). The reduced yield is proposed to be due to the sensitivity of the aldehyde functionality. In this case a second aldehyde-containing product (**228**) was observed in an approximate ratio of 4:1 of **221**:**228** as judged by analysis of the ^{1}H NMR spectrum of the crude reaction mixture. Repeating the reaction allowed the isolation of **228** and a second minor by-product **229**. The mass spectrum of **228** showed a single peak *m/z* 137 (ES) corresponding to $[M - H]^-$ and **228** gave rise to a band in the IR spectrum at 1676 cm^{-1} assigned to the acid C=O. Mass spectrometric analysis of **229** showed a peak corresponding to the parent molecular ion at *m/z* 193 (ES) and the corresponding IR spectrum showed bands at 1723 and 1644 cm^{-1}, which are assigned to the C=O of the aldehyde and the acid groups respectively. **228** is the result of oxidation of the aldehyde functionality whereas **229** is believed to result from breakdown of the secondary ozonide by dimethylsulfide via a competing acid-base process ($E1_{CB}$-type mechanism) forming the carboxylic acid product as a minor component of the reaction mixture (for further discussion on the mechanism see Section 4.2). [20]

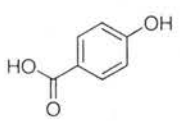

(228)

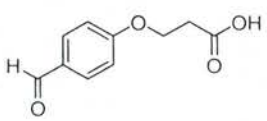

(229)

Figure 1.2. Structures assigned to the by-products obtained from deprotection of **225**. The formation of **228** accounts for the lower yield obtained in the ozonolytic deprotection of **225**.

2.9 THE USE OF TRIETHYLAMINE IN THE DEPROTECTION REACTION

Monitoring of product formation in the deprotection reaction by TLC proved difficult. The role of the base, triethylamine, was called into question because there was a possibility that the intermediate aldehyde was unstable and decomposed to the phenol product under either acidic work-up conditions or during chromatography. In order to test this, the deprotection reaction was repeated with **223**. After treatment with dimethylsulfide the reaction mixture was warmed to room temperature and split equally into four portions.

Each portion was subjected to a different work-up procedure as stated in Table 1.3 (reaction conditions: *a-d*). Based on TLC and ^{1}H NMR analyses, the phenol product was only observed under the basic conditions (entry 4, Table 1.3).

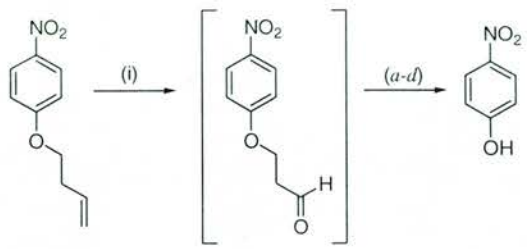

(223) **(230)** **(219)**

Scheme 1.8. The deprotection reaction of **223** was investigated further to consider the role of triethylamine.

Table 1.3. Deprotection conditions and observed product.

Entry	Reaction Conditions	Phenol 219	Aldehyde 230
1	*a*	×	✓
2	*b*	×	✓
3	*c*	×	✓
4	*d*	✓	×

Reagents and conditions: (i) O_3, DCM, –78 °C; $(CH_3)_2S$ (2 equiv.), –78 °C to RT; (*a*) Removal of solvent; (*b*) Addition of aqueous HCl and extraction; (*c*) Stirred with silica for 10 mins.; (*d*) Addition of NEt_3, 3 h, RT.

However, upon standing at room temperature it was observed that the intermediate aldehyde (**230**) decomposed to give the phenol product (**219**) and after 2–4 weeks **219** was observed as the only product.

It is known that decomposition of ozonides can occur using triethylamine.[20,21] Therefore, in theory, it may be possible to carry out the deprotection procedure using only triethylamine however, this was not experimentally investigated. No triethylamine *N*-oxide was detected in the decomposition reactions to suggest that triethylamine was not carrying out this role in the deprotection procedure using dimethylsulfide.

In summary, the extension of Barrett's butenyl protecting group strategy to the protection of phenols was successful, as expected. Electron-rich and electron-deficient aromatic phenols are tolerated and aldehyde functional groups, known to be sensitive in multi-step synthesis, are relatively stable under the mild deprotection conditions. The

addition of triethylamine to the reaction, following ozonolysis, was an essential step in the protocol, however, an acidic work-up could be omitted prior to purification without any significant reduction in yield.

3.0 APPLICATION OF PHENOL PROTECTION BY THE BUTENYL PROTECTING GROUP IN THE SYNTHESIS OF (*S*)-(–)-BLEBBISTATIN (2) ANALOGUES

To illustrate further the utility of the butenyl protecting group it has been applied in the synthesis of a phenol containing analogue of the small molecule, (*S*)-(–)-blebbistatin (**2**). This will be discussed in the following section.

3.1 THE SMALL MOLECULE TOOL (*S*)-(–)-BLEBBISTATIN (2)

The small molecule (*S*)-(–)-blebbistatin (**2**) is a relatively specific reversible inhibitor of NMMII (Chapter 1). Since its initial publication in 2003,[22] **2** has been the subject of 122 publications (as of the 10th March). For a recent review the reader is referred to reference.[23]

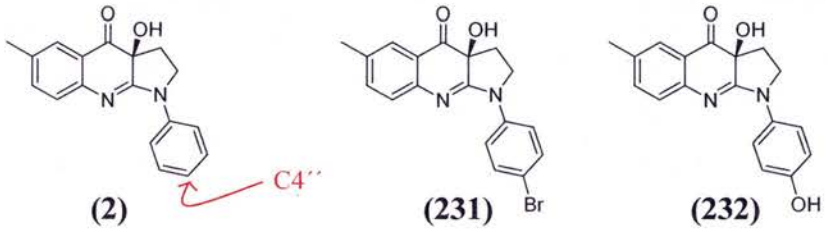

Figure 1.3. The small molecule tool (*S*)-(–)-blebbistatin (**2**) and the C-4'' bromo (**231**) and hydroxy (**232**) substituted derivatives.

A recent publication by the Rayment group of the crystal structure of (*S*)-(–)-blebbistatin (**2**) bound to the MgADP-vanadate complex of *Dictyostelium discoideum* myosin II clearly illustrates the structural basis for inhibition and specificity towards NMMII (Figure 1.4).[24]

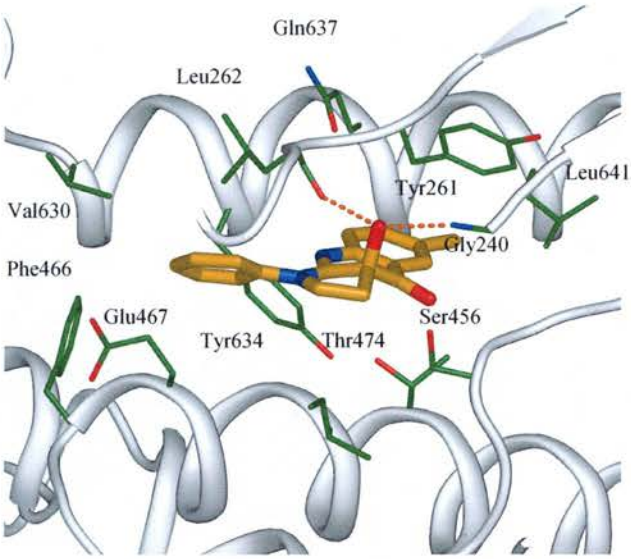

Figure 1.4. (*S*)-(–)-Blebbistatin-binding site in myosin II. Selected amino acids interacting with blebbistatin (shown in green stick representation) and hydrogen bonds between the OH group of (*S*)-(–)-blebbistatin (**2**) and the amino acids Leu262 and Gly240 (shown as red broken lines). Image reproduced from J. S. Allingham *et al.*, *Nat. Struct. Mol. Biol.* **2005**, *12*, 378-379.[24]

The crystallographic studies show that whilst **2** interacts with several key amino acids there is space associated with the *N*-phenyl ring, especially at the C4′′ position. It was envisaged that introducing diversity at C4′′ would pick up additional interactions with Glu467 or Val630 for example and may lead to the discovery of derivatives with improved biological activity.

3.2 IDENTIFICATION OF THE NEED FOR A PHENOL PROTECTING GROUP

In order to incorporate a handle with which to introduce diversity, a functional group at C4′′ was needed. Previous efforts in the Westwood laboratory have focussed on a C4′′ bromine derivative (**231**) attempting to exploit palladium catalysed carbon-carbon bond forming procedures. Interestingly, unpublished results from the Westwood, Sellers and Rayment groups have shown that incorporation of a bromine atom at this position leads to an increase in potency. In an alternative strategy, a free phenol containing derivative at C4′′ would be equally attractive for functionalisation (e.g. in C–O bond forming protocols). In contrast to the bromo-analogue (**231**), incorporating a hydroxyl group at C4′′ requires the use of a phenol protecting group for two reasons; Firstly, the proposed reterosynthetic route to **232** (Scheme 1.9) includes the use of LiHMDS, a strong base which would be expected to deprotonate the acidic phenolic proton. Secondly, the solubility of **232** in organic solvents, such as DCM or THF, would be expected to be lower than its protected counterpart (**240**, for structure see Scheme 1.9).

The application of the butenyl protecting group to a phenol functionality at C4'' was envisaged to provide a mild deprotection method that would allow diversity to be easily introduced at this position.

3.3 SYNTHESIS OF A BUTENYL-CONTAINING DERIVATIVE OF (*S*)-(–)-BLEBBISTATIN (240)

The first step in the synthesis was the protection of the phenol functionality in commercially available 4-iodophenol (**233**). This was achieved by the conventional Mitsunobu reaction[25] using triphenylphosphine, diethyl azodicarboxylate (DEAD), and 3-buten-1-ol with heating in toluene. Mass spectrometric analysis (EI) confirmed the mass of the product **234** to be 274 $[M]^{+\bullet}$ and also showed a fragmentation peak at *m/z* 220 corresponding to loss of the butenyl chain.

Preparation of the required pyrolidinone precursor (**235**) was accomplished using Buchwald coupling methodology.[26] The copper catalysed aryl amidation reaction with *N,N'*-dimethylethylenediamine in the presence of K_3PO_4, proceeded in a high yield of 88% to give **235**.

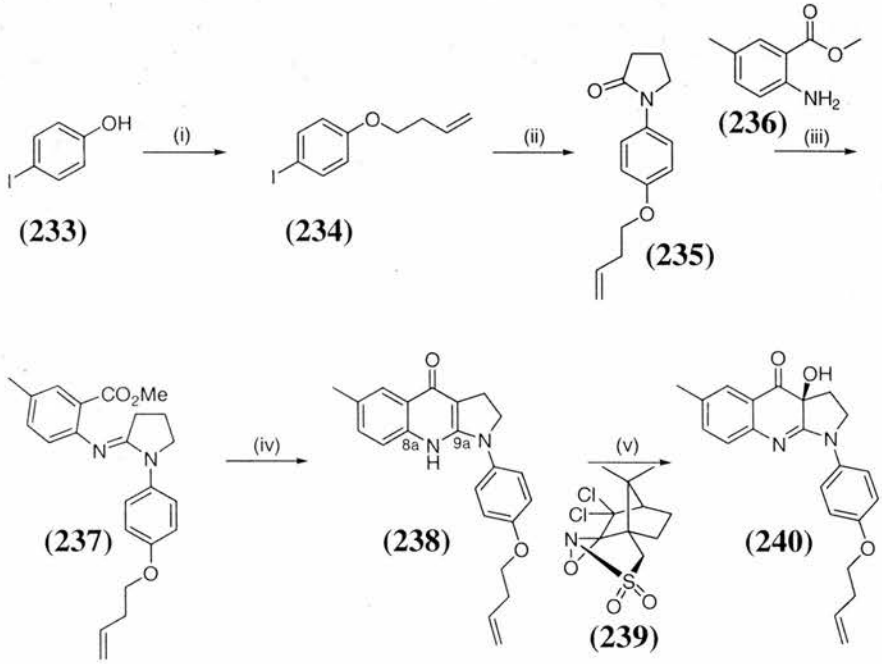

Scheme 1.9. Preparation of the butenyl-protected phenol- derivative of (*S*)-(–) blebbistatin (**240**). *Reagents and conditions:* (i) 3-buten-1-ol (1.3 equiv.), PPh_3 (1.3 equiv.), DEAD (1.6 equiv.), toluene, 80 °C, 24 h, 90%; (ii) 2-pyrrolidinone (1.8 equiv.), K_3PO_4 (2.0 equiv.), *N,N'*-dimethylethylenediamine (0.2 equiv.), CuI (cat.), reflux, 16 h; (iii) a) $POCl_3$ (0.9 equiv.), DCM, 25 °C, 3 h; b) methyl 5-methylanthranilate (**236**) (0.9 equiv.), reflux, 68 h, 20%; iv) LiHMDS (3.0 equiv), -78 °C to 0 °C, 3 h, 57%; v) a) LiHMDS (1.2 equiv), -78 °C to 0 °C, 30 min., THF; b) (–)-Davis oxaziridine (2.4 equiv.), –10 °C, THF, 16 h, 73%). LiHMDS = lithium bis(trimethylsilyl)amide.

The remainder of the synthesis was carried out using protocols analogous to those already established in the Westwood laboratory.[27,28] This route has proven to be an efficient method of preparing highly optically enriched **2** (>99% *ee*) and relies on the use of Davis oxaziridine methodology.[29-31]

The reaction of the butenyl pyrrolidinone **235** with the anthranilate **236** in the presence of phosphorous oxychloride afforded the desired amidine **237** in adequate yield (20%). Inclusion of the butenyl chain renders the amidine significantly less polar than other blebbistatin derivatives previously prepared in the Westwood group.[27] This has the disadvantage that **237** is more difficult to separate from excess reagent (**236**) that is required to drive the amidine forming reaction to a reasonable yield. The structure of the amidine product **237** was confirmed by ^{1}H NMR analysis and a single peak at *m/z* 379 in the mass spectrum, corresponding to $[M + H]^+$ of **237**. Bands in the IR spectrum of **237** were observed at 1720, 1663, and 1609 cm^{-1} and have been assigned to the C=O, C=N, and C=C respectively.

Subsequent cyclisation of the amidine **237** to the quinolone **238** was achieved using LiHMDS at –78 ° to 0 °C. Purification of the crude material was performed by flash column chromatography eluting with neat ethyl acetate due to the polarity of **238**. ^{1}H NMR analysis was performed in d_8-THF at 500 MHz to achieve resolution of the aromatic signals corresponding to the aromatic protons. ^{13}C NMR analysis was possible using 2D HSQC and long range HMBC due to the long relaxation times associated with the quaternary carbons C-8a and C-9a in **238**.

Stereoselective insertion of the α–hydroxy carbonyl functionality took advantage of the established Davis oxaziridine asymmetric hydroxylation. Treatment of the quinolone **238** with LiHMDS at –78 °C, under nitrogen, generated the lithium enolate of **238**. In a one-pot procedure the enolate was reacted with commercially available (–)-(8,8-dichlorocamphorylsulfonyl)-oxaziridine (**239**) (2.4 equiv.) and the reaction maintained at –10 °C for 16 hours. This temperature has previously been shown to give optimal asymmetric induction.[28] Following purification by acid-base extraction, **240** was isolated as a vivid yellow crystalline solid in a 73% yield: The intense yellow colour is a characteristic trait of blebbistatin analogues. Analysis of the crude product from the hydroxylation reaction by chiral HPLC showed two peaks corresponding to the two

enantiomers. This analysis demonstrated that a high enantiomeric excess (91%) with the enantiomer with t_R = 18.48 mins. dominating (Figure 1.5). IR analysis showed the presence of a broad OH stretch at 3423 cm^{-1} and the mass spectrum confirmed the formation of the desired product with a single peak at *m/z* 363 (ES) consistent with $[M + H]^+$ for **240**. A single recrystallisation of the crude reaction mixture from acetonitrile produced yellow needles of > 99% *ee* as determined by chiral HPLC analysis (Figure 1.5). The crystalline material of **240** gave an $[\alpha]_D^{24}$ = – 622.5 (*c* = 0.02, $CHCl_3$) compared to $[\alpha]_D^{24}$ – 550 (*c* = 0.02, $CHCl_3$) for the crude material. The *ee* based on $[\alpha]_D$ was therefore calculated to be 88%, in line with that obtained by chiral HPLC analysis. Unfortunately the crystals obtained were not of sufficient quality for X-ray analysis.

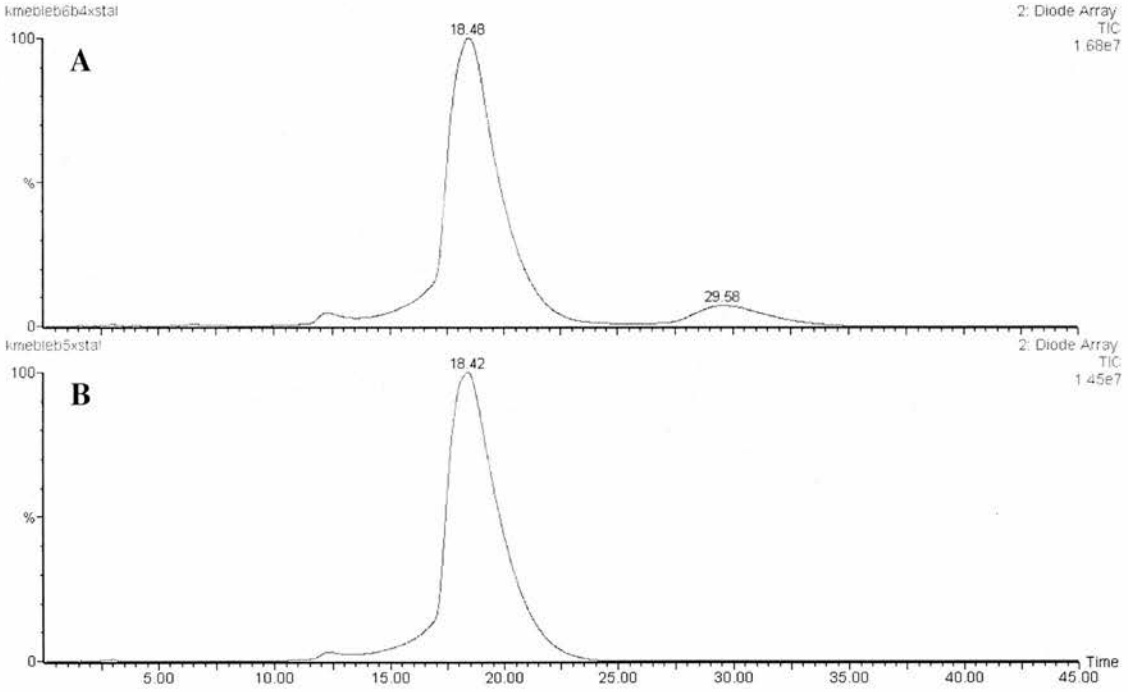

Figure 1.5. Chiral HPLC traces used to determine the *ee* of crude material of **240**. **A** Chromatogram of the crude mixture of **240**; first enantiomer t_R = 18.48 mins., λ_{max} = 249 nm; ESMS (+ve) $[M + H]^+$ = 363; second enantiomer t_R = 29.58 mins., λ_{max} = 249 nm; ESMS (+ve) $[M + H]^+$ = 363; *ee* 91% **B** recrystallised **240**, enantiomer t_R = 18.42 mins., λ_{max} = 249 nm; ESMS (+ve) $[M + H]^+$ = 363; *ee* > 99 %.

3.4 DEPROTECTION OF THE BUTENYL-CONTAINING DERIVATIVE OF (*S*)-(–)-BLEBBISTATIN (240)

Ozonolysis of **240** was carried out in DCM at –78 °C as described previously (Section 2.8). TLC analysis after treatment with ozone showed complete disapperance of starting material (**240**). Dimethylsulfide was the reducing agent of choice owing to the ease of removal of itself and the byproduct DMSO. *β*–Elimination of the assumed aldehyde intermediate using triethylamine afforded the desired phenol (**232**) in a moderate yield of 63% (Scheme 1.10). No precedent for racemisation is previously known for blebbistatin derivatives, therefore, loss of stereochemical integrity was not expected to occur in the deprotection step. A comparison of the optical activity measurements from samples of **232** synthesised from uncrystallised **240** with that obtained from the deprotection reaction showed values of $[\alpha]_D^{20}$ of – 303 and – 430 respectively (c = 0.02, CH_3OH). The difference in the absolute values indicates that the product from the deprotection reaction is of higher purity than the material prepared from uncrystallised material, suggesting that significant racemisation did not occur.

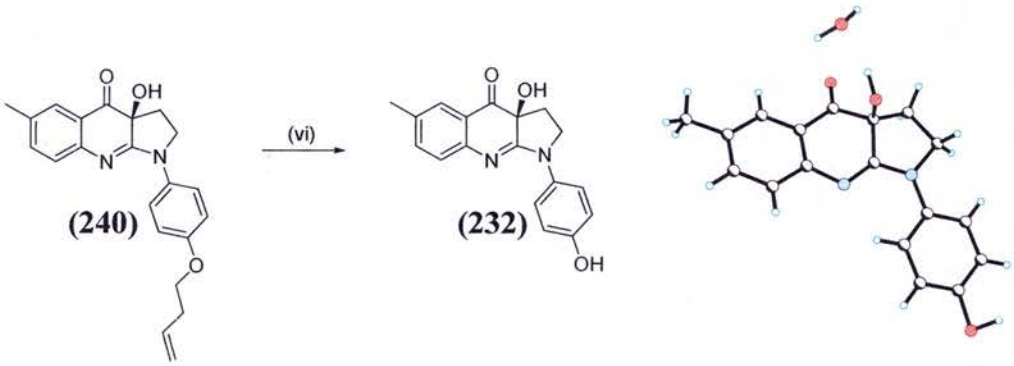

Scheme 1.10. Deprotection of butenyl protecting group applied to (*S*)-(–)-blebbistatin (**2**). *Reagents and conditions:* O_3, DCM, -78 °C; $(CH_3)_2S$ (2 equiv), 2 h, -78 °C to RT; Et_3N (2 equiv), RT, 3 h. Insert: X-ray crystal structure of **232** (orange crystals), confirmed the atom connectivity but could not confirm absolute configuration.

X-ray crystallographic analysis of a sample of **232**, collected as orange crystals from ethyl acetate/petroleum ether, confirmed the atom connectivity is as shown in Scheme 1.10. However, the single crystal was not of significant quality to determine the absolute configuration.

In the solid state, **232** is arranged in π-π stacked layers (Figure 1.6). Each layer contains a repeating unit of four stacks involved in hydrogen-bonding to two neighbouring

stacks of water molcules. An intricate network of intermolecular hydrogen-bonding occurs within the repeating unit involving the following interactions:

- phenol–OH····O=C of blebbistatin core
- phenol–O····H–O–H (water, × 2)
- chiral HO····H-8–Ar
- H_2O····H-3 of the blebbistatin core.

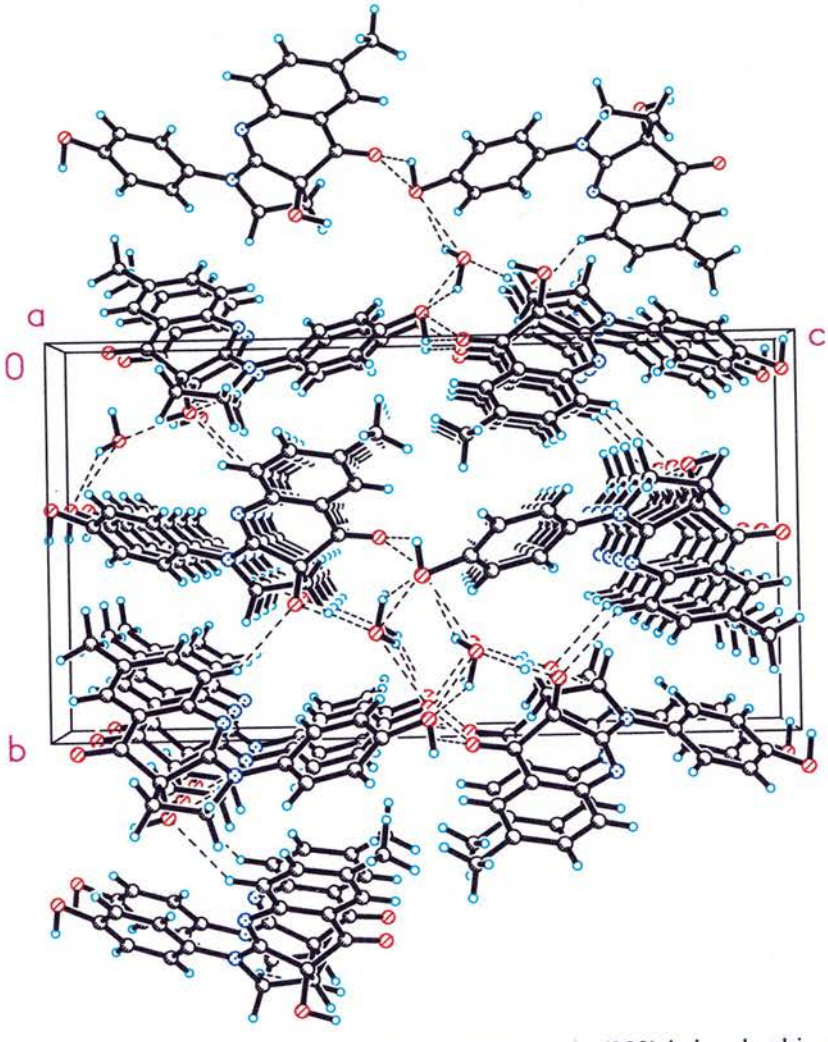

Figure 1.6. In the solid state the phenol derivative (*S*)-(–)-blebbistatin (**232**) is involved in π-π stacking and an intricate network of hydrogen-bonding involving two water molecules and four molecules of **232**.

3.5 SUMMARY

A series of 1-(but-3-en-1-yloxy)phenols have been prepared in good yields using two alternative protection methods. Deprotection occurred cleanly under mildly oxidative conditions in excellent yields. The utility of this protecting group was demonstrated in the synthesis of a phenol-containing derivative of (*S*)-(–)-blebbistatin (**232**). Identifying an

appropriate protecting group is often the decisive factor for success in a synthetic design (blueprint). Expanding the scope of the butenyl protecting group adds another protection method to the "tool-box" providing orthogonality and/or an option when availability is limited.

Finally, a reaction carried out within the Westwood group, subsequently converted phenol **232** to the methoxy derivative **241** (Figure 1.7) for which analytical data was consistent with material obtained by an alternative route.[27] This was achieved using Mitsunobu conditions, triphenylphosphine, DEAD and greater than stoichiometric methanol in toluene at room temperature. This approach provides a route for the synthesis of C4′′ substituted derivatives of **232** in order to try and discover more potent and specific inhibitors of the myosin II subclasses. Samples of the butenyl- and phenol-containing analogues of (*S*)-(–)- blebbistatin (**240** and **232**) have recently been sent to Prof. Rayment's laboratory in order to perform X-ray crystallographic studies aimed at obtaining a co-crystal structure with *Dictyostelium discoideum* myosin II.

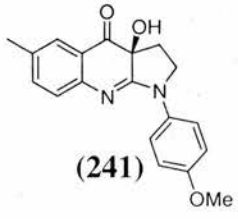

(241)

Figure 1.7. The chemical structure of the methoxy-containing derivative of (*S*)-(–)- blebbistatin (**241**) prepared by a Mitsunobu reaction from **240**.

4.0 ANILINE PROTECTION

The successful phenol protection led us to attempt protection of an amine nitrogen in a similar manner. Methyl anthranilate was chosen as an initial substrate based on a synthetic interest in the Westwood laboratory. It was hoped that this would offer an alternative route to the synthesis of (±)-blebbistatin analogues (Scheme 1.11). The idea involved the use of a traceless linker to immobilise the aniline building block onto a solid phase matrix. After a proposed acylation reaction to incorporate the lactam moiety, oxidative cleavage of the linker was envisaged to release the small molecule. Use of the base-mediated deprotection step would be investigated as a means to effect cyclisation to

the quinolone precursor. A one-pot procedure involving treatment with resin-bound Davis oxiziridine could then provide the final step leaving only the product and residual base in solution after removal of the resin beads. For this to be a valid proposal the initial stages involved in aniline protection were investigated and the results are presented herein.

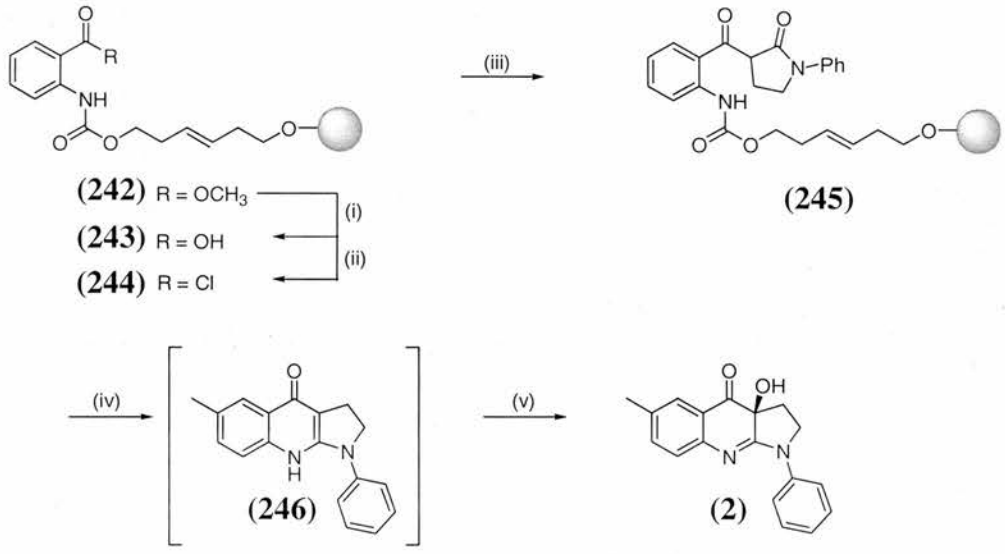

Scheme 1.11. The proposed alternative route to the synthesis of (±)-blebbistatin analogues on solid phase utilising a cleavable linker. Reagents and conditions: (i) H^+, MeOH, reflux; (ii) SO_2Cl; (iii) LiHMDS; (iv) O_3, DCM, –78 °C; DMS, –78 °C – 0 °C; NEt_3, RT; (v) LiHMDS; SP–(–)-Davis oxiziridine.

4.1 PROTECTION OF METHYL ANTHRANILATE (247)

The carbamate **248** was prepared according to a similar procedure reported by Parlo and Flynn,[32] using 3-butenyl chloroformate (**249**) and pyridine in DCM in excellent yield of 99% (Scheme 1.12). Slightly more than one equivalent of pyridine was used because it is required to act as a nucleophilic catalyst, in addition to sequestering hydrochloric acid.

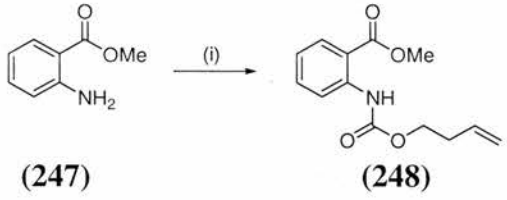

Scheme 1.12. Protection of methyl anthranilate (**247**) as the butenyl carbamate **248**. *Reagents and conditions:* (i) 3-butenyl chloroformate (**249**) (1.1 equiv.), pyridine (1.2 equiv.), DCM, RT, 99%.

4.2 Deprotection Optimisation of 248

The initial deprotection of **248** was carried out under the conditions reported by Barrett *et al.*[8] Under these conditions, a complex mixture of products was produced. The desired deprotected product, methyl anthranilate (**247**), was observed as a minor component, in only a 17% yield. Three by-products were isolated and characterised. As anticipated based on Section 2.8, the major by-product was the aldehyde (**250**), presumably formed via conjugate addition of the aniline nitrogen in **247** to acrolein, which was produced *in situ* during the deprotection reaction. For structural confirmation the aldehyde was prepared independently, by reaction of methyl anthranilate with acrolein. Interestingly it was found that triethylamine was required for the aldehyde forming reaction to proceed and in its absence only starting materials were observed by ^{1}H NMR spectroscopy and TLC analysis. All analytical data for **250** formed by this method was consistent with the aldehyde produced from the deprotection reaction of **248**. The product resulting from 1,2-addition to acrolein was not observed. The acetal (**251**) was isolated as a minor component of the reaction mixture, presumably by trapping of a hydroperoxide intermediate and protecting the aldehyde as an acetal in the presence of methanol. Only when the methanol was completely removed from the reaction was the formation of the acetal **251** prevented. The formation of the third by-product **252** is discussed in more detail in the next section.

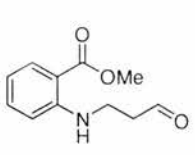

(250)

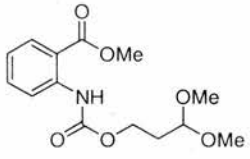

(251)

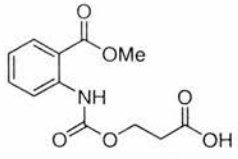

(252)

Figure 1.8. By-products isolated from the ozonolytic deprotection reaction of methyl anthranilate (**247**). *Reagents and conditions:* (i) O_3, DCM:MeOH 1:1 v/v, –78 °C; $(CH_3)_2S$, –78 °C to RT; NEt_3, RT; 10% aqueous HCl workup, **247** 17%; (ii) O_3, DCM:MeOH 10:1 v/v, –78 °C; $(CH_3)_2S$, –78 °C to RT; NEt_3, PS-*p*TsNHNH$_2$, RT, **247** 73%, **251** 14%, **252** NI; (iii) O_3, DCM, –78 °C; $(CH_3)_2S$, –78 °C to RT; NEt_3, PS-*p*TsNHNH$_2$, RT, **252** 8%. NI = not isolated.

4.3 Introduction of a Solid Phase "Scavenger" Resin

Addition of a scavenger to the deprotection reaction was proposed to remove acrolein (**206**, an α,β-unsaturated aldehyde, Figure 1.5) from the reaction mixture preventing the formation of **250**, therefore increasing the amount of **247**. Repeating the

solution phase deprotection with the addition of *p*-toluenesulfonyl hydrazine afforded **247** in 49% yield after purification. However, isolation was difficult owing to excess scavenger.

Polymer-bound scavengers are resins displaying reactive functional groups, which are added after a chemical reaction to remove excess reactants and/or unwanted by-products.[33] PS-*p*TsNHNH$_2$ (**253**) is the resin-bound equivalent of *p*-toluenesulfonyl hydrazine, developed for carbonyl scavenging applications, and has been shown to readily react with aldehydes and ketones.[34,35] Inclusion of PS-*p*TsNHNH$_2$ scavenger in the deprotection of **248** proved key. TLC analysis showed **247** to be the major product with one minor by-product present. The scavenger beads were easily removed by a simple filtration step and following column chromatography **247** was isolated in 73% yield and the by-product assigned as the carboxylic acid (**252**, Figure 1.8) was isolated in 8% yield. Previous literature by Hon and co-workers reported the formation of an acid product from ozonolytic cleavage of 1-phenylcyclopentene using dimethylsulfide.[20] Formation of the acid (**252**) demonstrates that dimethylsulfide is sufficiently basic to abstract the secondary ozonide ring proton. Both the oxidation-reduction (redox) process and to a lesser extent, the acid-base (El$_{CB}$ equivalent) mechanism occur when dimethylsulfide is used. On the other hand with triphenylphosphine, Hon *et al.* observed formation of the aldehyde as the sole product, resulting from attack of the peroxide linkage of the secondary ozonide.[20] Substituting dimethylsulfide with triphenylphosphine in the deprotection protocol eliminated the formation of the acid (**252**), as expected, and **247** was successfully isolated in a 98% yield.

Triphenylphosphine was considered as the scavenging reagent based on literature precedent for its reaction with acrolein (cf. Scheme 1.5).[36] Therefore, the deprotection reaction was repeated with the inclusion of the polymer supported tosyl hydrazine scavenger omitted. In this case, **247** was obtained in a moderate yield of 65%. Under these conditions the reaction performed adequately and aldehyde **250** was not observed by ^{1}H NMR or TLC analysis. However, the reaction did not proceed cleanly and therefore it was concluded that the optimal conditions for the deprotection reaction involved the combination of triphenylphenylphosphine and the scavenger resin **253** (entry 5, Table 1.4). The optimisation process is summarised in Table 1.4.

Table 1.4. Optimisation of the aniline deprotection using ozonolysis. [a] Isolated yields. NI = not isolated

Entry	Solvent Ratio v/v	Reducing agent	Base	Scavenger	Yield 247 (%)[a]
1	DCM:MeOH 1:1	$(CH_3)_2S$	NEt_3	–	17
2	DCM:MeOH 10:1	$(CH_3)_2S$	NEt_3	pTsNHNH$_2$	49
3	DCM:MeOH 10:1	$(CH_3)_2S$	NEt_3	PS-pTsNHNH$_2$	73
4	DCM	$(CH_3)_2S$	NEt_3	PS-pTsNHNH$_2$	NI
5	DCM	PPh_3	NEt_3	PS-pTsNHNH$_2$	98
6	DCM	PPh_3	NEt_3	–	65

Encouraged by the results from the optimised deprotection procedure for **248**, it was decided to study the scope of the ozonolytic deprotection methodology for several aniline derived carbamates (Scheme 1.13). A series of protected carbamates were efficiently prepared by reaction of the appropriate aniline with 3-butenyl chloroformate as previously described (Section 4.1). The protection reactions proceeded in high yields (89-99%) and were carried out across a range of concentrations (Table 1.5).

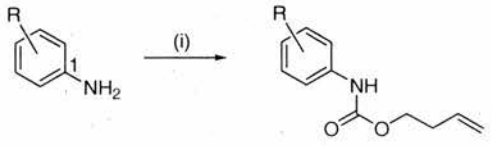

Scheme 1.13. Aniline protection. *Reagents and conditions:* (i) 3-butenyl chloroformate (1.1 equiv.), pyridine (1.2 equiv.), DCM, RT.

Table 1.5. Aniline protection. [a]

Entry	R		Protected Product	% yield [b]
1	2-COOMe	**(247)**	**248**	99
2	4-COOMe	**(254)**	**258**	89
3	2-COOMe, 4-Br	**(255)**	**259**	97
4	3-NO_2	**(256)**	**260**	99
5	4-OMe	**(257)**	**261**	98

[a] Reactions carried out across a range of concentrations, 0.1 – 0.2 M in aniline SM. [b] Isolated yields. Arbitrary numbering included for clarity.

4.4 DEPROTECTION RESULTS FOR ANILINES

Using the optimised protocol for ozonolytic deprotection the corresponding anilines were regenerated in moderate to high yields, 78-98% (entries 1-4, Table 1.6) with the exception of **257** (entry 5), which proceeded in the lower yield of 39%.

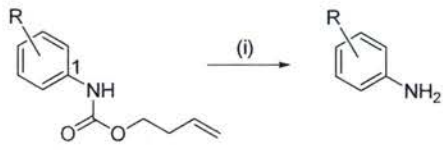

Scheme 1.14. Aniline deprotection. *Reagents and conditions:* (i) O_3, DCM, –78°C; PPh_3 (2 equiv), –78°C – RT 12-15 h; PS-*p*TsNHNH$_2$ (10 equiv), Et_3N (2 equiv), RT. Where R = 2/4-COOMe, 2-COOMe and 4-Br, 3-NO2, and 4-OMe.

Table 1.6. Aniline deprotection under optimised conditions. [a]

Entry	R		Deprotected Product	% yield [b]
1	2-COOMe	**(248)**	**247**	98
2	4-COOMe	**(254)**	**258**	78
3	2-COOMe, 4-Br	**(255)**	**259**	92
4	3-NO_2	**(256)**	**260**	80
5	4-OMe	**(257)**	**261**	39

[a] All reactions at 0.05 M in SM [b] Isolated yields. Arbitrary numbering included for clarity.

In all cases no by-products were observed by TLC or ^{1}H NMR analysis of the crude reaction mixture. To assess the resin beads after inclusion in the deprotection reaction, IR analysis was performed on a single bead (Figure 1.9). Despite the resin being used in 10-fold excess, differences were observed in this analysis.

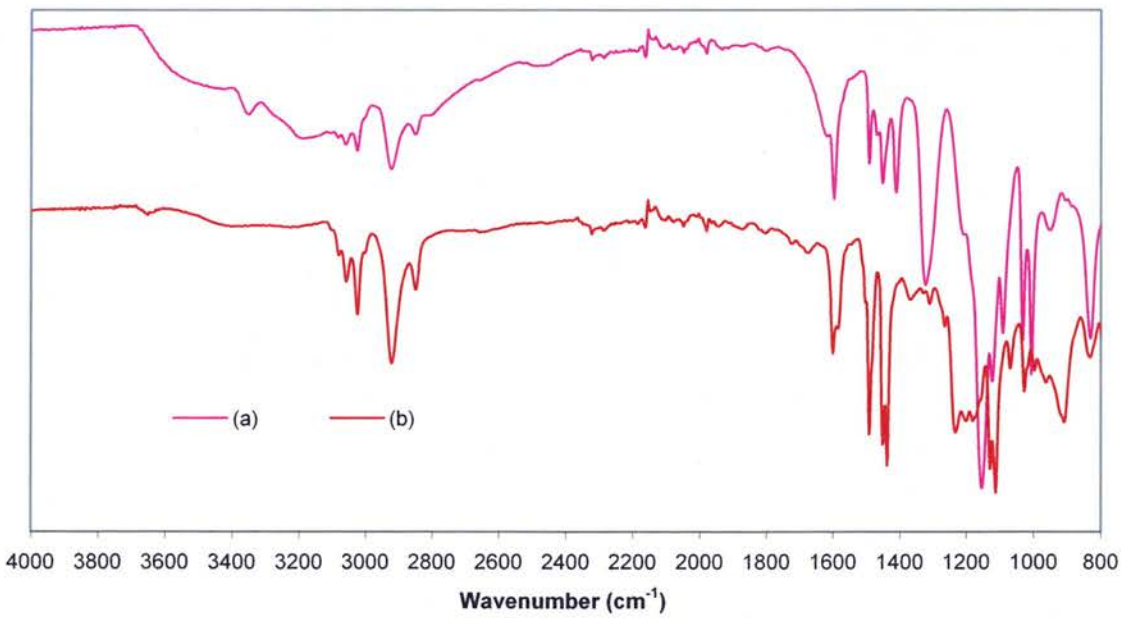

Figure 1.9. IR spectra of the PS-*p*TsNHNH$_2$ resin (**253**) before (a) and after (b) inclusion in the ozonolytic deprotection of **248**.

PS-*p*TsNHN$_2$ resin (**253**) has previously been characterised by IR spectroscopy.[34] PS-*p*TsNHN$_2$ (**253**) showed typical N-H stretching vibrations at 3590-3420 (broad band) and 3340 cm^{-1} and δ vibrations at 1595 and 945 cm^{-1} (Figure 1.9 (a)). Absorptions at 1320 and 1150 cm^{-1} characteristic of sulfonyl hydrazine were also present. The peaks at 1320, 1150, and 1005 cm^{-1} disappeared and the bands attributed to N-H stretching partly disappeared after reaction of polymer (**253**) in the ozonolytic deprotection (Figure 1.9 (b)). Additional peaks were observed at 1580 (C=N), 1230, 1110 and 905 cm^{-1} in polymer **253** after inclusion in the ozonolytic deprotection (Figure 1.9 (b)). Based on this evidence alone it is difficult to establish the product bound to the resin post inclusion in the deprotection protocol but it is proposed that the polymer-bound sulfonyl hydrazine scavenges the by-product acrolein (**206**), which becomes bound to the resin as the corresponding sulfonyl hydrazone derivative.[37]

4.5 Reusability of the PS-*p*TsNHNH$_2$ scavenger resin

Since the scavenger resin was employed in the deprotection protocol in 10-fold excess it was decided to investigate briefly its reusability. PS-*p*TsNHNH$_2$ resin (**253**) was retrieved from the deprotection of **259** to **255**. The recovered resin was collected in quantitative yield after drying *in vacuo* and applied to two further rounds of deprotection of **259**. The results as shown in Table 1.7 indicate that repeated use of the PS-*p*TsNHNH$_2$ resin (**253**) results in a drop in performance. The yield of **255** dropped to 71% on the third use of resin **253**. It is interesting to note that the analogous aldehyde to **250** was not observed and all reactions still proceeded cleanly.

Table 1.7. The efficacy of the re-use of polymer **253** in the ozonolytic deprotection reaction of **259**.

Entry	The *n*th use of polymer (n=)	Yield **255** (%) [b]
1	1	92
2	2	86
3	3	71

[a] All reactions at 0.05 M in SM. [b] Isolated yields.

4.6 SUMMARY

To summarise, the butenyl protecting group has been extended to the protection of aromatic amines as their corresponding carbamates. Modification of Barrett's deprotection protocol was necessary to prevent the formation of by-products that have been isolated and characterised. One such modification involved the use of a scavenger resin (**253**) for the by-product acrolein (**206**), which was observed to undergo a 1,4-conjugate addition reaction with the deprotected aniline species **247**. Several aniline derivatives have been easily protected in high yields and, using the optimised procedure, deprotection was efficiently achieved in moderate to high yields with a range of aromatic substituents studied.

Further extension of the protecting group was envisaged as the cleavable component of a traceless linker for solid phase chemistry, which is the subject of the next section.

5.0 A CLEAVABLE LINKER FOR SOLID PHASE CHEMISTRY

In solid phase chemistry, a cleavage method from the resin is arguably the most important synthetic step as it is required to release the target molecule from the resin. It is not surprising then that the design of new cleavable linkers is an active area of research for solid phase applications. Our proposed hexenyl-based linker system (**179**) incorporates a dual cleavage strategy that presents an interesting package. Currently, it takes months to progress from identifying a hit in a phenotype-based assay to affinity chromatography studies. Our approach aims to reduce this time.

A library of small molecules could be cleaved at one site from the solid phase resin (in a traceless manner (see later)) for screening in a forward chemical genetics assay. Traceless linkers boast the advantage of no workup procedures and therefore direct access to pure compounds on cleavage from the solid phase resin. Any hit compound could then be re-accessed quickly by returning to the library stock and cleaving the remaining beads under a second set of conditions that preserves the integrity of the linker unit. Ideally, this in turn could be directly attached to an affinity resin for preliminary target identifications studies (Figure 1.10).

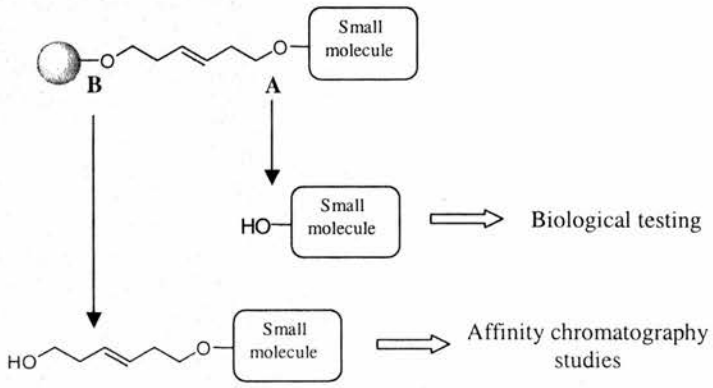

Figure 1.10. Schematic representation for an application of the doubly cleavable linker - from small molecule synthesis on solid phase to target identification studies.

A vast amount of chemistry has been explored in the synthesis of linkers for application to solid phase chemistry but surprisingly very few involve the incorporation of a double bond to effect cleavage. However, a limited number of examples are present in the literature.[38 -41] An exceptional example is displayed by Seeberger *et al.* with the use of an octenediol functionalised resin in the automated synthesis of a branched dodecasaccaride. The target oligosaccharide was readily cleaved from the solid support by olefin cross metathesis using Grubb's catalyst.

There is already an established precedent for ozone as a versatile reagent for solid phase synthesis.[42] Ozone has many advantages over alternative oxidants, which usually demonstrate low solubility and poor diffusion within the resin matrix and limited formation of by-products.[43] It is easily eliminated following reaction, simply by bubbling argon/nitrogen through the reaction mixture. Ozonolysis allows the product to be partially dependent on the workup reagent, thus an opportunity available for diversity (e.g. for the synthesis of DOS libraries).

The aim of this section was to demonstrate the relevance of the protecting group chemistry discussed thus far, and the linker unit introduced previously (Chapter 4) to solid phase library synthesis.

5.1 SYNTHESIS AND CLEAVAGE OF (*E*)-4-(6-(TRIALKYLSILYLOXY)HEX-3-ENYLOXY)BENZALDEHYDE FUNCTIONALISED RESIN (265)

The resin bound equivalent of the protected phenol **225** was prepared (Scheme 1.15). The phenol **221** was protected under standard Mitsunobu conditions (as previous, Section 2.7) using the mono-TIPS protected alcohol **180** (Chapter 4, Section 2.2.1). Fluoride deprotection of the TIPS group afforded the free alcohol **263** in 95% yield. Subsequent attachment of **263** to silicon-based 500-600 μm high capacity (1.43 mmol/g) polystyrene beads (**264**) through a Si–O bond to generate **265** was achieved following the protocol of Tallarico *et al.*[44] The resin **264** was chosen for its ease and efficiency of substrate loading and the ease at which it undergoes Si–O bond cleavage resulting in only volatile by-products. Loading of **263** to the resin was achieved in 62% yield (equivalent to 0.89 mmol/g), determined by mass increase of the resin beads and the amount of unloaded **263** recovered.

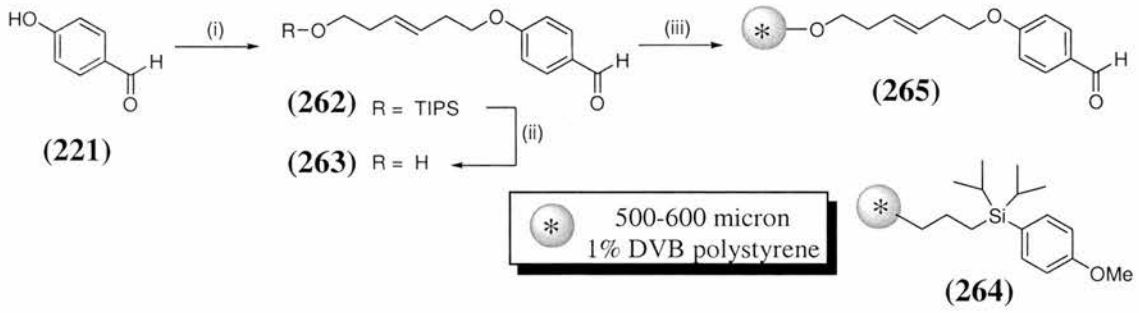

Scheme 1.15. Preparation of functionalised resin **265**. *Reagents and conditions:* (i) (*E*)-6-Triisopropylsilanyloxy-hex-3-en-1-ol (**180**), DEAD, toluene, 80 °C, 24 h, 69% (ii) TBAF, THF, RT, 3 h, 95%; (iii) a) Functionalised resin **264**, TfOH, DCM, 30 mins.; b) 2,6-lutidine, DCM, 15 mins.; **263**, DCM, 48 h, RT, 62% loading efficiency.

Treatment of the resin **265** with ozone followed by dimethylsulfide and triethylamine, afforded cleavage of 4-hydroxybenzaldehyde (**221**) in a 55% yield following column chromatography (Scheme 1.16, analogous to deprotection of **225** (Table 1.2, entry 4), based on 0.89 mmol/g loading). ^{1}H NMR and mass spectrometric analysis for **221** obtained by this method was consistent with data from the deprotection of **225** and with literature.[45] Conversely, a further Grignard reaction on the resin using phenylmagnesium bromide afforded the resin-bound alcohol **266**. A central feature of the silyl based resin is the cleavage under standard fluoride deprotection conditions. Therefore, treatment of resin **266** with TBAF afforded alcohol **267** in 47% yield following column chromatography.

Mass spectrometric analysis confirmed the formation of the desired product **267** with the major ionisation peak at *m/z* 321 (ES) consistent with $[M + Na]^+$. The alternate ozonolytic deprotection developed herein, gave 4-hydroxyphenyl-phenylmethanol (**268**) in 27% following column chromatography to remove a trace impurity. TLC analysis of a purified sample indicated that **268** was collected cleanly and ^{1}H NMR analysis was consistent with the literature.[46] The mass spectrum showed a peak at *m/z* 199 attributed to $[M - H]^-$ in ES and also several other ionisation peaks. Due to the small scale of the solid-phase deprotection, a second synthesis of **268** was performed in solution by reaction of 4-hydroxybenzaldehyde (**221**) with phenylmagnesium bromide for analytical verification. ^{1}H NMR and mass spectrometric analysis of **268** obtained by this route proved consistent with data obtained from the solid phase cleavage.

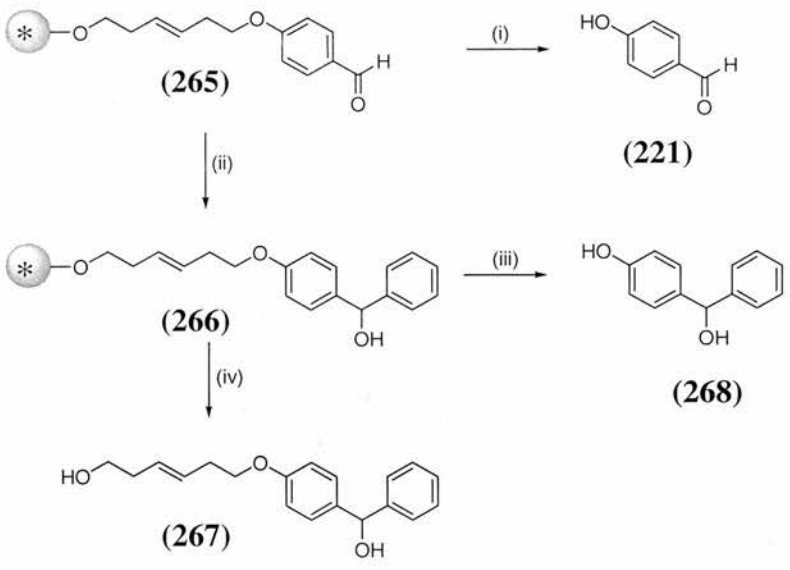

Scheme 1.16. Ozonolytic cleavage of resin **265** and preparation of resin **266** with subsequent dual cleavage. *Reagents and conditions:* (i) O_3, DCM, –78 °C; $(CH_3)_2S$ (12 equiv), 3 h, –78 °C to RT; Et_3N (6 equiv), RT, 12 h 55%; (ii) PhMgBr (10 equiv.), THF, RT, 12 h; (iii) O_3, DCM, –78 °C; $(CH_3)_2S$ (10 equiv), 3 h, –78 °C to RT; NEt_3 (5 equiv), RT, 12 h 27% (based on 62% loading); (iv) TBAF, THF, RT, 3 h, 47% (based on 62% loading).

This synthesis demonstrates that the hexenyl linker can be applied to solid phase chemistry and possesses the advantage of dual cleavability. However, ozonolytic cleavage suffers from a low yield for which, due to time constraints, optimisation was not attempted.

5.2 SUMMARY

In summary, the ozonolytic deprotection of the butenyl group originally developed by Barrett *et al.* has been incorporated into a linker system compatible with polystyrene resin as the support for solid phase synthesis. The linker reported here benefits from two cleavage methods and could serve to decrease the current time delay from solid phase library synthesis and identifying a hit in a phenotype-based assay to affinity chromatography studies. In a solid phase library synthesis, small molecules are prepared on resin beads using a linker. The linker allows cleavage of the small molecule from the resin by two methods: i) to allow the biological activity to be tested in the absence of a long linker unit; ii) to give the compound with the linker intact, enabling rapid attachment to an affinity matrix. Whilst dual cleavable linker systems are known,[47] none are known to have incorporated the use of ozone. However, one possible drawback of this methodology for solid phase synthesis is the obvious incompatibility of double (and triple) bonds and the sensitivity of aldehyde functional groups.

6.0 CONCLUSION

A mild and facile cleavable group is a versatile tool for organic synthesis. The methodology presented in this chapter should find useful applications in the development of small molecule libraries (e.g. blebbistatin) or could allow orthogonal protection in synthetic pathways (e.g. natural product targets).

CHAPTER 2

EXPERIMENTAL

1.0 General protocol for the synthesis of protected phenols: Method A

3-Buten-1-ol (9.60 mmol, 1.2 equiv.) and triphenylphosphine (9.60 mmol, 1.2 equiv) were added to a solution of phenol (8.00 mmol, 1 equiv) in anhydrous toluene (20 mL), with stirring, under nitrogen. DEAD (9.60 mmol, 1.2 equiv) was then added and the resulting solution was heated to 80 °C with stirring for 24 h. After cooling the reaction mixture was washed with aqueous sodium hydroxide solution (2.0 M, 2 × 200 mL) and distilled water (200 mL). The combined aqueous layers were extracted with ethyl acetate (3 × 200 mL) before the organic phases were combined, dried ($MgSO_4$), and concentrated *in vacuo*. Products were purified by flash column chromatography on silica gel (EA:hexane).

1.1 General protocol for the synthesis of protected phenols: Method B

Potassium carbonate (3 equiv.) was added to a solution of phenol (1 equiv.) in anhydrous DMF at room temperature, with stirring. After 10 mins. 4-bromobut-1-ene (2-4 equiv.) was added and the reaction stirred for 48-60 h. The reaction was diluted with distilled water (300 mL) and extracted with diethyl ether (3 × 150 mL). The combined organic phase was washed with distilled water (150 mL), dried ($MgSO_4$), and concentrated *in vacuo*. Products were purified by flash column chromatography on silica gel (EA:hexane).

1.2 General protocol for phenol deprotection: Method C

In a 50 mL pear shaped two-necked flask, equipped with a magnetic stirrer, a glass inlet tube and a bubbler, were placed the alkene (1 equiv.) and DCM (10 mL). A stream of ozone was bubbled through the solution at –78 °C (dry ice/acetone bath). Ozone treatment was terminated when the solution assumed a blue colour and/or in cases where the reaction mixture is coloured the use of a potassium iodide solution was used as an indicator. Excess ozone was then removed by purging the solution with oxygen, *c.* 10 mins., until the blue colour was discharged. The reducing agent (dimethylsulfide, 2 equiv.) was then

added to the solution, which was warmed to room temperature and stirred for 2 h. Triethylamine (2 equiv.) was added and the reaction mixture stirred for a further 3 h. The solvent was removed *in vacuo* and the crude reaction mixture purified by flash column chromatography on silica gel (EA:PE 40-60).

1.3 General protocol for the synthesis of protected anilines: Method D

3-Butenyl chloroformate (1.1-1.2 equiv) and anhydrous pyridine (1.2-1.3 equiv.) were added to a solution of the aniline (1.0 equiv.) in anhydrous DCM (0.1-0.2 M in aniline) with stirring. The reaction was stirred for 12-18 h at room temperature. Addition of saturated aqueous ammonium chloride solution (equivol.) and the aqueous layer extracted into DCM. The organic phase was dried ($MgSO_4$), filtered and concentrated *in vacuo*. Products were purified by flash column chromatography on silica gel (EA:hexane).

1.4 General protocol for aniline deprotection: Method E

In a 50 mL pear shaped two-necked flask, equipped with a magnetic stirrer, a glass inlet tube and a bubbler, were placed the alkene (1 equiv.) and solvent (10 mL, DCM). A stream of ozone was bubbled through the solution at –78 °C (dry ice/acetone bath). Ozone treatment was terminated when the solutions assumed a blue colour and/or in cases where the reaction mixture is coloured the use of a potassium iodide solution was used as an indicator. Excess ozone was then removed by purging the solution with oxygen, *c.* 10 mins., until the blue colour was discharged. The reducing agent (dimethylsulfide or triphenylphosphine, 2 equiv.) was then added to the solution, which was warmed to room temperature and stirred for 2 h. Triethylamine (2 equiv.) and scavenger (PS-*p*TsNHNH$_2$ washed and pre-swollen in DCM, 10 equiv. under optimal conditions) were added and the reaction mixture stirred for a further 3 h. The solvent was removed *in vacuo* and the crude reaction mixture purified by flash column chromatography on silica gel (EA:PE 40-60).

Preparation of 3-(but-3-enyloxy)nitrobenzene, 222

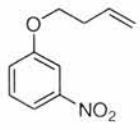

Prepared from **218** (1.11 g, 8.00 mmol) using the general method described for phenol protection (Method A). **222** was collected as a colourless oil (1.39 g, 7.19 mmol, 90%). **^{1}H NMR** (300 MHz, $CDCl_3$): δ 7.81 (ddd, ^3J = 8.2 Hz, ^4J = 2.2, 0.9 Hz, H-6), 7.73 (br t, 1H, ^4J = 2.2 Hz, H-2), 7.42 (br t, 1H, ^3J = 8.2 Hz, H-5), 7.22 (ddd, ^3J = 8.2 Hz, ^4J = 2.2, 0.9 Hz, H-4), 5.97-5.84 (m, 1H, C<u>H</u>=CH_2), 5.23-5.12 (m, 2H, CH=C<u>H</u>$_2$), 4.09 (t, ^3J = 6.6 Hz, 2H, OC<u>H</u>$_2$$CH_2$), 2.62-2.55 (2H, m, OCH_2C<u>H</u>$_2$); **^{13}C NMR** (75.5 MHz, $CDCl_3$): δ 159.4 (C3), 149.2 (C1), 133.8 (<u>C</u>H=CH_2), 129.9 (C5), 121.7 (C4), 117.5 (CH=<u>C</u>H_2), 115.7 (C6), 108.7 (C2), 67.8 (O<u>C</u>H_2), 33.3 (OCH_2<u>C</u>H_2); **MS-EI+** (*m/z*) 193 ($[M]^{+\bullet}$, 32%), 165 ($[M - CHCH_2]^{+\bullet}$, 22), 55 ($[C_2H_4CHCH_2]^{+\bullet}$, 100); **HRMS-EI$^+$** (*m/z*) Calcd for $C_{10}H_{11}NO_3$ $[M]^{+\bullet}$: 193.0739, found 193.0733. Also prepared from 3-nitrophenol (0.50 g, 3.60 mmol) using Method B for phenol protection. **222** was collected as a colourless oil (0.36 g, 1.88 mmol, 52%). Analytical data was consistent with the data for **222** obtained from Method A and with literature values.[48]

Preparation of 4-(but-3-enyloxy)nitrobenzene, 223

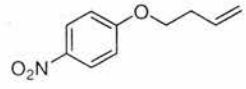

Prepared from **219** (1.11 g, 8.00 mmol) using the general method described for phenol protection (Method A). **223** was collected as a colourless oil (1.26 g, 6.53 mmol, 82%). **^{1}H NMR** (300 MHz, $CDCl_3$): δ 8.21-8.16 (m, 2H, AA′ part of AA′XX′, H-3 and H-5), 6.97-6.92 (m, 2H, XX′ part of AA′XX′, H-2 and H-6), 5.95-5.82 (m, 1H, C<u>H</u>=CH_2), 5.22-5.11 (m, 2H, CH=C<u>H</u>$_2$), 4.10 (t, ^3J = 6.7, 2H, OC<u>H</u>$_2$), 2.62-2.54 (m, 2H, OCH_2C<u>H</u>$_2$); **^{13}C NMR** (75.5 MHz, $CDCl_3$): δ 163.9 (C1), 141.4 (C4), 133.6 (<u>C</u>H=CH_2), 125.8 (C3 and C5), 117.8 (CH=<u>C</u>H_2), 114.4 (C2 and C6), 68.0 (O<u>C</u>H_2), 33.3 (OCH_2<u>C</u>H_2); **MS-EI+** (*m/z*) 193 ($[M]^{+\bullet}$, 17%), 165 ($[M - CHCH_2]^{+\bullet}$, 20), 55 ($[C_2H_4CHCH_2]^{+\bullet}$, 100); **MS-CI+** (*m/z*) 194 ($[M + H]^+$, 100%), 122 (20), 55 ($[C_2H_4CHCH_2]^+$, 14); **HRMS-CI$^+$** (*m/z*) Calcd for $C_{10}H_{12}NO_3$ $[M + H]^+$: 194.0813, found 194.0817. Also prepared from **219** (0.50 g, 3.60 mmol) using Method B for phenol protection. **223** was collected as a colourless oil (0.61 g, 3.15 mmol, 87%). Analytical data was consistent with the data for **223** obtained from Method A.

Preparation of 1-(4-methoxyphenoxy)butene, 224

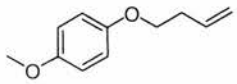

Prepared from **220** (0.99 g, 8.00 mmol) using the general method described for phenol protection (Method A). **224** was collected as a colourless oil (0.96 g, 5.36 mmol, 67%). **IR** (film) ν_{max}: 3076 (w), 2950-2834 (br m), 1641 (w) (C=C), 1509 (s), 1469 (m), 1232 (s), 1043 (m), 918 (w), 826 (m) and 739 (m) (ArC–H) cm^{-1}; **^{1}H NMR** (300 MHz, $CDCl_3$): δ 6.85 (s, 2H, ArH), 6.84 (s, 2H, ArH), 5.98-5.85 (m, 1H, CH=CH_2), 5.21-5.09 (m, 2H, CH=CH_2), 3.97 (t, ^3J = 6.7 Hz, OCH_2), 3.77 (s, 3H, OCH_3), 2.57-2.49 (m, 2H, OCH_2CH_2); **^{13}C NMR** (75.5 MHz, $CDCl_3$): δ 153.8 (C1 or C4), 153.0 (C1 or C4), 134.5 (CH=CH_2), 116.9 (CH=CH_2), 115.5 (C2 and C6), 114.6 (C3 and C5), 67.9 (OCH_2), 55.7 (OCH_3), 33.7 (OCH_2CH_2); **MS-CI+** (*m/z*) 179 ($[M + H]^+$, 100%), 178 ($[M]^+$, 20), 137 ($[M - C_2H_4CHCH_2]^+$, 29); **HRMS-CI$^+$** (*m/z*) Calcd for $C_{11}H_{15}O_2$ $[M + H]^+$: 179.1072, found 179.1074. Also prepared by the same procedure using **220** (0.40 g, 3.22 mmol), 3 buten-1-ol (0.24 g, 0.28 mL, 3.25 mmol), triphenylphosphine (0.85 g, 3.22 mmol), and diethyl azodicarboxylate (0.56 g, 0.59 mL, 3.24 mmol) to afford **224** (0.57 g, 3.19 mmol, 99%). Data are in agreement with literature values.[49]

Preparation of 4-(but-3-enyloxy) benzaldehyde, 225

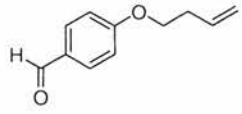

Prepared from **221** (0.98 g, 8.00 mmol) using the general method described for phenol protection (Method A). **225** was collected as a colourless oil (0.72 g, 4.11 mmol, 51%). **IR** (film) ν_{max}: 3077 (s), 2940-2740 (s), 1699 (s) (C=O), 1643 (s), 1577 (s), 1509 (s), 1162 (s), 1028 (s), 921 (m), 834 (s) (ArC–H), 652 (m) cm^{-1}; **^{1}H NMR** (300 MHz, $CDCl_3$): δ 9.88 (s, 1H, CHO), 7.84-7.82 (m, 2H, AA′ part of the AA′XX′ system, H-2 and H-6), 7.01-6.98 (m, 2H, XX′ part of the AA′XX′ system, H-3 and H-5), 5.97-5.83 (m, 1H, CH=CH_2), 5.22-5.12 (m, 2H, CH=CH_2), 4.10 (t, ^3J = 6.7 Hz, 2H, OCH_2), and 2.62-2.54 (m, 2H, OCH_2CH_2); **^{13}C NMR** (75.5 MHz, $CDCl_3$): δ 190.8 (CHO), 163.9 (C4), 133.8 (CH=CH_2), 132.0 (C2 and C6), 129.9 (C1), 117.5 (CH=CH_2), 114.7 (C3 and C5), 67.5 (OCH_2) and 33.4 (OCH_2CH_2); **MS-ES+** (*m/z*) 199 ($[M + Na]^+$, 100%), 177 ($[M + H]^+$, 39); **HRMS-ES$^+$** (*m/z*) Calcd for $C_{11}H_{12}O_2Na$ $[M + Na]^+$: 199.0735, found 199.0735. Also prepared from **221** (1.00 g, 8.19 mmol) using Method B for phenol protection. **225**

was collected as a colourless oil (0.96 g, 5.45 mmol, 67%). Analytical data was consistent with the data for **225** obtained from Method A and with literature values.[50]

Deprotection of 222 to 3-nitrophenol, 218

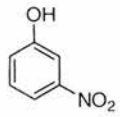

Treatment of **222** using the general method described for phenol deprotection (Method C), gave **218** as a colourless solid (0.26 g, 1.85 mmol, 92%); mp 96-97 °C (lit. 95 °C).[51] **^{1}H NMR** (300 MHz, $CDCl_3$): δ 7.81 (ddd, ^3J = 8.2 Hz, ^4J = 2.2 Hz, ^4J = 0.9 Hz, H-4), 7.70 (br t, 1H, ^4J = 2.2 Hz, H-2), 7.41 (br t, 1H, ^3J = 8.2 Hz, H-5), 7.18 (ddd, ^3J = 8.2 Hz, ^4J = 2.2, 0.9 Hz, H-6), 5.67 (br s, 1H, OH); **^{13}C NMR** (75.5 MHz, $CDCl_3$): δ 156.3 (C1), 149.0 (C3), 130.3 (C5), 122.0 (C6), 115.8 (C4), 110.5 (C2); **MS-ES–** (*m/z*) 138 ([M – H]$^-$, 100%).

1-Butoxy-3-nitrobenzene, 227: **^{1}H NMR** (300 MHz, $CDCl_3$): δ 7.80 (ddd, ^3J = 8.2 Hz, ^4J = 2.3, 0.9 Hz, H-4), 7.71 (br t, 1H, ^4J = 2.3 Hz, H-2), 7.41 (br t, 1H, ^3J = 8.2 Hz, H-5), 7.21 (ddd, ^3J = 8.2 Hz, ^4J = 2.3, 0.9 Hz, H-6), 4.03 (t, ^3J = 6.5 Hz, 2H, OCH_2), 1.85-1.75 (m, 2H, OCH_2CH_2), 1.57-1.45 (m, 2H, CH_2CH_3), 0.99 (t, ^3J = 7.4 Hz, 3H, CH_3); **^{13}C NMR** (75.5 MHz, $CDCl_3$): δ 159.7 (C1), 149.2 (C3), 129.8 (C5), 121.7 (C6), 115.5 (C4), 108.6 (C2), 68.3 (OCH_2), 31.0 (OCH_2CH_2), 19.1 (CH_2CH_3), 13.8 (CH_3). Data are in agreement with literature values.[18]

Deprotection of 223 to 4-nitrophenol, 219

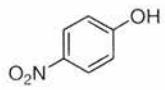

Treatment of **223** using the general method described for phenol deprotection (Method C), gave **219** as as a colourless solid (0.24 g, 1.75 mmol, 87%); mp 109.0-111.0 °C (lit. 113-114 °C, H_2O).[52] **^{1}H NMR** (300 MHz, $CDCl_3$): δ 8.20-8.15 (m, AA′ part of AA′XX′, 2H, H-3 and H-5), 6.95-6.90 (m, XX′ part of AA′XX′, 2H, H-2 and H-6), 6.18 (br s, 1H, OH); **^{13}C NMR** (75.5 MHz, $CDCl_3$): δ 161.4 (C1), 141.6 (C4), 126.3 (C3 and C5), 115.7 (C2 and C6); **MS-ES–** (*m/z*) 138 ([M – H]$^-$, 100%). Data are in agreement with literature values.[53]

Deprotection of 224 to 4-methoxy-phenol, 220

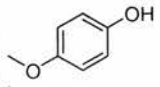

Treatment of **224** using the general method described for phenol deprotection (Method C), gave **220** as a white solid (0.25 g, 1.98 mmol, 99%); mp 49.5-51.0 °C (lit. 54-55 °C).[54] **^{1}H NMR** (300 MHz, $CDCl_3$): δ 6.78 (d, ^3J = 0.9, 4H, Ar-H), 4.88 (br s, 1H, OH), 3.77 (s, 3H, OCH_3); **^{13}C NMR** (75.5 MHz, $CDCl_3$): δ 153.6 (C4), 149.5 (C1), 116.0 (C2 and C6), 114.8 (C3 and C5), 55.8 (CH_3); **MS-ES–** (*m/z*) 108 ($[M - H]^-$, 100%). Data are in agreement with literature values.[54]

Deprotection of 225 to 4-hydroxybenzaldehyde, 221

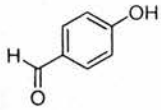

Treatment of **225** using the general method described for phenol deprotection (Method C), gave **221** as a white crystalline solid (0.16 g, 1.32 mmol, 66%); mp 116.0-118.0 °C (lit. 117 °C).[55] **^{1}H NMR** (300 MHz, $CDCl_3$): δ 9.87 (s, 1H, CHO), 7.84-7.80 (m, AA′ part of AA′XX′, 2H, H-2 and H-6), 6.99-6.94 (m, XX′ part of AA′XX′, 2H, H-3 and H-5), 5.93 (br s, 1H, OH); **^{13}C NMR** (75.5 MHz, $CDCl_3$): δ 191.3 (CHO), 161.7 (C4), 132.5 (C2 and C6), 129.8 (C1), 116.0 (C3 and C5); **MS-ES–** (*m/z*) 121 ($[M - H]^-$, 100%). Data are in agreement with literature values.[45] In addition, **228** was isolated as a white powdery solid (17 mg, 0.12 mmol, 14%) and **229** collected as colourless crystals (15 mg, 0.07 mmol, 9%) as by-products.

4-Hydroxybenzoic acid, 228

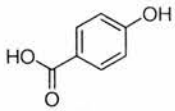

IR (NaCl, Nujol) ν_{max}: 3385 (br s) (OH), 1676 (s) (C=O, acid), 1608 (s) (CO_2^-), 1595 (s) (ArC–C), 1510 (m), 1425 (m) cm^{-1}; **^{1}H NMR** (300 MHz, CD_3OD): δ 7.86-7.80 (m, AA′ part of the AA′XX′ system, 2H, H-2 and H-6), 6.79-6.74 (m, XX′ part of the AA′XX′ system, 2H, H-3 and H-5); **^{13}C NMR** (75.5 MHz, CD_3OD): δ 170.1 (C=O), 163.4 (C4), 133.1 (C2 and C6), 122.8 (C1), 116.1 (C3 and C5); **MS-ES–** (*m/z*) 137 ($[M - H]^-$, 100). Data are in agreement with literature values.[56]

3-(4-Formylphenoxy)propionoic acid, 229

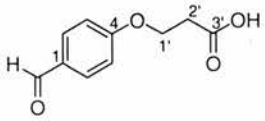

IR (NaCl, Nujol) ν_{max}: 3384 (br w) (OH), 1723 (s) (C=O, aldehyde), 1644 (m) (C=O, acid), 1600 (s) (CO_2^-), 1572 (s) (ArC–C) cm^{-1}; **^{1}H NMR** (300 MHz, $CDCl_3$): δ 9.79 (s, 1H, CHO), 7.85-7.79 (m, AA′ part of the AA′XX′ system, 2H, H-2 and H-6), 7.08-7.02 (m, XX′ part of the AA′XX′ system, 2H, H-3 and H-5), 4.30 (t, ^3J = 6.0, 2H, CH_2-1′), 2.75 (t, ^3J = 6.0, 2H, CH_2-2′); **^{13}C NMR** (75.5 MHz, $CDCl_3$): δ 192.9 (CHO), 174.6 (COOH), 165.5 (C4), 133.1 (C2 and C6), 131.5 (C1), 116.0 (C3 and C5), 65.3 (C1′), 35.1 (C2′); **MS-ES–** (*m/z*) 387 ([2M – H]$^-$, 51%), 193 ([M – H]$^-$, 100), 121 ([M – $(CH_2)_2$COOH]$^-$, 19).

Preparation of 4-bromobut-1-ene, 226 [19]

3-Buten-1-ol (1.26 g, 1.50 mL, 17.4 mmol) in pyridine (0.55 g, 0.57 mL, 7.00 mmol) was added to phosphorous tribromide (1.91 g, 0.67 mL, 6.97 mmol) at –5 °C (ice-salt bath) with stirring. The reaction mixture was stirred for 1 h at –5 °C before warming to room temperature and stirring for a further 2h. Purification by distillation gave **226** as a colourless oil (1.42 g, 10.5 mmol, 60%); bp. 96 – 100 °C (lit. 97.5 °C).[19] **^{1}H NMR** (300 MHz, $CDCl_3$): δ 5.87-5.73 (m, 1H, H-2), 5.17-5.10 (m, 2H, CH_2-1), 3.41 (t, ^3J = 7.0 Hz, 2H, CH_2-4), 2.66-2.58 (m, 2H, CH_2-3); **^{13}C NMR** (75.5 MHz, $CDCl_3$): δ 135.1 (C2), 117.5 (CH_2-1), 36.9 (CH_2-4), 32.0 (CH_2-3).

Preparation of 1-(but-3-en-1-yloxy)-4-iodobenzene, 234

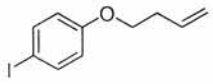

Prepared from **233** (5.00 g, 22.7 mmol), 3-buten-1-ol (2.11 g, 2.52 mL, 29.3 mmol), triphenylphosphine (7.67 g, 29.3 mmol), and DEAD (6.43 g, 6.73 mL, 36.9 mmol) in anhydrous toluene (375 mL) using the general method described for phenol protection (Method A). **234** was collected as a colourless oil (5.60 g, 20.4 mmol, 90%). **IR** (thin film) ν_{max}: 3078 (w) (=CH_2 st), 1643 (w), 1586 and 1571 (m) (ArC–C), 1487 (s) (C=C), 1470 (m) (ArC–C), 1283 (m), 1244 (s) (C–O), 1175 (m), 1033 (m), 999 and 919 (CH=CH_2), 820 (m) (ArC-H) cm^{-1}; **^{1}H NMR** (300 MHz, $CDCl_3$): δ 7.57–7.52 (m, 2H, AA′ part of the AA′XX′ system, H-3 and H-5), 6.70-6.65 (m, 2H, XX′ part of the

AA′XX′ system, H-2 and H-6), 5.95–5.82 (m, 1H, CH=CH_2), 5.20–5.09 (m, 2H, CH=CH_2), 3.97 (t, ^{3}J = 6.7 Hz, 2H, OCH_2), 2.57–2.49 (m, 2H, OCH_2CH_2); **^{13}C NMR** (75.5 MHz, $CDCl_3$): δ 158.7 (C1), 138.1 (C3), 134.1 (C3′), 117.2 (C4′), 116.9 (C2), 82.7 (C4), 67.3 (C1′), 33.5 (C2′); **MS-EI+** (*m/z*) 274 ($[M]^{+\bullet}$, 91%), 220 ($[M - CH_2CH_2CHCH_2]^+$, 100); **HRMS-EI+** (*m/z*) Calcd for $C_{10}H_{11}OI$ $[M]^{+\bullet}$: 273.9855, found 273.9848.

Preparation of 1-[4 -(but-3-en-1-yloxy)phenyl]pyrrolidin-2-one, 235

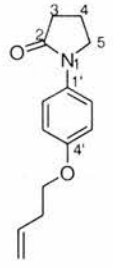

To a solution of **234** (5.00 g, 18.2 mmol), 2-pyrrolidinone (2.73 g, 32.1 mmol) and potassium phosphate (7.64 g, 36.0 mmol) in anhydrous toluene (170 mL) were added *N,N′*-dimethylethylenediamine (0.32 g, 300 μL, 3.68 mmol). After addition of copper iodide (0.34 g, 0.18 mmol) the reaction mixture was heated to reflux for 16 h. After cooling the resulting mixture was passed through a silica plug which was washed with MeOH:Et_2O (1:4) and the eluent concentrated *in vacuo* to give a dark brown oil. Purification by flash column chromatography on silica gel (ethyl acetate:PE 40-60 2:3) gave **235** as a white solid (3.65 g, 15.8 mmol, 88%); mp 93.5-94.5 °C. **IR** (KBr) ν_{max}: 3082 (w), 1883 (w), 1690 (s), 1657 (m), 1644 (m), 1517 (s), 1427 (m), 1400 (s), 1254 (m), 1227 (m), 1034 (s), 914 (s), 831 (s) cm^{-1}; **^{1}H NMR** (300 MHz, $CDCl_3$): δ 7.50–7.45 (m, 2H, AA′ part of the AA′XX′ system, H-2 and H-6), 6.92–6.87 (m, 2H, XX′ part of the AA′XX′ system, H-3 and H-5), 5.97–5.83 (m, 1H, CH=CH_2), 5.20-5.08 (m, 2H, CH=CH_2), 4.00 (t, ^3J = 6.7 Hz, 2H, OCH_2), 3.83 (t, ^3J = 7.0 Hz, 2H, CH_2-5′), 2.59 (t, ^3J = 7.8 Hz, 2H, CH_2-3′), 2.58–2.50 (m, 2H, OCH_2CH_2), 2.20-2.10 (m, 2H, CH_2-4′); **^{13}C NMR** (75.5 MHz, $CDCl_3$): δ 173.9 (C2′), 155.9 (C4), 134.4 (CH=CH_2), 132.6 (C1), 121.8 (C2), 117.1 (CH=CH_2), 114.8 (C3), 67.4 (OCH_2), 49.2 (C5′), 33.6 (OCH_2CH_2), 32.5 (C3′), 18.0 (C4′); **MS-ES+** (*m/z*) 254 ($[M + Na]^+$, 100%); **HRMS-ES+** (*m/z*) Calcd for $C_{14}H_{17}NO_2Na$ $[M + Na]^+$: 254.1157, found 254.1160; **Anal.** Calcd for $C_{14}H_{17}NO_2$: C, 72.70; H, 7.41; N, 6.06. Found: C, 72.54; H, 7.40; N, 6.03.

Preparation of methyl 5-methyl-2-[1-(4-(but-3-en-1-yloxy)phenyl)pyrrolidin-2-ylideneamino]benzoate, 237

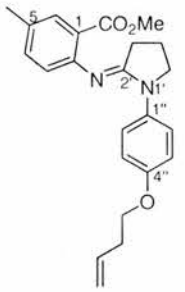

To a solution of **235** (1.70 g, 7.35 mmol) in anhydrous dichloromethane (8.2 mL) was added phosphorus oxychloride (1.06 g, 630 μL, 6.68 mmol) dropwise with stirring, under nitrogen. The reaction was stirred for 3 h at room temperature. A solution of methyl 5-methylantranilate (1.10 g, 6.68 mmol) in anhydrous DCM (47.3 mL) was then added and the reaction heated to reflux for 68 h. The reaction was then cooled and concentrated *in vacuo*. The resulting solid was redissolved in aqueous hydrochloric acid (3.0 M, 25 mL) and extracted with DCM (2 × 5 mL). The pH of the aqueous phase was adjusted to 7/8 (aqueous 2.0 M sodium hydroxide) and extracted with ethyl acetate (3 × 100 mL). The first organic extracts were concentrated *in vacuo* and the resulting solid was carried through the above extraction procedure multiple times. All ethyl acetate extracts were combined, dried ($MgSO_4$), filtered and concentrated *in vacuo* to afford **237** as a viscous colourless oil (544 mg, 1.44 mmol, 20%). **IR** (thin film) ν_{max}: 3077 (w), 1720 (s) (C=O), 1663 (s) (C=N), 1609 (m) (C=C), 1509 (m) (aryl-H), 1434 (m), 1401 (m), 1241 and 1204 (m) (C-O), 1077 (m), 1038 (m), 999 and 918 (m) ($CH=CH_2$), 901 (m), 831 (m) and 794 (w) (ArC-H) cm^{-1}; **^{1}H NMR** (300 MHz, $CDCl_3$): δ 7.69-7.64 (m, 3H, H-6 and AA′ part of the AA′XX′ system, H-2′′ and H-6′′), 7.18 (br d, ^3J = 8.0 Hz, 1H, H-4), 6.91-6.88 (m, 2H, XX′ part of the AA′XX′ system, H-3′′ and H-5′′), 6.78 (d, ^3J = 8.0 Hz, 1H, H-3), 5.96-5.82 (m, 1H, $CH=CH_2$), 5.19-5.07 (m, 2H, $CH=CH_2$), 3.99 (t, ^3J = 6.7 Hz, 2H, OCH_2), 3.85 (t, ^3J = 6.8 Hz, 2H, CH_2-5′), 3.82 (s, 3H, OCH_3), 2.55-2.48 (m, 4H, OCH_2CH_2 and CH_2-3′), 2.30 (s, 3H, CH_3), 2.09-2.00 (m, 2H, CH_2-4′); **^{13}C NMR** (75.5 MHz, $CDCl_3$): δ 167.8 (C=O), 160.4 (C2′), 155.2 (C4′′), 149.9 (C2), 134.4 ($CH=CH_2$), 134.3 (C1′′), 133.5 (C4), 131.2 (C5), 130.9 (C6), 123.5 (C3), 122.6 (C2′′), 122.1 (C1), 116.9 ($CH=CH_2$), 114.8 (C3′′), 67.5 (OCH_2), 51.8 OCH_3), 51.5 (C5′), 33.6 (OCH_2CH_2), 29.1 (C3′), 20.6 (CH_3), 19.8 (C4′); **MS-ES+** (*m/z*) 379 ($[M + H]^+$, 100%); **HRMS-ES+** (*m/z*) Calcd for $C_{22}H_{27}N_2O_3$ $[M + H]^+$: 379.2022, found 379.2010.

Preparation of 1-(4-(but-3-enyloxy)phenyl)-6-methyl-2,3-dihydro-1*H*-pyrrolo[2,3-*b*]quinolin-4-one, 238

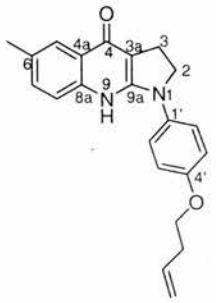

A solution of amidine **237** (500 mg, 1.32 mmol) in anhydrous THF (50 mL) was cooled to –78 °C and stirred under nitrogen for 15 mins. Lithium bis(trimethylsilyl)amide (1.0 M in THF, 4.00 mL, 3.97 mmol) was added dropwise to the reaction mixture, which was warmed to 0 °C over 3 h and quenched at 0 °C with saturated aqueous ammonium chloride (50 mL). Further saturated aqueous ammonium chloride (150 mL) was added. The aqueous phase was extracted with DCM (3 × 150 mL) and the combined organic phases dried ($MgSO_4$), filtered and concentrated *in vacuo* to give a brown solid. Purification by flash column chromatography on silica gel (neat ethyl acetate) gave **238** as a beige glassy solid (259 mg, 0.75 mmol, 57%); mp 110.0-112.0 °C. **IR** (KBr) ν_{max}: 1633 (s) (C=C), 1577 (s) (C=O), 1509 (s) (aryl-H), 1471 (m), 1451 (m), 1420 (m), 1383 (w), 1242 (m) (C–O), 1070 (m), 1035 (m), 990 and 916 (m) ($CH=CH_2$), 825 (m) (ArC–H) and 554 (s) cm^{-1}; **^{1}H NMR** (300 MHz, $CDCl_3$): δ 7.96 (br s, 1H, H-5), 7.45 (d, ^3J = 8.3 Hz, 1H, H-8), 7.26-7.20 (m, 3H, H-7 and AA′ part of the AA′XX′ system, H-2′ and H-6′), 6.78-6.74 (m, 2H, XX′ part of the AA′XX′ system, H-3′ and H-5′), 5.92-5.78 (m, 1H, $CH=CH_2$), 5.18-5.07 (m, 2H, $CH=CH_2$), 3.87 (t, ^3J = 8.5 Hz, 2H, CH_2-2), 3.77 (t, ^3J = 6.7 Hz, 2H, OCH_2), 3.04 (t, ^3J = 8.5 Hz, 2H, CH_2-3), 2.50-2.44 (m, 2H, OCH_2CH_2), 2.39 (s, 3H, CH_3); **^{13}C NMR** (75.5 MHz, $CDCl_3$) δ 156.6 (C4′), 155.1 (C4 and C9a), 137.9 (C8a), 134.2 (C3′′), 133.0 (C1′), 132.0 (C6), 130.8 (C7), 124.4 (C2′), 124.0 (C5), 123.8 (C4a), 118.4 (C8), 117.1 (C4′′), 115.4 (C3′), 102.9 (C3a), 67.3 (C1′′), 53.5 (C2), 33.5 (C2′′), 23.6 (C3), 21.1 (CH_3); **^{1}H NMR** (500 MHz, d_8-THF): δ 7.87 (br s, 1H, H-5), 7.82-7.80 (m, 2H, AA′ part of the AA′XX′ system, H-2′ and H-6′), 7.46 (d, ^3J = 8.4 Hz, 1H, H-8), 7.22 (dd, ^3J = 8.4 Hz, ^4J = 1.7 Hz, 1H, H-7), 6.87-6.89 (m, 2H, XX′ part of the AA′XX′ system, H-3′ and H-5′), 5.96-5.88 (m, 1H, $CH=CH_2$), 5.16-5.13 (m, 1H, $CH=CH_2$), 5.06-5.04 (m, 1H, $CH=CH_2$), 3.99-3.94 (m, 4H, CH_2-2 and OCH_2), 3.17 (t, ^3J = 8.2 Hz, 2H, CH_2-3), 2.52-2.48 (m, 2H, OCH_2CH_2), 2.41 (s, 3H, CH_3); **^{13}C NMR** (125 MHz, d_8-THF)

δ 159.2 (C4 and C9a), 155.3 (C4′), 145.5 (C8a), 136.5 (C1′), 135.8 (C3′′), 131.3 (C6), 130.7 (C7), 124.7 (C8), 122.3 (C5), 121.1 (C2′ and C4a), 116.8 (C4′′), 115.2 (C3′), 105.7 (C3a), 68.0 (C1′′), 50.8 (C2), 34.6 (C2′′), 23.2 (C3), 21.3 ($\underline{C}H_3$); **MS-ES+** (*m/z*) 347 ([M + H]$^+$, 100%); **MS-ES–** (*m/z*) 345 ([M – H]$^-$, 100%); **HRMS-ES+** (*m/z*) Calcd for $C_{22}H_{23}N_2O_2$ [M + H]$^+$: 347.1760, found 347.1755.

Preparation of *S*-3a-hydroxy-1-(4-(but-3-enyloxy)phenyl)-6-methyl-2,3,3a,4-tetrahydro-1*H*-pyrrolo[2,3-*b*]quinolin-4-one, 240

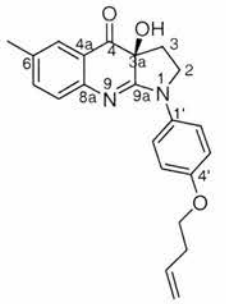

A solution of quinolone **238** (150 mg, 0.43 mmol) in anhydrous THF (32 mL) was added dropwise to a solution of lithium bis(trimethylsilyl)amide (1.0 M in THF, 520 μL, 0.52 mmol) in anhydrous THF (3.0 mL) at –78 °C under nitrogen. The reaction mixture was stirred for 30 mins. at –78 °C and a solution of (–)-(8,8-dichlorocamphorylsulfonyl)-oxaziridine (310 mg, 1.04 mmol) in anhydrous THF (5.0 mL) was added. After 16 h at –10 °C, saturated aqueous ammonium iodide (3.0 mL) and Et_2O (4 mL) were added and the reaction gradually warmed to room temperature. Saturated aqueous sodium thiosulfate (15 mL) was added and the reaction extracted with Et_2O (3 × 15 mL). The combined organic extracts were dried ($MgSO_4$), filtered and concentrated *in vacuo* to give a yellow solid. The solid was partitioned between DCM (100 mL) and aqueous hydrochloric acid solution (3.0 M, 100 mL). The aqueous phase was washed with DCM (3 × 100 mL), brought to pH 8 with aqueous sodium hydroxide solution (2.0 M) and extracted with ethyl acetate (2 × 50 mL). The DCM phase was subjected to the above extraction procedure multiple times. The combined ethyl acetate extracts were dried ($MgSO_4$), filtered and concentrated *in vacuo* to give **238** as a bright yellow solid (0.114g, 0.31 mmol, 73%); The *ee* of **238** was 92% as determined by chiral-phase HPLC analysis. $[\alpha]_D^{24}$ = – 550 (*c* = 0.02, $CHCl_3$); HPLC (acetonitrile: water + 1% acetonitrile 50:50, flow rate 0.8 mL min^{-1}, λ = 254 nm): major enantiomer: t_R = 18.48 min., and minor enantiomer: t_R = 29.58 min.

An analytical sample of **238** was prepared by recrystallisation from acetonitrile to afford bright yellow needles; mp 190.0-191.0 °C (recrystallised from acetonitrile); Chiral-phase HPLC analysis showed that after a single recrystallisation (acetonitrile), **238** was prepared with an *ee* of >99%. $[\alpha]_D^{24}$ = – 622.5 (*c* = 0.02, $CHCl_3$). HPLC (acetonitrile: water + 1% acetonitrile 50:50, flow rate 0.8 mL min^{-1}, λ = 254 nm): major enantiomer: t_R = 18.42 min. **IR** (KBr) ν_{max}: 3423 (br) (OH), 1698 (s), 1621 (s), 1603 (s), 1512 (s), 1482 (s), 1298 (w), 1246 (m) (C–O), 1109 (m), 1061 (w), 1037 (m), 917 (w) ($CH=CH_2$), and 832 (m) (ArC–H) cm^{-1}; **^{1}H NMR** (300 MHz, $CDCl_3$): δ 7.74-768 (m, 2H, AA′ part of the AA′XX′ system, H-2′and H-6′), 7.60 (br d, ^4J = 2.0 Hz, 1H, H-5), 7.05 (dd, ^3J = 8.2 Hz, ^4J = 2.0 Hz, 1H, H-7), 6.97-6.92 (m, 2H, XX′ part of the AA′XX′ system, H-3′ and H-5′), 6.88 (d, ^3J = 8.2 Hz, 1H, H-8), 5.99-5.85 (m, 1H, $CH=CH_2$), 5.23-5.11 (m, 2H, $CH=CH_2$), 4.89 (br s, 1H, OH), 4.04 (t, ^3J = 6.8 Hz, 2H, OCH_2), 3.78-3.64 (m, 2H, CH_2-2), 2.60-2.53 (m, 2H, OCH_2CH_2), 2.39-2.33 (m, 1H, CH_2-3), 2.33 (s, 3H, CH_3), 2.22-2.12 (m, 1H, CH_2-3); **^{13}C NMR** (75.5 MHz, $CDCl_3$): δ 194.0 (C=O), 160.4 (C2′), 164.4 (C9a), 155.9 (C4′), 148.2 (C8a), 137.1, (C7), 134.3 ($CH=CH_2$), 132.9 (C6 and C1′), 127.1, (C5), 125.4 (C8), 122.0 (C2′), 119.9 (C4a), 117.2 ($CH=CH_2$), 114.6 (C3′), 73.8 (C3a), 67.5 (OCH_2), 48.9 (C2), 33.6 (OCH_2CH_2), 29.1 (C3), 20.6 (CH_3); **MS-ES+** (*m/z*) 363 ($[M + H]^+$, 100%); **HRMS-ES+** (*m/z*) Calcd for $C_{22}H_{23}N_2O_3$ $[M + H]^+$: 363.1709, found 363.1706; Anal. Calcd for $C_{22}H_{22}N_2O_3$: C, 72.91; H, 6.12; N, 7.73. Found: C, 72.66; H, 6.50; N, 7.29.

Preparation of *S*-3a-hydroxy-1-(4-phenol)-6-methyl-2,3,3a,4-tetrahydro-1*H*-pyrrolo[2,3-*b*]quinolin-4-one, 232

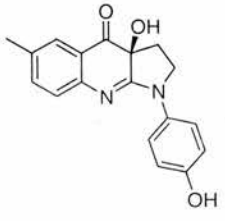

Prepared from **240** (36.5 mg, 0.10 mmol) using the general method described for phenol deprotection (Method C). **232** was collected as an orange crystalline solid (19.5 mg, 0.06 mmol, 63%); mp 194.5-196.5 °C; $[\alpha]_D^{20}$ = – 430 (*c* = 0.02, CH_3OH). Chiral-phase HPLC (acetonitrile: water + 1% acetonitrile 50:50, flow rate 0.8 mL min^{-1}, λ = 254 nm): t_R = 3.83 min. **IR** (KBr) ν_{max}: 3469 (br) (OH), 3244 (br) (OH), 1670 (s), 1604 (s), 1510 (s), 1479 (s), 1301 (w), 1244 (m) (C–O), 1212 (w), 1143 (w), 842 (w) (ArC–H), 831

(w) and 806 (w) (ArC–H) cm^{-1}; **^{1}H NMR** (300 MHz, CD_3OD) δ 7.60 (br d, ^4J = 2.0 Hz, 1H, H-5), 7.57-7.52 (m, 2H, AA′ part of the AA′XX′ system, H-2′and H-6′), 7.32 (dd, ^3J = 8.2 Hz, ^4J = 2.0 Hz, 1H, H-7), 7.06 (d, ^3J = 8.2 Hz, 1H, H-8), 6.88-6.83 (m, 2H, XX′ part of the AA′XX′ system, H-3′ and H-5′), 4.16-4.07 (m, 1H, CH_2-2), 3.93-3.86 (m, 1H, CH_2-2), 2.36-2.31 (m, 2H, CH_2-3), 2.31 (s, 3H, CH_3); **^{13}C NMR** (75.5 MHz, CD_3OD) δ; 196.7 (C=O), 167.4 (C9a), 156.7 (C4′), 151.1 (C8a), 138.0 (C7), 133.6 (C6), 133.1 (C1′), 127.9 (C5), 126.3 (C8), 125.5 (C2′), 122.2 (C4a), 116.7 (C3′), 74.9 (C3a), 60.0 (C2), 30.4 (C3), 20.6 (CH_3); **MS-ES+** (*m/z*) 309 ($[M + H]^+$, 100%); **HRMS-ES+** (*m/z*) Calcd for $C_{18}H_{17}N_2O_3$ $[M + H]^+$: 309.1239, found 309.1242. An analytical sample of **232** was prepared by recrystallisation from ethyl acetate/PE 40-60 to afford orange crystals suitable for X-ray analysis.

Preparation of methyl 2-(but-3-enyloxycarbonylamino)benzoate, 248

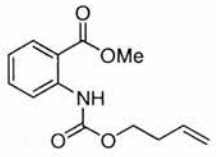

Prepared from **247** (500 mg, 3.31 mmol) using the general method described for aniline protection (Method D). **248** was collected as a pale yellow oil (820 mg, 3.30 mmol, 99%). **IR** (film) ν_{max}: 3303 (br s) (NH, H-bonded), 2955 (m) (CH), 1738 (s) (C=O, ester), 1695 (s) (C=O, carbamate), 1592 (s), 1530 (s) (C=C), 1452 (s), 1062 (m), 755 (m) (ArC–H) cm^{-1}; **^{1}H NMR** (300 MHz, $CDCl_3$): δ 10.48 (br s, 1H, NH), 8.44 (dd, ^3J = 8.6 Hz, ^4J = 1.2 Hz, 1H, H-3), 8.00 (dd, ^3J = 8.0 Hz, ^4J = 1.6 Hz, 1H, H-6), 7.56-7.50 (m, 1H, H-4), 7.05-6.70 (m, 1H, H-5), 5.91-5.77 (m, 1H, $CH=CH_2$), 5.19-5.07 (m, 2H, $CH=CH_2$), 4.22 (t, ^3J = 6.8 Hz, 2H, OCH_2), 3.92 (s, 3H, OCH_3), 2.49-2.42 (m, 2H, OCH_2CH_2); **^{13}C NMR** (75.5 MHz, $CDCl_3$): δ 168.5 (C=O, ester), 153.6 (C=O), 141.8 (C2), 134.6 (C4), 134.9 ($CH=CH_2$), 130.8 (C6), 121.5 (C5), 118.8 (C3), 117.3 ($CH=CH_2$), 114.5 (C1), 64.3 (OCH_2), 52.2 (OCH_3), 33.3 (OCH_2CH_2); **MS-CI+** (*m/z*) 250 ($[M + H]^+$, 100%), 218 ($[M - OCH_3]^+$ 12); **HRMS-ES$^+$** (*m/z*) Calcd for $C_{13}H_{15}NO_4Na$ $[M + Na]^+$: 272.0899, found 272.0899.

Deprotection of 248 to methyl anthranilate, 247

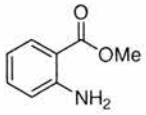

Method 1: Deprotection of carbamate 248 in DCM/MeOH 1/1 v/v using $(CH_3)_2S$

Following Method E, treatment of **248** (0.46 g, 1.84 mmol) in DCM (8 mL) and MeOH (8 mL) using dimethylsulfide (0.42 g, 0.5 mL, 6.76 mmol) and triethylamine (0.36 g, 0.5 mL, 3.59 mmol) afforded following column chromatography **247** as a colourless oil (47 mg, 0.31 mmol, 17%).

Method 2: Deprotection of carbamate 248 in DCM/MeOH 10/1 v/v using $(CH_3)_2S$ and *p*TsNHNH$_2$

Following Method E, treatment of **248** (0.19 g, 0.76 mmol) in DCM (10 mL) and MeOH (1 mL) using dimethylsulfide (0.30 g, 350 μL, 4.77 mmol), triethylamine (0.25 g, 350 μL, 2.51 mmol) and *p*TsNHNH$_2$ (2.84 g, 15.3 mmol) afforded, following column chromatography **247** as a colourless oil (0.06 g, 0.37 mmol, 49%).

Method 3: Deprotection of carbamate 248 in DCM:MeOH 10/1 v/v using $(CH_3)_2S$ and PS-*p*TsNHNH$_2$

Following Method E, treatment of **248** (70 mg, 0.28 mmol) in DCM (10.0 mL) and MeOH (1.0 mL) using dimethylsulfide (0.21 g, 0.25 mL, 3.4 mmol). PS-*p*TsNHNH$_2$ (2.75 mmol, 2.5 mmol/g loading, 10 equiv) was weighed into a 50 mL pear shaped flask and allowed to swell in DCM (15.0 mL) for 30 mins. and the reaction mixture added, followed by triethylamine (0.18 g, 0.25 mL, 1.78 mmol), which, after column chromatography afforded **247** as a colourless oil (31 mg, 0.21 mmol, 73%).

Method 4: Deprotection of carbamate 248 in DCM using $(CH_3)_2S$ and PS-*p*TsNHNH$_2$

Following Method E, treatment of **248** (104 mg, 0.42 mmol) in DCM (10.0 mL) using dimethylsulfide (0.21 g, 0.25 mL, 3.4 mmol). PS-*p*TsNHNH$_2$ (2.75 mmol, 2.5 mmol/g loading, 10 equiv) was weighed into a 50 mL pear shaped flask and allowed to swell in DCM (15.0 mL) for 30 min. and the reaction mixture added, followed by triethylamine (0.18 g, 0.25 mL, 1.78 mmol), which, after column chromatography afforded **247** as confirmed by ^{1}H NMR and TLC analysis but was not isolated.

Method 5: Deprotection of carbamate 248 in DCM using PPh_3 and PS-*p*$TsNHNH_2$

Following Method E, treatment of **248** (125 mg, 0.50 mmol) in DCM (10.0 mL) using triphenylphosphine (0.26 g, 1.00 mmol). PS-*p*$TsNHNH_2$ (2.75 mmol, 2.5 mmol/g loading, 10 equiv) was weighed into a 50 mL pear shaped flask and allowed to swell in DCM (15.0 mL) for 30 min. and the reaction mixture added, followed by triethylamine (0.10 g, 140 μL, 1.00 mmol), which, after column chromatography afforded **247** as a colourless oil (74 mg, 0.49 mmol, 98%).

Method 6: Deprotection of carbamate 248 in DCM using PPh_3

Following Method E, treatment of **248** (200 mg, 0.80 mmol) in DCM (10.0 mL) using triphenylphosphine (0.42 g, 1.61 mmol), followed by triethylamine (0.16 g, 225 μL, 1.61 mmol), which, after column chromatography afforded **247** as a colourless oil (79 mg, 0.52 mmol, 65%).

IR (film) ν_{max}: 1694 (s) (C=O, ester), 1618 (s), 1590 (s), 1296 (m), 1249 (m), 739 (m) (ArC–H) cm^{-1}; **^{1}H NMR** (300 MHz, $CDCl_3$): δ 7.85 (dd, ^3J = 7.9 Hz, ^4J = 1.6 Hz, 1H, H-6), 7.26 (ddd, ^3J = 8.5, 7.2 Hz, ^4J = 1.6 Hz, 1H, H-4), 6.67-6.62 (m, 2H, H-5 and H-3), 5.72 (br s, 2H, NH_2), 3.87 (s, 3H, OCH_3); **MS-ES+** (*m/z*) 183 ($[M + MeOH]^+$, 39%), 174 ($[M + Na]^+$, 87), 152 ($[M + H]^+$, 100). Data are in agreement with the literature values.[57]

Preparation of methyl 2-(3-oxopropylamino)benzoate, 250

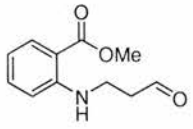

250 was isolated from the ozonolytic deprotection of **248** using Method 1. Also prepared by addition of triethylamine (0.22 g, 300 μL, 2.18 mmol) and acrolein (0.22 g, 260 μL, 0.40 mmol) to a solution of **247** (0.30 g, 2.00 mmol) in DCM (10 mL) at room temperature. After stirring for 18 h, the reaction mixture was washed with saturated aqueous ammonium chloride solution (10 mL) and extracted with DCM (3 × 25 mL). The organic phase was dried ($MgSO_4$) and concentrated *in vacuo*. Purification by flash column chromatography on silica gel (EA:PE 40-60, 1:9) gave **250** as a pale yellow oil (0.17 g, 0.84 mmol, 42%). **IR** (film) ν_{max}: 3500-3350 (br s) (NH, H-bonded), 2951 and 2929 (w) (CH stretching), 1722 (s) (C=O, ester), 1684 (s) (C=O, aldehyde), 1608 (s), 1582 (s), 1519

(s), 1457 (m), 1438 (m), 752 and 703 (m) (ArC–H) cm^{-1}; **^{1}H NMR** (300 MHz, $CDCl_3$): δ 9.86 (t, ^3J = 1.2 Hz, 1H, CHO), 7.90 (dd, ^3J = 8.0 Hz, ^4J = 1.7 Hz, 1H, H-3), 7.78 (br s, 1H, NH), 7.37 (ddd, ^3J = 8.5, 7.1 Hz, ^4J = 1.7 Hz, 1H, H-5), 6.69 (br d, ^3J = 8.5 Hz, 1H, H-6), 6.62 (ddd, ^3J = 8.0, 7.1 Hz, ^4J = 1.1 Hz, 1H, H-4), 3.85 (s, 3H, OCH_3), 3.61-3.55 (m, 2H, NCH_2), 2.84 (td, ^3J = 6.7 Hz, ^4J = 1.2 Hz, 2H, CH_2CHO); **^{13}C NMR** (75.5 MHz, $CDCl_3$): δ 200.6 (CHO), 169.0 (C=O, ester), 150.5 (C1), 134.7 (C5), 131.8 (C3), 115.0 (C4), 110.9 (C6), 110.4 (C2), 51.5 (OCH_3), 43.3 (NCH_2), 36.0 (CH_2CHO); **MS-ES+** (*m/z*) 230 ([M + Na]$^+$, 100%), 164 ([M – CH_2COH]$^+$, 74); **HRMS-ES$^+$** (*m/z*) Calcd for $C_{11}H_{13}NO_3Na$ [M + Na]$^+$: 230.0793, found 230.0796.

Methyl 2-((3,3-dimethoxypropoxy)carbonylamino)benzoate, 251

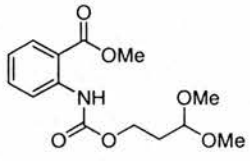

251 was collected as a pale yellow oil (0.012 g, 0.04 mmol, 14%) using Method 3. **^{1}H NMR** (300 MHz, $CDCl_3$): δ 10.50 (br s, 1H, NH), 8.44 (dd, ^3J = 8.6 Hz, ^4J = 1.2 Hz, 1H, H-3), 8.01 (dd, ^3J = 8.0 Hz, ^4J = 1.7 Hz, 1H, H-6), 7.56-7.50 (m, 1H, H-4), 7.06-7.00 (m, 1H, H-5), 4.57 (t, ^3J = 5.8 Hz, 1H, CH), 4.25 (t, ^3J = 6.5 Hz, 2H, OCH_2), 3.92 (s, 3H, OCH_3, ester), 3.36 (s, 6H, 2 × OCH_3, acetal), 2.04-1.98 (m, 2H, OCH_2CH_2); **^{13}C NMR** (125.7 MHz, $CDCl_3$): δ 168.4 (C=O, ester), 153.3 (C=O, carbamate), 141.6 (C2), 134.6 (C4), 131.0 (C6), 121.1 (C5), 118.7 (C3), 114.4 (C1), 101.4 (CH), 61.2 (OCH_2), 52.8 (OCH_3, acetal), 52.1 (OCH_3, ester), 32.2 (CH_2); **MS-ES+** (*m/z*) 320 ([M + Na]$^+$, 100%); **HRMS-ES$^+$** (*m/z*) Calcd for $C_{14}H_{19}NO_6Na$ [M + Na]$^+$ 320.1110, found 320.1115.

Isolation of 3-(2-(methoxycarbonyl)phenylcarboxy)propanoic acid, 252

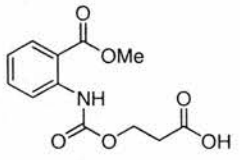

252 was collected as a pale yellow oil (9 mg, 0.03 mmol, 8%) using Method 4. **IR** (film) ν_{max}: 3310-3280 (br m) (OH, NH, H-bonded), 3055 (m), 1737 (br s) (C=O, ester and carboxylic acid), 1695 (s) (C=O, carbamate), 1592 (m), 1530 (m) cm^{-1}; **^{1}H NMR** (300 MHz, $CDCl_3$): δ 10.52 (br s, 1H, NH), 8.42 (dd, ^3J = 8.5 Hz, ^4J = 1.1 Hz, 1H, H-3), 8.00 (dd, ^3J = 8.0 Hz, ^4J = 1.6 Hz, 1H, H-6), 7.56-7.50 (m, 1H, H-4), 7.06-7.01 (m, 1H, H-5),

4.46 (t, ^3J = 6.4 Hz, 2H, OC$\underline{H}_2$), 3.91 (s, 3H, OC$\underline{H}_3$), 2.79 (t, ^3J = 6.4 Hz, 2H, OCH$_2$C$\underline{H}_2$); **^{13}C NMR** (75.5 MHz, $CDCl_3$): δ 175.4 (C=O, ester), 153.2 (C=O, carbamate), 141.5 (C1), 134.6 (C5), 130.9 (C3), 121.7 (C4), 118.8 (C6), 114.6 (C2), 60.2 (OC$\underline{H}_2$), 52.3 (OC$\underline{H}_3$), 33.7 (OCH$_2$C$\underline{H}_2$); **MS-ES+** (*m/z*) 290 ([M + Na]$^+$, 100%); **MS-ES–** (*m/z*) 533 ([2M – H]$^-$, 34%), 266 ([M – H]$^-$, 87).

Preparation of methyl 4-((but-3-enyloxy)carbonylamino)benzoate, 258

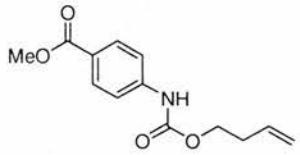

Prepared from **254** (250 mg, 1.65 mmol) using the general method described for aniline protection (Method D). **258** was collected as a white powdery solid (365 mg, 1.46 mmol, 89%); mp 130.0-132.0 °C. **IR** (Nujol, NaCl) ν_{max}: 3316 (br s) (NH, H-bonded) 1730 (s) (C=O, ester), 1699 (s) (C=O, carbamate), 1607 (s) (C=C), 1537 (m) (ArC–C), 1291 (m), 1217 (s), 1050 (m), 855 and 770 (w) (ArC–H) cm^{-1}; **^{1}H NMR** (300 MHz, $CDCl_3$): δ 8.02-7.97 (m, AA′ part of the AA′XX′ system, 2H, $\underline{H}$-2 and $\underline{H}$-6), 7.48-7.43 (m, XX′ part of the AA′XX′ system, 2H, $\underline{H}$-3 and $\underline{H}$-5), 6.77 (br s, 1H, N$\underline{H}$), 5.89-5.75 (m, 1H, C$\underline{H}$=CH$_2$), 5.19-5.09 (m, 2H, CH=C$\underline{H}_2$), 4.25 (t, ^3J = 6.7 Hz, 2H, OC$\underline{H}_2$), 3.89 (s, 3H, OC$\underline{H}_3$), 2.49-2.41 (m, 2H, OCH$_2$C$\underline{H}_2$); **^{13}C NMR** (75.5 MHz, $CDCl_3$): δ 166.7 (C=O, ester), 153.0 (C=O, carbamate), 142.2 (C4), 133.8 (C$\underline{H}$=CH$_2$), 130.9 (C2 and C6), 124.7 (C1), 117.50 (C3 and C5), 117.46 (CH=C$\underline{H}_2$), 64.6 (OC$\underline{H}_2$), 52.0 (CH_3), 33.2 (OCH$_2$C$\underline{H}_2$); **MS-EI+** (*m/z*) 249 ([M]$^{+\bullet}$, 66%), 195 (41), 164 (26), 120 (22), 55 ([(CH$_2$)$_2$CHCH$_2$]$^{+\bullet}$100); **HRMS-EI+** (*m/z*) Calcd for $C_{13}H_{15}NO_4$ [M]$^{+\bullet}$: 249.1001, found 249.0998; **Anal.** Calcd for $C_{13}H_{15}NO_4$: C, 62.64; H, 6.07; N, 5.62. Found: C, 62.91; H, 6.17; N, 5.49.

Preparation of methyl 5-bromo-2-((but-3-enyloxy)carbonylamino)benzoate, 259

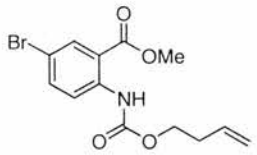

Prepared from **255** (500 mg, 2.17 mmol) using the general method described for aniline protection (Method D). **259** was collected as a white amorphous powder (688 mg, 2.10 mmol, 97%); mp 49.0 – 50.0 °C. **IR** (Nujol, NaCl) ν_{max}: 3305 (br s) (NH, H-bonded) 1742 (s) (C=O, ester), 1702 (s) (C=O, carbamate), 1586 (m) (C=C), 1518 (s) (ArC–C),

1238 (s), 1215 (m), 1056 (m), 830 (w) (ArC–H) cm^{-1}; **^{1}H NMR** (300 MHz, $CDCl_3$): δ 10.39 (br s, 1H, NH), 8.36 (d, ^3J = 9.1 Hz, 1H, H-3), 8.11 (d, ^4J = 2.4 Hz, 1H, H-6), 7.60 (dd, ^3J = 9.1 Hz, ^4J = 2.4 Hz, 1H, H-4), 5.89-5.76 (m, 1H, $CH=CH_2$), 5.18-5.07 (m, 2H, $CH=CH_2$), 4.21 (t, ^3J = 6.8 Hz, 2H, OCH_2), 3.92 (s, 3H, OCH_3), 2.48-2.41 (m, 2H, OCH_2CH_2); **^{13}C NMR** (75.5 MHz, $CDCl_3$): δ 167.3 (C=O, ester), 153.4 (C=O, carbamate), 140.9 (C2), 137.3 (C4), 133.8 ($CH=CH_2$), 133.3 (C6), 120.5 (C3), 117.4 ($CH=CH_2$), 116.0 (C1), 113.8 (C5), 64.5 (OCH_2), 52.5 (OCH_3), 33.2 (OCH_2CH_2); **MS-EI+** (*m/z*) 329 ($[M]^{+\bullet}$, ^{81}Br, 37%), 327 ($[M]^{+\bullet}$, ^{79}Br, 37), 257 (34), 255 (34), 231 (58), 229 (59), 226 (94), 224 (100), 199 (41), 197 (41), 170 (42), 168 (35), 55 ($[(CH_2)_2CHCH_2]^{+\bullet}$, 48); **HRMS-EI+** (*m/z*) Calcd for $C_{13}H_{14}{}^{79}BrNO_4$ $[M]^{+\bullet}$: 327.0106, found 327.0096. **Anal.** Calcd for $C_{13}H_{14}BrNO_4$: C, 47.58; H, 4.30; N, 4.27. Found: C, 47.63; H, 4.21; N, 4.18.

Preparation of but-3-enyl 3-nitrophenylcarbamate, 260

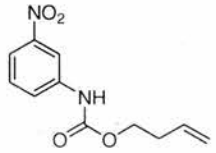

Prepared from **256** (500 mg, 3.62 mmol) using the general method described for aniline protection (Method D). **260** was collected as a a pale yellow crystalline solid (846 mg, 3.58 mmol, 99%); mp 51.0 – 52.0 °C. **IR** (Nujol, NaCl) ν_{max}: 3387 (br s) (NH, H-bonded), 3127 (w), 1719 (s) (C=O, carbamate), 1553 (s) (C=C), 1538 (s) (NO_2), 1350 (s) (NO_2), 1285 (m), 1237 (m), 928 (m), 883 (m), 804 (w), 766 (m), 737 (s), 671 (w) cm^{-1}; **^{1}H NMR** (300 MHz, $CDCl_3$): δ 8.30 (t, ^4J = 2.2 Hz, 1H, H-2), 7.90 (ddd, ^3J = 8.2 Hz, ^4J = 2.2, 0.9 Hz, 1H, H-4), 7.74 (br d, ^3J = 8.2 Hz, 1H, H-6), 7.46 (t, ^3J = 8.2 Hz, 1H, H-5), 6.98 (br s, 1H, NH), 5.88-5.75 (m, 1H, $CH=CH_2$), 5.19-5.08 (m, 2H, $CH=CH_2$), 4.26 (t, ^3J = 6.6, 2H, OCH_2), 2.48-2.41 (m, 2H, OCH_2CH_2); **^{13}C NMR** (75.5 MHz, $CDCl_3$): δ 153.2 (C=O), 148.7 (C3), 139.1 (C1), 133.7 ($CH=CH_2$), 129.8 (C5), 124.1 (C6), 118.0 (C4), 117.6 ($CH=CH_2$), 113.3 (C2), 64.8 (OCH_2), 33.2 (OCH_2CH_2); **MS-EI+** (*m/z*) 236 ($[M]^{+\bullet}$, 11%), 182 (75), 178 (79), 134 (100), 55 ($[(CH_2)_2CHCH_2]^{+\bullet}$, 72); **HRMS-EI+** (*m/z*) Calcd for $C_{11}H_{12}N_2O_4$ $[M]^{+\bullet}$: 236.0797, found 236.0788.

Preparation of but-3-enyl 4-methoxyphenylcarbamate, 261

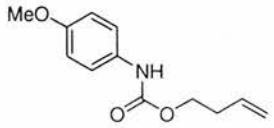

Prepared from **257** (500 mg, 4.06 mmol) using the general method described for aniline protection (Method D). **261** was collected as a a pale yellow crystalline solid (876 mg, 3.96 mmol, 98%); mp 38.0-39.0 °C. **IR** (NaCl, Nujol) ν_{max}: 3306 (br s) (NH, H-bonded), 1693 (s) (C=O, carbamate), 1599 (w), 1530 (s), 1242 (s), 1084 (m), 1029 (m), 826 (s) (ArC–H) cm^{-1}; **^{1}H NMR** (300 MHz, $CDCl_3$): δ 7.31-7.25 (br m, AA′ part of AA′XX′ system, 2H, H-2 and H-6), 6.87-6.81 (m, XX′ part of AA′XX′ system, 2H, H-3 and H-5), 6.61 (br s, 1H, NH), 5.89-5.75 (m, 1H, $CH=CH_2$), 5.18-5.07 (m, 2H, $CH=CH_2$), 4.22 (t, ^3J = 6.7 Hz, 2H, OCH_2), 3.78 (s, 3H, OCH_3), 2.46-2.39 (m, 2H, OCH_2CH_2); **^{13}C NMR** (75.5 MHz, $CDCl_3$): δ 155.7 (C4), 153.9 (C=O, carbamate), 134.0 ($CH=CH_2$), 130.9 (C1), 120.5 (C2 and C6), 117.1 ($CH=CH_2$), 114.0 (C3 and C5), 64.0 (OCH_2), 55.3 (OCH_3), 33.3 (OCH_2CH_2) **MS-CI+** (*m/z*) 222 ($[M + H]^+$, 100%); **HRMS-ES$^+$** (*m/z*) Calcd for $C_{12}H_{16}NO_3$ $[M + H]^+$: 222.1130, found 222.1123; **Anal.** Calcd for $C_{12}H_{15}NO_3$: C, 65.14; H, 6.83; N, 6.33. Found: C, 65.00; H, 7.14; N, 6.33.

Deprotection of 258 to methyl 4-aminobenzoate, 254

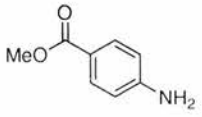

Treatment of **258** using the general method described for aniline deprotection (Method E) gave **254** as a white solid (0.06 g, 0.39 mmol, 78%); mp 107.0-108.0 °C (lit. 107-110 °C).[58] **^{1}H NMR** (300 MHz, $CDCl_3$): δ 7.87-7.83 (m, AA′ part of the AA′XX′ system, 2H, H-2 and H-6), 6.66-6.62 (m, XX′ part of the AA′XX′ system, 2H, H-3 and H-5), 4.02 (br s, 2H, NH_2), 3.85 (s, 3H, OCH_3); **^{13}C NMR** (75.5 MHz, $CDCl_3$): δ 167.2 (C=O, ester), 150.8 (C4), 131.6 (C2 and C6), 119.7 (C1), 113.8 (C3 and C5), 51.6 (CH_3); **MS-ES+** (*m/z*) 174 ($[M + Na]^+$, 100%). Data are in agreement with literature values.[58]

Deprotection of 259 to methyl 2-amino-5-bromobenzoate, 255

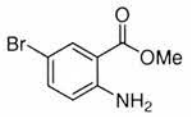

Treatment of **259** using the general method described for aniline deprotection (Method E) gave **255** as a white crystalline solid (0.106 g, 0.46 mmol, 92%); mp 67.-69.0 °C; (lit. mp 68-69 °C).[59] **^{1}H NMR** (300 MHz, $CDCl_3$): δ 7.95 (d, ^4J = 2.4 Hz, 1H, H-6), 7.31 (dd, ^3J = 8.8 Hz, ^4J = 2.4 Hz, 1H, H-4), 6.55 (d, ^3J = 8.8 Hz, 1H, H-3), 5.75 (br s, 2H, NH_2), 3.86 (s, 3H, OCH_3); **^{13}C NMR** (75.5 MHz, $CDCl_3$): δ 167.5 (C=O, ester), 149.3 (C2), 136.7 (C4), 133.4 (C6), 118.3 (C3), 112.0 (C1), 107.3 (C5), 51.8 (OCH_3); **MS-ES+** (*m/z*) 232 ($[M + H]^+$, ^{81}Br, 74%), 230 ($[M + H]^+$, ^{79}Br, 100), 223 (30), 221 (32), 219 (82); **HRMS-ES$^+$** (*m/z*) Calcd for $C_8H_9{}^{81}BrNO_2$ $[M + H]^+$: 231.9796, found 231.9796; **HRMS-ES$^+$** (*m/z*) Calcd for $C_8H_9{}^{79}BrNO_2$ $[M + H]^+$: 229.9817, found 229.9812.

Deprotection of 260 to 3-Nitroaniline, 256

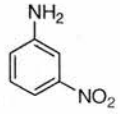

Treatment of **260** using the general method described for aniline deprotection (Method E) gave **256** as a bright yellow crystalline solid (0.055 g, 0.40 mmol, 80%); mp 111.0-113.0 °C (lit. 112.5 °C).[60] **^{1}H NMR** (300 MHz, $CDCl_3$): δ 7.57 (ddd, ^3J = 8.1 Hz, ^4J = 2.3, 0.8 Hz 1H, H-4), 7.49 (t, ^4J = 2.4 Hz, 1H, H-2), 7.27 (t, ^3J = 8.1 Hz, 1H, H-5), 6.94 (ddd, ^3J = 8.1 Hz, ^4J = 2.3, 0.8 Hz 1H, H-6), 4.00 (br s, 2H, NH_2); **^{13}C NMR** (75.5 MHz, $CDCl_3$): δ 149.1 (C3), 147.4 (C1), 129.9 (C5), 120.6 (C6), 113.1 (C4), 109.0 (C2); **MS-ES–** (*m/z*) 137 ($[M - H]^-$, 100%). Data are in agreement with literature values.[61]

Deporotection of 261 to 4-Methoxyaniline, 257

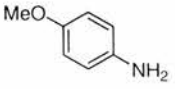

Treatment of **261** using the general method described for aniline deprotection (Method E) gave **257** as a pale green semi-solid (0.024 g, 0.19 mmol, 39%); **^{1}H NMR** (300 MHz, $CDCl_3$): δ 6.78-6.72 (m, AA′ part of the AA′BB′ system, 2H, H-3 and H-5), 6.67-6.62 (m, BB′ part of the AA′BB′ system, 2H, H-2 and H-6), 3.74 (s, 3H, OCH_3), 3.27 (br s, 2H, NH_2); **MS-ES+** (*m/z*) 124 ($[M + H]^+$, 100%).

Preparation of (*E*)-4-(6-(triisopropylsilyloxy)hex-3-enyloxy)benzaldehyde, 262

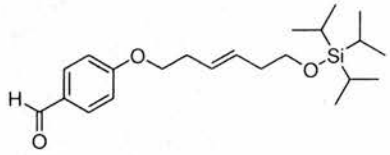

Prepared from **180** (200 g, 0.73 mmol), **221** (90 mg, 0.73 mmol), triphenylphosphine (193 mg, 0.73 mmol), and DEAD (128 mg, 0.13 mL, 0.73 mmol) using the general method described for phenol protection (Method A). Purification by column chromatography on silica (EA:hexane 1:19) gave **262** as a colourless oil (192 mg, 0.51 mmol, 69%). **IR** (NaCl, Nujol) ν_{max}: 2735 (w), 1697 (s) (C=O, aldehyde), 1602 (s) (C=C), 1578 (m) (ArC–C), 1509 (m) (ArC–C), 1258 (s) (C–O–C) cm^{-1}; **^{1}H NMR** (300 MHz, $CDCl_3$): δ 9.87 (s, 1H, C<u>H</u>O), 7.84-7.79 (m, AA′ part of AA′XX′ system, 2H, <u>H</u>-2 and <u>H</u>-6), 7.00-6.95 (m, AA′ part of AA′XX′ system, 2H, <u>H</u>-3 and <u>H</u>-5), 5.68-5.50 (m, 2H, <u>H</u>-3′ and <u>H</u>-4′), 4.04 (t, ^3J = 6.8 Hz, 2H, C<u>H</u>$_2$-1′), 3.70 (t, ^3J = 6.7 Hz, 2H, C<u>H</u>$_2$-6′), 2.55-2.48 (m, 2H, C<u>H</u>$_2$-2′), 2.30-2.24 (m, 2H, C<u>H</u>$_2$-5′), 1.06-1.04 (m, 21H, Si(C<u>H</u>(C<u>H</u>$_3$)$_2$)$_3$); **^{13}C NMR** (75.5 MHz, $CDCl_3$): δ 190.8 (C=O), 164.0 (C4), 131.9 (C2 and C6), 130.2 (C3′), 129.7 (C1), 126.8 (C4′), 114.7 (C3 and C5), 68.0 (C1′), 63.2 (C6′), 36.4 (C5′), 32.4 (C2′), 17.8 (SiC<u>C</u>H$_3$), 11.9 (Si<u>C</u>CH$_3$); **MS-ES+** (*m/z*) 399 ([M + Na]$^+$, 100%); **HRMS-ES$^+$** (*m/z*) Calcd for $C_{22}H_{36}O_3SiNa$ [M + Na]$^+$: 399.2331, found 399.2321.

Preparation of (*E*)-4-(6-hydroxyhex-3-enyloxy)benzaldehyde, 263

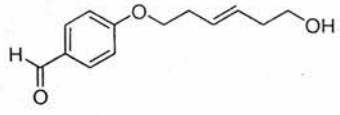

To a solution of **262** (160 mg, 0.43 mmol) in THF (9.0 mL) was added TBAF (0.64 mL, 1.0 M in THF, 0.64 mmol) at room temperature, with stirring. After 2 h the reaction was quenched by addition of water (25 mL) and partitioned between Et_2O (3 × 50 mL) and water. The organic phase was dried ($MgSO_4$) and concentrated *in vacuo*. Purification by flash column chromatography on silica gel (EA:Hexane, 1:9 to 1:1) gave **263** as a colourless oil (89 mg, 0.40 mmol, 95%). **IR** (film) ν_{max}: 3448 (br s) (OH), 3055 (w), 2936 (m), 2746 (w), 1686 (s) (C=O, aldehyde), 1601 (s) (C=C), 1578 (m) and 1509 (m) (ArC–C), 1265 (s) (C–O–C), 1161 (s), 1021 (m), 834 and 738 (ArC–H) cm^{-1}; **^{1}H NMR** (300 MHz, $CDCl_3$): δ 9.86 (s, 1H, C<u>H</u>O), 7.84-7.79 (m, AA′ part of AA′XX′ system, 2H, <u>H</u>-2 and <u>H</u>-6), 7.00-6.95 (m, AA′ part of AA′XX′ system, 2H, <u>H</u>-3 and <u>H</u>-5), 5.68-5.52 (m, 2H,

H-3′ and H-4′), 4.06 (t, ^3J = 6.6 Hz, 2H, CH_2-1′), 3.65 (t, ^3J = 6.2 Hz, 2H, CH_2-6′), 2.57-2.51 (m, 2H, CH_2-2′), 2.33-2.27 (m, 2H, CH_2-5′), 1.72 (br s, 1H, OH); **^{13}C NMR** (75.5 MHz, $CDCl_3$): δ 190.8 (COH), 163.9 (C4), 132.0 (C2 and C6), 129.8 (C1), 129.4 (C4′), 128.5 (C3′), 114.7 (C3 and C5), 67.7 (C1′), 61.8 (C6′), 35.9 (C5′), 32.3 (C2′); **MS-ES+** (*m/z*) 243 ([M + Na]$^+$, 100%); **HRMS-ES$^+$** (*m/z*) Calcd for $C_{13}H_{16}O_3Na$ [M + Na]$^+$: 243.0997, found 243.0995.

Preparation of (*E*)-4-(6-(trialkylsilyloxy)hex-3-enyloxy)benzaldehyde functionalised resin, 265

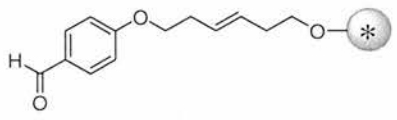

Activation of tetralkylsilane 264 to silyl triflate functionalised resin 264a. Silicon functionalised resin **264** (1.43 mequiv. Si/g or mmol/g) that had been dried under hi-vac for 12 h was weighed (185 mg, 0.26 mmol, 1 equiv.) into a 10 mL polypropylene PD-10 column fitted with a teflon™ stopcock and swollen in DCM (2.0 mL) under an atmosphere of N_2 for 30 mins. The solvent was then drained under positive N_2 pressure and 4% trifluoromethanesulfonic acid in DCM (5.0 mL) solution added. The resin turned pink/orange upon acid treatment and was then gently agitated for 30 mins. while still under N_2 atmosphere. Once activation was completed, the beads were washed with DCM (2 × 5 mL) to remove excess acid.

Loading of (*E*)-4-(6-hydroxyhex-3-enyloxy)benzaldehyde (263) onto resin 264a. Treatment of a suspension of **264a** in DCM (3.0 mL) with 2,6-lutidine (227 mg, 0.25 mL, 2.12 mmol, 8 equiv. relative to Si) for 15 mins. followed by addition of an azeotropically dried solution of **263** (77 mg, 0.35 mmol, 1.3 equiv.) in DCM (3 mL) resulted in colourless resin beads. The beads were then gently agitated for 48 h at room temperature under N_2 atmosphere. The beads were drained and washed in DCM (3 × 10 mL × 30 mins.). The resin was then air-dried for 1 h and then placed under hi-vac for 24 h to remove trace solvent. The mass of the loaded and dried resin was 221.0 mg, an increase in mass of 36.0 mg, indicating an apparent loading efficiency of 62% based on weight gain. The resin washes were combined and the solvent removed in vacuo. The resulting residue was purified by column chromatography on silica gel (EA:Hexane, 3:17 to 1:4) to recover **263** as a colourless oil (41 mg).

Cleavage of 221 from resin. Method 2. Ozonolytic cleavage

Vacuum-dried resin **264a** was weighed (20.0 mg) into a 50 mL pear shaped flask and allowed to swell in DCM (5.0 mL) for 30 mins. The DCM solution was removed and replaced with fresh DCM (10 mL). Treatment of the suspension of **264a** using the general method described for phenol deprotection (Method C) with $(CH_3)_2S$ (21 mg, 25 μL, 0.34 mmol) and triethylamine (18 mg, 25 μL, 0.18 mmol). The solution was removed and the beads washed in DCM (4 × 10 mL × 30 mins.). The resin washes were combined and concentrated *in vacuo*. The resulting residue was purified by column chromatography on silica gel (EA:Hexane, 1:9 to 1:4) to afford **221** as a white solid (1.2 mg, 0.01 mmol). Based on the assumption that 100% of the material loaded onto the resin is cleaved and recovered, this amount of material represents 55% of the theoretical maximum from beads **264a** with a loading efficiency of 62% i.e. 0.89 mmol/g). ^{1}H NMR was consistent with data for **221** from the deprotection of **225** also by Method C.

Preparation of (*E*)-phenyl[4-(6-(trialkylsilyloxy)hex-3-enyloxy)phenyl]methanol functionalised resin, 266

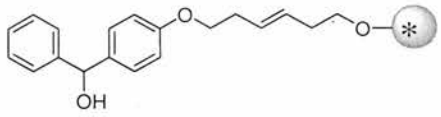

Grignard coupling to produce resin 266. Vacuum-dried resin **264a** was weighed (40.0 mg) into a 25 mL pear shaped flask and allowed to swell in THF (10.0 mL) for 30 min. The THF solution was removed and replaced with fresh THF (20.0 mL) and a solution of phenylmagnesium bromide (0.57 mL, 1.0 M in THF) was added. The beads were then gently agitated for 12 h at room temperature under N_2 atmosphere. The solution was removed and the beads washed in DCM (6 × 20 mL × 30 mins.). The resin was then air-dried for 1 h and then placed under hi-vac for 24 h to remove trace solvent. The mass of the loaded and dried resin was 48.7 mg, an increase in mass of 8.7 mg.

(*E*)-6-[4-(Hydroxy(phenyl)methyl)phenoxy]hex-3-en-1-ol, 267

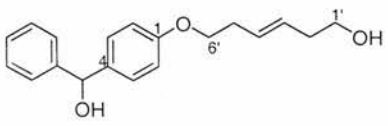

Cleavage of 267 from resin: Method 1. Fluoride cleavage: Vacuum-dried resin **266** was weighed (20.0 mg, 0.43 mmol) into a 25 mL pear shaped flask and allowed to swell in THF (5.0 mL) for 30 min. The THF solution was removed and replaced with fresh THF

(5.0 mL) and a solution of TBAF (43 μL, 1.0 M in THF, 0.04 mmol) added. The beads were then gently agitated for 1.5 h at room temperature. Additional TBAF (43 μL, 1.0 M in THF, 0.04 mmol) was added and the suspension agitated for a further 1.5 h. The solution was removed and the beads washed in CH_2Cl_2 (3 × 20 mL × 30 min.). The combined organics were partitioned between Et_2O (3 × 20 mL) and water. The organic phase was dried ($MgSO_4$) and concentrated *in vacuo* to afford a pale yellow oil which by ^{1}H NMR analysis appeared to contain a trace impurity resulting in aliphatic signals. Purification by flash column chromatography on silica gel (EA:Hexane, 1:4 to 2:3) gave **267** as a pale yellow oil (2.5 mg, 0.008 mmol). Based on the assumption that 100% of the material loaded onto the resin is cleaved and recovered, this amount of material represents 47% of the theoretical maximum from beads **266** with a loading efficiency of 62% i.e. 0.89 mmol/g). **^{1}H NMR** (300 MHz, $CDCl_3$): δ 7.39-7.23 (m, 7H, included AA′ part of the AA′XX′ system, H-2 and H-6, and 5 × ArH), 6.85 (m, 2H, XX′ part of the AA′XX′ system, H-3 and H-5,), 5.81 (s, 1H, CH, methylene), 5.68-5.49 (m, 2H, H-3′ and H-4′), 3.98 (t, ^3J = 6.8 Hz, 2H, CH_2-6′), 3.63 (t, ^3J = 6.2 Hz, 2H, CH_2-1′), 2.53-2.45 (m, 2H, CH_2-5′), 2.32-2.26 (m, 2H, CH_2-2′), 2.15 (br s, 1H, CHOH), 1.39 (br s, 1H, OH); **MS-ES+** (*m/z*) 321 ([M + Na]$^+$, 100%), 281 ([M – OH]$^+$, 16); **HRMS-ES$^+$** (*m/z*) Calcd for $C_{19}H_{22}O_3Na$ [M + Na]$^+$: 321.1467, found 321.1461.

4-Hydroxy benzhydrol, 268

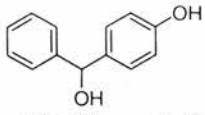

Cleavage of 268 from resin: Method 2. Ozonolytic cleavage: Vacuum-dried resin **266** was weighed (25.0 mg) into a 25 mL pear shaped flask and allowed to swell in DCM (5.0 mL) for 30 min. The DCM solution was removed and replaced with fresh DCM (10 mL). Treatment of the suspension of **266** using the general method described for phenol deprotection (Method C) with $(CH_3)_2S$ (21 mg, 25 μL, 0.34 mmol) and triethylamine (18 mg, 25 μL, 0.18 mmol). The solution was removed and the beads washed in DCM (4 × 10 mL × 30 min.). The resin washes were combined and concentrated *in vacuo*. The resulting residue was purified by column chromatography on silica gel (EA:Hexane, 1:9 to 2:3) to afford 268 as a white solid (1.2 mg, 0.006 mmol). Based on the assumption that 100% of the material loaded onto the resin is cleaved and recovered, this amount of material represents 27% of the theoretical maximum from beads **266** with a loading efficiency of 62% i.e. 0.89 mmol/g). **^{1}H NMR** (300 MHz, $CDCl_3$): δ 7.37-7.19 (m, 7H,

H-3 and H-5 and 5 ×ArH), 6.82-6.75 (m, XX′ part of AA′XX′ system, 2H, H-2 and H-6), 6.12 (s, 1H, OH), 6.08 (s, 1H, CH); **MS-ES–** (*m/z*) 381 (81), 255 (20), 199 ([M – H]$^-$, 47%), 197 (100), 181 (26), 121 (27).

Prepared by Grignard coupling. To a solution of **221** (45 mg, 0.37 mmol) in THF (20.0 mL) was added a solution of phenylmagnesium bromide (0.37 mL, 1.0 M in THF, 0.37 mmol) at room temperature, with stirring. After 30 min. the reaction was quenched by addition of saturated ammonium chloride solution (25 mL) and extracted into DCM (3 × 50 mL). The combined organic phases were dried ($MgSO_4$) and concentrated *in vacuo* to afford a white solid. Purification by flash column chromatography on silica gel (EA:Hexane, 1:4) gave **268** as a white crystalline solid (59 mg, 0.29 mmol, 80%); mp 156.0-158.0 °C recrystallised from ethanol/H_2O (lit. 161-162 °C, ethanol/H_2O).[62] **IR** (NaCl, Nujol) ν_{max}: 3399 (s) (OH), 3162 (br s) (OH, H-bonded), 3038 (w), 1612 and 1596 (m) (ArC–C), 1236 and 1220 (m), 1006 (s) (C–O), cm^{-1}; **^{1}H NMR** (300 MHz, $CDCl_3$): δ 7.40-7.23 (m, includes AA′ part of AA′XX′ system, 7H, H-3 and H-5 and 5 ×ArH), 6.81-6.76 (m, XX′ part of AA′XX′ system, 2H, H-2 and H-6), 5.81 (s, 1H, CH); **^{1}H NMR** (300 MHz, CD_3OD): δ 7.37-7.13 (m, includes AA′ part of AA′XX′ system, 7H, H-3 and H-5 and 3 ×ArH), 6.74-6.70 (m, XX′ part of AA′XX′ system, 2H, H-2 and H-6), 5.69 (s, 1H, CH), 4.75 (s, 1H, OH); **^{13}C NMR** (75.5 MHz, CD_3OD): δ 157.8 (C1), 146.3 (C1′), 136.9 (C4), 129.2 (4 ×ArC) 128.1 (ArC), 127.6 (2 ×ArC), 116.0 (C2 and C6), 76.7 (CH, methylene); **MS-ES–** (*m/z*) 255 (11%), 199 ([M – H]$^-$, 100), 181 (8), 121 (4). Data are in agreement with literature values.[46] ^{1}H NMR was consistent with data for **268** from the cleavage of **266** from the resin.

REFERENCES

REFERENCES

1. Greene, T. W.; Wuts, P. G. M. *Protective Groups in Organic Synthesis 3rd Ed.*, John Wiley & Sons Inc. **1999**, Chapter 3, 246-287.
2. Gerstenberger, B. S.; Konopelski, J. P. *J. Org. Chem.* **2005**, *70*, 1467-1470.
3. Kocienski, P. J. *Protecting groups*, Georg Thieme Verlag, Stuttgart, Germany, **1994**.
4. Sartori, G.; Ballini, R.; Bigi, F.; Bosica, G.; Maggi, R.; Righi, P. *Chem. Rev.* **2004**, *104*, 199-250.
5. Jarowicki, K.; Kocienski, P. *J. Chem. Soc., Perkin Trans I* **1998**, 4005-4037.
6. Schreiber, S. L. *Science* **2000**, *287*, 1964-1969.
7. Pelish, H. E.; Westwood, N. J.; Feng, Y.; Kirchhausen, T.; Shair, M. D. *J. Am. Chem. Soc.* **2001**, *123*, 6740-6741.
8. Barrett, A. G. M.; Lebold, S. A.; Zhang, X. *Tetrahedron Lett.* **1989**, *30*, 7317-7320.
9. Barrett, A. G. M.; Lebold, S. A. *J. Org. Chem.* **1990**, *55*, 5818-5820.
10. Hardy, P. M.; Rydon, H. N.; Thompson, R. C. *Tetrahedron Lett.* **1968**, *9*, 2525-2526.
11. Westwood, N. J. PhD Thesis, 1995, therein.
12. Veysoglu, T.; Mitscher, L. A.; Swayze, J. *Synthesis* **1980**, 807-810.
13. Slomp, G. J.; Johnson, J. L. *J. Am. Chem. Soc.* **1958**, *80*, 915-921.
14. Criegee, R. *Angew. Chem. Int. Ed.* **1975**, *14*, 745-752.
15. Smith, M. B., March, J. *March's Advanced Organic Chemistry: Reactions, Mechanisms, and Structure*, 5th Ed. John Wiley & Sons, Inc. 2001.
16. Pappas, J. J.; Keaveney, W. P. *Tetrahedron Lett.* **1966**, *36*, 4273-4278.
17. Mitsunobu, O. *Synthesis* **1981**, 1-28.
18. Torraca, K. E.; Huang, X.; Parrish, C. A.; Buchwald, S. L. *J. Am. Chem. Soc.* **2001**, *123*, 10770-10771.
19. Frankel, M. B.; Witucki, E. F.; Rowley, G. L.; Warner, M. *J. Org. Chem.* **1972**, *37*, 152-154.
20. Hon, Y-S.; Lin, S-W.; Lu, L.; Chen, Y-J. *Tetrahedron* **1995**, *51*, 5019-5034.
21. Aurell, M. J.; Ceita, L.; Mestres, R.; Tortajada, A. *Tetrahedron* **1997**, *53*, 10883-10898.
22. Straight, A. F.; Cheung, A.; Limouze, J.; Chen, I.; Westwood, N. J.; Sellers, J. R.; Mitchison, T. J. *Science* **2003**, *299*, 1743-1747.

23. Patterson, S.; Lucas-Lopez, C.; Westwood, N. J. *Beilstein-Institut Proc. Bozen 2004*, **2005**, 147-166.
24. Allingham, J. S.; Smith, R.; Rayment, I. *Nat. Struct. Mol. Biol.* **2005**, *12*, 378-379.
25. Mitsunobu, O.; Yamada, M. *Bull. Chem. Soc. Jpn.* **1967**, *40*, 2380-2382.
26. Klapars, A.; Huang, X.; Buchwald, S. L. *J. Am. Chem. Soc.* **2002**, *124*, 7421-7428.
27. Lucas-Lopez, C. PhD Thesis, July 2005, therein.
28. Lucas-Lopez, C.; Patterson, S.; Blum, T.; Straight, A. F.; Toth, J.; Slawin, A. M. Z.; Mitchison, T. J.; Sellers, J. R.; Westwood, N. J. *Eur. J. Org. Chem.* **2005**, 1736-1740.
29. Davis, F. A.; Sheppard, A. C.; *Tetrahedron* **1989**, *45*, 5703-5742.
30. Davis, F. A.; Sheppard, A. C.; Chen, B-C.; Haque, M. S. *J. Am. Chem. Soc.* **1990**, *112*, 6679-6690.
31. Davis, F. A.; Weismiller, M. C.; Murphy, C. K.; Reddy, R. T.; Chen, B-C. *J. Org. Chem.* **1992**, *57*, 7274-7285.
32. Parlow, J. J.; Flynn, D. L. *Tetrahedron* **1998**, *54*, 4013-4031.
33. Kirschning, A.; Monenschein, H.; Wittenberg, R. *Chem. Eur. J.* **2000**, *6*, 4445-4450.
34. Galioğlu, O.; Akar, A. *Eur. Polym. J.* **1989**, *25*, 313-316.
35. Hu, Y.; Baudart, S.; Porco, J. A. Jr. *J. Org. Chem.* **1999**, *64*, 1049-1051.
36. Goese, M.; Eisenreich, W.; Kupfer,E.; Stohler, P.; Weber, W.; Leuenberger, H. G.; Bacher, A. *J. Org. Chem.* **2001,** *66,* 4673-4678.
37. Emerson, D. W.; Emerson, R. R.; Joshi, S. C.; Sorensen, E. M.; Turek, J. E. *J. Org. Chem.* **1979**, *44*, 4634-4640.
38. Hall, B. J.; Sutherland, J. D. *Tetrahedron Lett.* **1998**, *39*, 6593-6596.
39. Plante, O. J.; Palmacci, E. R.; Seeberger, P. H. *Science* **2001**, *291*, 1523-1527.
40. Fréchet, J. M.; Schuerch, C. *Carbohyd. Res.* **1972**, *22*, 399-412.
41. Paris, M.; Pothion, C.; Goulleux, L.; Heitz, A.; Martinez, J.; Fehrentz, J-A. *React. Funct. Polym.* **1999**, *41*, 255-261.
42. Hanessian, S.; Xie, F. *Tetrahedron Lett.* **1998**, *39*, 737-740.
43. Sylvain, C.; Wagner, A.; Mioskowski, C. *Tetrahedron Lett.* **1997**, *38*, 1043-1044.
44. Tallarico, J. A.; Depew, K. M.; Pelish, H. E.; Westwood, N. J.; Lindsley, C. W.; Shair, M. D.; Schreiber, S. L.; Foley, M. A. *J. Comb. Chem.* **2001**, *3*, 312-318.
45. Yasuhara, A.; Kasano, A.; Sakamoto, T. *J. Org. Chem.* **1999**, *64*, 4211-4213.

46. Hattori, K.; Sajiki, H.; Hirota, K. *Tetrahedron*, **2001**, *57*, 4817-4824.

47. Scicinski, J. J.; Congreve, M. S.; Kay, C.; Ley, S. V. *Curr. Med. Chem.* **2002**, *9*, 2103-2127.

48. Ventrice, T.; Campi, E. M.; Jackson, W. R.; Patti, A. F. *Tetrahedron* **2001**, *57*, 7557-7574.

49. Corey, E. J.; Guzman-Perez, A.; Noe, M. C. *J. Am. Chem. Soc.* **1995**, *117*, 10805-10816.

50. Nicolaou, K. C.; Cho, S. Y.; Hughes, R.; Winssinger, N.; Smethurst, C.; Labischinski, H.; Endermann, R. *Chem. Europ. J.* **2001**, *7*, 3798-3823.

51. Sarma, J. A. R. P.; Nagaraju, A. *J. Chem. Soc. Perkin Trans. II* **2000**, *6*, 1113-1118.

52. Hudson, R. F.; Loveday, G. *J. Chem. Soc.* **1962**, 1068-1075.

53. Krapcho, P. A.; Waterhouse, D. *Synth. Commun.* **1998**, *28*, 3415-3422.

54. Webb, K. S.; Ruszkay, S. J. *Tetrahedron* **1998**, *54*, 401-410.

55. Sarma, J. A. R. P.; Nagaraju, A.; Majumdar, K. K.; Samuel, P. M.; Das, I.; Roy, S.; McGhie, A. J. *J. Chem. Soc. Perkin Trans I* **2000**, *6*, 1119-1124.

56. Levin, J. I.; Du, M. T. *Synth. Commun.* **2002**, *32*, 1401-1406.

57. Webb, R. G.; Haskell, M. W.; Stammar, C. H. *J. Org. Chem.* **1969**, *34*, 576-577.

58. Sellarajah, S.; Lekishvili, T.; Bowring, C.; Thompsett, A. R.; Rudyk, H.; Birkett, C. R.; Brown, D. R.; Gilbert, I. H. *J. Med. Chem.* **2004**, *47*, 5155-5134.

59. Leiby, R. W. *J. Org. Chem.* **1985**, *50*, 2926-2929.

60. Berliner, J. F. T.; May, O. E. *J. Am. Chem. Soc.* **1925**, *47*, 2350-2356.

61. Crank, D. J.; Levy, G. L.; Brownlee, R. T. C. *J. Org. Chem.* **1983**, *48*, 1601-1606.

62. Vittum, P. W.; Brown, G. H. *J. Am. Chem. Soc.* **1949**, *71*, 2287-2290.

CONCLUSIONS AND FUTURE WORK

CONCLUSIONS

In this thesis, the reactivity of 2,3-bis(bromomethyl)quinoxaline 1,4-dioxide (**27**) with primary and secondary amines is presented. Unexpectedly, the results showed that a double nucleophilic substitution reaction involving two equivalents of the amine is preferred to a cyclisation pathway. However, in the absence of the *N*-oxide functional groups a cyclisation reaction was preferred. These studies raise the intriguing possibility that two protein-based nucleophilic residues are required in close proximity to achieve covalent modification of a target protein by **27**.

Our studies have shown that synthetic modification of **27** at C-6/7 has interesting regioisomeric consequences for the mechanism for the reaction with amines. In all cases, the presence of an *N*-oxide functional group has been shown to influence the outcome of the reaction of 2,3-bis(bromomethyl)quinoxaline derivatives with amines. NMR, computuational modelling techniques and X-ray crystallographic analysis have been used to rationalise the experimental findings.

A range of derivatives of **27** have been successfully prepared and characterised, including a biotinylated affinity reagent. Biological activity data has shown that incorporation of bromine at C-6 in **27** increases the potency of the small molecule as an invasion inhibitor of *Toxoplasma gondii* parasites into host cells. Preliminary target identification experiments using the biotinylated affinity reagent have shown promising results.

The development of the butenyl group introduced by Barrett *et al.* as a protecting group for phenols and anilines (as the carbamate) has been achieved. An ozonolytic deprotection protocol has been used that is suitable for application in both solution and solid phase synthesis. The utility of the butenyl protecting group has been demonstrated in the synthesis of a phenol-containing derivative of (*S*)-(–)-blebbistatin (**232**). The synthetic route disclosed provides an approach towards the synthesis of blebbistatin analogues containing a C-4′′ substiuent. In addition, the structure of **232** has been confirmed by X-ray crystallographic analysis.

In conclusion, the goals set at the outset of this research project (page 29) have been achieved.

FUTURE WORK

Ideas for future work have been threaded throughout this thesis. Much of the synthetic work presented in the body of this thesis enables the development of new synthetic projects. These could include:

I. The potential development of **27** as a chemical proteomic probe.

II. The synthesis of the hydrobromide salt analogue of **27** (**184**) may be used in the synthesis of a set of reagents applicable to *in vivo* target identification studies.

III. Further extension of the butenyl protecting group to amine and alcohol function groups.

IV. The synthesis of the phenol-containing derivative of (*S*)-(–)-blebbistatin (**232**) provides an important starting material for the synthesis of analogues. Chemical modification at the C-4′′ position (OH group) utilising C–O bond forming procedures (eg. Mitsunobu chemistry) will allow the introduction of diversity at this position. This may potentially lead to the discovery of more potent and/or selective inhibitors of the myosin subclasses.

V. Future development of the hexenyl-based linker unit (**180**) should remain a key approach to the design of a cleavable linker for affinity chromatography and for applications in solid phase synthesis.

APPENDIX

1.0 SUPPLEMENTARY INFORMATION

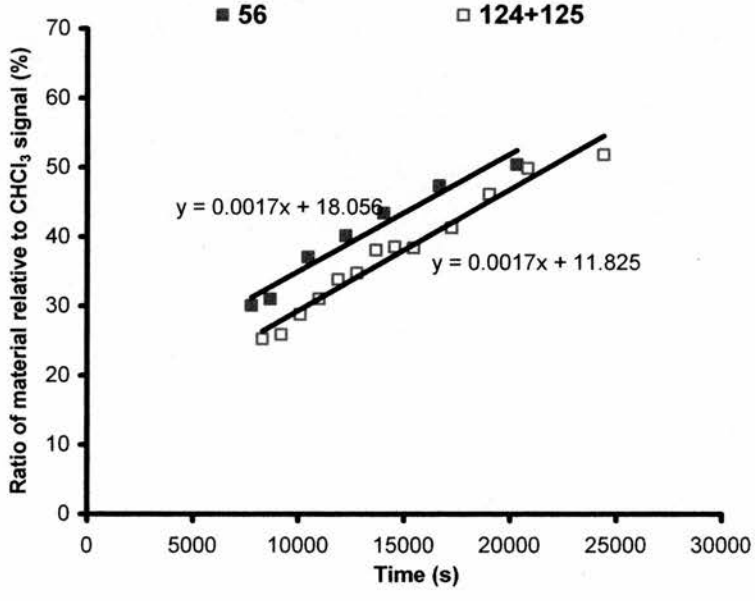

Figure 1. Total product formation in the reactions of **27** and **110** with *n*-butylamine. The rate of product formation between t = 7800 and 24 500 s is similar based on the calculated gradient.

2.0 ^{1}H NMR Data analysed for the reaction of 27 with *n*-butylamine at 4 mM.

Specific peaks chosen for analysis are indicated.

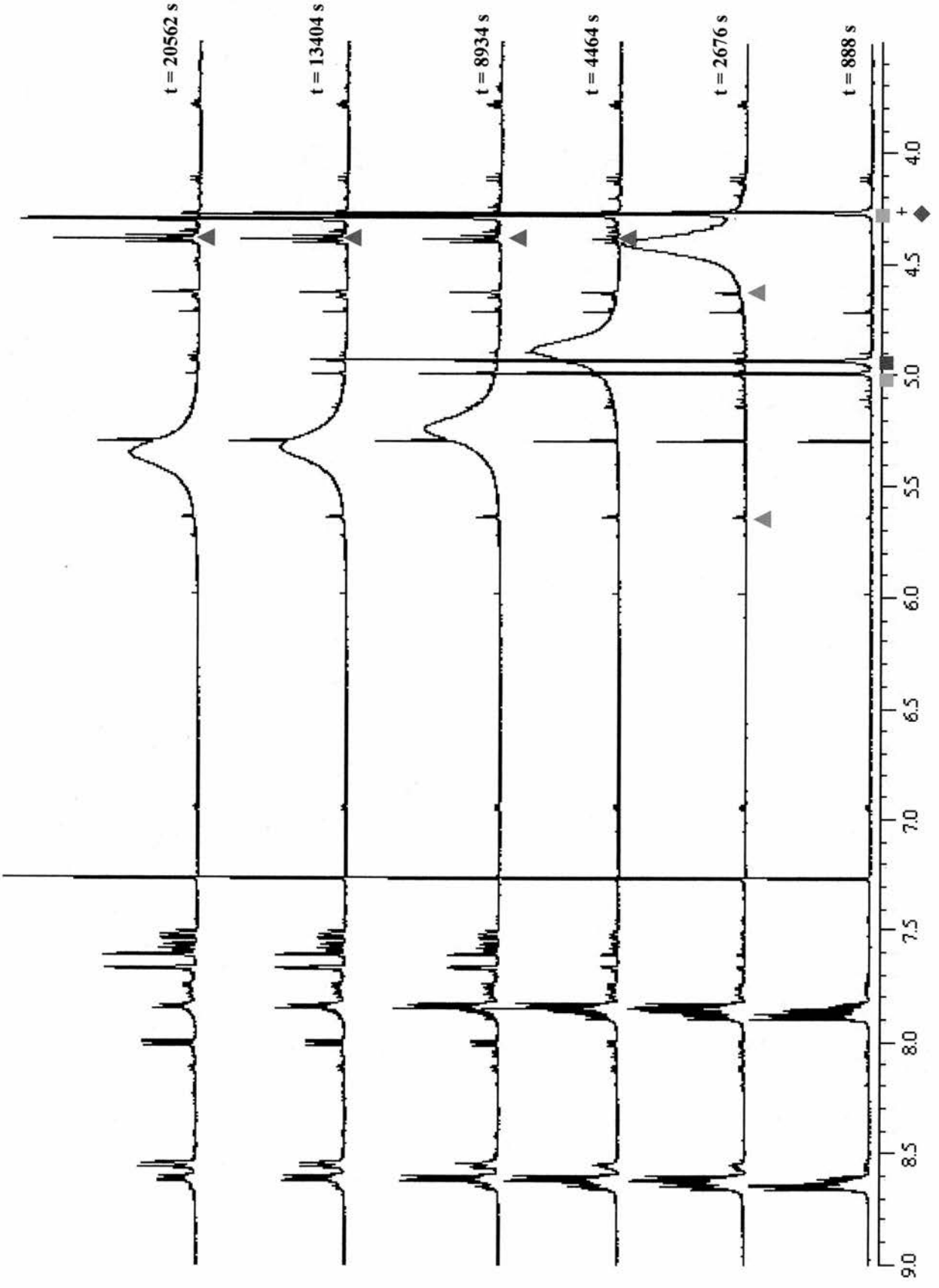

3.0 CRYSTALLOGRAPHIC DATA

3.1 Crystal data and structure refinement for kenw8. *tert*-Butyl 2,3-bis(bromomethyl)quinoxalin-6-ylcarbamate 1,4-dioxide, 110

Identification code	kenw8	
Empirical formula	C15 H17 Br2 N3 O4	
Formula weight	463.14	
Temperature	93(2) K	
Wavelength	0.71073 Å	
Crystal system	Monoclinic	
Space group	P2(1)/n	
Unit cell dimensions	a = 14.181(2) Å	α= 90°.
	b = 6.9634(10) Å	β= 106.362(9)°.
	c = 17.674(3) Å	γ = 90°.
Volume	1674.6(4) $Å^3$	
Z	4	
Density (calculated)	1.837 Mg/m^3	
Absorption coefficient	4.866 mm^{-1}	
F(000)	920	
Crystal size	0.200 x 0.020 x 0.010 mm^3	
Theta range for data collection	2.99 to 25.34°.	
Index ranges	-15<=h<=17, -7<=k<=6, -20<=l<=21	
Reflections collected	10969	
Independent reflections	2875 [R(int) = 0.0854]	
Completeness to theta = 25.34°	93.9 %	
Absorption correction	Multiscan	
Max. and min. transmission	1.0000 and 0.6337	
Refinement method	Full-matrix least-squares on F^2	
Data / restraints / parameters	2875 / 1 / 222	
Goodness-of-fit on F^2	1.074	
Final R indices [I>2sigma(I)]	R1 = 0.0739, wR2 = 0.1515	
R indices (all data)	R1 = 0.0928, wR2 = 0.1615	
Largest diff. peak and hole	0.787 and -0.632 $e.Å^{-3}$	

3.2 Crystal data and structure refinement for kenw7. 2,3-Bis(bromomethyl)-6-bromoquinoxaline 1,4-dioxide, 142

Identification code	kenw7	
Empirical formula	C10 H7 Br3 N2 O2	
Formula weight	426.91	
Temperature	93(2) K	
Wavelength	0.71073 Å	
Crystal system	Monoclinic	
Space group	P2(1)/c	
Unit cell dimensions	a = 9.693(3) Å	α= 90°.
	b = 7.704(2) Å	β= 97.143(13)°.
	c = 15.975(5) Å	γ = 90°.
Volume	1183.7(6) $Å^3$	
Z	4	
Density (calculated)	2.395 Mg/m^3	
Absorption coefficient	10.213 mm^{-1}	
F(000)	808	
Crystal size	0.200 x 0.030 x 0.010 mm^3	
Theta range for data collection	2.94 to 25.35°.	
Index ranges	-11<=h<=10, -6<=k<=8, -11<=l<=18	
Reflections collected	6379	
Independent reflections	2022 [R(int) = 0.0581]	
Completeness to theta = 25.35°	93.4 %	
Absorption correction	Multiscan	
Max. and min. transmission	1.0000 and 0.8077	
Refinement method	Full-matrix least-squares on F^2	
Data / restraints / parameters	2022 / 0 / 155	
Goodness-of-fit on F^2	1.024	
Final R indices [I>2sigma(I)]	R1 = 0.0512, wR2 = 0.0911	
R indices (all data)	R1 = 0.0806, wR2 = 0.1001	
Largest diff. peak and hole	1.362 and -0.729 $e.Å^{-3}$	

3.3 Crystal data and structure refinement for kenw10. 2,3-Bis(bromomethyl)-6-bromoquinoxaline 4-oxide, 152

Identification code	kenw10	
Empirical formula	C10 H7 Br3 N2 O	
Formula weight	410.91	
Temperature	93(2) K	
Wavelength	0.71073 Å	
Crystal system	Triclinic	
Space group	P-1	
Unit cell dimensions	a = 7.483(2) Å	α= 100.412(9)°.
	b = 7.6916(19) Å	β= 93.102(5)°.
	c = 10.345(3) Å	γ = 95.459(10)°.
Volume	581.4(3) $Å^3$	
Z	2	
Density (calculated)	2.347 Mg/m^3	
Absorption coefficient	10.385 mm^{-1}	
F(000)	388	
Crystal size	0.0300 x 0.0300 x 0.1500 mm^3	
Theta range for data collection	2.74 to 25.33°.	
Index ranges	-9<=h<=6, -9<=k<=7, -11<=l<=12	
Reflections collected	3712	
Independent reflections	2018 [R(int) = 0.0439]	
Completeness to theta = 25.33°	95.0 %	
Absorption correction	Multiscan	
Max. and min. transmission	1.0000 and 0.5494	
Refinement method	Full-matrix least-squares on F^2	
Data / restraints / parameters	2018 / 0 / 146	
Goodness-of-fit on F^2	0.739	
Final R indices [I>2sigma(I)]	R1 = 0.0273, wR2 = 0.0667	
R indices (all data)	R1 = 0.0299, wR2 = 0.0678	
Largest diff. peak and hole	1.128 and -0.638 $e.Å^{-3}$	

3.4 Crystal data and structure refinement for kenw6. 2,3-Bis(bromomethyl)-7-bromoquinoxaline 1-oxide, 153

Identification code	kenw6	
Empirical formula	C10 H7 Br3 N2 O	
Formula weight	410.91	
Temperature	93(2) K	
Wavelength	0.71073 Å	
Crystal system	Triclinic	
Space group	P-1	
Unit cell dimensions	a = 7.4673(16) Å	α= 86.162(14)°.
	b = 7.8862(17) Å	β= 88.275(13)°.
	c = 10.833(2) Å	γ = 65.970(11)°.
Volume	581.4(2) $Å^3$	
Z	2	
Density (calculated)	2.347 Mg/m^3	
Absorption coefficient	10.386 mm^{-1}	
F(000)	388	
Crystal size	0.130 x 0.030 x 0.010 mm^3	
Theta range for data collection	2.83 to 25.35°.	
Index ranges	-7<=h<=8, -9<=k<=9, -11<=l<=13	
Reflections collected	3937	
Independent reflections	1817 [R(int) = 0.0734]	
Completeness to theta = 25.35°	85.3 %	
Absorption correction	Multiscan	
Max. and min. transmission	1.0000 and 0.9572	
Refinement method	Full-matrix least-squares on F^2	
Data / restraints / parameters	1817 / 0 / 137	
Goodness-of-fit on F^2	0.883	
Final R indices [I>2sigma(I)]	R1 = 0.1077, wR2 = 0.2714	
R indices (all data)	R1 = 0.1120, wR2 = 0.2762	
Extinction coefficient	0.002(4)	
Largest diff. peak and hole	2.824 and -2.188 $e.Å^{-3}$	

3.5 Crystal data and structure refinement for kenw13. 2,3-Bis(bromomethyl)-6-nitroquinoxaline 1-oxide, 154

Identification code	kenw13	
Empirical formula	C10 H7 Br2 N3 O3	
Formula weight	377.01	
Temperature	93(2) K	
Wavelength	0.71073 Å	
Crystal system	Monoclinic	
Space group	P2(1)/c	
Unit cell dimensions	a = 7.3962(19) Å	α= 90°.
	b = 24.731(6) Å	β= 111.789(5)°.
	c = 6.9611(17) Å	γ = 90°.
Volume	1182.3(5) Å^3	
Z	4	
Density (calculated)	2.118 Mg/m^3	
Absorption coefficient	6.860 mm^{-1}	
F(000)	728	
Crystal size	0.1000 x 0.1000 x 0.0100 mm^3	
Theta range for data collection	2.97 to 25.35°.	
Index ranges	-8<=h<=8, -29<=k<=29, -8<=l<=7	
Reflections collected	7435	
Independent reflections	2145 [R(int) = 0.0459]	
Completeness to theta = 25.35°	98.8 %	
Absorption correction	Multiscan	
Max. and min. transmission	1.0000 and 0.3016	
Refinement method	Full-matrix least-squares on F^2	
Data / restraints / parameters	2145 / 0 / 164	
Goodness-of-fit on F^2	1.079	
Final R indices [I>2sigma(I)]	R1 = 0.0304, wR2 = 0.0666	
R indices (all data)	R1 = 0.0360, wR2 = 0.0690	
Largest diff. peak and hole	0.706 and -0.866 e.Å^{-3}	

3.6 Crystal data and structure refinement for kenw11. 2,3-Bis(bromomethyl)-7-nitroquinoxaline 1-oxide, 155

Identification code	kenw11	
Empirical formula	C10 H7 Br2 N3 O3	
Formula weight	377.01	
Temperature	93(2) K	
Wavelength	0.71073 Å	
Crystal system	Triclinic	
Space group	P-1	
Unit cell dimensions	a = 7.3140(13) Å	α= 87.946(15)°.
	b = 7.7055(11) Å	β= 89.412(13)°.
	c = 11.226(3) Å	γ = 72.355(10)°.
Volume	602.5(2) $Å^3$	
Z	2	
Density (calculated)	2.078 Mg/m^3	
Absorption coefficient	6.730 mm^{-1}	
F(000)	364	
Crystal size	0.1000 x 0.0300 x 0.0100 mm^3	
Theta range for data collection	2.78 to 25.34°.	
Index ranges	-7<=h<=8, -7<=k<=9, -13<=l<=8	
Reflections collected	3971	
Independent reflections	2144 [R(int) = 0.0291]	
Completeness to theta = 25.34°	97.4 %	
Absorption correction	Multiscan	
Max. and min. transmission	1.0000 and 0.5135	
Refinement method	Full-matrix least-squares on F^2	
Data / restraints / parameters	2144 / 0 / 164	
Goodness-of-fit on F^2	1.048	
Final R indices [I>2sigma(I)]	R1 = 0.0270, wR2 = 0.0709	
R indices (all data)	R1 = 0.0314, wR2 = 0.0739	
Largest diff. peak and hole	0.795 and -0.636 $e.Å^{-3}$	

3.7 Crystal data and structure refinement for kenw12. *S*-3a-hydroxy-1-(4-phenol)-6-methyl-2,3,3a,4-tetrahydro-1*H*-pyrrolo[2,3-*b*]quinolin-4-one, 232

Identification code	kenw12	
Empirical formula	C18 H18 N2 O4	
Formula weight	326.34	
Temperature	93(2) K	
Wavelength	0.71073 Å	
Crystal system	Orthorhombic	
Space group	P2(1)2(1)2(1)	
Unit cell dimensions	a = 5.840(4) Å	α= 90°.
	b = 11.728(8) Å	β= 90°.
	c = 21.6494(14) Å	γ = 90°.
Volume	1482.9(13) $Å^3$	
Z	4	
Density (calculated)	1.462 Mg/m^3	
Absorption coefficient	0.105 mm^{-1}	
F(000)	688	
Crystal size	0.2000 x 0.0300 x 0.0100 mm^3	
Theta range for data collection	1.88 to 25.45°.	
Index ranges	-4<=h<=6, -12<=k<=14, -26<=l<=25	
Reflections collected	9738	
Independent reflections	2600 [R(int) = 0.0988]	
Completeness to theta = 25.45°	97.1 %	
Absorption correction	Multiscan	
Max. and min. transmission	1.0000 and 0.6122	
Refinement method	Full-matrix least-squares on F^2	
Data / restraints / parameters	2600 / 4 / 227	
Goodness-of-fit on F^2	1.126	
Final R indices [I>2sigma(I)]	R1 = 0.0950, wR2 = 0.1831	
R indices (all data)	R1 = 0.1273, wR2 = 0.2039	
Absolute structure parameter	-1(4)	
Largest diff. peak and hole	0.278 and -0.297 $e.Å^{-3}$	